ION CHANNELS AND TRANSPORTERS IN CA^{2+} -DEPENDENT FUNCTIONS OF LYMPHOCYTES

EDITED BY: Péter Béla Hajdu, Barbara Niemeyer, Ildikò Szabò and Heike Wulff

PUBLISHED IN: Frontiers in Pharmacology and Frontiers in Physiology

frontiers Research Topics

ISSN 1664-8714
ISBN 978-2-88976-697-0
DOI 10.3389/978-2-88976-697-0

About Frontiers

Frontiers is more than just an open-access publisher of scholarly articles: it is a pioneering approach to the world of academia, radically improving the way scholarly research is managed. The grand vision of Frontiers is a world where all people have an equal opportunity to seek, share and generate knowledge. Frontiers provides immediate and permanent online open access to all its publications, but this alone is not enough to realize our grand goals.

Frontiers Journal Series

The Frontiers Journal Series is a multi-tier and interdisciplinary set of open-access, online journals, promising a paradigm shift from the current review, selection and dissemination processes in academic publishing. All Frontiers journals are driven by researchers for researchers; therefore, they constitute a service to the scholarly community. At the same time, the Frontiers Journal Series operates on a revolutionary invention, the tiered publishing system, initially addressing specific communities of scholars, and gradually climbing up to broader public understanding, thus serving the interests of the lay society, too.

Dedication to Quality

Each Frontiers article is a landmark of the highest quality, thanks to genuinely collaborative interactions between authors and review editors, who include some of the world's best academicians. Research must be certified by peers before entering a stream of knowledge that may eventually reach the public - and shape society; therefore, Frontiers only applies the most rigorous and unbiased reviews.
Frontiers revolutionizes research publishing by freely delivering the most outstanding research, evaluated with no bias from both the academic and social point of view. By applying the most advanced information technologies, Frontiers is catapulting scholarly publishing into a new generation.

What are Frontiers Research Topics?

Frontiers Research Topics are very popular trademarks of the Frontiers Journals Series: they are collections of at least ten articles, all centered on a particular subject. With their unique mix of varied contributions from Original Research to Review Articles, Frontiers Research Topics unify the most influential researchers, the latest key findings and historical advances in a hot research area! Find out more on how to host your own Frontiers Research Topic or contribute to one as an author by contacting the Frontiers Editorial Office: frontiersin.org/about/contact

ION CHANNELS AND TRANSPORTERS IN CA^{2+} -DEPENDENT FUNCTIONS OF LYMPHOCYTES

Topic Editors:
Péter Béla Hajdu, University of Debrecen, Hungary
Barbara Niemeyer, Saarland University, Germany
Ildikò Szabò, University of Padua, Italy
Heike Wulff, University of California, Davis, United States

Citation: Hajdu, P. B., Niemeyer, B., Szabò, I., Wulff, H., eds. (2022). Ion Channels and Transporters in Ca^{2+} -Dependent Functions of Lymphocytes. Lausanne: Frontiers Media SA. doi: 10.3389/978-2-88976-697-0

Table of Contents

frontiers | Frontiers in Physiology

EDITORIAL
published: 07 July 2022
doi: 10.3389/fphys.2022.962110

Editorial: Ion Channels and Transporters in Ca^{2+} -Dependent Functions of Lymphocytes

Peter Hajdu[1,2]*, *Heike Wulff*[3], *Barbara A. Niemeyer*[4] and *Ildikó Szabó*[5]

[1]Department of Biophysics and Cell Biology, University of Debrecen, Debrecen, Hungary, [2]Department of Dental Biochemistry, Faculty of Dentistry, University of Debrecen, Debrecen, Hungary, [3]Department of Pharmacology, School of Medicine, University of California, Davis, CA, Davis, United States, [4]Department of Molecular Biophysics, Faculty of Medicine, Saarland University, Homburg, Germany, [5]Department of Biology, Faculty of Sciences, University of Padua, Padua, Italy

Keywords: ion channels, ion transporter, lymhocyte, Ca^{2+}- signaling, cancer, autoimmunity, pharmacology

Editorial on the Research Topic

Ion Channels and Transporters in Ca^{2+}-Dependent Functions of Lymphocytes

Ion channels and transporters have been shown to play essential roles in the physiology of lymphocytes since their discovery in the 1980s. Understanding the specific interplay between lymphocyte ion channels and the particular roles of defined ion channels and transporters for immune cells and subtype specific functions is crucial for untangling the pathophysiological mechanisms behind numerous immune system related diseases and may uncover new targets for pharmaceutical intervention.

This special topic, which is jointly issued in Frontiers in Physiology and Frontiers in Pharmacology, contains 8 original research studies and one review article. The articles cover topics ranging from classical pharmacology of ion channels, the effects of excess intracellular Ca^{2+} induced by exercise to the role/expression of various ion channels under pathological conditions, and it is noteworthy, that the included articles report on almost all major ion channels/transporter described in lymphocytes.

Two articles in our collection focus on the role of ion channels and expression level changes in disease. In their study Markakis et al. show increases in functional Kv1.3 expression in T cells from multiple sclerosis (MS) patients, which is more pronounced in patients with secondary progressive MS status (Markakis et al.). Furthermore, the authors also reveal that TASK-2 channels have no influence on the increased K^+ conductance detected in MS patients. In the second article by Gawali et al., we learn about the effect of immune checkpoint therapies on K+ channel function in $CD8^+$ cells: treatment with both anti-PD1 (pembrolizumab) and anti-PD-L1 (atezolizumab) antibodies facilitate the function of KCa3.1 and Kv1.3 in head and neck squamous cell carcinoma patients' peripheral lymphocytes (Gawali et al.). Treatment of $CD8^+$ cells isolated from healthy donors with PD-L1 reduced KCa3.1 activity, an effect that could be attributed to the modulation by PI3 kinase. However, addition of anti-PD1 did not change the expression level of Kv1.3, KCa3.1, and Orai1/STIM1 as determined by flow cytometry.

Three articles report on the pharmacology of lymphocyte ion channels, thus providing insight into therapy development or explaining side effects of clinically used drugs. Loureirin B (LrB), which is a flavonoid extracted from Resina Draconis ("dragon's blood"), was shown to inhibit Kv1.3 channels as well as CRAC channels constituted of STIM1/Orai1 complexes in a concentration-dependent manner (Shi et al.). Moreover, LrB reduces Ca^{2+} influx and IL-2 production in Jurkat T cells. Hence, loureirin B may serve as a template for developing new small molecule inhibitors to treat autoimmune diseases. In a second article, several broadly-used

OPEN ACCESS

Edited and reviewed by:
Christoph Fahlke,
Helmholtz Association of German Research Centres (HZ), Germany

***Correspondence:**
Peter Hajdu
hajdup@med.unideb.hu

Specialty section:
This article was submitted to Membrane Physiology and Membrane Biophysics, a section of the journal Frontiers in Physiology

Received: *05 June 2022*
Accepted: *15 June 2022*
Published: *07 July 2022*

Citation:
Hajdu P, Wulff H, Niemeyer BA and Szabó I (2022) Editorial: Ion Channels and Transporters in Ca^{2+} -Dependent Functions of Lymphocytes. Front. Physiol. 13:962110. doi: 10.3389/fphys.2022.962110

NSAID compounds (naproxen, ibuprofen, salicylate, and aspirin) are shown to inhibit TRPM7 currents (Chokshi et al.). It turned out that these molecules develop use-dependent block slowly and reduce cell viability in a concentration dependent manner, however, they do not bind directly to TRPM7 channels but impair TRPM7 function via acidification of the cytosolic compartment. A specific mutation within TRPM7 (S1170R) renders the channel resistant to intracellular pH changes, Mg^{2+} and PIP_2 and, indeed, is resistant to NSAID application. The pH-change induced inhibition did not require activity of cyclooxygenase enzymes, another well-known target of NSAIDs. In the final article of this set, Naseem et al. describe a new expression system suitable for production of peptide toxins with a high yield and purity (three-fold higher as compared to other systems) (Naseem et al.). As these toxins often are very specific inhibitors of subtype specific ion channels, the more technical paper is of interest to scientists studying the role of ion channels for immune cell pathologies. The authors chose margatoxin (MgTx), which is a high affinity antagonist of Kv1.2 and Kv1.3 and produced the toxin in *Pichia pastoris* (a methylotrophic yeast species) in a tagged (TrMgTx, with 6xHis tag) and an untagged (UrMgTx) version. Both variants had an inhibitory effect comparable to wild-type MgTx, and they could show that toxins were able to inhibit the expression of early activation markers (IL2 receptor or CD25 and CD40L or CD154) in $CD4^+$ effector memory T cells. The *Pichia pastoris* expression system proves to be efficient tool in generating cysteine rich small peptides such as recombinant toxins applied in study of ion channels function and expression.

Another set of three articles was devoted to aspects of Ca^{2+} signaling in T cells. Much recent interest focusses on the role of mitochondrial Ca^{2+} handling. Wu et al. report on the role of the mitochondrial Ca^{2+} uniporter (MCU), which is one pathway for Ca^{2+} uptake into mitochondria for various T cell functions (Wu et al.). Using mice with T cell-specific genetic elimination of MCU, the authors conclude that lack of MCU has no influence on the respiratory chain activity, T cell differentiation or effector functions in both regulatory and inflammatory T cell populations *in vitro*. *In vivo,* mouse model experiments demonstrate that MCU also does not appear to play a significant role: not for the development of T-cell mediated autoimmunity and not for immune responses against viral infections. These results draw attention to the fact that compensatory mechanisms may override effects of genetic ablation of MCU as well as suggest that antagonists used in other studies might not be specific towards MCU. In the paper by Liu et al. the effects of exercise (running in/on treadmill) on Ca^{2+} levels in T cells was reported: basal resting cytosolic Ca^{2+}-concentrations as well as agonist-induced Ca^{2+}-responses in cells isolated 3 h (E3 group) after workout were higher as compared to the 0 h (E0 group) and 24 h (E24 group) groups. In contrast, proliferation rates in the E3 group were lower relative to the other groups (Liu et al.). Transcriptional levels of SERCA, PMCA, TRPC1 and P2X7 are downregulated in E3 T cells, while IP_3R2 and RyR2 expression levels are up-regulated: these changes could account for the increased cytosolic Ca^{2+} level of E3 T cells. However, the suppressed, mitogen-induced proliferation of E3 cells contradicts data obtained for Ca^{2+} levels in the E3 group cells and suggests that different pathway are responsible for exercise-related immune-suppression. Finally, a study on various lymphoma cell lines and primary lymphoma cells (DLBCL: diffuse large B cell lymphoma) analyzed expression of several Ca_V channel genes as well as the Orai-STIM-ORAI gene set (Stanwood et al.). Cav1.2 expression was higher in classical Hodgkin lymphoma (CHL) cell lines as compared to other B cell lymphoma cell lines, while STIM2-Orai2-levels were decreased. Activated B cell like DLBCL (ABC-DLBCL) cells had higher levels of $Ca_V1.3$, while $Ca_V1.1$, $Ca_V1.2$ and $Ca_V1.4$ were reduced in comparison to germinal center DLCBL cells, and no difference in STIM-ORAI expression was reported. Other proteins related to the Ca^{2+}-regulated activation pathway (NFAT, calcineurin, calmodulin) displayed elevated expression in CHL cell lines with respect to other B lymphoma cell lines. In contrast, the calmodulin and Ca^{2+}-dependent pathway was downregulated in ABC-DLBCL patient cells. A recent study reported that Ca_V channel transcripts lacking huge parts of 5' exons were present in T cells, which probably transcribes their mRNA into non-functional truncated Ca_V proteins: no Ca^{2+} channels were detected by electrophysiology tools (patch–clamp, Ca^{2+}-imaging) (Erdogmus et al., 2022). The situation may be the same for B cells, hence, functional studies are required to clarify role of Ca_V in B lymphocytes and lymphoma cells.

Last, but not least, a review by Bohmwald et al. described the role of Ca^{2+}-signaling in viral infection and showcases how viruses highjack host cell Ca^{2+} channels to facilitate both their entry into cells as well as their replication and budding capacity (Bohmwald et al.). The authors summarize the data on ion channels expressed in B and T lymphocytes, and selected viruses (Hepatitis B, SARS-CoV-2, Herpes simplex, hRSV, and HIV), all of which utilize Ca^{2+}-signaling pathways by modifying Ca^{2+} channel function in order to enter cells and/or replicate.

Taken together, this article collection highlights the importance of ion channels and transporters regulating calcium signaling in lymphocytes in health and disease.

AUTHOR CONTRIBUTIONS

PH was invited by Frontiers in Physiology, suggested the title of this special issue and invited IS, BN, and HW as co-editors. The Editorial was written by PH, HW, and BN with comments from IS.

REFERENCE

Erdogmus, S., Concepcion, A. R., Yamashita, M., Sidhu, I., Tao, A. Y., Li, W., et al. (2022). Cavβ1 Regulates T Cell Expansion and Apoptosis Independently of Voltage-Gated Ca^{2+} Channel Function. *Nat. Commun.* 13 (1), 2033. doi:10.1038/S41467-022-29725-3

Conflict of Interest: The authors declare that the research was conducted in the absence of any commercial or financial relationships that could be construed as a potential conflict of interest.

Publisher's Note: All claims expressed in this article are solely those of the authors and do not necessarily represent those of their affiliated organizations, or those of the publisher, the editors and the reviewers. Any product that may be evaluated in this article, or claim that may be made by its manufacturer, is not guaranteed or endorsed by the publisher.

frontiers in Pharmacology

ORIGINAL RESEARCH
published: 25 June 2021
doi: 10.3389/fphar.2021.685092

Loureirin B Exerts its Immunosuppressive Effects by Inhibiting STIM1/Orai1 and K_V1.3 Channels

*Shujuan Shi[1†], Qianru Zhao[1†], Caihua Ke[1], Siru Long[1], Feng Zhang[1], Xu Zhang[1], Yi Li[1], Xinqiao Liu[1], Hongzhen Hu[2] and Shijin Yin[1]**

[1]Department of Chemical Biology, School of Pharmaceutical Sciences, South-Central University for Nationalities, Wuhan, China, [2]Department of Anesthesiology, the Center for the Study of Itch & Sensory Disorders, Washington University School of Medicine, St. Louis, MO, United States

Loureirin B (LrB) is a constituent extracted from traditional Chinese medicine Resina Draconis. It has broad biological functions and an impressive immunosuppressive effect that has been supported by numerous studies. However, the molecular mechanisms underlying Loureirin B-induced immune suppression are not fully understood. We previously reported that Loureirin B inhibited K_V1.3 channel, calcium ion (Ca^{2+}) influx, and interleukin-2 (IL-2) secretion in Jurkat T cells. In this study, we applied CRISPR/Cas9 to edit K_V1.3 coding gene KCNA3 and successfully generated a K_V1.3 knockout (KO) cell model to determine whether K_V1.3 KO was sufficient to block the Loureirin B-induced immunosuppressive effect. Surprisingly, we showed that Loureirin B could still inhibit Ca^{2+} influx and IL-2 secretion in the Jurkat T cells in the absence of K_V1.3 although KO K_V1.3 reduced about 50% of Ca^{2+} influx and 90% IL-2 secretion compared with that in the wild type cells. Further experiments showed that Loureirin B directly inhibited STIM1/Orai1 channel in a dose-dependent manner. Our results suggest that Loureirin B inhibits Ca^{2+} influx and IL-2 secretion in Jurkat T cells by inhibiting both K_V1.3 and STIM1/Orai1 channels. These studies also revealed an additional molecular target for Loureirin B-induced immunosuppressive effect, which makes it a promising leading compound for treating autoimmune diseases.

Keywords: LrB, Kv1.3, Jurkat T cell, CRISPR/ Cas9, STIM1/Orai1, Ca^{2+} influx, IL-2

OPEN ACCESS

Edited by:
Barbara Niemeyer, Saarland University, Germany

Reviewed by:
Olivier DELLIS, Institut National de la Santé et de la Recherche Médicale (INSERM), France
Martin Vaeth, Julius-Maximilians-Universität, Germany

****Correspondence:***
Shijin Yin
yinshijinyf@163.com

†These authors have contributed equally to this work

Received: *24 March 2021*
Accepted: *11 May 2021*
Published: *25 June 2021*

Citation:
Shi S, Zhao Q, Ke C, Long S, Zhang F, Zhang X, Li Y, Liu X, Hu H and Yin S (2021) Loureirin B Exerts its Immunosuppressive Effects by Inhibiting STIM1/Orai1 and K_V1.3 Channels. Front. Pharmacol. 12:685092. doi: 10.3389/fphar.2021.685092

INTRODUCTION

Loureirin B (LrB) is a Resina Draconis (RD)-derived flavonoid and a traditional Chinese medicine bearing multifaceted effects on numerous diseases (Fan et al., 2014; Bai et al., 2015). LrB was reported to be a plasminogen activator inhibitor-1 (PAI-1) that promoted blood circulation and reduced the size of arterial thrombus (Jiang et al., 2017). LrB alone or combined with other RD constituents inhibited voltage-gated sodium (Na_V) channel, transient receptor potential vanilloid 1 channel, and acid-sensing ion channel in dorsal root ganglion (DRG) neurons and ameliorated inflammatory pain (Chen et al., 2018; Wan et al., 2019). Besides its analgesic effect, LrB and RD also possess promising immunosuppressive effects. The ethylacetated RD inhibited inflammatory responses in vascular smooth muscle cells and macrophages by suppressing ROS production (Heo et al., 2010). A recent study showed that LrB could reduce the severity of inflammation in Crohn's disease *via* inhibiting the expression levels of inflammatory cytokines interleukin-1 (IL-1), IL-6, and tumor necrosis

factor-alpha (TNF-α) (Sun et al., 2020). However, the mechanisms behind LrB-induced immune suppression have not been fully elucidated.

Ion channels are critically involved in regulating proliferation and apoptosis of lymphocytes (Cahalan and Chandy, 2009). Calcium signaling plays a pivotal role in linking ion channels and numerous functions of T lymphocytes (Feske et al., 2015). When an antigen stimulates a T cell and binds to a T cell receptor (TCR), the downstream phospholipase C gamma (PLCγ) will hydrolyze PIP_2 into DAG and inositol triphosphate (IP_3) (Zhong et al., 2016; Zhu et al., 2017). The newly synthesized IP_3 binds to IP_3 receptor (IP_3R) on endoplasmic reticulum (ER) membrane and depletes calcium ion (Ca^{2+}) stored in ER pool (Zhong et al., 2016; Cao et al., 2019). Another ER membrane protein - stromal interaction molecule (STIM) - could sense Ca^{2+} depletion in ER and change its own conformation to contact and subsequently open a Ca^{2+} channel - Orai channel on the plasma membrane (Lewis, 2020). This process is named Store-operated Calcium Entry (SOCE) and results in Ca^{2+} influx which ultimately activates the downstream signaling pathways such as CaM-CaN-NFATc1 and NFκB to produce inflammatory cytokines (Feske et al., 2012; Trebak and Kinet, 2019). During these processes, the STIM1/Orai1 complex - also called calcium release-activated calcium (CRAC) channel - is the "major player" to trigger immune responses of T cells, while other ion channels, such as potassium ion (K^+) channel, could modulate calcium signals by changing the membrane potential of T cells and providing a driving force for Ca^{2+} entry (Cahalan and Chandy, 2009).

$K_V1.3$ is a predominantly expressed K^+ channel in T cells (Nicolaou et al., 2009) and regulates immune responses stimulated by antigens and cell volume of T cells (Nicolaou et al., 2009; Bobak et al., 2011). Pharmacological blockade of $K_V1.3$ in myelin basic protein - specific encephalitogenic T cell line inhibited cytokine secretion through reducing Ca^{2+} influx, which improved encephalomyelitis (EAE) symptoms in rats (Beeton et al., 2001). $K_V1.3$ blockade also suppressed the activation and motility of T_{EM} (memory effector T) cells and delayed-type hypersensitivity in rats (Matheu et al., 2008). Surprisingly, although $K_V1.3$ plays an important role in T cells, $K_V1.3$ knockout (KO) mice lived normally and their immune systems showed no impairment (Koni et al., 2003). The expression level of chloride ion (Cl^-) channels was found to have increased 10-fold in T lymphocytes from these KO animals, which could compensate for the function of $K_V1.3$ to sustain a normal membrane potential and did not affect proliferation or activation of T cells (Koni et al., 2003). Another report studied the effects of $K_V1.3$ deletion in the EAE model and found that the number of activated $CD4^+$ T cells and secretion of IFN-γ and IL-17 in $K_V1.3$ KO mice were all decreased significantly (Gocke et al., 2012). A recent study showed that T helper (Th) cells isolated from the $K_V1.3$ KO mice developed into a novel type of Th cell which differed in gene expression and functions compared with Th cell in wild type animals when stimulated with Myelin oligodendrocyte glycoprotein (MOG) (Grishkan et al., 2015). These inconsistent results in $K_V1.3$ KO mice suggest that selective $K_V1.3$ deletion in specific lymphocyte type might help to pinpoint the mechanisms underlying $K_V1.3$-mediated regulation of immune responses in healthy or pathological organisms.

We previously used Jurkat T cell as a model to study the effects of LrB and reported that LrB inhibited $K_V1.3$ currents, Ca^{2+} influx, and IL-2 release in a dose-dependent manner (Yin et al., 2014). In this study, we applied CRISPR/Cas9 system to knock out KCNA3 gene to explore whether $K_V1.3$ deletion could block effects of LrB on Ca^{2+} influx and cytokine secretion. We showed that KO $K_V1.3$ in Jurkat T cell decreased but did not abolish the effects of LrB on Ca^{2+} influx and IL-2 secretion. We further demonstrated that LrB could decrease Ca^{2+} influx and IL-2 secretion through inhibiting STIM1/Orai1 channels in the absence of $K_V1.3$. These findings suggest that LrB has an immunosuppressive effect by inhibiting both $K_V1.3$ and STIM1/Orai1 channels.

MATERIALS AND METHODS

Drugs

LrB was synthesized by our group (**Supplementary Scheme S1**) and dissolved in DMSO. $K_V1.3$ inhibitor ADWX-1 was purchased from More Biotechnology Co. Ltd. (Cat. MPK-001A, Wuhan, China) and dissolved in double-distilled water. Agonist of T cell - Concanavalin A (ConA) was purchased from MP Biomedicals (Cat. 195,283, Santa Ana, CA, United States) and dissolved in 1x Phosphate Buffer Saline (PBS). Calcium-ATPase inhibitor Cyclopiazonic Acid (CPA) was purchased from Sigma-Aldrich (Cat. C1530, St.Louis, MO, United States) and dissolved in DMSO. SK_{Ca} inhibitor Scytx was purchased from More Biotechnology Co. Ltd. (Cat. MPK-001C, Wuhan, China).

Cell Culture

Jurkat T cell line was bought from National Platform of Cell Line Resource for Sci-Tech (Wuhan, China). Wild type and $K_V1.3$ knockout Jurkat T cells were suspended in culture medium which consisted of Roswell Park Memorial Institute (RPMI) 1,640 basic (Cat. C11875500, Gibco, NY, United States) supplemented with 10% fetal bovine serum (FBS) (Cat. 40130ES76, YESEN, Shanghai, China) and 1% Penicillin-Streptomycin (Cat. 15070063, Gibco, NY, United States). Cell density was counted using Cellometer K2 (Nexcelom, San Diego, CA, United States) and suspended cells were seeded in 6-well plate with 1×10^6 cells/well in 2 ml culture medium under 5% CO_2 and 37°C. After being pretreated with 0.01, 0.1, or 1 μM LrB for 1 h, 10 μg/ml ConA was added in the culture medium as stimulus group, and the same volume of 1x PBS was added in control group. After incubating with ConA or PBS for 24 h, the culture medium was harvested in Eppendorf (Ep) tube for ELISA assay (Cat. DY202-05, R&D, Minneapolis, MN, United States) to test IL-2 secretion by Jurkat T cells with or without ConA stimulation.

sgRNA Design and Plasmid Construct

sgRNA was designed to target the first exon (exon1) of KCNA3 gene, which consists of the functional domain of $K_V1.3$ subunit. The target DNA sequence was submitted to http://crispr.mit.edu/ website and two sgRNA sequences with the highest editing efficiency scores were selected and synthesized by Tskingke Company (Peking, China). Sequences of DNA fragments expressing sgRNAs CTACCCCGCCTCGACGTCGC (sgRNA1) and GAGATCCGCTTCTACCAGCT (sgRNA2) are used in our study (**Supplementary Figures S1A,B**). The pX458 plasmid is a gift from Lu Xue lab (School of Life Sciences, Central-South University for Nationalities, Wuhan, China) and used to express SpCas9 and sgRNA simultaneously to edit the target genes. This plasmid expresses GFP as a fluorescence reporter to indicate vector transfection of the cells. The plasmid was digested with Fast Digest BbsI enzyme (Cat. ER1011, Thermo Scientific, Waltham, MA, United States) and linked with synthesized sgRNA fragments by T4 ligase (Cat. D2011A, Kyoto, Takara, Japan). The sgRNA sequence insertion in plasmid was confirmed by gene sequencing (**Supplementary Figure S1A,B**).

Electroporation and Cell Sorting

Cultured Jurkat T cells were transfected with the constructed plasmids using a CTX-1500A EX Electroporator (Celetrix Biotechnologies, Manassas, VA, United States). Cultured Jurkat T cells were suspended into single cells and sorted with Fluorescence Activated Cell Sorter (FACS) (MA900, Sony, Tokyo, Japan) 48 h after transfection. The single cells expressing GFP were selected and seeded in a 96-well plate and passed to a 24-well and then a 6-well plate to amplify the single colony. Genomes and proteins were extracted from each colony for confirmation of $K_V1.3$ KO.

Confirmation of Gene Editing Efficiency

Before cell sorting by FACS, Jurkat T cells transfected with the constructed plasmids were tested for editing efficiency first. Genomes in different groups were extracted using Genome Extraction kit (Cat. 7E491E0, Vazyme, Suzhou, China) and the target sequence was amplified with Polymerase Chain Reaction (PCR) from the genome. The PCR primers were FP: GTCATC AACATCTCCGGGCT, RP: TACTCGAAGAGCAGCCACAC. Products of PCR were used for T7EN1 digestion and DNA gel first. Gray analysis of the digested fragments compared with the whole quantities of the PCR products was used to calculate the editing efficiency of CRISPR/Cas9. After we obtained the single cell colony, the target sequence was amplified with PCR and ligated into commercial pMD™19 T vector (Cat. 6,013, Kyoto, Takara, Japan) to check the mutation of each single colony edited by PX458-sgRNA1 or PX458-sgRNA2.

Western Blot

Cultured cells were collected by centrifugation at 6,000 rpm for 5 min and washed with ice cold 1x PBS twice. Cells were lysed with Radio Immunoprecipitation Assay (RIPA) solution (Cat. P0013B, Beyotime, Peking, China) for 30 min. The lysis solution was centrifuged again at 12,000 rpm under 4°C for 15 min and the supernatant was collected and mixed with 2x Sodium dodecyl sulfate (SDS) loading buffer and boiled for 5 min. Before loading, the total protein concentration of each group was determined by BCA kit and scanned with a microplate photospectrometer (SPARK 10M, Tecan, Hombrechtikon, Swiss). Proteins were loaded based on the total protein concentration of each group to assure equal quantities per lane. Proteins were separated on a 10% SDS-polyacrylamide gel and transferred to Polyvinylidene fluoride (PVDF) membranes (Millipore, Billerica, MA). The membranes were blocked with 10% nonfat milk and incubated at 4°C overnight with the following antibodies: rabbit polyclonal antibody against $K_V1.3$ (1:1,000, Cat. APC101; alomone labs, Jerusalem, Israel) and rabbit polyclonal antibody against β-actin (1:1,000, Cat. AC006; Abclonal, Boston, United States). After washing in Tris-Buffered Saline (TBS) with 0.3% Tween three times for 45 min, the membranes were incubated with HRP-conjugated goat anti-rabbit IgG (1:10,000, Cat. AS014; Abclonal, Boston, United States) for 2 h at room temperature. Chemiluminescent signals were generated using a Super Signal West Pico trial kit (Pierce Protein Biology, Thermo Fisher Scientific, Waltham, MA, United States) and detected using the ChemiDoc XRS System (Bio-Rad, Hercules, CA, United States). Image Lab software (Bio-Rad, Hercules, CA, United States) was used for background subtraction and quantification of immunoblotting data.

Electrophysiology Recording

Whole-cell patch-clamp recordings were performed using an EPC9 amplifier (HEKA Elektronik, Lambre-cht/Pfalz, Germany) at room temperature (22–24°C). Pipettes pulled from borosilicate glass (Cat. BF 150-86-10, Sutter Instrument Co., Novato, CA, United States) had resistances of 2–4 MΩ when filled with the internal solution. The internal pipette solution for recording voltage-gated potassium (K_V) currents contained KCl 140 mM, $MgCl_2$ 1 mM, EGTA 1 mM, Na_2ATP 3 mM, and HEPES 10 mM (pH 7.3 with KOH). For recording CRAC, currents contained Cs Methanesulfonate 120 mM, $MgCl_2$ 10 mM, EGTA 4 mM, $CaCl_2$ 2 mM, and HEPES 10 mM (pH 7.3 with CsOH). The formula of internal pipette solution for recording small conductance Ca^{2+}-activated K^+ channels (SK_{Ca}) currents was calculated by Winmaxc software to guarantee that the concentration of free Ca^{2+} in cytoplasm was kept at 2 μM and contained KCl 140 mM, HEPES 10 mM, HEDTA 5 mM, and $CaCl_2$ 2 mM (pH 7.2 with KOH). The external solution for recording K_V currents contained KCl 5 mM, NaCl 140 mM, HEPES 10 mM, $CaCl_2$ 2 mM, $MgCl_2$ 1 mM, and D-Glucose 10 mM (pH 7.4 with NaOH). For recording CRAC currents, the external solution contained NaCl or NaGlu 140 mM, KCl 5 mM, HEPES 10 mM, or $CaCl_2$ 2.5 mM (pH 7.3 with NaOH). For recording SK_{Ca} currents the external solution contained KCl 140 mM, $MgCl_2$ 1 mM, Glucose 10 mM, $CaCl_2$ 2 mM, and HEPES 10 mM (pH 7.4 with KOH). K_V currents were elicited by +50 mV, 400 ms depolarizing pulse from the holding potential of −60 mV every 20 s. CRAC currents were elicited by +10 mV, 100 ms depolarizing ramp from the holding potential of -60 mV every 10 s, and SK_{Ca} currents were elicited by from −100 mV to +100 mV for 200 ms depolarizing ramp from the holding potential of 0 mV every 10 s. Using IGOR (WaveMetrics, Lake

Oswego, OR, United States) software, concentration–response relationships were fitted according to modified Hill equation: $I_{toxin}/I_{control} = 1/1 + ([drug]/IC_{50})$, where I is the steady-state current and [drug] is the concentration of LrB. The parameter to be fitted was concentration of half-maximal effect (IC_{50}).

IL-2 Secretion

IL-2 secretion from Jurkat T cells was measured using an ELISA kit (Cat. DY202-05, R&D System, Minneapolis, MN, United States) following manufacturer's instructions. The goodness of fit for the ELISA kit was between 10 pg/ml to 1,000 pg/ml. Cells were centrifuged at 1,500 rpm for 10 min, and the supernatants were collected to measure IL-2 concentrations. Reactions were performed in 96-well plates coated with the capture antibody and stopped with 1 M phosphoric acid. Absorbance was measured at 450 nm. Each experiment was repeated at least three times in duplicate.

Calcium Imaging

Jurkat T cells were loaded with 4 μM Fura-2 AM (Cat.40702ES50, YEASEN, Shanghai, China) for 60 min at 37 °C. Cells were then washed three times and incubated in Hank's Balanced Salt Solution (HBSS) for 30 min at room temperature before use. Fluorescence at 340 and 380 nm excitation wavelengths was recorded on an inverted Nikon Ts2R microscope (Tokyo, Japan) equipped with 340, 360, and 380 nm excitation filter wheels using NIS-Elements imaging software (Nikon). 510 nm Fura-2 emission fluorescence ratios (F340/F380) reflect changes in intracellular Ca^{2+} concentration ($[Ca^{2+}]_i$) upon stimulation. Data were obtained from 100 to 250 cells in time-lapse images from each coverslip. To make sure that Fura-2 loading was the same in individual cells, we selected the cells with the same baseline level of fluorescence intensity at the beginning of the calcium imaging experiment.

Statistics Analysis

All data are presented as mean ± SEM for independent observations. Statistical analysis of differences between groups was carried out using one-way ANOVA combined with Turkey's post-hoc test. $p < 0.05$ was considered significantly different.

RESULTS

CRISPR/Cas9-Mediated $K_V1.3$ Knockout in Jurkat T Cells

We constructed the pX458-sgRNA1 and pX458-sgRNA2 plasmids to express Cas9 and sgRNA simultaneously and confirmed the insertion of sgRNA with sequencing (**Supplementary Figure S1A,B**). The Jurkat T cells were transfected by electroporation with the constructed plasmids that also express GFP as a reporter (**Supplementary Figure S1C**). The target sequence was amplified with PCR and digested by T7EN1 enzyme to confirm editing efficacy. If the target sequence had been edited by CRISPR/Cas9, the hybridized double strand DNA would be mismatched and form a neck and ring structure. T7EN1 enzyme could recognize the mismatched DNA structure and cut it into small fragments. DNA gel of the digestion products showed that the control group only had one single band, which is consistent with the molecular weight of the target sequence, while sgRNA1 and the sgRNA2 editing groups both had bands smaller than the target sequence. These bands matched the fragments cut by T7EN1 (**Supplementary Figure S1D**). The editing efficiencies of sgRNA1 and sgRNA2 calculated according to the gray analysis of T7EN1 digestion were 25 and 34%, respectively.

To obtain the KCNA3 knock out Jurkat T cell, we used FACS to select GFP-expressing cells which had been transfected with pX458-sgRNA plasmid and edited by CRISPR/Cas9 system. Single cells were then seeded in a 96-well plate and cultured for colony expansion. Proliferated cells were harvested and lysed with RIPA solution to extract proteins to examine the expression of $K_V1.3$ using Western Blot. We found that cell colonies edited either by sgRNA1 or sgRNA2 expressed much less $K_V1.3$ than the control group (**Figure 1A**). $K_V1.3$ expression in the colony edited by sgRNA2 was lower than that by sgRNA1, and almost completely knocked out by CRISPR/Cas9 editing (**Figure 1A**). We therefore used the sgRNA2-edited cells for further experiments.

The genome of sgRNA2-edited cells was extracted and the target sequence of $K_V1.3$ was amplified with PCR. The PCR product was sequenced and nucleotide deletion started around the recognition site of sgRNA, which indicates Indel mutations from this site. To further confirm the mutation of the targeted sequence, the PCR fragments were ligated into pMD™19 T vector and sequenced again. We found that one cell colony (KO-1) lost one bp (**Figures 1C,F**) compared with the wild type group (**Figures 1B,F**). Another cell colony (KO-2) lost four and five bp (**Figures 1D–F**), respectively. We compared the sequences of KO-1 and KO-2 with wild type sequence and confirmed that these two colonies both had frameshift mutations starting from the sgRNA guided site and changed the open reading frame of KCNA3, thus changing the normal $K_V1.3$ translation.

$K_V1.3$ Current Elimination in Jurkat T Cell After CRISPR/Cas9 Editing

After confirmation of KCNA3 editing efficiency and $K_V1.3$ expression deletion, we studied the electrophysiology properties of the $K_V1.3$ KO cells and compared the changes in membrane currents with wild type cells. Previous studies showed that $K_V1.3$ and type II SK_{Ca} ($K_{Ca}2.2$) channels were the two main types of K^+ channels expressed in Jurkat T (Cahalan and Chandy, 2009; Valle-Reyes et al., 2018). To determine whether KO $K_V1.3$ eliminates the function of $K_V1.3$ in Jurkat T cell, we used whole-cell patch-clamp recording to measure K^+ currents in Jurkat T cells. The holding potential was set as −60mV and depolarized to +50 mV for 400 ms and a Ca^{2+}-free external solution with added tetrodotoxin (TTX) to block Na_V currents was used to record K^+ currents. A large outward current was recorded in wild type Jurkat T cells, which was blocked by the $K_V1.3$ inhibitor ADWX-1 (**Figure 1G**). The outward current amplitude was much smaller in the $K_V1.3$ KO Jurkat T cells and was resistant to 10 nM ADWX-1 (**Figure 1H**), suggesting that

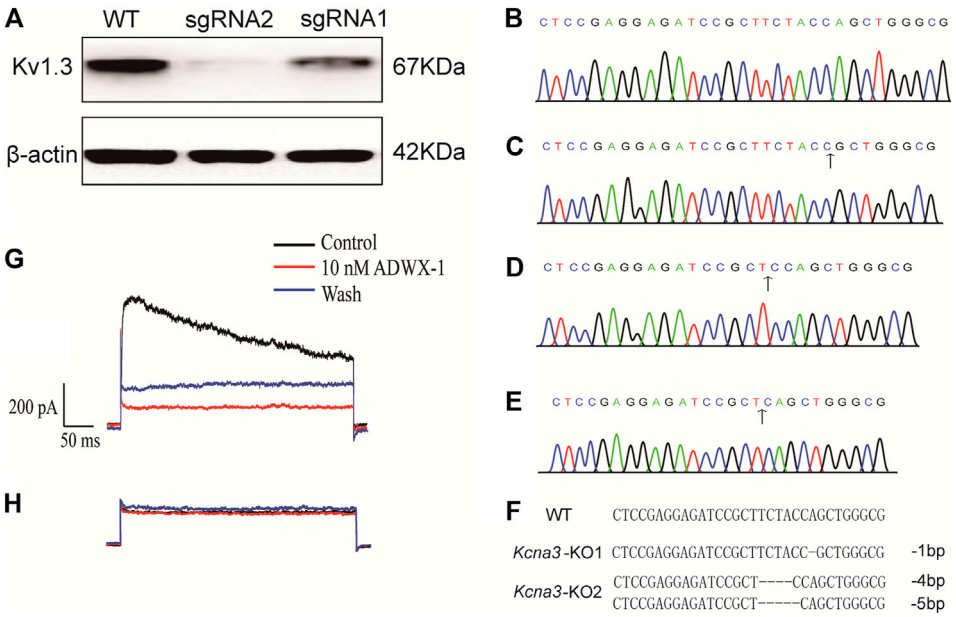

FIGURE 1 | Confirmation of Kv1.3 KO in Jurkat T cells. **(A)** Western Blot for K_V1.3 expression in wild type and Kv1.3 KO cells (n = 3); **(B)** Sequencing of target gene in wild type Jurkat T cells; **(C)** Sequencing of target gene in KO-1 colony which has one bp nucleotide loss compared with wild type, the black arrow indicates the start point of CRISPR/Cas9 editing; **(D,E)** KO-2 colony has four and five bp nucleotide loss respectively, the black arrow indicates the start point of CRISPR/Cas9 editing; **(F)** Alignment of the wild type, KO-1 and KO-2 Jurkat T cell colonies; **(G)** Membrane current of a wild type Jurkat T cell was irreversibly inhibited by 10 nM ADWX-1 (n = 3); **(H)** Membrane current of a Kv1.3 knockout Jurkat T cell was nearly abolished and the remaining residual current was not further inhibited by ADWX-1 (n = 3).

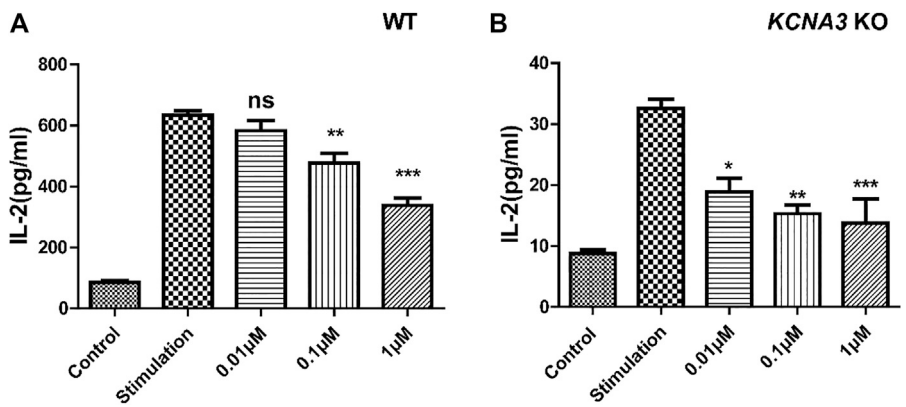

FIGURE 2 | Effects of Kv1.3 KO on IL-2 secretion. **(A)** Changes of IL-2 secretion in wild type Jurkat T cells under control, ConA stimulation, and LrB treatment with different concentrations (n = 5); **(B)** Changes of IL-2 secretion in the Kv1.3 KO Jurkat T cells under control, ConA stimulation, and LrB treatment with different concentrations (n = 5). Data were presented as mean ± SEM. Statistical analysis of differences between groups was carried out using one-way ANOVA combined with Turkey's post-hoc test. ***, p < 0.001.

Jurkat T cells edited by CRISPR/Cas9 system completely lost K_V1.3 conducted current.

LrB-Induced Inhibiton of IL-2 Secretion in Jurkat T Cells

Concanavalin A (ConA) is a phytohemagglutinin activating T cells and increasing K_V1.3 expression on T cell membrane (Yin et al., 2014; Yabuuchi et al., 2017). ConA also induced IL-2 release through a Ca^{2+}-dependent pathway in Jurkat T cells (Sharma et al., 2019). We therefore used ConA as a cytokine stimulant. The control group and K_V1.3 KO Jurkat T cells under the same culture conditions were pretreated with 0.01, 0.1, or 1 μM LrB separately for 1 h, then 10 ug/mL ConA was added in the culture medium to activate Jurkat T cells. 24 h after ConA incubation, the supernatant of culture medium was collected and tested for IL-2 concentration using an ELISA kit. The quantity of IL-2 secreted by the K_V1.3 KO

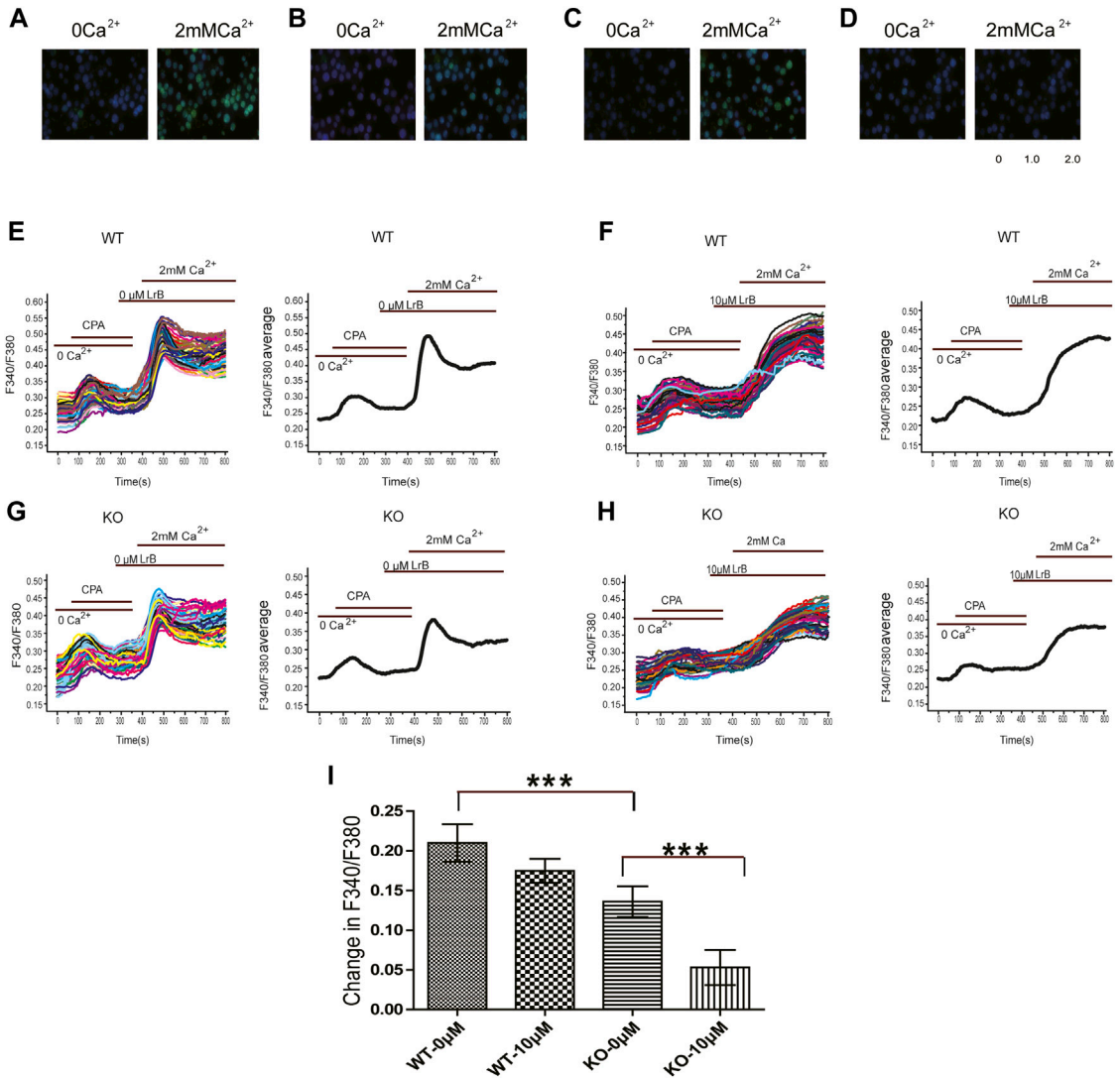

FIGURE 3 | Effects of LrB on $[Ca^{2+}]_i$ in Jurkat T cells. **(A)** $[Ca^{2+}]_i$ responses of wild type Jurkat T cells before **(left)** and after **(right)** 2 mM Ca^{2+}perfusion; **(B)** $[Ca^{2+}]_i$ responses of wild type Jurkat T cells pretreated with 10 μM LrB before **(left)** and after **(right)** 2 mM Ca^{2+}perfusion; **(C)** $[Ca^{2+}]_i$ responses of the Kv1.3 KO Jurkat T cells before **(left)** and after **(right)** 2 mM Ca^{2+}perfusion; **(D)** $[Ca^{2+}]_i$ responses of the Kv1.3 KO Jurkat T cells pretreated with 10 μM LrB before **(left)** and after **(right)** 2 mM Ca^{2+}perfusion; **(E,F)** Representative traces of F340/F380 ratio show $[Ca^{2+}]_i$ in wild type Jurkat T cells treated with and without LrB; the first small peak was caused by 10 μM CPA depletion of ER Ca^{2+}store, the second peak was caused by 2 mM Ca^{2+}perfusion; **(G,H)**. Representative traces of F340/F380 ratio in the Kv1.3 KO Jurkat T cells treated with and without LrB; **(I)** Statistic analysis of changes in F340/F380 in the wild type and Kv1.3 KO cells after 2 mM Ca^{2+}perfusion between control and LrB treatment groups (n = 3, 100–250 cells were selected each batch). Data were presented as mean ± SEM. Statistical analysis of differences between groups was carried out using one-way ANOVA combined with Turkey's post-hoc test. ***, $p < 0.001$.

group (8.73 ± 0.66 pg/ml) without any treatment was 10-fold lower compared with the wild type group (85.00 ± 6.46 pg/ml) (**Figures 2A,B**). Surprisingly, LrB in a relatively low concentration still significantly inhibited IL-2 secretion although most IL-2 release was blocked by KO $K_V1.3$ (**Figure 2B**). Moreover, the inhibitory effect of LrB on IL-2 secretion in the wild type Jurkat T cells was dose-dependent ($p < 0.001$) in both wild type and $K_V1.3$ KO cells treated with 0.01, 0.1, or 1 μM LrB. Therefore, LrB could inhibit IL-2 release in the absence of $K_V1.3$.

Decreased Ca^{2+} Influx in $K_V1.3$ KO Jurkat T Cells

$K_V1.3$ conducts an outward K current and hyperpolarizes the membrane potential, which provides a driving force for Ca^{2+} influx (Chandy et al., 2004; Nicolaou et al., 2009) to maintain T cell Ca^{2+} homeostasis (Nicolaou et al., 2009; Trebak and Kinet, 2019). Our results showed that LrB reduced IL-2 secretion in the absence of $K_V1.3$ KO in Jurkat T cells, which suggests that LrB might be able to directly regulate intracellular Ca^{2+} concentration ($[Ca^{2+}]_i$) in Jurkat T cells. To test this possibility, we examined

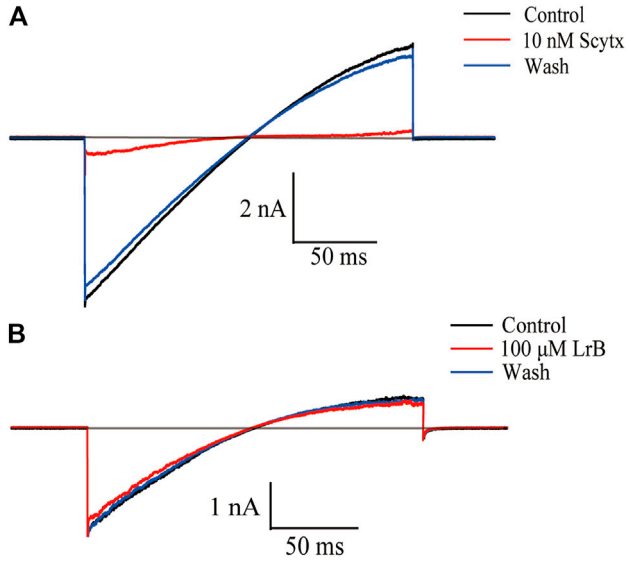

FIGURE 4 | Effects of LrB on SK_{Ca} currents. **(A)** Representative whole-cell currents recorded in $K_{Ca}2.2$ expressing HEK293T cells with or without the treatment of 10 nM Scytx. Black trace represents the baseline control current, red trace represents the currents recorded after Scytx treatment, and the blue trace is the current under external solution washing off Scytx. (*n* = 5). **(B)** Representative whole-cell currents recorded in $K_{Ca}2.2$ expressing HEK293 T cells with and without the treatment of 100 μM LrB. Black trace represents the baseline control current, red trace represents the currents recorded after LrB treatment, and the blue one is the current under external solution washing off LrB (*n* = 5).

whether LrB affects $[Ca^{2+}]_i$ after Ca^{2+} stored in ER was depleted by the Ca^{2+}-ATPase inhibitor CPA. After CPA exhausts Ca^{2+} in ER, CRAC channel will sense the Ca^{2+} depletion and mediate Ca^{2+} influx (Hoth and Penner, 1992; McCarl et al., 2010). We incubated the cells with 0 Ca^{2+} HBSS first and conducted calcium imaging to observe the effects of LrB on $[Ca^{2+}]_i$. 10 μM CPA caused a small instant $[Ca^{2+}]_i$ increase in Jurkat T cells. After CPA treatment for 6 min, perfusion with HBSS adding 2 mM Ca^{2+} led to a large $[Ca^{2+}]_i$ peak followed by a stable plateau (**Figure 3E,G**). Interestingly, the $[Ca^{2+}]_i$ reached a peak but would not go down when the cells were pretreated with 10 μM LrB in both wild type and $K_V1.3$ KO groups (**Figure 3F,H**), which suggests that LrB might block the Ca^{2+} reuptake of the Jurkat T cells. F340/F380 ratio representing $[Ca^{2+}]_i$ of wild type Jurkat T cells was changed by 0.21 ± 0.024 after 2 mM Ca^{2+} perfusion, while in the $K_V1.3$ KO Jurkat T cells it was changed by 0.14 ± 0.019, which is significantly smaller than the wild type group (**Figure 3I**). LrB pretreatment inhibited Ca^{2+} influx induced by 2 mM Ca^{2+}in both the wild type (0.1748 ± 0.015) and $K_V1.3$ KO Jurkat T cells (0.053 ± 0.022) (**Figure 3I**). Although $[Ca^{2+}]_i$ changes in the $K_V1.3$ KO Jurkat T cells were significantly smaller than that in the wild type cells, LrB further reduced the $[Ca^{2+}]_i$ in the $K_V1.3$ KO cells from 0.14 ± 0.019 to 0.053 ± 0.022 (**Figure 3I**). These results suggest that LrB inhibited Ca^{2+} influx in the absence of $K_V1.3$, which is consistent with the results for IL-2 secretion.

Inhibition of STIM1/Orai1 Current by LrB

$K_V1.3$ and $K_{Ca}2.2$ are two main K^+ channels expressed in Jurkat T cells and regulate membrane potential and T cell activation (Grissmer et al., 1992; Desai et al., 2000). To exclude the possibility that LrB affects SK_{Ca} to inhibit IL-2 secretion or Ca^{2+} influx in $K_V1.3$ KO cells, we transfected HEK293 T cells with $K_{Ca}2.2$ plasmids and recorded SK_{Ca} currents with or without LrB treatment. As predicted, 10 nM SK_{Ca} inhibitor Scytx (Wu et al., 2004) nearly blocked the SK_{Ca} currents (**Figure 4A**). In marked contrast, a relatively high concentration (100 μM) of LrB could not inhibit SK_{Ca} currents (**Figure 4B**), suggesting that SK_{Ca} is unlikely the mediator of LrB's inhibition on IL-2 release and Ca^{2+} influx.

Although $K_V1.3$ and $K_{Ca}2.2$ provide the driving force for Ca^{2+} influx, STIM1/Orai1 channel is the "key player" to trigger Ca^{2+} influx after ER depletion and T cell activation (McCarl et al., 2010; Trebak and Kinet, 2019). Since LrB continued to decrease Ca^{2+} influx after $K_V1.3$ knockout and did not inhibit SK_{Ca}, we speculated that LrB might directly inhibit STIM1/Orai1 channel and block Ca^{2+} influx in Jurkat T cells, resulting in immunosuppression. To test this possibility, we transfected the HEK293 T cells with STIM1 and Orai1 plasmids. 24 h after transfection, cells were stimulated with a ramp protocol (depolarizing the cell with a slope from the holding potential −60 to 10 mV) to record STIM1/Orai1 current. Indeed, LrB inhibited the STIM1/Orai1 current in a concentration-dependent manner. Moreover, the inhibition was partly reversed by washing off LrB in the external solution (**Figure 5A**). Statistics analysis with Igor Pro four Hill software showed that LrB inhibited STIM1/Orai1 current with an IC_{50} of 17.11 ± 2.17 μM (**Figure 5B**).

DISCUSSION

In this study, we used Jurkat T cell as a T cell model and applied CRISPR/Cas9 system to KO $K_V1.3$ to study the effects of LrB on Ca^{2+} influx and cytokine release in the absence of $K_V1.3$. We found that although KO $K_V1.3$ reduced IL-2 secretion and Ca^{2+} influx after T cell activation, it did not abolish the inhibitory effect of LrB on IL-2 secretion and Ca^{2+} influx. We further demonstrated that LrB did not affect SKCa channels but directly inhibited the STIM1/Orai1 channel in heterologous cells. Our results suggest that LrB acts on multiple targets in Jurkat T cells to impact cytokine production and release. Recognizing the promiscuous property of LrB-induced inhibition of T cell function should shed new light on its immunosuppressive functions.

$K_V1.3$ and SK_{Ca} channels are two predominant K channels expressed in T lymphocytes (Valle-Reyes et al., 2018; Trebak and Kinet, 2019). Both of them can regulate membrane potential and provide a driving force for Ca^{2+} influx in T cells (Cahalan and Chandy, 2009; Nicolaou et al., 2009), which subsequently modulates proliferation, activation, and apoptosis of T cells (Cahalan and Chandy, 2009; Valle-Reyes et al., 2018). It was reported that $K_V1.3$ joins the immunological synapse (IS) of T cells which contacts with the antigen-presenting cell (APC)

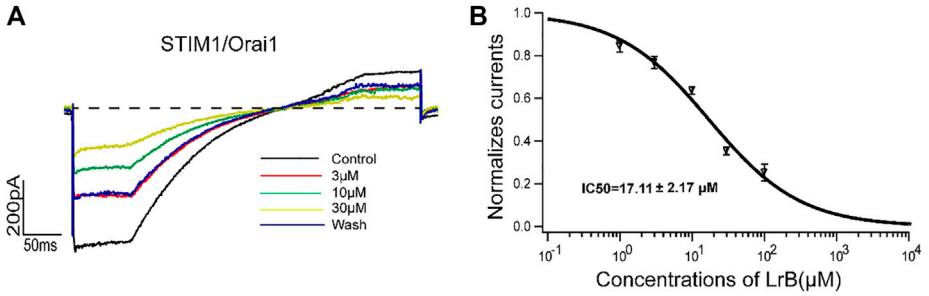

FIGURE 5 | Effects of LrB on STIM1/Orai1 currents. **(A)** Representative whole-cell currents recorded in STIM1/Orai1 expressing HEK293 T cells after treatment with 3, 10, or 30 μM LrB, black trace represents the baseline control current. Red, green, and yellow traces represent the currents recorded after the treatment of 3, 10, and 30 μM LrB, respectively, and the blue trace is the current under external solution washing off LrB. **(B)** Concentration-response curve of LrB inhibition on STIM1/Orai1 currents (IC50 = 17.11 ± 2.17 μM, n = 5, Mean ± SEM).

when the antigens activate TCR (Nicolaou et al., 2007; Nicolaou et al., 2009). The redistribution to IS and function of $K_V1.3$ were disrupted in many immunology diseases such as systemic lupus erythematosus and rheumatic arthritis (Nicolaou et al., 2007). To investigate the mechanisms underlying $K_V1.3$-mediated regulation of immune responses in diseases, numerous studies have used the $K_V1.3$ KO animals, which have greatly extended our knowledge about $K_V1.3$ and its functions in immune system. Initially, $K_V1.3$ KO mice were found to manifest a normal phenotype with unaltered T cell proliferation and activation (Koni et al., 2003). On the other hand, the expression of Cl^- channels in T cells in the absence of $K_V1.3$ was increased 10-fold, which is considered as a compensatory factor for the loss of $K_V1.3$ to sustain the membrane potential of T cell and driving force for Ca^{2+} influx (Koni et al., 2003). Proliferation of $CD4^+$ T cells and secretion of IL-17 and TNF-α were significantly decreased when EAE was induced in the $K_V1.3$ KO animals compared with the wild type group (Gocke et al., 2012). These changes render the Kv1.3 KO mice resistant to EAE and support $K_V1.3$ as a target to treat autoimmune diseases (Gocke et al., 2012). Another study using Th cells isolated from the $K_V1.3$ KO mice expressing MOG-specific TCR (2D2-Kv1.3 KO) demonstrated that Ca^{2+} oscillation and NFATc1 activation in Th cells did not differ between $K_V1.3$ KO and wild type cells after antigen stimulation, but part of the Th cells grew into a novel phenotype which is similar to regulatory T (Treg) cells (Grishkan et al., 2015). Collectively, these studies demonstrated that different types of T cells or the same cells in different stages may show divergent effects after $K_V1.3$ deletion. We chose the commonly used Jurkat T cell line and applied CRISPR/Cas9 to KO $K_V1.3$, which might help to reveal the effects of LrB on T cells in the absence of $K_V1.3$ acutely since it may avoid the changes in Cl^- channel expression or other molecular compensation mechanisms during T cell development *in vivo*. This approach could be developed into a useful *in vitro* model to complement the studies using *in vivo* $K_V1.3$ KO animals.

STIM1/Orai1 signaling plays pivotal roles in regulating activation, proliferation, and motility of T cells (Lewis, 2020), as reflected by the lethality of Orai1 knockout mice (Vig et al., 2008; Oh-Hora et al., 2013). Humans with Orai1 mutations also suffer from severe combined immunodeficiency (SCID) (Le Deist et al., 1995; Feske et al., 2006). STIM1/Orai1 and $K_V1.3$ channels crosstalk with each other and dynamically regulate Ca^{2+} homeostasis and the downstream signaling pathways of T cells (Lioudyno et al., 2008; Nicolaou et al., 2009). It is reported that after T cell activation, STIM1/Orai1 expression is up-regulated and Ca^{2+} influx increases through a positive feedback loop (Lioudyno et al., 2008). In addition to the role of sustaining a hyperpolarization state of plasma membrane and providing a driving force for Ca^{2+} influx, $K_V1.3$ anchors molecules on plasma membranes to stabilize IS and generate a sustained Ca^{2+} influx (Hanada et al., 1997; Levite et al., 2000). Our results from calcium imaging and IL-2 secretion assays showed that both Ca^{2+} influx and IL-2 secretion were reduced significantly in $K_V1.3$ KO cells and the effect on IL-2 secretion was higher than that for Ca^{2+} influx. In $K_V1.3$ KO cells, CRAC channels may still sense Ca^{2+} depletion in ER and mediate an instant Ca^{2+} influx when 2 mM Ca^{2+} was present in the external solution, however, this low level of Ca^{2+} increase may not be enough to form a positive feedback loop to further upregulate the downstream signaling as occurs in the wild type cells. This may explain the discrepancy between the changes of Ca^{2+} influx and IL-2 secretion. A detailed analysis of the long-term changes of Ca^{2+} oscillations and activation of signaling molecules such as CaN and NFATc1 in $K_V1.3$ KO Jurkat T cell is needed to test this possibility.

We showed that LrB significantly inhibited Ca^{2+} influx in the $K_V1.3$ KO Jurkat T cell and STIM1/Orai1 currents in HEK293 T cell. Although IL-2 secretion was largely blocked by KO $K_V1.3$, the remaining IL-2 was further inhibited by LrB in even at 0.01 uM concentration. This result suggests that LrB is a potent inhibitor for STIM1/Orai1 in T cells and inhibits IL-2 release in a relatively low concentration. This might be caused by the fact that other than crosslinking with $K_V1.3$, STIM1/Orai1 were also closely working with other molecules to cooperatively regulate the activation of T cells (Trebak and Kinet, 2019). For instance, after the initial Ca^{2+} influx mediated by CRAC channel, mitochondria and plasma membrane calcium ATPase (PMCAs) would move close to STIM1/Orai1 channel in the IS and form a microdomain where Ca^{2+} concentration was kept in a lower level to avoid the Ca^{2+} inactivation of CRAC channel and keep a sustained Ca^{2+} elevation globally to activate Ca^{2+} signals and cytokine expression (Quintana et al., 2011). In addition, Orai1, STIM1/2, and ryanodine receptor type1 (RyR1) could also form

Ca^{2+} microdomains when T cell was activated and spread Ca^{2+} increase deeper in the cell (Diercks et al., 2018). The cooperation between STIM1/Orai1 and PMCAs or RyRs may be able to explain the inhibition of Ca^{2+} reuptake by LrB in both wild type and $K_V1.3$ KO Jurkat T cells. Blockade of STIM1/Orai1 by LrB might further inhibit the function of other Ca^{2+}-related components such PMCAs and RyRs and block Ca^{2+} reuptake in the cytoplasm. Ca^{2+} influx through CRAC channel is also required for dynamic polymerization and depolymerization of actin and affects function and motility of the T cells (Hartzell et al., 2016; Dong et al., 2017). Therefore, CRAC channel is a highly sensitive Ca^{2+} modulator through which even a small decrease of Ca^{2+} influx could be sensed and amplified by Ca^{2+} compartmentation and cooperation with other Ca^{2+} signal regulation components. Because the numbers of CRAC channel inhibitor is limited, our finding that LrB is a potent CRAC inhibitor might provide a new direction for the development of CRAC inhibitors based on the structure of LrB, which will also facilitate the use of LrB and its derivatives as potentially highly effective medicines to treat autoimmune diseases.

DATA AVAILABILITY STATEMENT

The original contributions presented in the study are included in the article/**Supplementary Material**, further inquiries can be directed to the corresponding author.

AUTHOR CONTRIBUTIONS

Conceived and designed the experiments: SY and HH. Performed the experiments: SS, QZ, CK, SL, FZ, XZ, YL, and XL. Analyzed the data: SY, SS, and QZ. Wrote the paper: QZ, SS, and SY. All authors read and approved the final article.

FUNDING

This work is supported partly by grants from the National Natural Sciences Foundation of China to SY (81373379, 81641186), the National Natural Sciences Foundation of China (32000685) and Natural Sciences Foundation of Hubei Province, China (2020CFB348) to QZ, the Fundamental Research Funds for the Central Universities, South-Central University for Nationalities to SY (CZZ19005), and the National Key R and D Program of China to XL (2018YFC1708004).

SUPPLEMENTARY MATERIAL

The Supplementary Material for this article can be found online at: https://www.frontiersin.org/articles/10.3389/fphar.2021.685092/full#supplementary-material

REFERENCES

Bai, X., He, T., Liu, J., Wang, Y., Fan, L., Tao, K., et al. (2015). Loureirin B Inhibits Fibroblast Proliferation and Extracellular Matrix Deposition in Hypertrophic Scar via TGF-β/Smad Pathway. *Exp. Dermatol.* 24 (5), 355–360. doi:10.1111/exd.12665

Beeton, C., Barbaria, J., Giraud, P., Devaux, J., Benoliel, A.-M., Gola, M., et al. (2001). Selective Blocking of Voltage-Gated K+ Channels Improves Experimental Autoimmune Encephalomyelitis and Inhibits T Cell Activation. *J. Immunol.* 166 (2), 936–944. doi:10.4049/jimmunol.166.2.936

Bobak, N., Bittner, S., Andronic, J., Hartmann, S., Mühlpfordt, F., Schneider-Hohendorf, T., et al. (2011). Volume Regulation of Murine T Lymphocytes Relies on Voltage-dependent and Two-Pore Domain Potassium Channels. *Biochim. Biophys. Acta (Bba) - Biomembranes* 1808 (8), 2036–2044. doi:10.1016/j.bbamem.2011.04.013

Cahalan, M. D., and Chandy, K. G. (2009). The Functional Network of Ion Channels in T Lymphocytes. *Immunol. Rev.* 231 (1), 59–87. doi:10.1111/j.1600-065X.2009.00816.x

Cao, X., Chen, J., Li, D., Xie, P., Xu, M., Lin, W., et al. (2019). ORP4L Couples IP3to ITPR1 in Control of Endoplasmic Reticulum Calcium Release. *FASEB J.* 33 (12), 13852–13865. doi:10.1096/fj.201900933RR

Chandy, K. G., Wulff, H., Beeton, C., Pennington, M., Gutman, G. A., and Cahalan, M. D. (2004). K+ Channels as Targets for Specific Immunomodulation. *Trends Pharmacol. Sci.* 25 (5), 280–289. doi:10.1016/j.tips.2004.03.010

Chen, S., Wan, Y., Liu, X., and Pan, X. (2018). Inhibitive Effect of Loureirin B Plus Capsaicin on Tetrodotoxin-Resistant Sodium Channel. *J. Tradit Chin. Med.* 38 (6), 842–852.

Desai, R., Peretz, A., Idelson, H., Lazarovici, P., and Attali, B. (2000). Ca2+-activated K+ Channels in Human Leukemic Jurkat T Cells. *J. Biol. Chem.* 275 (51), 39954–39963. doi:10.1074/jbc.M001562200

Diercks, B. P., Werner, R., Weidemuller, P., Czarniak, F., Hernandez, L., Lehmann, C., et al. (2018). ORAI1, STIM1/2, and RYR1 Shape Subsecond Ca2+ Microdomains upon T Cell Activation. *Sci. Signaling* 11 (561), Eaat0358, 2018 , ARTN. doi:10.1126/scisignal.aat0358

Dong, T. X., Othy, S., Greenberg, M. L., Jairaman, A., Akunwafo, C., Leverrier, S., et al. (2017). Intermittent Ca2+ Signals Mediated by Orai1 Regulate Basal T Cell Motility. *Elife* 6, e27827. doi:10.7554/eLife.27827

Fan, J.-Y., Yi, T., Sze-To, C.-M., Zhu, L., Peng, W.-L., Zhang, Y.-Z., et al. (2014). A Systematic Review of the Botanical, Phytochemical and Pharmacological Profile of Dracaena Cochinchinensis, a Plant Source of the Ethnomedicine "Dragon's Blood". *Molecules* 19 (7), 10650–10669. doi:10.3390/molecules190710650

Feske, S., Gwack, Y., Prakriya, M., Srikanth, S., Puppel, S.-H., Tanasa, B., et al. (2006). A Mutation in Orai1 Causes Immune Deficiency by Abrogating CRAC Channel Function. *Nature* 441 (7090), 179–185. doi:10.1038/nature04702

Feske, S., Skolnik, E. Y., and Prakriya, M. (2012). Ion Channels and Transporters in Lymphocyte Function and Immunity. *Nat. Rev. Immunol.* 12 (7), 532–547. doi:10.1038/nri3233

Feske, S., Wulff, H., and Skolnik, E. Y. (2015). Ion Channels in Innate and Adaptive Immunity. *Annu. Rev. Immunol.* 33, 291–353. doi:10.1146/annurev-immunol-032414-112212

Gocke, A. R., Lebson, L. A., Grishkan, I. V., Hu, L., Nguyen, H. M., Whartenby, K. A., et al. (2012). Kv1.3 Deletion Biases T Cells toward an Immunoregulatory Phenotype and Renders Mice Resistant to Autoimmune Encephalomyelitis. *J.I.* 188 (12), 5877–5886. doi:10.4049/jimmunol.1103095

Grishkan, I. V., Tosi, D. M., Bowman, M. D., Harary, M., Calabresi, P. A., and Gocke, A. R. (2015). Antigenic Stimulation of Kv1.3-Deficient Th Cells Gives Rise to a Population of Foxp3-independent T Cells with Suppressive Properties. *J.I.* 195 (4), 1399–1407. doi:10.4049/jimmunol.1403024

Grissmer, S., Lewis, R. S., and Cahalan, M. D. (1992). Ca(2+)-activated K+ Channels in Human Leukemic T Cells. *J. Gen. Physiol.* 99 (1), 63–84. doi:10.1085/jgp.99.1.63

Hanada, T., Lin, L., Chandy, K. G., Oh, S. S., and Chishti, A. H. (1997). Human Homologue of the Drosophila Discs Large Tumor Suppressor Binds to P56 Tyrosine Kinase and Shaker Type Kv1.3 Potassium Channel in T Lymphocytes. *J. Biol. Chem.* 272 (43), 26899–26904. doi:10.1074/jbc.272.43.26899

Hartzell, C. A., Jankowska, K. I., Burkhardt, J. K., and Lewis, R. S. (2016). Calcium Influx through CRAC Channels Controls Actin Organization and Dynamics at the Immune Synapse. *Elife* 5, e14850, 2016 , ARTN. doi:10.7554/elife.14850

Heo, S.-K., Yi, H.-S., Yun, H.-J., Ko, C.-H., Choi, J.-W., and Park, S.-D. (2010). Ethylacetate Extract from Draconis Resina Inhibits LPS-Induced Inflammatory Responses in Vascular Smooth Muscle Cells and Macrophages via Suppression of ROS Production. *Food Chem. Toxicol.* 48 (5), 1129–1136. doi:10.1016/j.fct.2009.06.043

Hoth, M., and Penner, R. (1992). Depletion of Intracellular Calcium Stores Activates a Calcium Current in Mast Cells. *Nature* 355 (6358), 353–356. doi:10.1038/355353a0

Jiang, Y., Zhang, G., Yan, D., Yang, H., Ye, Z., and Ma, T. (2017). Bioactivity-Guided Fractionation of the Traditional Chinese Medicine Resina Draconis Reveals Loureirin B as a PAI-1 Inhibitor. *Evidence-Based Complement. Altern. Med.* 2017, 1–8. doi:10.1155/2017/9425963

Koni, P. A., Khanna, R., Chang, M. C., Tang, M. D., Kaczmarek, L. K., Schlichter, L. C., et al. (2003). Compensatory Anion Currents in Kv1.3 Channel-Deficient Thymocytes. *J. Biol. Chem.* 278 (41), 39443–39451. doi:10.1074/jbc.M304879200

Le Deist, F., Hivroz, C., Partiseti, M., Thomas, C., Buc, H., Oleastro, M., et al. (1995). A Primary T-Cell Immunodeficiency Associated with Defective Transmembrane Calcium Influx. *Blood* 85 (4), 1053–1062. doi:10.1182/blood.v85.4.1053.bloodjournal8541053

Levite, M., Cahalon, L., Peretz, A., Hershkoviz, R., Sobko, A., Ariel, A., et al. (2000). Extracellular K+ and Opening of Voltage-Gated Potassium Channels Activate T Cell Integrin Function. *J. Exp. Med.* 191 (7), 1167–1176. doi:10.1084/jem.191.7.1167

Lewis, R. S. (2020). Store-Operated Calcium Channels: From Function to Structure and Back Again. *Cold Spring Harbor Perspect. Biol.* 12 (5), a035055, 2020 , ARTN. doi:10.1101/cshperspect.a03505510.1101/cshperspect.a035055

Lioudyno, M. I., Kozak, J. A., Penna, A., Safrina, O., Zhang, S. L., Sen, D., et al. (2008). Orai1 and STIM1 Move to the Immunological Synapse and Are Up-Regulated during T Cell Activation. *Proc. Natl. Acad. Sci.* 105 (6), 2011–2016. doi:10.1073/pnas.0706122105

Matheu, M. P., Beeton, C., Garcia, A., Chi, V., Rangaraju, S., Safrina, O., et al. (2008). Imaging of Effector Memory T Cells during a Delayed-type Hypersensitivity Reaction and Suppression by Kv1.3 Channel Block. *Immunity* 29 (4), 602–614. doi:10.1016/j.immuni.2008.07.015

McCarl, C.-A., Khalil, S., Ma, J., Oh-hora, M., Yamashita, M., Roether, J., et al. (2010). Store-Operated Ca2+Entry through ORAI1 Is Critical for T Cell-Mediated Autoimmunity and Allograft Rejection. *J.Immunol.* 185 (10), 5845–5858. doi:10.4049/jimmunol.1001796

Nicolaou, S. A., Neumeier, L., Steckly, A., Kucher, V., Takimoto, K., and Conforti, L. (2009). Localization of Kv1.3 Channels in the Immunological Synapse Modulates the Calcium Response to Antigen Stimulation in T Lymphocytes. *J. Immunol.* 183 (10), 6296–6302. doi:10.4049/jimmunol.0900613

Nicolaou, S. A., Szigligeti, P., Neumeier, L., Molleran Lee, S., Duncan, H. J., Kant, S. K., et al. (2007). Altered Dynamics of Kv1.3 Channel Compartmentalization in the Immunological Synapse in Systemic Lupus Erythematosus. *J. Immunol.* 179 (1), 346–356. doi:10.4049/jimmunol.179.1.346

Oh-Hora, M., Komatsu, N., Pishyareh, M., Feske, S., Hori, S., Taniguchi, M., et al. (2013). Agonist-selected T Cell Development Requires strong T Cell Receptor Signaling and Store-Operated Calcium Entry. *Immunity* 38 (5), 881–895. doi:10.1016/j.immuni.2013.02.008

Quintana, A., Pasche, M., Junker, C., Al-Ansary, D., Rieger, H., Kummerow, C., et al. (2011). Calcium Microdomains at the Immunological Synapse: How ORAI Channels, Mitochondria and Calcium Pumps Generate Local Calcium Signals for Efficient T-Cell Activation. *EMBO J.* 30 (19), 3895–3912. doi:10.1038/emboj.2011.289

Sharma, N., Baek, K., Shimokawa, N., and Takagi, M. (2019). Effect of Temperature on Raft-dependent Endocytic Cluster Formation during Activation of Jurkat T Cells by Concanavalin A. *J. Biosci. Bioeng.* 127 (4), 479–485. doi:10.1016/j.jbiosc.2018.09.014

Sun, X., Wen, K., Xu, Z., He, Z., Wu, B., Yang, X., et al. (2020). Effect of Loureirin B on Crohn's Disease Rat Model Induced by TNBS via IL-6/STAT3/NF-κB Signaling Pathway. *Chin. Med.* 15, 2. doi:10.1186/s13020-019-0282-5

Trebak, M., and Kinet, J.-P. (2019). Calcium Signalling in T Cells. *Nat. Rev. Immunol.* 19 (3), 154–169. doi:10.1038/s41577-018-0110-7

Valle-Reyes, S., Valencia-Cruz, G., Liñan-Rico, L., Pottosin, I., and Dobrovinskaya, O. (2018). Differential Activity of Voltage- and Ca2+-dependent Potassium Channels in Leukemic T Cell Lines: Jurkat Cells Represent an Exceptional Case. *Front. Physiol.* 9, 499. doi:10.3389/fphys.2018.00499

Vig, M., DeHaven, W. I., Bird, G. S., Billingsley, J. M., Wang, H., Rao, P. E., et al. (2008). Defective Mast Cell Effector Functions in Mice Lacking the CRACM1 Pore Subunit of Store-Operated Calcium Release-Activated Calcium Channels. *Nat. Immunol.* 9 (1), 89–96. doi:10.1038/ni1550

Wan, Y., Yu, Y., Pan, X., Mo, X., Gong, W., Liu, X., et al. (2019). Inhibition on Acid-Sensing Ion Channels and Analgesic Activities of Flavonoids Isolated from Dragon's Blood Resin. *Phytotherapy Res.* 33 (3), 718–727. doi:10.1002/ptr.6262

Wu, Y., Cao, Z., Yi, H., Jiang, D., Mao, X., Liu, H., et al. (2004). Simulation of the Interaction between ScyTx and Small Conductance Calcium-Activated Potassium Channel by Docking and MM-PBSA. *Biophysical J.* 87 (1), 105–112. doi:10.1529/biophysj.103.039156

Yabuuchi, S., Endo, S., Baek, K., Hoshino, K., Tsujino, Y., Vestergaard, M. d. C., et al. (2017). Raft-dependent Endocytic Movement and Intracellular Cluster Formation during T Cell Activation Triggered by Concanavalin A. *J. Biosci. Bioeng.* 124 (6), 685–693. doi:10.1016/j.jbiosc.2017.06.009

Yin, S., Hu, Q., Luo, J., Li, Y., Lu, C., Chen, X., et al. (2014). Loureirin B, an Essential Component of Sanguis Draxonis, Inhibits Kv1.3 Channel and Suppresses Cytokine Release from Jurkat T Cells. *Cell Biosci.* 4, 78. doi:10.1186/2045-3701-4-78

Zhong, W., Yi, Q., Xu, B., Li, S., Wang, T., Liu, F., et al. (2016). ORP4L Is Essential for T-Cell Acute Lymphoblastic Leukemia Cell Survival. *Nat. Commun.* 7, 12702. doi:10.1038/ncomms12702

Zhu, L., Yuan, C., Ding, X., Jones, C., and Zhu, G. (2017). The Role of Phospholipase C Signaling in Bovine Herpesvirus 1 Infection. *Vet. Res.* 48 (1), 45. doi:10.1186/s13567-017-0450-5

Conflict of Interest: The authors declare that the research was conducted in the absence of any commercial or financial relationships that could be construed as a potential conflict of interest.

frontiers in Pharmacology

ORIGINAL RESEARCH
published: 27 August 2021
doi: 10.3389/fphar.2021.742862

Immune Checkpoint Inhibitors Regulate K^+ Channel Activity in Cytotoxic T Lymphocytes of Head and Neck Cancer Patients

*Vaibhavkumar S. Gawali[1], Ameet A. Chimote[1], Hannah S. Newton[1], Manuel G. Feria-Garzón[1], Martina Chirra[1], Edith M. Janssen[2,3], Trisha M. Wise-Draper[4] and Laura Conforti[1]**

[1]Department of Internal Medicine, Division of Nephrology, University of Cincinnati, Cincinnati, OH, United States, [2]Division of Immunobiology, Cincinnati Children's Hospital Medical Center, Cincinnati, OH, United States, [3]Immunology, Janssen Research and Development, Spring House, PA, United States, [4]Department of Internal Medicine, Division of Hematology Oncology, University of Cincinnati, Cincinnati, OH, United States

Programmed death receptor-1 (PD-1) and its ligand (PD-L1) interaction negatively regulates T cell function in head and neck squamous cell carcinoma (HNSCC). Overexpression of PD-1 reduces intracellular Ca^{2+} fluxes, and thereby T cell effector functions. In HNSCC patients, PD-1 blockade increases KCa3.1 and Kv1.3 activity along with Ca^{2+} signaling and mobility in $CD8^+$ peripheral blood T cells (PBTs). The mechanism by which PD-L1/PD-1 interaction regulates ion channel function is not known. We investigated the effects of blocking PD-1 and PD-L1 on ion channel functions and intracellular Ca^{2+} signaling in $CD8^+$ PBTs of HNSCC patients and healthy donors (HDs) using single-cell electrophysiology and live microscopy. Anti-PD-1 and anti-PD-L1 antibodies increase KCa3.1 and Kv1.3 function in $CD8^+$ PBTs of HNSCC patients. Anti-PD-1 treatment increases Ca^{2+} fluxes in a subset of HSNCC patients. In $CD8^+$ PBTs of HDs, exposure to PD-L1 reduces KCa3.1 activity and Ca^{2+} signaling, which were restored by anti-PD-1 treatment. The PD-L1-induced inhibition of KCa3.1 channels was rescued by the intracellular application of the PI3 kinase modulator phosphatidylinositol 3-phosphate (PI3P) in patch-clamp experiments. In HNSCC $CD8^+$ PBTs, anti-PD-1 treatment did not affect the expression of KCa3.1, Kv1.3, Ca^{2+} release activated Ca^{2+} (CRAC) channels, and markers of cell activation (CD69) and exhaustion (LAG-3 and TIM-3). Our data show that immune checkpoint blockade improves T cell function by increasing KCa3.1 and Kv1.3 channel activity in HNSCC patients.

Keywords: ion channels, immune checkpoint inhibitors, KCa3.1 (intermediate-conductance Ca^{2+}-activated K^+ channel), Kv1.3 channel, Ca^{2+} signalling, head and neck (H&N) cancer, immunotharapy

OPEN ACCESS

Edited by:
Ildikò Szabò,
University of Padua, Italy

Reviewed by:
Timm Danker,
University of Tübingen, Germany
Hongguang Nie,
China Medical University, China

****Correspondence:***
Laura Conforti
laura.conforti@uc.edu

Specialty section:
This article was submitted to Pharmacology of Ion Channels and Channelopathies, a section of the journal Frontiers in Pharmacology

Received: *16 July 2021*
Accepted: *16 August 2021*
Published: *27 August 2021*

Citation:
Gawali VS, Chimote AA, Newton HS, Feria-Garzón MG, Chirra M, Janssen EM, Wise-Draper TM and Conforti L (2021) Immune Checkpoint Inhibitors Regulate K^+ Channel Activity in Cytotoxic T Lymphocytes of Head and Neck Cancer Patients. Front. Pharmacol. 12:742862. doi: 10.3389/fphar.2021.742862

INTRODUCTION

Head and neck squamous cell cancer (HNSCC) is the seventh most common cancer worldwide (Chow, 2020; Sung et al., 2021). Conventional treatments include surgery, radiotherapy, chemotherapy, and multimodal approaches. However, the prognosis of locally advanced disease remains poor, with a 5 years overall survival <50% (Chow, 2020). The discovery of immunotherapy has changed the landscape of HNSCC treatment by offering long term

response in a subset of patients. Programmed cell death receptor-1 (PD-1) immune checkpoint inhibitors have shown promising responses in the treatment of HNSCC. Hence, they have been approved by the FDA since 2016 (Sharma et al., 2017; Chow, 2020). However, over 80% of HNSCC patients do not respond to PD-1 blockade (Bauml et al., 2019). Resistance to immunotherapy remains a big challenge as the majority of patients do not show a response to the treatment (primary resistance) (Sharma et al., 2017). Furthermore, some patients who initially respond and receive benefit from the treatment, later show disease relapse (acquired resistance) (Sharma et al., 2017). Therefore, better understanding of PD-1 signaling is necessary to develop new therapeutic options. The interaction of PD-1 ligand -1 and 2 (PD-L1/2) with their receptor PD-1 on cytotoxic T cells negatively regulates T cell function and causes apoptosis, anergy, and exhaustion (Zhou et al., 2017). PD-L1 is constitutively present in T cells and other immune cells, and it's over expression by tumor cells contributes to immune evasion (Zhou et al., 2017). PD-L1 is also present, and biologically active, in the plasma of HNSCC patients in a secreted form and bound to exosomes contributing to immune evasion (Theodoraki et al., 2018). However, the mechanisms of PD-L1-mediated PD-1 signaling on T cell function are not fully understood.

Ion channels in T lymphocytes orchestrate the influx of intracellular Ca^{2+} required for downstream effector functions, such as migration and proliferation. Calcium release activated Ca^{2+} (CRAC), voltage-gated K^+ (Kv1.3) and Ca^{2+} activated K^+ (KCa3.1) channels are involved in the early phase of T cell activation and regulate the Ca^{2+} influx necessary for their effector functions. Ca^{2+} influx is triggered by the T cell receptor (TCR) mediated-depletion of Ca^{2+} stores in the endoplasmic reticulum and opening of the CRAC channels, and it is aided by Kv1.3 and KCa3.1 channels, which allow maintenance of the negative membrane potential necessary for Ca^{2+} influx through the CRAC channels (Feske et al., 2015). KCa3.1 channels also control chemotaxis (Chimote et al., 2018; Chimote et al., 2020). Defective ion channel function leads to alterations in Ca^{2+} signaling and downstream effector functions (Feske et al., 2006). In HNSCC patients, reduced expression of Kv1.3 in tumor infiltrating lymphocytes (TILs) contributes to lower Ca^{2+} response and cytotoxicity (Chimote et al., 2017). Furthermore, reduced activity of KCa3.1 in $CD8^+$ peripheral blood T cells (PBTs) of HNSCC patients causes these cells to be hypersensitive to adenosine found in the tumor microenvironment, ultimately reducing their migratory abilities and restricting their infiltration into tumors (Chimote et al., 2013; Chimote et al., 2018).

It has been reported that overexpression of PD-1 influences TCR-dependent effector functions, such as Ca^{2+} fluxing, secretion of cytokines and cytotoxic activity (Wei et al., 2013). Furthermore, TILs of melanoma patients with high expression of PD-1 have decreased Ca^{2+} responses to TCR stimulation (Chapon et al., 2011). We have recently shown that treatment of HNSCC patients with pembrolizumab, a monoclonal blocking antibody against PD1 (αPD-1), increases KCa3.1 and Kv1.3 activities in $CD8^+$ TILs and PBTs, along with their Ca^{2+} fluxing and migratory abilities (Newton et al., 2020). Furthermore, a specific pattern of K^+ channel reinvigoration was associated with a pathological response to therapy (Newton et al., 2020). However, these studies did not allow us to dissect the mechanisms by which PD-1 signaling affects ion channel activity. Herein, we conducted *in vitro* studies that further our understanding of the interconnection between PD-1 and ion channels in T cells. These studies showed that blockade of PD-L1/PD-1 interaction leads to the rapid activation of KCa3.1 and Kv1.3 channels to ultimately regulate Ca^{2+} signaling in HNSCC patients' T cells.

TABLE 1 | Demographic and clinical data of HNSCC patients enrolled in the study.

Age (at the time of sample collection)	**Years**
Range	18–90
Mean	59
Variable	**Number (%)**
Sex	
Male	23 (71)
Female	9 (39)
Site	
Oral Cavity	10 (31)
Oropharynx	14 (43)
Larynx	07 (21)
Hypopharynx	0 (0)
Nasopharynx	0 (0)
Unknown Primary	1 (3)
Primary Tumor	
T1	8 (25)
T2	10 (31)
T3	5 (16)
T4	8 (25)
Unknown	1 (3)
Nodal Status	
N0	7 (21)
N1	11 (34)
N2	11 (34)
N3	3 (9)
Unknown	0 (0)
ECOG performance status	
0	6 (19)
1	13 (41)
2	4 (12)
3	1 (3)
Unknown	8 (25)
Smoking	
No (<10 pack years)	14 (44)
Yes (>10 pack years)	18 (56)
Alcohol	
No (<5 drinks/week)	22 (69)
Yes (>5 drinks/week)	9 (28)
Unknown	1(3)
p16 status	
Positive	12 (38)
Negative	13 (41)
Unknown	7 (22)

HNSCC patients (n = 32) were enrolled in the study upon fulfillment of eligibility criteria. TNM staging system was used to stage tumor size and nodal involvement. T1 to T4 refers to the size and invasion of the tumors. N1 to N3 refers to the assessment of number and location of the regional lymph nodes. The ECOG (Eastern Cooperative Oncology Group) performance status indicates daily quality of life of individuals affected by diseases on a scale of 0–5. Smoking status (pack years) was calculated by multiplying the number of packs of cigarettes smoked per day by the number of years the person has smoked. We used a cutoff of 10 packs per year to differentiate the smoking status.

MATERIALS AND METHODS

Human Subjects

Peripheral blood samples from de-identified HNSCC patients (n = 32) were obtained from the University of Cincinnati Medical Center. HNSCC patients included in this study were treatment-naïve and had a positive diagnosis of HNSCC by tissue biopsy (See **Table 1** for a summary of patient demographics and **Supplementary Table S1** for clinical information). Peripheral blood samples of 7 healthy donors (HDs, 4 males and 3 females, age range between 30 and 65 years) were collected from individual donors and from discarded blood units (Hoxworth Blood Center, University of Cincinnati). The demographics of the donors from Hoxworth Blood center were not available. Informed consent was obtained from all HNSCC patients and HDs. The data collected in the study were managed using the Research Electronic Data Capture (REDCap) tools licensed to the University of Cincinnati. Sample collection was approved by the University of Cincinnati Institutional Review Board (IRB no. 2014-4755).

Reagents and Chemicals

Human serum, L-glutamine, sodium hydroxide, poly-L-lysine, LY294002 HCl, ionomycin, calmodulin, poly-L-lysine, thapsigargin (TG), tetraethylammonium-chloride (TEA-Cl), 1,2-Bis(2-Aminophenoxy)ethane-*N,N,N′,N′*-tetraacetic acid (BAPTA), $MgCl_2$ were purchased from Millipore Sigma. Sterile, 4-(2-hydroxyethyl)-1-piperazineethanesulfonic acid (HEPES), RPMI-1640 medium, fetal bovine serum, penicillin, streptomycin, Fura-2 and phosphate buffered saline (PBS) were obtained from ThermoFisher. Phosphatidylinositol 3-phosphate diC16 (PI3P) was purchased from Echelon Biosciences. Pembrolizumab (Merck Sharpe and Dohme Corp) samples used in this study were received from the leftover pharmacy supply at Cincinnati Children's Hospital. Atezolizumab was purchased from Biovision life sciences. PD-L1-Fc chimera was obtained from R&D systems. Stock solutions of LY394002 and TG were prepared in dimethyl sulfoxide and used at 0.1% dilution. Stock solutions of PD-L1-Fc, pembrolizumab and atezolizumab were prepared in sterile PBS.

Cell isolation and *in vitro* Activation

Peripheral blood mononuclear cells were isolated from whole blood by Ficoll-Paque density gradient centrifugation (Cytiva) as previously described (Chimote et al., 2018). $CD8^+$ PBTs were isolated by negative selection using EasySep Human $CD8^+$ T cell Enrichment kit (StemCell Technologies). Post isolation, $CD8^+$ PBTs were maintained in RPMI-1640 medium supplemented with 10% human serum, 200 U/ml penicillin, 200 mg/ml streptomycin, 1 mM L-glutamine, and 10 mM HEPES. Activation of cells was performed either by adding 40.5 nM of phorbol-12-myristate-13-acetate (PMA, Millipore Sigma) and 1.5 μM of ionomycin (Millipore Sigma) or in cell culture plates coated with 10 μg/ml anti-CD3 and anti-CD28 antibodies (BioLegend) for 72–96 h (h) as previously described (Chimote et al., 2016; Chimote et al., 2018). After isolation, some fresh cells were used for functional studies, the remaining cells were frozen and used later on for flow cytometry experiments.

Treatment With αPD-1/PD-L1 Antibodies and PD-L1-Fc

$CD8^+$ PBTs from HNSCC patients were activated for 72–96 h using PMA and ionomycin followed by treatment with the αPD-1 antibody pembrolizumab (10 μg/ml) and/or the αPD-L1 antibody atezolizumab (1 and 10 μg/ml) for 6 h prior to performing functional studies. $CD8^+$ PBTs from HDs were plated on cell culture plates coated with PD-L1 (PD-L1-Fc, R&D Systems) (10 μg/ml) and activated with either PMA and ionomycin or (with anti-CD3/CD28 antibodies for 72–96 h followed by treatment with the αPD-1 antibody pembrolizumab (10 μg/ml) for 6 h before performing functional studies. For prolonged treatment with PD-L1, cells were activated for 120 h with plate-bound anti-CD3/CD8 antibodies along with PD-L1-Fc in T cell medium supplemented with 20 IU/ml of IL-2.

Electrophysiology

Whole cell patch-clamp electrophysiology was used to measure the activity of KCa3.1 and Kv1.3 channels in activated $CD8^+$ PBTs cells of HDs and HNSCC patients as described previously (Chimote et al., 2020). The external solution consisted of (in mM): 160 NaCl, 4.5 KCl, 1 $MgCl_2$, 10 HEPES, pH 7.4. Internal solution consisted of (in mM): 145 K-Aspartate, 2 $MgCl_2$, 8.5 $CaCl_2$, 10 EGTA, 10 HEPES, pH 7.2 TRIS buffer (1 μM free Ca^{2+} concentration). Borosilicate glass (World Precision Instruments) pipettes (4–5 MΩ resistance) were fabricated using a P-97 horizontal puller (Sutter Instruments). A voltage-ramp pulse protocol (from −120 to + 50 mV, for 200 ms, holding potential of −70 mV, every 15 s) was used to elicit the currents from $CD8^+$ PBTs. Currents were recorded, amplified and digitalized (Axon 200B and Digidata 1320A, Molecular Devices) through a 16-bit A-D/D-A interface. Data acquisition was performed using pClamp 8.0 software (Molecular Devices) and signals were low pass filtered at 2 kHz and digitalized at 100 kHz. The conductance (G) of KCa3.1 channels was calculated as, the ratio of linear fraction of the currents to the slope of ramp voltage stimulus (measured in the voltage range between −100 and −80 mV) after subtraction of leak current. (Chimote et al., 2018). The G of Kv1.3 channels was determined from the same recordings by measuring the peak currents at +50 mV after subtraction of KCa3.1 currents extrapolated by linear regression. This protocol accurately record and separate KCa3.1 and Kv1.3 currents (Newton et al., 2020). LY294002 was delivered extracellular *via* a manual perfusion system. Calmodulin and PI3P were dissolved in the internal solution and delivered intracellularly *via* the patch-pipette. The KCa3.1 and Kv1.3 Gs were measured in at least three to five cells for each condition per individual patient.

For divalent free (DVF) currents, cells patched in the whole-cell configuration were pre-incubated with TG (1 μM) in external solution without Ca^{2+} for 10 min followed by perfusion with 20 mM Ca^{2+} for 1 min and, finally, with DVF solution for 2 min (Vaeth et al., 2017). DVF currents were measured to amplify the CRAC currents. The DVF Ringer's solution contained (in mM): 150 NaCl, 10 HEDTA, 1 EDTA and 10 HEPES (pH 7.4 with NaOH). The 20 mM Ca^{2+} external solution consisted of (in mM):

130 NaCl, 4.5 KCl, 20 $CaCl_2$, 10 D-glucose and 5 HEPES (pH 7.4 with NaOH). 10 mM TEA-Cl was added to all extracellular solutions to block voltage-gated K^+ channels. The pipette solution contained (in mM): 135 Cs aspartate, 8 $MgCl_2$, 8 BAPTA and 1 HEPES (pH 7.2 with CsOH). A ramp (-100 to +100 mV, holding potential of +30 mV) protocol was used for 100 m every 1.5 s to record DVF currents. Analysis of DVF current was performed by measuring the peak current value at the voltage of −100 mV during the ramp step protocol.

Ca^{2+} Flux Measurements

Intracellular Ca^{2+} fluxes were measured in activated $CD8^+$ PBTs using the ratiometric Ca^{2+} sensitive dye Fura-2. Perfusion with the sarco-endoplasmic pump inhibitor TG allowed us to measure Ca^{2+} fluxes that are independent of TCR stimulation and only rely on downstream signaling events initiated by the release of Ca^{2+} from the endoplasmic reticulum (Robbins et al., 2005). T cells were plated on poly-L-lysine coated coverslips followed by treatment with 1 μM Fura-2 AM (ThermoFisher) at 37°C for ~30 min. Cells were then washed with RPMI-1640 and maintained at 37°C prior to recordings using InCyt-Im2 Ca^{2+} imaging system (Intracellular Imaging). Coverslips were mounted on the microscope and perfused with a Ca^{2+} free solution for 5 min, followed by perfusion with 1 μMTG in Ca^{2+} free solution for other 5 min to deplete the Ca^{2+} from the intracellular Ca^{2+} stores and open the CRAC channels. Finally, 0.5 mM Ca^{2+} solution was perfused for 10–15 min to allow Ca^{2+} influx through CRAC channels. Ca^{2+} free solution had the following composition (in mM): 155 NaCl, 4.5 KCl, 1 $MgCl_2$, 10 HEPES, 10 glucose, 2 EGTA, pH 7.4. The 0.5 mM Ca^{2+} solution had the following composition (in mM): 155 NaCl, 4.5 KCl, 2.5 $MgCl_2$, 10 HEPES, 10 glucose, 0.5 $CaCl_2$, pH 7.4. A standard calibration curve was used to correlate ratiometric Fura-2 values (340/380 nm ratio) with known Ca^{2+} concentrations as per the protocol provided by the manufacturer. Changes in Ca^{2+} values [Delta (Δ) Ca^{2+}], a measure of Ca^{2+} fluxing ability, were determined as the difference between the peak of Ca^{2+} reached after 0.5 mM Ca^{2+} and the baseline Ca^{2+} after the perfusion with 1 μMTG in Ca^{2+} free solution, immediately before the addition of 0.5 mM Ca^{2+}. Statistical analysis was performed to detect significant difference in ΔCa^{2+} values post treatment for an individual patient or healthy donor. Only those donors who showed a statistically significant increase in the Ca^{2+} values before and after αPD-1 were included in the positive response (PR) group while those who did not show any statistically significant increase were included in the no-response (NR) group. Individual single cell ΔCa^{2+} values from donors in the PR group and the NR group were then combined to detect significance differences between the two groups. This is because of low sample quantity and variable cell count per patient.

Flow Cytometry

$CD8^+$ PBT cells were maintained at a density of 1×10^6 cells/mL and stimulated with PMA/ionomycin for 72 h. Cells were then rinsed with 1x PBS, followed by staining for flow cytometry. The proportion of dead cells were determined using the Zombie UV fixable viability kit (Biolegend). The cells were then fixed with 1% paraformaldehyde (ThermoFisher), washed with 1x PBS and stained overnight with mouse anti-human anti-KCa3.1 biotinylated antibodies (clone 6C1, Alomone). Then, the cells were washed with 1x PBS and incubated for 30 min at room temperature with the following anti-human antibodies (all from Biolegend): anti-CD8-PacificBlue (cloneHIT8A), anti-CD69-APCFire750 (clone FN50), anti-LAG3-BV510 (clone 11C3C56), anti-PD1-BV605 (clone EH12. 2H7), anti-TIM3-BV786 (clone F38-2F2), and anti-streptavidin-PECy7 (clone). Next, the cells were washed with 1x PBS, and permeabilized with BD Cytofix/Cytoperm kit (BD Biosciences) as per the manufacturer's instructions, and incubated for 30 min at 4°C with mouse anti-human anti-Calmodulin-PerCP (clone 2D1, NOVUS Biologicals), and anti-human anti-Ki67-BV711 (Biolegend).

For determination of ion channel expression, cells were fixed with 4% paraformaldehyde, washed with PBS followed by overnight incubation at 4°C with the following primary antibodies, mouse anti-human KCa3.1 (6C1/ATTO-488), guinea pig anti-human Kv1.3, rabbit anti-human Orai1 (all from Alomone labs) followed by anti-guinea pig (Dy350 goat anti-guinea pig IgG/Thermo Fisher) and anti-rabbit (Alexa Fluor 594 goat anti-rabbit IgG/Thermo Fisher) secondary antibodies. To stain for intracellular ion channel epitopes, cells were permeabilized with BD Cytofix/Cytoperm kit (BD Biosciences) as per manufacturer's instructions. Cells were then stained for rabbit anti-human STIM1 (Proteintech) primary antibodies followed by secondary antibodies (Alexa Fluor 594 goat anti-rabbit IgG/Thermo Fisher). Specificity of these antibodies was previously reported by our laboratory (Chimote et al., 2018; Newton et al., 2020). All flow cytometry data were collected on LSR Fortessa or LSR II flow cytometer (BD Biosciences), using the FACS Diva software v.6.0. At least 30,000 total events were acquired. Fluorescence minus one controls were also included. The flow cytometry data were analyzed using FlowJo Software version 10.6.1 ((BD Biosciences).

Statistical Analysis

Statistical analyses were performed using Student's *t* test (paired or unpaired), Mann-Whitney rank sum test (in experiments where samples failed normality or had unequal variance), and ANOVA or ANOVA on Ranks as indicated. Post hoc testing on ANOVA was done by multiple pairwise comparison procedures using the Holm-Sidak, Dunn's or Tukey's methods depending on sample normality and variance. Statistical analysis was performed using SigmaPlot 13.0 (Systat Software Inc.). *p* value of less than or equal to 0.05 was considered as statistically significant.

RESULTS

PD-1 Blockade improves KCa3.1 and Kv1.3 Activity in $CD8^+$ PBTs of HNSCC Patients

Ion channels are fundamental regulators of T cell Ca^{2+} signaling and effector functions (Feske et al., 2015) and we have shown that treatment of HNSCC patients with pembrolizumab increases

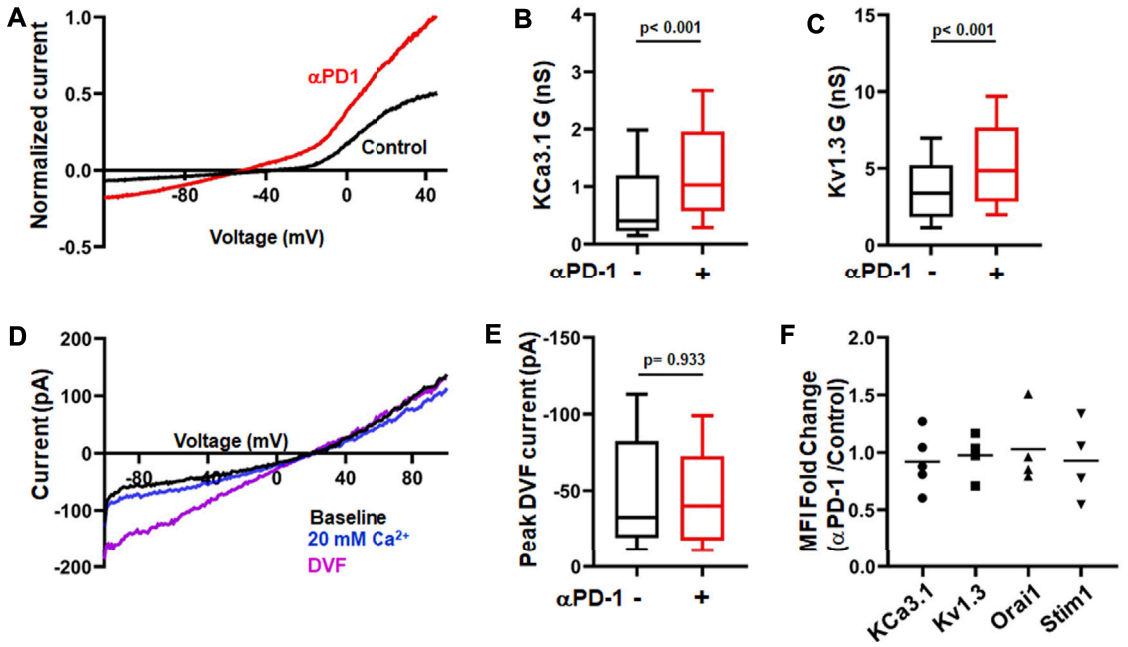

FIGURE 1 | αPD-1 treatment increases K^+ channel activity in HNSCC T cells. **(A)** Representative current traces of KCa3.1 and Kv1.3 channels recorded in whole-cell mode of voltage-clamp configuration in activated $CD8^+$ PBTs cells from a HNSCC patient in absence or presence of αPD-1 (10 μg/ml, for 6 h). Data are normalized to maximum current at +50 mV recorded using a ramp pulse protocol from −120 mV to +50 mV for 200 ms every 15 s. The holding potential used was −70 mV. **(B,C)** KCa3.1 **(B)** and Kv1.3 **(C)** conductance **(G)** measured in the absence or presence of αPD-1 (10 μg/ml, 6 h incubation) in $CD8^+$ PBTs of HNSCC patients (n = 68 cells without pembrolizumab and n = 55 cells with pembrolizumab from 14 patients). **(D)** Representative current traces of divalent free current (DVF) through CRAC channels recorded in whole-cell mode of voltage-clamp configuration in activated $CD8^+$ PBTs from a HNSCC patient. Data were recorded using a ramp pulse protocol from −100 to +100 mV with at holding potential of +30 mV every 1.5 s. Cells were perfused with 0 mM Ca^{2+} solution (1 min) followed by 20 mM Ca^{2+} (1 min) and DVF solutions (2 min, see methods) to amplify currents during recordings. **(E)** Peak DVF current values measured in absence and presence of αPD-1 (10 μg/ml, 6 h incubation) in $CD8^+$ PBTs of HNSCC patients (n = 34 cells without αPD-1 and n = 31 cells with αPD-1 from 8 patients). The values in panels **(B,C)** and **(E)** are represented as box plots: the horizontal line indicates the median; the lower box is the 25th percentile; the upper box is the 75th percentile; and the whiskers represent the 10th and 90th percentiles. **(F)** Ion channel expression (KCa3.1, Kv1.3, Orai1 and STIM1) in HNSCC patient T cells after treatment with αPD-1 (10 μg/ml for 6 h). Effect of αPD-1 treatment is shown as ratio of mean fluorescence intensity (MFI, fold change) values of treatment versus control group. Data are represented as scatter plot where each symbol represents an individual patient (n = 4–5). Horizontal line represents mean values for each group. Data in panels **(B,C,E)** were analyzed by Mann-Whitney rank sum test.

KCa3.1 and Kv1.3 activity in $CD8^+$ PBTs (Newton et al., 2020). Herein, we conducted *in vitro* experiments to study in detail the effect of pembrolizumab on ion channels in HNSCC T cells. We tested the effect of a short exposure (6 h) to pembrolizumab (αPD-1 antibody) (10 μg/ml) on activated $CD8^+$ PBTs. Whole-cell currents were measured before and after αPD-1 treatment to assess KCa3.1 and Kv1.3 activity (**Figure 1A**). αPD-1 treatment increased the conductance of both KCa3.1 and Kv1.3 channels (**Figures 1B,C**). We did not detect any effect of αPD-1 on CRAC channel activity (**Figures 1D,E**). Further control experiments ruled out the possibility that the increase in KCa3.1 and Kv1.3 activity was an artefact due to the extra 6 h the cells treated with αPD-1 were maintained in culture. The KCa3.1 and Kv1.3 conductance in untreated cells at the beginning of the experiment (0 h) and after 6 h (equivalent to the time of exposure to αPD-1) were comparable (**Supplementary Figure S1**). There was no difference in the capacitance values, an arbitrary measure of cell size and activation state, before and after treatment with pembrolizumab (**Supplementary Figure S2**). Furthermore, flow cytometry experiments showed no changes in the expression of either ion channels or activation and exhaustion markers in $CD8^+$ PBTs from HNSCC patients after αPD-1 treatment (**Figure 1F**; **Supplementary Figures S3–S4**). These findings indicate that αPD-1 treatment increases KCa3.1 and Kv1.3, but not CRAC channel, activity in $CD8^+$ PBTs of HNSCC patients. Furthermore, αPD-1 treatment did not change the expression of typical markers associated with exhaustion and activation in $CD8^+$ PBTs of HNSCC patients.

PD-1 Blockade increases Ca^{2+} Fluxing Abilities in T Cells From a Subset of HNSCC Patients

Since K^+ channels regulate T cell Ca^{2+} signaling and effector functions, we investigated the functional consequences of the increase in K^+ channel activity in $CD8^+$ PBTs of HNSCC patients induced by αPD-1 treatment. We measured the Ca^{2+} fluxing abilities of $CD8^+$ PBTs from HNSCC patients using a TG-based protocol that allows us to assess Ca^{2+} fluxes dependent on ion

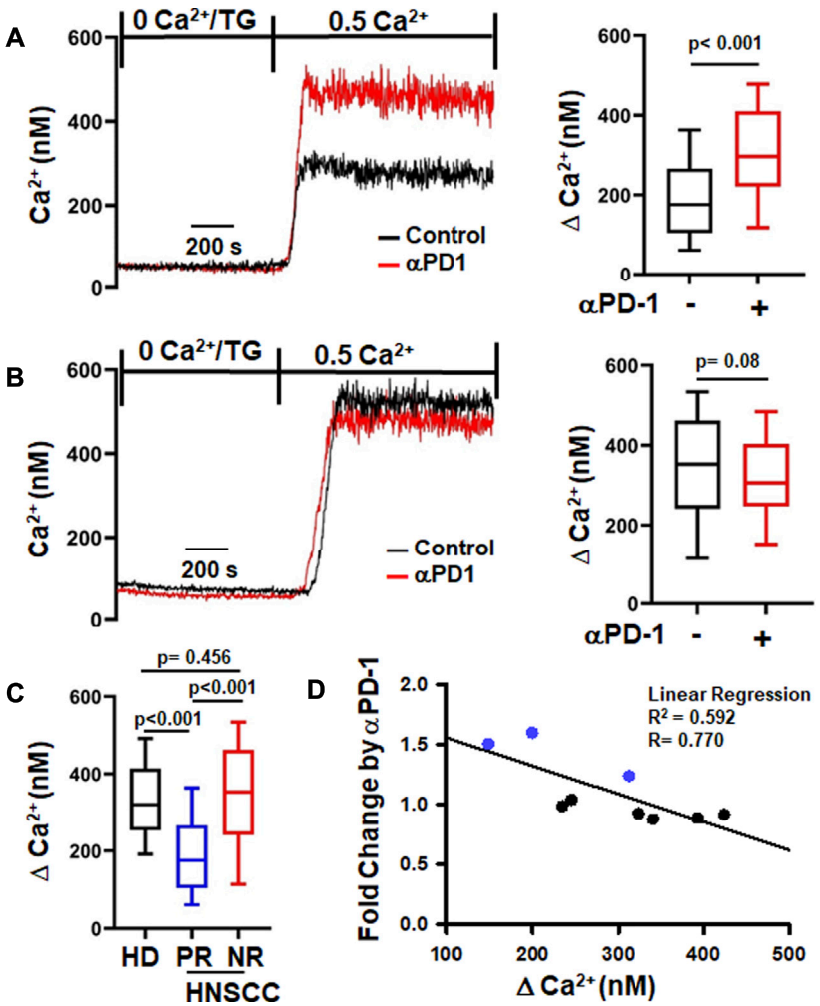

FIGURE 2 | αPD-1 increases Ca^{2+} fluxes in PBTs of a subset of HNSCC patients. **(A,B)** Representative intracellular Ca^{2+} recordings in activated $CD8^+$ PBTs of HNSCC patients are shown on the left side. Cells loaded with Fura-2 were perfused with thapsigargin (TG) in 0 mM Ca^{2+}. Perfusion with 0.5 mM Ca^{2+} yields a rapid influx of Ca^{2+} (See *Material and Methods*). Two types of Ca^{2+} responses to αPD-1 were observed. A significant increase in Ca^{2+} after αPD-1 (10 μg/ml for 6 h) was defined as positive response, PR **(A, left)** while no change in Ca^{2+} response was defined as no-response, NR **(B, left)**. The subset of HNSCC patients (n = 3/9) showing positive Ca^{2+} response are reported in panel **(A, right)** while patients (n = 6/9) with no-response are shown in panel **(B, right)**. The corresponding single cell ΔCa^{2+} values (peak minus baseline before peak) measured in the absence and presence of αPD-1 of PR and NR are shown in the right panels (n = 82–99 cells from 3 patients in PR and n = 140–149 cells from 6 patients in NR). **(C)** Comparison of ΔCa^{2+} values of activated $CD8^+$ PBTs from HDs n = 376 cells from nine donors and PR (n = 82 cells from 3 patients) and NR (n = 146 cells from 6 patients) HNSCC patients at baseline (before αPD-1). The ΔCa^{2+} values in panels **(A,B,C)** are represented as box and whisker plots. The lower and upper bound of the box represent 25^{th} and 75^{th} percentiles respectively. Median values are shown as horizontal line in the box. The lower and upper error represents 10^{th} and 90^{th} percentile respectively. **(D)** Relationship between ΔCa^{2+} values before αPD-1 treatment and fold increase in ΔCa^{2+} after treatment with αPD-1 antibody in $CD8^+$ PBTs of HNSCC patients (n = 9) are represented as correlation analysis. Individual patients from PR and NR group are marked in blue (PR) and black (NR). Data for panel **(A)** were analyzed using unpaired student's t-test. Data for panel **(B)** were analyzed using Mann-Whitney rank-sum test. Data in panel C were analyzed using ANOVA (p < 0.001) followed by Dunn's test and data in panel D were analyzed using linear regression.

channel activity while bypassing the TCR (Newton et al., 2020). Activated $CD8^+$ PBTs from HNSCC patients were treated with αPD-1 for 6 h (same protocol as **Figure 1**) and Ca^{2+} fluxes were measured. We observed variable Ca^{2+} responses in these patients' samples. Therefore, we defined the presence or absence of a response to αPD-1 based on a statistically significant increase in ΔCa^{2+} values before and after *in vitro* αPD-1 treatment in individual patients. In a subset of patients (n = 3/9), αPD-1 treatment increased the Ca^{2+} response of T cells (**Figure 2A**). We termed these patients as "positive-response" (PR) patients. Patients whose T cells did not show any increase in the Ca^{2+} response to αPD-1 treatment *in vitro* were defined as "no-response" (NR) patients (n = 6/9), (**Figure 2B**). αPD-1 treatment induced a 46% increase in ΔCa^{2+} in the PR group (**Figure 2A**). Interestingly, we observed that the ΔCa^{2+} at baseline (before αPD-1 treatment) of $CD8^+$ PBTs from PR patients was 67% lower than NR patients; even lower than that of HDs $CD8^+$ PBTs (**Figure 2C**). Indeed, we observed a significant negative

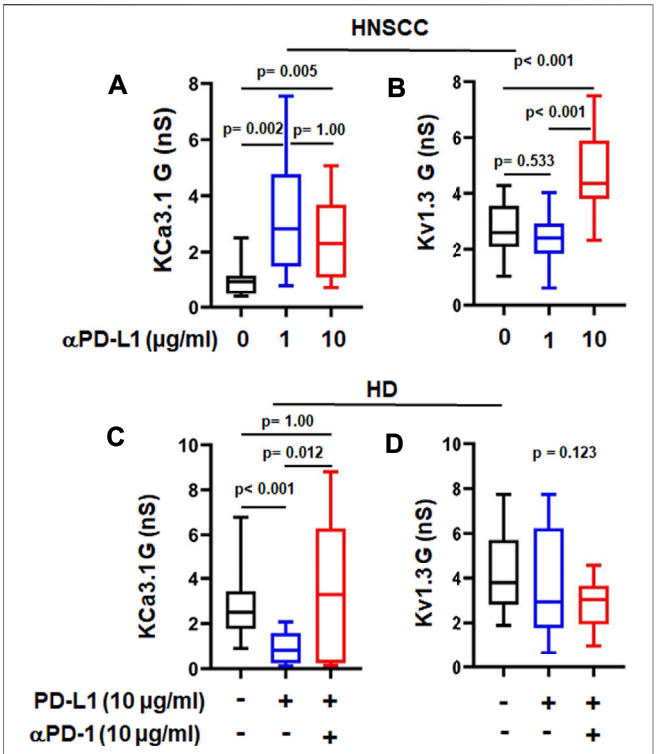

FIGURE 3 | αPD-L1 treatment increases K^+ channel activity in HNSCC patients. **(A)** KCa3.1 and **(B)** Kv1.3 conductance values **(G)** measured with and without the αPD-L1 antibody, atezolizumab (1 and 10 μg/ml for 6 h) in activated $CD8^+$ PBTs of HNSCC patients. **(C)** KCa3.1 and **(D)** Kv1.3 G measured in presence of PD-L1 and αPD-1 antibody pembrolizumab in activated $CD8^+$ PBTs of HDs. Activated cells were treated with plate-bound PD-L1 (PD-L1-Fc 10 μg/ml) +/- αPD-1 (untreated cells were used as a control) and activated for 72 h using PMA/Ionomycin. αPD-1 was added to treatment group for 6 h. Data in the lower and upper bound of the box represent 25^{th} and 75^{th} percentiles respectively. Median values are shown as horizontal lines. The lower and upper error bars represents 10^{th} and 90^{th} percentile respectively, n = 8–23 cells from 3 HNSCC patients, n = 30 cells from 6 HDs (control and PD-L1) and n = 15 cells from 3 HDs (PD-L1 + αPD-1). Five cells were recorded for each individual donor. Data in **(A,C,D)** were analyzed by ANOVA on ranks test ($p < 0.001$) followed by Dunn's post hoc analysis. Data in **(B)** were analyzed by One way ANOVA ($p < 0.001$) followed by Holm-Sidak test.

correlation between the increase in ΔCa^{2+} (fold change for individual patient) induced by αPD-1 versus the baseline ΔCa^{2+} of all HNSCC patients (**Figure 2D**). We performed this type of analysis because we wanted to assess whether the mean baseline ΔCa^{2+} of a patient could be a predictor of his/her ability to respond to pembrolizumab. This indicates that HNSCC patients whose $CD8^+$ PBTs have low baseline Ca^{2+} fluxing abilities were more likely to show a positive response to αPD-1 treatment. Overall, these results indicate that αPD-1 treatment has a rapid effect on ion channel-regulated Ca^{2+} fluxes of HNSCC $CD8^+$ PBTs and point to baseline Ca^{2+} fluxing ability of T cells as a possible predictive marker of αPD-1 treatment response. However, questions still remain about the mechanisms by which αPD-1 antibody regulates K^+ channel activity: is this effect the result of blocking PD-L1/PD-1 binding, and what are the downstream signaling pathways involved?

The Effect of αPD-1 Treatment on K^+ Channels is due to the Disruption of PD-L1/PD-1 Binding

We tested the corollary of our earlier observation with αPD-1 treatment hypothesizing that prevention of or breaking the interaction of PD-L1 with PD-1 is responsible for the improved K^+ channel function. While we have no cancer cells in our *in vitro* setting, $CD8^+$ PBTs of HDs and HNSCC patients can be a source of PD-L1 as both express it (**Supplementary Figure S5**). Others have shown that human $CD3^+$ T cells express PD-L1 (Succaria et al., 2020). Therefore, we next tested the effect of an anti-PD-L1 antibody (αPD-L1), atezolizumab, on KCa3.1 and Kv1.3 channels in activated $CD8^+$ PBTs of HNSCC patients reasoning that if the effect of pembrolizumab is due to the disruption of PD-L1/PD-1 binding, a similar effect should be produced by αPD-L1. Short-term treatment of HNSCC T cells with atezolizumab (1 and 10 μg/ml for 6 h) increased KCa3.1 function, while Kv1.3 function was increased only at the higher concentration (**Figures 3A,B**). These results suggest that engagement of PD-L1 by PD-1 may have negative effects on K^+ channel function in HNSCC T cells and disruption of its binding to the cognate receptor restores the channel's function. Therefore, we tested the effect of PD-L1 (plate-bound PD-L1-Fc; 10 μg/ml) on KCa3.1 and Kv1.3 in $CD8^+$ PBTs of HDs. Cells were incubated with PD-L1 for 72 h followed by treatment with αPD-1 antibody (10 μg/ml) for 6 h. Our data showed that PD-L1 reduced KCa3.1 activity by 65.44%, but, at this concentration, had no effect on Kv1.3 (**Figures 3C,D**). A similar effect was observed after 5 days exposure to PD-L1 (**Supplementary Figure S6**). Furthermore, αPD-1 treatment reversed the effect of PD-L1 on KCa3.1 activity (**Figure 3C**). These results show that, in HDs $CD8^+$ PBTs, KCa3.1 channels appear highly sensitive to PD-1 signaling, more than Kv1.3.

We then measured Ca^{2+} fluxes in activated $CD8^+$ PBTs cells of HDs exposed to PD-L1 to assess the functional effect of PD-L1. Nine out of twelve samples from HDs showed response to PD-L1 and only the $CD8^+$ PBTs samples from donors that showed this response were used in analysis. Cells exposed to PD-L1 showed a small (14%) decrease in ΔCa^{2+} as compared to control cells (**Figure 4B**). Treatment with pembrolizumab significantly increased ΔCa^{2+} by 39% in PD-L1 exposed cells, and by 25% in 9/12 HDs in the control untreated group (**Figures 4A,B**). It is noteworthy that treatment with pembrolizumab showed a similar increase of 45% in ΔCa^{2+} in HNSCC $CD8^+$ PBTs (**Figure 2A**). These results indicate that PD-L1 reduced Ca^{2+} fluxing abilities of T cells in HDs thus supporting the notion that high exposure to PD-L1 may decrease the Ca^{2+} fluxing ability of HNSCC $CD8^+$ PBTs like it occurs for TILs (Chimote et al., 2017). Furthermore, they suggest that KCa3.1 may be highly sensitive to PD-1 signaling, more than Kv1.3. We thus proceeded to investigate the mechanism through which PD-1 regulates KCa3.1 activity.

PI3K Signaling and CaM Mediate PD-L1 inhibition of KCa3.1 Channels

Activation and function of KCa3.1 is controlled by a variety of molecules and phosphorylation events (Ohya and Kito, 2018).

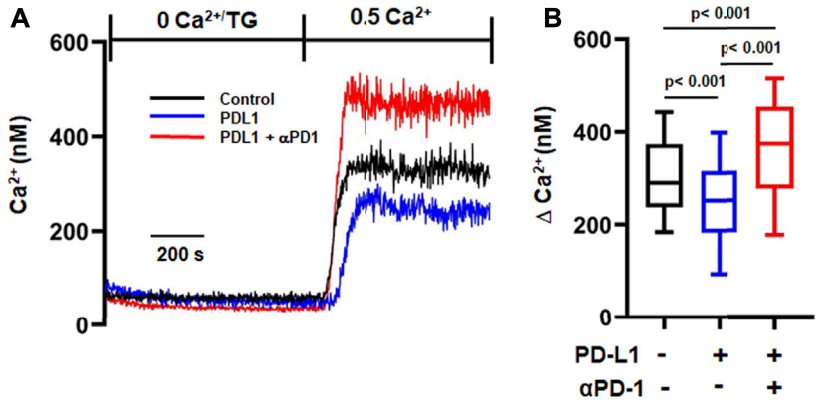

FIGURE 4 | αPD-1 rescues the reduced Ca^{2+} influx induced by PDL-1-Fc in HDs. **(A)** Representative traces of intracellular Ca^{2+} response in activated $CD8^+$ PBTs of HDs. Cells were loaded with Fura-2 and Ca^{2+} fluxes were elicited by TG/0 mM Ca^{2+} followed by 0.5 mM Ca^{2+} (See *Material and Methods*). Cells were incubated with plate bound PD-L1 (PD-L1-Fc, 10 μg/ml for 72 h) followed by treatment with αPD-1 (10 μg/ml for 6 h). **(B)** Summary of ΔCa^{2+} values of activated $CD8^+$ PBTs of HDs (n = 160–255 cells from nine HDs, 20–50 cells were recorded from a single HD, see *Methods*). The values in panel B are represented as box and whisker plots. The lower and upper bound of the box represent 25^{th} and 75^{th} percentiles respectively. Median values are shown as horizontal line. The lower and upper error bars represents 10^{th} and 90^{th} percentile respectively. Data were analyzed using ANOVA ($p < 0.001$) on ranks followed by Dunn's *post hoc* analysis.

KCa3.1 function requires binding of the intracellular Ca^{2+} sensor calmodulin (CaM). We recently showed that $CD8^+$ PBTs of HNSCC patients have reduced levels of CaM which diminished their KCa3.1 activity (Chimote et al., 2020). PD-L1 is available in the plasma of HNSCC patients both as soluble molecule or carried by exosomes, and the presence of PD-$L1^+$ exosomes has been correlated with the increased immune suppressive state of these patients (Theodoraki et al., 2018). These findings raise the possibility that a reduction in CaM by PD-L1 mediates the suppression of KCa3.1 currents. Therefore, we proceeded to determine the signaling pathways involved in PD-L1/PD-1 signaling by exposing HD T cells to PD-L1 for 3 days (72 h; like in the experiments reported above) and 5 days. The latter resembles more the HNSCC patients' setting where T cells are exposed to PD-L1, both in circulation and in the tumor, for a long time. Exposure to PD-L1 for 3 days did not reduce CaM expression (**Figures 5A,B**) and, consequently, intracellular supplementation of CaM did not rescue KCa3.1 inhibition (**Figures 5C,D**). We thus investigated whether the phosphoinositide 3-kinase (PI3K)—phosphatidylinositol-3 phosphatase (PI3P) signaling pathway was instead involved. In T lymphocytes, PI3K favors the production of PI3P from phosphatidylinositol (PI); PI3P activates the nucleoside diphosphate kinase B (NDPK-B) which, ultimately, increases KCa3.1 activity *via* histidine phosphorylation (Srivastava et al., 2005; Srivastava et al., 2006b). PD-1 signaling in T cells involves the blockade of PI3K and, consequently, the suppression of downstream effector functions (Patsoukis et al., 2013). We performed patch-clamp experiments to determine if the inhibition of KCa3.1 activity by PD-L1 can be mimicked by the PI3K inhibitor LY294002 and rescued by PI3P. Activated $CD8^+$ PBTs from HDs were pretreated with LY294002 (10 μM, for 15 min) followed by measurement of KCa3.1 in presence and absence of PI3P (100 nM) delivered intracellularly *via* patch pipette (**Figure 6A**). LY294002, similar to PD-L1, reduced KCa3.1 currents while PI3P reversed this inhibition in both LY294002 and PD-L1 treated cells. (**Figures 6A–C**). These results provide the evidence of involvement of PI3K in the early (3 days) effect of PD-L1 on KCa3.1 activity. Longer exposure to PD-L1 revealed a diminished contribution of PI3K signaling and a role for CaM becomes evident (**Figures 6D,E**). Electrophysiological experiments showed that PI3P only partially restored the KCa3.1 activity of HDs $CD8^+$ PBTs treated with PD-L1 for 5 days (**Figure 6D**). Flow-cytometry data showed that at this time point there was a significance 40% reduction in CaM expression and not KCa3.1. Interestingly, we observed also a selective reduction in Stim1 (the partner protein of Orai1 that forms CRAC channels) (**Figure 6E**). Overall, these findings support a role for PI3P signaling and CaM in mediating the effect of PD-L1/PD-1 interaction on KCa3.1 channels in $CD8^+$ T cells.

DISCUSSION

Resistance to immunotherapy in cancer is attributed to a weak or blunted immune response. Engagement of the immune checkpoint receptor PD-1 by its ligand PD-L1 is part of the immune escape mechanism of cancer cells (Farhood et al., 2019). Herein, we provide evidence of a role for K^+ channels as early regulators of PD-L1/PD-1 mediated suppression of cytotoxic T cells in HNSCC patients.

It is well established that blockade of PD-L1/PD-1 interaction increases T cell function and antitumor immunity (Alsaab et al., 2017). In this study, we report that disruption of PD-L1/PD-1 binding by αPD-1 and αPD-L1 antibodies, rapidly (within 6 h) increased KCa3.1 and Kv1.3 activities in $CD8^+$ PBTs of HNSCC patients. Studies in murine models and human subjects with solid malignancies show that αPD-1 treatment improves T cell activation as indicated by the increased expression of

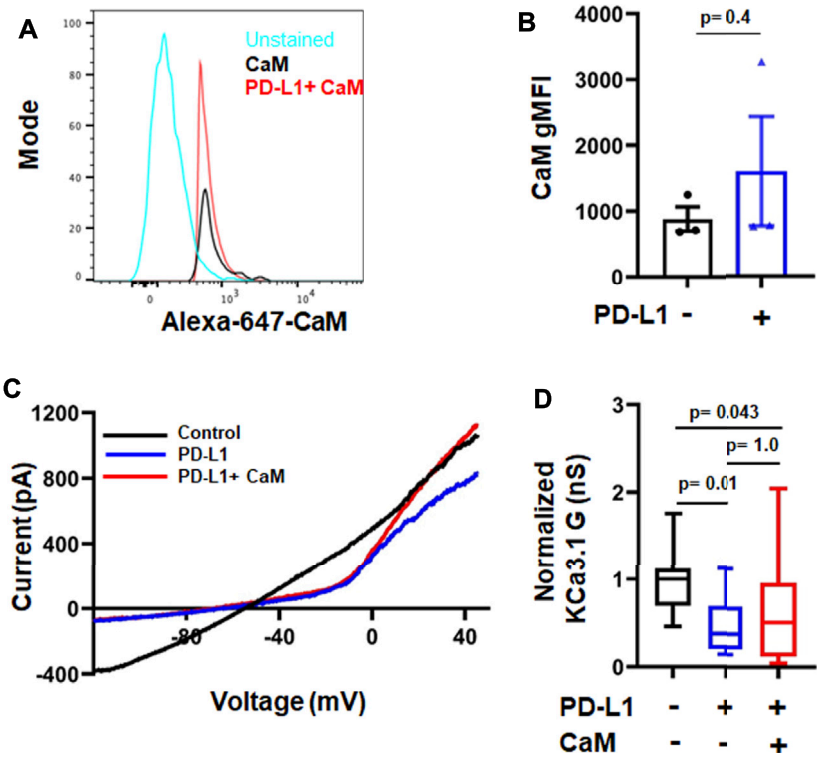

FIGURE 5 | Short-time treatment with PD-L1 decreases KCa3.1 activity in a calmodulin-independent manner. **(A)** Flow cytometry histogram and geometric mean fluorescence intensity (gMFI) values **(B)** for CaM expression in activated $CD8^+$ PBTs from HD donors ($n = 3$) in the absence and presence of PD-L1. **(C)** Representative recordings of KCa3.1 currents in activated $CD8^+$ PBTs from HDs showing the effect of PD-L1 (PD-L1-Fc, 10 μg/ml) and CaM (50 μM). **(D)** Average normalized KCa3.1 conductance (**G**, nS) measured in the absence and presence of PD-L1, with and without CaM. All conductance values are normalized to average conductance value obtained from control recordings. Cells were pre-incubated with plate-bound PD-L1 (PD-L1-Fc,10 μg/ml, for 72 h) activated using anti-CD3/CD28 antibodies and treated with or without CaM (50 μM), that was delivered intracellularly *via* patch pipette during recordings ($n = 15–18$ cells per group from 3 HDs). The values in panel **(B)** are represented as bar graphs. Each symbol represent an individual HD. The values are represented as mean ± SEM. The values in panel **(D)** are represented as box and whisker plots. The lower and upper bound of the box represent 25^{th} and 75^{th} percentiles respectively. Median values are shown as horizontal line. The lower and upper error bars represents 10^{th} and 90^{th} percentile respectively. Data in panel **(B)** were analyzed by *t*-test and data in panel **(D)** were analyzed by ANOVA on ranks ($p = 0.008$) with Dunn's *post hoc* analysis.

activation markers (Peng et al., 2012; Ascierto et al., 2019). Herein, we showed that short treatment with αPD-1 antibody (pembrolizumab) was not sufficient to change the expression of the T cell activation marker CD69, and yet produced changes in the activity of K^+ channels. These data suggest that activation of K^+ channels may be among the earliest changes produced by interruption of PD-1 signaling in $CD8^+$ PBTs of HNSCC patients. We also showed that αPD-1 treatment affected exclusively K^+ channels as it did not alter CRAC channels. Furthermore, the effect of αPD-1 antibody on K^+ channels could not be ascribed to changes in channel protein expression or activation/exhaustion state of T cells as markers of T cell activation and exhaustion and ion channel proteins were all unchanged. This is in agreement with what we observed in T cells from HNSCC patients treated with pembrolizumab (Newton et al., 2020).

A well-established functional consequence of increased KCa3.1 and Kv1.3 activities in T cells is an increase in Ca^{2+} fluxing abilities that is necessary for cytokine production and cytotoxicity (Feske et al., 2012). In the present study, we measured TCR-independent Ca^{2+} fluxes to assess the consequences of the positive effect of αPD-1 treatment on K^+ channel activity. Indeed, we observed that pembrolizumab produces a rapid increase in Ca^{2+} fluxing abilities of $CD8^+$ PBTs in a subset of HNSCC patients. The *in vitro* positive Ca^{2+} response to pembrolizumab was observed in 33% of patients. This response is in line with the objective response reported in a recent clinical trial (KEYNOTE-048) in HNSCC patients (Burtness et al., 2019; Kok, 2020). We also observed that a low baseline Ca^{2+} fluxing ability of $CD8^+$ PBTs from HNSCC patients predicts the response to pembrolizumab. It is possible that HNSCC patients whose T cells display lower Ca^{2+} fluxing abilities *in vitro* had a higher exposure to circulating PD-L1 (either soluble or *via* tumor-derived exosomes) *in vivo*, and they will ultimately benefit the most from αPD-L1 and αPD-1 blockade. An *in vitro* study showed that PD-L1 decreases TCR dependent Ca^{2+} fluxes in a dose dependent manner in human T cells overexpressing the PD-1 receptor (Wei et al., 2013). In agreement with this study, we reported here that PD-L1 inhibits ion channel-dependent Ca^{2+} fluxes in $CD8^+$ T cells. Furthermore, multiple studies have shown that a high PD-L1 expression in

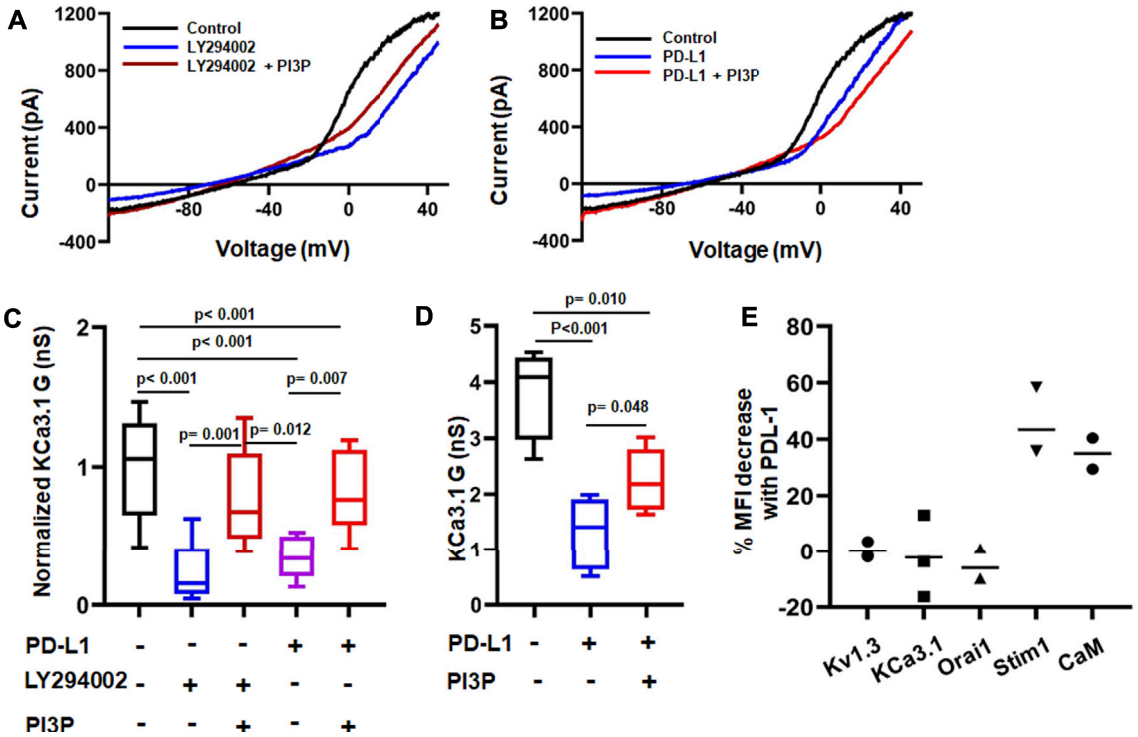

FIGURE 6 | Differential time-dependent involvement of PI3K and calmodulin on PD-L1 mediated inhibition of KCa3.1 channels. **(A,B)** Representative recordings of KCa3.1 channels in activated $CD8^+$ PBTs from HDs showing the effect of the PI3K inhibitor LY294002 (10 μM) +/– phosphatidylinositol-3 phosphatase (PI3P) (100 nM) **(A)** and PD-L1 (PD-L1-Fc, 10 μg/ml) +/– PI3P (100 nM) **(B). (C)** Summary of the pharmacological modulation of KCa3.1 channels byLY294002 and PI3P in the absence and presence of plate bound PD-L1 in activated $CD8^+$ PBTs of HDs. Cells were activated using anti-CD3/CD28 antibodies for 72 h. Cells were perfused with LY294002 for 15 min followed by patch clamp recordings with and without PI3P, delivered intracellularly *via* patch pipette (*n* = eight to nine cells per group from 3 HDs). All KCa3.1 conductance **(G)** values are normalized to the average G of the control group (drug-free). **(D)** KCa3.1 G measured in absence or presence of PD-L1 in activated $CD8^+$ PBTs of HDs. Cells were treated with plate-bound PD-L1 (PD-L1-Fc, 10 μg/ml) and activated using anti-CD3/CD28 antibodies for 120 h PI3P was delivered intracellularly *via* the patch pipette during the electrophysiological experiments (drug-free control). Cells were held at −70 mV, *n* = four to five cells per group from one HD. The values in panel **(C,D)** are represented as box and whiskers plot. The lower and upper bound of the box represent 25^{th} and 75^{th} percentiles respectively. Median values are shown as horizontal line. The lower and upper error bars represents 10^{th} and 90^{th} percentile respectively. **(E)** Percentage change in mean fluorescence intensity (MFI) of ion channels (Kv1.3, KCa3.1, Orai1, Stim1) and Calmodulin (CaM) measured using flow cytometry. Each dot represents an individual HD and the horizontal black line represents the mean value. Data in panel **(C)** were analyzed by One Way ANOVA ($p < 0.001$) followed by Holm-Sidak's *post hoc* analysis. Data in **(D)** were analyzed by One way ANOVA followed by Holm-Sidak's *post hoc* analysis.

cancer cells correlate with a good response to αPD-1/αPDL-1 blocking antibodies (Evrard et al., 2020).

Our data showed that while KCa3.1 and Kv1.3 channels mediate the response to αPD-1 and αPD-L1 antibodies, there may be a difference in sensitivity. Indeed, a higher concentration of αPD-L1 was necessary to unleash Kv1.3 activity in HNSCC T cells. Furthermore, the concentration of PD-L1 activating antibodies (PD-L1-Fc) we used (10 μg/ml) suppressed KCa3.1, but not Kv1.3, currents in $CD8^+$ PBTs of HDs, and, in this setting, αPD-1 antibody increased KCa3.1, but not Kv1.3, conductance. It is possible that inhibition of Kv1.3 requires higher concentrations of PDL-1 and/or a longer exposure. Our earlier observations *in vivo* in HNSCC patients treated with pembrolizumab showed increases KCa3.1, but not Kv1.3, channels activity in $CD8^+$ PBTs shortly after treatment (Newton et al., 2020). The effect of PD-1 blockade on Kv1.3 is only evident a long time after pembrolizumab administration. However, it is also possible that higher levels of PD-L1 may be needed for Kv1.3 inhibition. This could explain what we observed untreated HNSCC patients (Chimote et al., 2018; Newton et al., 2020). We reported low KCa3.1 activity in $CD8^+$ PBTs, which is further reduced in TILs (Chimote et al., 2018; Newton et al., 2020). However, while we did not observe any reduction in Kv1.3 activity in HNSCC circulating T cells, there was a profound suppression of this channel activity/expression in TILs, particularly those in close proximity with cancer cells, (Chimote et al., 2018; Newton et al., 2020) where the levels of PD-L1 are higher than in circulation. Secreted PD-L1 is detected in the plasma of HNSCC patients contributing to reduced T cell function (Zhou et al., 2020). While we showed that $CD8^+$ PBTs express PD-L1, we do not know the PD-L1 levels in our cell cultures and how they compare with those of PD-L1-Fc used in our experiments. The presence of T cell generated PD-L1 (endogenous PD-L1) explains the response to αPD-1 and αPD-L1 antibodies without pre-treatment with PD-L1-Fc (**Figures 1**, **3**). It is very likely that PD-L1-Fc is in addition to the endogenous PD-L1. This explains why αPD-1 brings the Ca^{2+} response of PD-L1-Fc treated cells to levels higher than

"untreated" cells that are exposed to the endogenous PD-L1 (**Figure 4B**).

The high sensitivity of KCa3.1 to PD-L1 may be explained by the mechanisms by which PD-1 regulates this channel which imply a fast kinase-mediated signaling event. We observed that the response of KCa3.1 channels to PD-1 ligation is mediated by PI3K-PI3P signaling and that this is the earliest pathway engaged. CaM downregulation follows in time. In T cells, activation of TCR signaling cascade leads to activation of PI3K/Akt [phosphatidylinositol 3-kinase (PI3K) and Akt/Protein Kinase B)], while ligation of PD-1 results in a decrease in TCR proximal signaling through inhibition of PI3K activity (Seidel et al., 2018). PI3K has also been implicated in KCa3.1 regulation (Ohya and Kito, 2018). KCa3.1 channels have a histidine residue (H358) in the carboxy-terminus whose phosphorylation is regulated by PI3K, PI3P and NDPK-B kinase (Srivastava et al., 2006b; Srivastava et al., 2009; Srivastava et al., 2016). KCa3.1 channels in healthy human $CD4^+$ T cells are inhibited by the non-selective PI3K blocker LY294002, while PI3P (whose formation from PI is facilitated by PI3K) reverses this inhibition (Srivastava et al., 2006a). NDPK-B (the enzyme mediating PI3P effect on KCa3.1) knock-down decreases KCa3.1 without affecting the activity of Kv1.3 (Srivastava et al., 2006b). Similarly, in this study we showed that PD-L1-Fc at the concentration we used only inhibited KCa3.1, that this effect was reproduced by LY294002, and reversed by PI3P. While the PI3K/PI3P signaling pathway is the dominant regulatory mechanism early upon PD-1 ligation, a reduction in CaM expression contributes to reduced KCa3.1 activity later on. CaM serves as binding partner and intracellular Ca^{2+} sensor for KCa3.1 allowing the activation of this Ca^{2+}-dependent channel (Cahalan and Chandy, 2009; Sforna et al., 2018). We have recently reported that membrane CaM levels are downregulated in activated $CD8^+$ T cells of HNSCC patients (Chimote et al., 2020). In this study, the long-term effect of PD-1 ligation in healthy $CD8^+$ T cells is a decrease in CaM expression. CaM downregulation is not contributing to KCa3.1 suppression at earlier time points as indicated by the lack of effect of intracellular supplementation of CaM on KCa3.1 channels in PBTs of HDs treated for 72 h with PD-L1-Fc. At this stage, it is not clear if there is a correlation between PI3K and CaM. However, it is possible that the decrease in Ca^{2+} fluxing abilities that follows the reduction in KCa3.1 by PI3K inhibition may lead to reduced CaM. It has been reported that CaM gene expression is regulated by Ca^{2+} (Bosch et al., 1994).

Overall, our *in vitro* studies showed that αPD-1 induces an increase in Kv1.3, KCa3.1 and Ca^{2+} fluxing that ultimately will lead to improved anti-tumor response. Ca^{2+} signaling in fact regulates multiple effector functions of T cells, including the production of cytokines like IL-2 and IFN-γ, and cytotoxicity (Feske et al., 2003). These are highly desirable anti-tumor functions. In agreement with the studies presented here, we have recently reported that *in vivo* administration of αPD-1 blockade followed by surgical resection increases Ca^{2+} fluxing abilities of $CD8^+$ T cells by increasing the KCa3.1 and Kv1.3 channel function in head and neck cancer patients (Newton et al., 2020). Furthermore, a recent report on combination of immune checkpoint inhibitors, anti-PD-1 and anti-LAG-3 antibodies, showed significant increase in peak Ca^{2+} levels of T cells resulting in increased cytotoxicity (Sullivan et al., 2020).

In conclusion, the data presented in this manuscript highlight the crucial role of K^+ channels as early modulators of PD-1 signaling and point to them as therapeutic targets in restoring anti-tumor immunity in HNSCC patients. This study paves the way for further investigations about new therapeutic strategies in cancer that incorporate K^+ channel activators along with immune checkpoint inhibitors.

DATA AVAILABILITY STATEMENT

The original contributions presented in the study are included in the article/**Supplementary Material**, further inquiries can be directed to the corresponding author/s.

ETHICS STATEMENT

The studies involving human participants were reviewed and approved by University of Cincinnati Institutional Review Board (IRB no. 2014-4755). The patients/participants provided their written informed consent to participate in this study.

AUTHOR CONTRIBUTIONS

Conceptualization and design: LC, and VG Development of Methodology: VG, AC and MF-G, Formal analysis: VG, and AC Investigation: VG, AC, HN, MC, and MF-G. Resources: MC, MF-G, and HN. Writing (original draft): VG, and LC. Writing (review and editing): VG, AC, and LC Visualization: VG, AC, and MF-G Supervision: LC Project administration: VG, EJ, TW-D, and LC. Funding acquisition: LC, EJ, and TW-D. All authors discussed the results and commented on the manuscript.

FUNDING

This work was supported by the Office of the Assistant Secretary of Defense for Health Affairs, through the Peer Reviewed Cancer Research Program, under Award No W81XWH-17-1-0374 (LC, TW-D, and EJ). Opinions, interpretations, conclusions and recommendations are those of the authors and are not necessarily endorsed by the Department of Defense. The United States Army Medical Research Acquisition Activity, Fort Detrick, Maryland is the awarding and administering acquisition office. Additional funding was provided by the National Institutes of Health (grant R01-CA95286) to LC. HN was supported by NIH training grant T32 CA117846.

ACKNOWLEDGMENTS

We would like to acknowledge the clinical coordinators (Bethany Fuhrman and Shireen Desai) for their assistance in patient sample collection (Clinical Trials Office, University of Cincinnati Cancer

Center). All flow cytometry data were acquired using equipment maintained by the Research Flow Cytometry Core (Division of Rheumatology) at Cincinnati Children's Hospital Medical Center and Shriners Hospital for Children Flow Cytometry Core, Cincinnati, OH.

SUPPLEMENTARY MATERIAL

The Supplementary Material for this article can be found online at: https://www.frontiersin.org/articles/10.3389/fphar.2021.742862/full#supplementary-material

REFERENCES

Alsaab, H. O., Sau, S., Alzhrani, R., Tatiparti, K., Bhise, K., Kashaw, S. K., et al. (2017). PD-1 and PD-L1 Checkpoint Signaling Inhibition for Cancer Immunotherapy: Mechanism, Combinations, and Clinical Outcome. *Front. Pharmacol.* 8, 561. doi:10.3389/fphar.2017.00561

Ascierto, P. A., Bifulco, C., Buonaguro, L., Emens, L. A., Ferris, R. L., Fox, B. A., et al. (2019). Perspectives in Immunotherapy: Meeting Report from the "Immunotherapy Bridge 2018" (28-29 November, 2018, Naples, Italy). *J. Immunother. Cancer* 7 (1), 332. doi:10.1186/s40425-019-0798-3

Bauml, J. M., Aggarwal, C., and Cohen, R. B. (2019). Immunotherapy for Head and Neck Cancer: where Are We Now and where Are We Going? *Ann. Transl. Med.* 7 (Suppl. 3), S75. doi:10.21037/atm.2019.03.58

Bosch, M., López-Girona, A., Bachs, O., and Agell, N. (1994). Protein Kinase C Regulates Calmodulin Expression in NRK Cells Activated to Proliferate from Quiescence. *Cell Calcium* 16 (6), 446–454. doi:10.1016/0143-4160(94)90074-4

Burtness, B., Harrington, K. J., Greil, R., Soulières, D., Tahara, M., de Castro, G., Jr., et al. (2019). Pembrolizumab Alone or with Chemotherapy versus Cetuximab with Chemotherapy for Recurrent or Metastatic Squamous Cell Carcinoma of the Head and Neck (KEYNOTE-048): a Randomised, Open-Label, Phase 3 Study. *Lancet* 394 (10212), 1915–1928. doi:10.1016/s0140-6736(19)32591-7

Cahalan, M. D., and Chandy, K. G. (2009). The Functional Network of Ion Channels in T Lymphocytes. *Immunol. Rev.* 231 (1), 59–87. doi:10.1111/j.1600-065X.2009.00816.x

Chapon, M., Randriamampita, C., Maubec, E., Badoual, C., Fouquet, S., Wang, S. F., et al. (2011). Progressive Upregulation of PD-1 in Primary and Metastatic Melanomas Associated with Blunted TCR Signaling in Infiltrating T Lymphocytes. *J. Invest. Dermatol.* 131 (6), 1300–1307. doi:10.1038/jid.2011.30

Chimote, A. A., Balajthy, A., Arnold, M. J., Newton, H. S., Hajdu, P., Qualtieri, J., et al. (2018). A Defect in KCa3.1 Channel Activity Limits the Ability of CD8+ T Cells from Cancer Patients to Infiltrate an Adenosine-Rich Microenvironment. *Sci. Signal.* 11 (527), eaaq1616. doi:10.1126/scisignal.aaq1616

Chimote, A. A., Gawali, V. S., Newton, H. S., Wise-Draper, T. M., and Conforti, L. (2020). A Compartmentalized Reduction in Membrane-Proximal Calmodulin Reduces the Immune Surveillance Capabilities of CD8+ T Cells in Head and Neck Cancer. *Front. Pharmacol.* 11, 143. doi:10.3389/fphar.2020.00143

Chimote, A. A., Hajdu, P., Kottyan, L. C., Harley, J. B., Yun, Y., and Conforti, L. (2016). Nanovesicle-targeted Kv1.3 Knockdown in Memory T Cells Suppresses CD40L Expression and Memory Phenotype. *J. Autoimmun.* 69, 86–93. doi:10.1016/j.jaut.2016.03.004

Chimote, A. A., Hajdu, P., Kucher, V., Boiko, N., Kuras, Z., Szilagyi, O., et al. (2013). Selective Inhibition of KCa3.1 Channels Mediates Adenosine Regulation of the Motility of Human T Cells. *J. Immunol.* 191 (12), 6273–6280. doi:10.4049/jimmunol.1300702

Chimote, A. A., Hajdu, P., Sfyris, A. M., Gleich, B. N., Wise-Draper, T., Casper, K. A., et al. (2017). Kv1.3 Channels Mark Functionally Competent CD8+ Tumor-Infiltrating Lymphocytes in Head and Neck Cancer. *Cancer Res.* 77 (1), 53–61. doi:10.1158/0008-5472.CAN-16-2372

Chow, L. Q. M. (2020). Head and Neck Cancer. *N. Engl. J. Med.* 382 (1), 60–72. doi:10.1056/NEJMra1715715

Evrard, D., Hourseau, M., Couvelard, A., Paradis, V., Gauthier, H., Raymond, E., et al. (2020). PD-L1 Expression in the Microenvironment and the Response to Checkpoint Inhibitors in Head and Neck Squamous Cell Carcinoma. *Oncoimmunology* 9 (1), 1844403. doi:10.1080/2162402X.2020.1844403

Farhood, B., Najafi, M., and Mortezaee, K. (2019). CD8+ Cytotoxic T Lymphocytes in Cancer Immunotherapy: A Review. *J. Cel. Physiol.* 234 (6), 8509–8521. doi:10.1002/jcp.27782

Feske, S., Gwack, Y., Prakriya, M., Srikanth, S., Puppel, S. H., Tanasa, B., et al. (2006). A Mutation in Orai1 Causes Immune Deficiency by Abrogating CRAC Channel Function. *Nature* 441 (7090), 179–185. doi:10.1038/nature04702

Feske, S., Okamura, H., Hogan, P. G., and Rao, A. (2003). Ca2+/calcineurin Signalling in Cells of the Immune System. *Biochem. Biophys. Res. Commun.* 311 (4), 1117–1132. doi:10.1016/j.bbrc.2003.09.174

Feske, S., Skolnik, E. Y., and Prakriya, M. (2012). Ion Channels and Transporters in Lymphocyte Function and Immunity. *Nat. Rev. Immunol.* 12 (7), 532–547. doi:10.1038/nri3233

Feske, S., Wulff, H., and Skolnik, E. Y. (2015). Ion Channels in Innate and Adaptive Immunity. *Annu. Rev. Immunol.* 33, 291–353. doi:10.1146/annurev-immunol-032414-112212

Kok, V. C. (2020). Current Understanding of the Mechanisms Underlying Immune Evasion from PD-1/pd-L1 Immune Checkpoint Blockade in Head and Neck Cancer. *Front. Oncol.* 10, 268. doi:10.3389/fonc.2020.00268

Newton, H. S., Gawali, V. S., Chimote, A. A., Lehn, M. A., Palackdharry, S. M., Hinrichs, B. H., et al. (2020). PD1 Blockade Enhances K+ Channel Activity, Ca2+ Signaling, and Migratory Ability in Cytotoxic T Lymphocytes of Patients with Head and Neck Cancer. *J. Immunother. Cancer* 8 (2), e000844. doi:10.1136/jitc-2020-000844

Ohya, S., and Kito, H. (2018). Ca2+-Activated K+ Channel KCa3.1 as a Therapeutic Target for Immune Disorders. *Biol. Pharm. Bull.* 41 (8), 1158–1163. doi:10.1248/bpb.b18-00078

Patsoukis, N., Li, L., Sari, D., Petkova, V., and Boussiotis, V. A. (2013). PD-1 Increases PTEN Phosphatase Activity while Decreasing PTEN Protein Stability by Inhibiting Casein Kinase 2. *Mol. Cel. Biol.* 33 (16), 3091–3098. doi:10.1128/MCB.00319-13

Peng, W., Liu, C., Xu, C., Lou, Y., Chen, J., Yang, Y., et al. (2012). PD-1 Blockade Enhances T-Cell Migration to Tumors by Elevating IFN-γ Inducible Chemokines. *Cancer Res.* 72 (20), 5209–5218. doi:10.1158/0008-5472.Can-12-1187

Robbins, J. R., Lee, S. M., Filipovich, A. H., Szigligeti, P., Neumeier, L., Petrovic, M., et al. (2005). Hypoxia Modulates Early Events in T Cell Receptor-Mediated Activation in Human T Lymphocytes via Kv1.3 Channels. *J. Physiol.* 564 (Pt 1), 131–143. doi:10.1113/jphysiol.2004.081893

Seidel, J. A., Otsuka, A., and Kabashima, K. (2018). Anti-PD-1 and Anti-CTLA-4 Therapies in Cancer: Mechanisms of Action, Efficacy, and Limitations. *Front. Oncol.* 8, 86. doi:10.3389/fonc.2018.00086

Sforna, L., Megaro, A., Pessia, M., Franciolini, F., and Catacuzzeno, L. (2018). Structure, Gating and Basic Functions of the Ca2+-Activated K Channel of Intermediate Conductance. *Curr. Neuropharmacol.* 16 (5), 608–617. doi:10.2174/1570159x15666170830122402

Sharma, P., Hu-Lieskovan, S., Wargo, J. A., and Ribas, A. (2017). Primary, Adaptive, and Acquired Resistance to Cancer Immunotherapy. *Cell* 168 (4), 707–723. doi:10.1016/j.cell.2017.01.017

Srivastava, S., Choudhury, P., Li, Z., Liu, G., Nadkarni, V., Ko, K., et al. (2006a). Phosphatidylinositol 3-phosphate Indirectly Activates KCa3.1 via 14 Amino Acids in the Carboxy Terminus of KCa3.1. *Mol. Biol. Cel.* 17 (1), 146–154. doi:10.1091/mbc.e05-08-0763

Srivastava, S., Di, L., Zhdanova, O., Li, Z., Vardhana, S., Wan, Q., et al. (2009). The Class II Phosphatidylinositol 3 Kinase C2beta Is Required for the Activation of the K+ Channel KCa3.1 and CD4 T-Cells. *Mol. Biol. Cel.* 20 (17), 3783–3791. doi:10.1091/mbc.e09-05-0390

Srivastava, S., Li, Z., Ko, K., Choudhury, P., Albaqumi, M., Johnson, A. K., et al. (2006b). Histidine Phosphorylation of the Potassium Channel KCa3.1 by Nucleoside Diphosphate Kinase B Is Required for Activation of KCa3.1 and CD4 T Cells. *Mol. Cel.* 24 (5), 665–675. doi:10.1016/j.molcel.2006.11.012

Srivastava, S., Li, Z., Lin, L., Liu, G., Ko, K., Coetzee, W. A., et al. (2005). The Phosphatidylinositol 3-phosphate Phosphatase Myotubularin- Related Protein 6

(MTMR6) Is a Negative Regulator of the Ca2+-Activated K+ Channel KCa3.1. *Mol. Cel. Biol.* 25 (9), 3630–3638. doi:10.1128/mcb.25.9.3630-3638.2005

Srivastava, S., Panda, S., Li, Z., Fuhs, S. R., Hunter, T., Thiele, D. J., et al. (2016). Histidine Phosphorylation Relieves Copper Inhibition in the Mammalian Potassium Channel KCa3.1. *Elife* 5, e16093. doi:10.7554/eLife.16093

Succaria, F., Kvistborg, P., Stein, J. E., Engle, E. L., McMiller, T. L., Rooper, L. M., et al. (2020). Characterization of the Tumor Immune Microenvironment in Human Papillomavirus-Positive and -negative Head and Neck Squamous Cell Carcinomas. *Cancer Immunol. Immunother.* 70, 1227–1237. doi:10.1007/s00262-020-02747-w

Sullivan, M. R., Ugolini, G. S., Sarkar, S., Kang, W., Smith, E. C., McKenney, S., et al. (2020). Quantifying the Efficacy of Checkpoint Inhibitors on CD8+ Cytotoxic T Cells for Immunotherapeutic Applications via Single-Cell Interaction. *Cell Death Dis.* 11 (11), 979. doi:10.1038/s41419-020-03173-7

Sung, H., Ferlay, J., Siegel, R. L., Laversanne, M., Soerjomataram, I., Jemal, A., et al. (2021). Global Cancer Statistics 2020: GLOBOCAN Estimates of Incidence and Mortality Worldwide for 36 Cancers in 185 Countries. *CA A. Cancer J. Clin.* 71, 209–249. doi:10.3322/caac.21660

Theodoraki, M. N., Yerneni, S. S., Hoffmann, T. K., Gooding, W. E., and Whiteside, T. L. (2018). Clinical Significance of PD-L1+ Exosomes in Plasma of Head and Neck Cancer Patients. *Clin. Cancer Res.* 24 (4), 896–905. doi:10.1158/1078-0432.Ccr-17-2664

Vaeth, M., Yang, J., Yamashita, M., Zee, I., Eckstein, M., Knosp, C., et al. (2017). ORAI2 Modulates Store-Operated Calcium Entry and T Cell-Mediated Immunity. *Nat. Commun.* 8, 14714. doi:10.1038/ncomms14714

Wei, F., Zhong, S., Ma, Z., Kong, H., Medvec, A., Ahmed, R., et al. (2013). Strength of PD-1 Signaling Differentially Affects T-Cell Effector Functions. *Proc. Natl. Acad. Sci. U S A.* 110 (27), E2480–E2489. doi:10.1073/pnas.1305394110

Zhou, J., Mahoney, K. M., Giobbie-Hurder, A., Zhao, F., Lee, S., Liao, X., et al. (2017). Soluble PD-L1 as a Biomarker in Malignant Melanoma Treated with Checkpoint Blockade. *Cancer Immunol. Res.* 5 (6), 480–492. doi:10.1158/2326-6066.Cir-16-0329

Zhou, K., Guo, S., Li, F., Sun, Q., and Liang, G. (2020). Exosomal PD-L1: New Insights into Tumor Immune Escape Mechanisms and Therapeutic Strategies. *Front. Cel. Dev. Biol.* 8, 569219. doi:10.3389/fcell.2020.569219

Conflict of Interest: The authors declare that the research was conducted in the absence of any commercial or financial relationships that could be construed as a potential conflict of interest.

Publisher's Note: All claims expressed in this article are solely those of the authors and do not necessarily represent those of their affiliated organizations, or those of the publisher, the editors and the reviewers. Any product that may be evaluated in this article, or claim that may be made by its manufacturer, is not guaranteed or endorsed by the publisher.

frontiers in Pharmacology

ORIGINAL RESEARCH
published: 23 September 2021
doi: 10.3389/fphar.2021.714841

Kv1.3 Channel Up-Regulation in Peripheral Blood T Lymphocytes of Patients With Multiple Sclerosis

*Ioannis Markakis[1,2†], Ioannis Charitakis[1†], Christine Beeton[3,4†], Melpomeni Galani[1], Elpida Repousi[1,2], Stella Aggeloglou[2], Petros P. Sfikakis[1], Michael W. Pennington[5], K. George Chandy[3,6] and Cornelia Poulopoulou[1]**

[1]National and Kapodistrian University of Athens, Medical School, Athens, Greece, [2]Department of Neurology, "St. Panteleimon" General State Hospital, Nikaia, Greece, [3]Department of Physiology and Biophysics, University of California, Irvine, Irvine, CA, United States, [4]Department of Molecular Physiology and Biophysics, Baylor College of Medicine, Houston, TX, United States, [5]Ambiopharm, Inc., North Augusta, SC, United States, [6]Lee Kong Chian School of Medicine, Nanyang Technological University, Nanyang Ave, Singapore

OPEN ACCESS

Edited by:
Péter Béla Hajdu, University of Debrecen, Hungary

Reviewed by:
Andrea Olschewski, Medical University of Graz, Austria
Hubert Hannes Kerschbaum, University of Salzburg, Austria
Ameet A. Chimote, University of Cincinnati, United States

***Correspondence:**
Cornelia Poulopoulou
cpoulop@med.uoa.gr

†These authors have contributed equally to this work and share first authorship

Specialty section:
This article was submitted to Pharmacology of Ion Channels and Channelopathies, a section of the journal Frontiers in Pharmacology

Received: *26 May 2021*
Accepted: *09 September 2021*
Published: *23 September 2021*

Citation:
Markakis I, Charitakis I, Beeton C, Galani M, Repousi E, Aggeloglou S, Sfikakis PP, Pennington MW, Chandy KG and Poulopoulou C (2021) Kv1.3 Channel Up-Regulation in Peripheral Blood T Lymphocytes of Patients With Multiple Sclerosis. Front. Pharmacol. 12:714841. doi: 10.3389/fphar.2021.714841

Voltage-gated Kv1.3 potassium channels are key regulators of T lymphocyte activation, proliferation and cytokine production, by providing the necessary membrane hyperpolarization for calcium influx following immune stimulation. It is noteworthy that an accumulating body of *in vivo* and *in vitro* evidence links these channels to multiple sclerosis pathophysiology. Here we studied the electrophysiological properties and the transcriptional and translational expression of T lymphocyte Kv1.3 channels in multiple sclerosis, by combining patch clamp recordings, reverse transcription polymerase chain reaction and flow cytometry on freshly isolated peripheral blood T lymphocytes from two patient cohorts with multiple sclerosis, as well as from healthy and disease controls. Our data demonstrate that T lymphocytes in MS, manifest a significant up-regulation of Kv1.3 mRNA, Kv1.3 membrane protein and Kv1.3 current density and therefore of functional membrane channel protein, compared to control groups ($p < 0.001$). Interestingly, patient sub-grouping shows that Kv1.3 channel density is significantly higher in secondary progressive, compared to relapsing-remitting multiple sclerosis ($p < 0.001$). Taking into account the tight connection between Kv1.3 channel activity and calcium-dependent processes, our data predict and could partly explain the reported alterations of T lymphocyte function in multiple sclerosis, while they highlight Kv1.3 channels as potential therapeutic targets and peripheral biomarkers for the disease.

Keywords: T cells, potassium channels, Kv1.3, multiple sclerosis, patch clamp, calcium regulation

INTRODUCTION

Multiple sclerosis (MS) is a chronic autoimmune disorder of the central nervous system (CNS), characterized by white matter demyelination and intense perivascular infiltration by macrophages and auto-reactive T cells (Lassmann, 2004; Goverman, 2009; Gourraud et al., 2012) that migrate into the CNS and initiate myelin destruction, following their activation in the peripheral blood (PB) (Goverman, 2009; Severson and Hafler, 2010). With T cell activation being central in MS pathophysiology (Zhang et al., 1994), cellular components that control this process are of great importance and investigations concerning their expression and function could help the understanding of disease pathogenesis and the development of effective therapies.

Particularly relevant molecules in this context are the voltage-gated Kv1.3 channels, the main potassium conductance of T cells at rest and during the initial steps of their activation (Wulff et al., 2003; Cahalan and Chandy, 2009). Most importantly, these channels are part of the signalosome that clusters at the immunological synapse during antigenic stimulation (Panyi et al., 2003; Panyi et al., 2004), serving as key regulators of the calcium signaling required for cellular homeostasis and T cell activation. The activity of Kv1.3 channels, during the early events of T cell antigenic stimulation, determines the degree of membrane hyperpolarization and therefore the strength of the electrochemical driving force necessary for extracellular calcium entry into the cell via the calcium release activated calcium (CRAC) channels, the main calcium conductance of T cell plasma membrane (Cahalan and Chandy, 2009). Thus, Kv1.3 channel activity plays a central role in regulating the magnitude and duration of calcium responses during the initial steps of T cell activation and subsequently determines T cell fate and function (Lewis, 2001; Malissen and Bongrand, 2015).

Aside from their key role in T cell physiology, the interest in Kv1.3 channels in MS is further corroborated by a wealth of data associating these channels with the pathophysiology of the disease. Kv1.3 channels are up-regulated in activated effector memory T cells (T_{EM} cells) (Wulff et al., 2003; Cahalan and Chandy, 2009), a subset enriched in the myelin-specific T cell pool of MS patients. These cells specifically up-regulate Kv1.3 and not KCa3.1 channels, and are characterized as $Kv1.3^{high}KCa3.1^{low}$ (1,500 Kv1.3/cell and 50 KCa3.1/cell) (Wulff et al., 2003; Cahalan and Chandy, 2009). Interestingly, while quiescent myelin-specific T cells are present in the PB of both healthy individuals and MS patients (Zhang et al., 1994), activated $Kv1.3^{high}KCa3.1^{low}$ myelin-specific T_{EM} cells are only present in the PB of MS patients (Wulff et al., 2003). Additionally, inflammatory infiltrates in the lesions of MS brains are enriched in T_{EM} cells of the $Kv1.3^{high}$ phenotype (Rus et al., 2005). The role of Kv1.3 channels in MS is further strengthened by reports showing that Kv1.3-selective blockers (Beeton et al., 2001; Beeton et al., 2006) and genetic knockout of Kv1.3 (Gocke et al., 2012), ameliorate disease in animal models of multiple sclerosis. Furthermore, a recent genetic study (Lioudyno et al., 2021) identified a link between a gain-of-function polymorphic allele of the Kv1.3 gene and rapid disease progression, more severe disease phenotype and increased PB $CXCR3^+$ T_{EM} cells in MS patients.

Herein, we used a combination of patch clamp, flow cytometry and semi-quantitative PCR to study Kv1.3 channels in freshly isolated, unsorted, un-manipulated, non-cultured T cells from the PB of MS patients, patients with other neurological disorders (OND), patients with other inflammatory neurological disorders (OIND), patients with clinical isolated syndrome (CIS) and healthy controls with similar demographic characteristics. Our data demonstrate that resting T cells of patients with relapsing-remitting (RRMS) and secondary progressive MS (SPMS) manifest a significant increase in Kv1.3 expression, compared to healthy and disease controls. Moreover, it is shown, for the first time to our knowledge, that T cells from SPMS patients, express significantly higher numbers of functional Kv1.3 channels, compared to RRMS. Our findings suggest that Kv1.3 may serve as a useful peripheral biomarker for the disease, and support the use of Kv1.3 channel inhibitors for the treatment of MS and especially for SPMS, where treatment options are limited.

MATERIALS AND METHODS

Patients and Controls- Greek Cohort

Study protocol had received prior approval by the Scientific and Ethics committee of St Panteleimon General State Hospital of Nikaia. Patients came from either the outpatient department or the neurological clinic of the above Hospital; Informed consent for blood sample collection as well as for clinical and demographic data use was obtained from all participating subjects.

Our study included 38 patients with definite MS according to the McDonald criteria (Thompson et al., 2018); twenty had relapsing-remitting and 18 secondary progressive disease. MS subtypes were defined according to clinical phenotypes (Lublin et al., 2014); a minimum of 12 months of gradual worsening was required to define SPMS. Nineteen (11 RRMS, 8 SPMS) patients were receiving immunomodulatory treatment during enrollment. Disability was measured using the Expanded Disability Status Scale (EDSS). All patients were enrolled in the Neurology department of St. Panteleimon General Hospital of Nikaia. Exclusion criteria comprised: evidence of MS relapse or corticosteroid treatment within the previous 30 days, active systemic bacterial, viral or fungal infection, coexisting systemic autoimmune disease, a history or presence of malignancy. Twenty-one healthy controls with similar demographic characteristics and similar exclusion criteria were also included. Additionally, 31 patients were enrolled as neurological controls: 16 patients with other neurological disorders (OND), 9 patients with other inflammatory neurological disorders (OIND) and 6 with clinical isolated syndrome (CIS) (**Table 1**).

Patients and Controls–US Cohort

In a previous study, we analyzed peripheral blood T cells from unrelated, non-Hispanic Caucasians with clinically definite MS. Patients were obtained from the MS clinic at the University of California Irvine; age- and sex-matched healthy controls were also included in the study (Mkhikian et al., 2011). Here, archived residual peripheral blood T cells from that study (9 MS patients and 22 healthy individuals) (**Table 2**) were used for flow cytometry to characterize cell surface $K_V1.3$ expression.

Cell Preparation

Mononuclear cells were isolated from heparinized whole blood by Ficoll-Hypaque density gradient centrifugation (Boyum, 1968). The isolated buffy coat was washed 3X with PBS without Ca^{2+} and re-suspended in RPMI 1640 culture medium and monocytes ($CD14^+$ cells) and B cells ($CD19^+$) were depleted by the use of magnetic beads (Dynabeads CD14 and CD19 ThermoFisher). The isolated T cells were separated into two pools: one for electrophysiology experiments on the same day of isolation and the second for RNA isolation.

TABLE 1 | Characteristics of multiple sclerosis (MS) patients and controls. Greek cohort of MS patients and controls. *CIS*: Clinically Isolated Syndrome (3 optic neuropathy, 3 transverse myelitis). *OND*: Other Neurological Disorders (3 early-onset Alzheimer's disease, 3 early-onset Parkinson's disease, 2 motor neuron disease, 3 ischemic stroke, four epileptic seizures, one Vitamin B12 deficiency). *OIND*: Other Inflammatory Neurological Disorders (2 limbic encephalopathy, five acute lymphocytic meningitis, one lupus-associated myelopathy, one neuro-Behçet syndrome). Values are expressed as means ± SD.

Disease	*n*	Sex (M/F)	Age (years)	Treated/untreated	Disease duration (years)	EDSS
MS	38	16/22	37.2 ± 7.4	26/12	8.5 ± 5.7	3.5 ± 1.8
Relapsing remitting	20	10/11	36.2 ± 7.2	13/7	6.7 ± 4.8	2 ± 1.2
Secondary progressive	18	7/11	38.4 ± 7.6	13/5	10.9 ± 5.8	4.83 ± 1.3
CIS	6	2/4	38.5 ± 3.8	2/4	2.8 ± 1.5	1.5 ± 1.4
OND	16	9/7	40.9 ± 10.8	—	—	—
OIND	9	5/4	39.6 ± 4.2	9/0	1,3 ± 0,8	—
Healthy controls	21	10/11	38.1 ± 8	—	—	—

TABLE 2 | Characteristics of multiple sclerosis (MS) patients and controls. North American Cohort of MS patients. *ND*: Non-disclosed, *FH:* Family History; *AID:* Autoimmune Disease; *AITD*: autoimmune thyroid disease.

Patient ID	Age	Gender	MS type	FH of AID	Rx
Pa1	35	F	RR MS	No	No
Pa2	51	M	RR MS	No	No
Pa3	46	F	RR MS	MS	No
Pa4	ND	F	RR MS	ND	No
Pa5	75	F	SP MS	MS	No
Pa6	40	M	PP MS	No	No
Pa8	48	F	RR MS	No	No
Pa11	47	F	MS	ND	?
PaJ	67	F	PP MS	MS, AITD	No

Solutions

The standard extracellular solution used in patch clamp experiments contained 135 mM NaCl, 5mM KCl, 1 mM $CaCl_2$,1 mM $MgCl_2$, and 10 mM HEPES, pH 7.4; osmolality, 280 mOsmol/kg). The standard pipette solution was composed of 100 mM KCl, 40 mM KF, 1 mM $CaCl_2$, 1 mM $MgCl_2$, 10 mM EGTA, and 10 mM HEPES, pH 7.4; osmolality, 290 mOsmol/kg), having low calcium concentrations, well below the K_{Ca} channel activation threshold (Poulopoulou et al., 2008). Pipettes were filled with solutions filtered through a 0.22 μm-syringe filter (Thermo Scientific). Modified solutions were also used in some experiments and their composition is stated in the text.

Electrophysiological Recordings

All patch clamp experiments were performed in the whole-cell configuration. We focused on patch clamping small size (resting) T cells (average cell capacitance 1.6 pF) and avoided the enlarged ones. Membrane currents were measured in the whole-cell configuration of the patch clamp technique, as previously described (Poulopoulou et al., 2005a). Membrane currents were corrected for liquid junction potentials. Pipettes were fabricated from R-series Borosilicate Glass Capillaries (World Precision Instruments, Sarasota, FL) using a two-stage puller (L/M-3P-A; List Medical) and had resistances between 3 and 5 MΩ. All experiments were performed at room temperature (20–25°C). Currents were low-pass filtered at 2 kHz. Kv1.3 currents were recorded in response to 150 ms voltage ramps from −100 to +100 mV, out of a holding potential of −90 mV. Peak currents were also measured from the same holding potential, in response to 1000-ms voltage-steps from −80 to +40 mV, in 15 mV increments, given every 60 s, and conductance-to-voltage curves (g-V) were constructed using the chord equation (Hille, 2001). The voltage dependence of steady-state inactivation was estimated by clamping the cell membrane at -90 mV and then stepping to various pre-pulse potentials (−120 to 0 mV, in 15-mV increments) for 100 s and then to a test pulse of +40 mV for 100 ms. Current measurements were performed using the pClamp software (Axon Instruments). The majority of T cells studied were resting T cells (cell capacitance 1.6 pF). To normalize for cell size, we determined channel density/μm^2 of cell surface area, by dividing the average channel number/cell by the average cell surface area, determined from cell capacitance measurements (1 pF = 100 μm^2). Data were further analyzed using Origin technical graphics and data analysis program (OriginLab Corp., Northampton, MA). Peak conductance-to-voltage and steady-state inactivation curves were fitted to Boltzmann functions. Kinetic parameters were calculated by fitting whole-cell currents to the Hodgkin-Huxley n4 j kinetic model (Cahalan, et al., 1985).

RNA Preparation, Reverse Transcription, and Polymerase Chain Reaction

Total RNA isolation and cDNA synthesis were performed as follows (Poulopoulou et al., 2005b): 1 μl of cDNA synthesized by 2 μg of total RNA, extracted using the RNAeasy kit (Qiagen, Chatsworth, CA) following the manufacturer's instructions. The PCR amplification was performed in a final volume of 50 μl (1xPCR Buffer, 200 μl of each dNTP, 25 pmol of each primer and 2.5 μl of HotStarTaq DNA Polymerase (Qiagen). All samples used had produced negative results when total RNA was used instead of cDNA, confirming the absence of DNA contamination from the sample. The efficacy and the integrity of the cDNA in all our samples were assessed by the amplification of the housekeeping gene glyceraldehyde-3-phosphate dehydrogenase (GAPDH). The initial denaturation step of the PCR was performed at 94°C for 15 min followed by 35 cycles at 94°C

for 1 min for Kv1.3, TASK-2 and KCa3.1 gene and 30 cycles for GAPDH gene, at the appropriate annealing temperature (54° C for all four genes) for 1 min and at 72°C for 1 min. The last cycle was followed by a final extension step at 72°C for 10 min. The PCR products were subjected to electrophoresis in 1.5 (w/v) agarose gels.

PCR products that were run in 1.5 (w/v) agarose gels demonstrated: one band with a molecular size of 103 bp, corresponding to K_V1.3 transcripts, one band with a molecular size of 106 bp, corresponding to TASK-2 transcripts, one band with a molecular size of 125 bp, corresponding to KCa3.1 transcripts and one band with a molecular size of 117 bp, corresponding to GAPDH transcripts.

The intensity of each band was measured by densitometric scanning, and the value of each Kv1.3, TASK-2 and KCa3.1 band from each sample was normalized to the intensity value of the housekeeping gene Glyceraldehyde-3-Phosphate Dehydrogenase (GAPDH) (Poulopoulou et al., 2005b). The RefSeq accession number, the sequence of the PCR primers, the number of cycles and the amplified fragment size, were as follows:

Kv1.3: (NM_002232.5) F:5'-GTGTCTTGACCA TCGCATTG-3', R:5'-ACGTGCATGTACTGGGATTG-3', 35 cycles, bp:103; TASK-2: (NM_003740.4) F:5'-TGGTGATCCCACCCTTCGTA -3', R: 5'-ACAAAG TCACCGAAGCCGAT-3', 35 cycles, bp:106; KCa3.1 (NM_002250.3): F:5'-ATGCAGAGATGCTGTGGTTCG-3',R:5'-GACCTCTTTGGCATGAAAGGC-3', 35 cycles, bp:125; GAPDH: (NM_002046.7) F:5-CTCCAAAATC AAGTGGGGCG-3, R:5'-ATGATGACCCTTTTGGCTC CC -3', 30 cycles, bp:117.

Human brain total RNA was purchased from TAKARA BIO and was used as our positive internal control for all primers.

Flow Cytometry Experiments

K_V1.3 expression was detected on peripheral blood mononuclear cells by flow cytometry using a validated fluorescein-conjugated ShK-F6CA assay. ShK-F6CA is a highly specific K_V1.3 inhibitor that blocks the channel with low picomolar affinity and binds to the channel tetramer (Beeton et al., 2003). Peripheral blood T cells were washed twice with phosphate buffered saline (PBS) and incubated in the dark at room temperature with 100 nm ShK-F6CA in PBS +2% goat serum (Sigma) for 30 min and then washed 3× with PBS +2% goat serum before flow cytometry analysis. Stained mononuclear cells were analyzed by flow cytometry on a BD Biosciences FACScan as described previously (Beeton et al., 2003). Data were further analyzed using CellQuest software. For each subject, staining intensity was compared between cells stained with ShK-F6CA versus unlabeled ShK using the Kolmogorov-Smirnov Test (Cell Quest software) to subtract autofluorescence (D values).

Statistics

Statistical analysis was performed using Student's t test with an accepted level of $p < 0.05$. For multiple comparisons one-way analysis of variance was applied with Bonferroni *post hoc* correction. Normality of data was assessed using the Kolmogorov-Smirnov test. The goodness of data fit to exponential or Boltzmann functions was evaluated with the Hamilton's R coefficient. All results presented in the text are mean ± standard error.

RESULTS

T Lymphocytes of MS Patients Exhibit Higher Kv1.3 Currents Compared to Healthy and Disease Controls

Previous studies of MS patients measured Kv1.3 expression in antigen-specific T cell lines or MHC-tetramer-sorted T cells that had been activated and expanded through repeated *in vitro* antigenic stimulations before patch clamp analysis (Wulff et al., 2003; Beeton et al., 2006). Here, we performed whole-cell patch clamp experiments in negatively selected, freshly isolated T cells from MS patients and various control groups in order to investigate the biophysical characteristics of Kv1.3 currents and calculate the number of functional channels/surface area of each cell.

We recorded outward potassium currents in response to voltage ramp protocols (*see methods section*) (N = ~70 T cells/subject). In a subset of these cells (N = ~20 T cells/subject) we also recorded currents in response to: 1) voltage-step activation and 2) steady-state inactivation protocols (*see methods section*). Cell capacitance was constantly monitored. Currents were identified as Kv1.3 based on the presence of cumulative inactivation, a distinctive property of Kv1.3 and their total inhibition by 1 nM of the Kv1.3-selective blocker ShK-186 (Matheu et al., 2008). Kinetic measurements of Kv1.3 current activation and inactivation and calculated whole-cell activation and steady-state inactivation conductance-to-voltage relations showed that Kv1.3 currents from MS T lymphocytes have similar biophysical characteristics with currents recorded from either healthy individuals or patients with other neurological disorders (**Table 3**). Interestingly, T lymphocytes isolated from MS patients (n = 38) exhibited currents with significantly higher peak amplitudes than those of healthy (n = 21) and disease controls (n = 31) (**Figures 1A,B**). Given that Kv1.3 currents from both MS patients and controls have similar gating and kinetic properties, it follows that the increased current amplitude in MS T lymphocytes is due to up-regulation in the number of Kv1.3 channels.

Channel-Specific Protocols Exclude TASK-2 Contribution in the Potassium Current Up-Regulation of MS T Lymphocytes

An earlier study (Bittner et al., 2010) has also reported increased potassium currents in T cells of MS patients but they attributed this up-regulation to pH-sensitive TASK-2 channels, rather than Kv1.3 channels. For this reason, we examined the potential contribution of TASK-2 conductance to our potassium current recordings by taking advantage of the very distinct biophysical properties of these channels. TASK-2 channels are voltage-independent, non-inactivating, do not

TABLE 3 | Electrophysiological properties of Kv1.3 channels, in patients with multiple sclerosis (MS) (n = 38) and control groups (n = 52). Data are presented as means ± SEM. (t_n: activation time constant; t_j: inactivation time constant; V_n: potential of half-maximal activation; V_j: potential of half-maximal steady-state inactivation; I_{max}: peak current amplitude following depolarization to +40 mV; C_m: membrane capacitance).

Group	Activation threshold	τ_n (ms)	τ_j (ms)	V_n (mV)	V_j (mV)	I_{max} (pA)	C_m (pF)	Kv1.3 channel density (channels/ μm^2)
Definite MS	–35 mV	3.4 ± 0.4	169 ± 4.2	–32.3 ± 2.5	–53.5 ± 1.9	636.3 ± 29.3	1.67 ± 0.1	2.5 ± 0.04
Relapsing remitting	–35 mV	3.5 ± 0.3	167 ± 3.2	–31.8 ± 2.1	–53.1 ± 2.2	596.7 ± 32.2	1.68 ± 0.1	2.4 ± 0.04
Secondary progressive	–35 mV	3.4 ± 0.5	171 ± 5	–32.7 ± 2.6	–53.7 ± 2.1	680.5 ± 28.4	1.65 ± 0.2	2.7 ± 0.05
CIS	–35 mV	3.5 ± 0.3	169 ± 4.7	–31.9 ± 2.5	–52.8 ± 2.3	432.6 ± 36.8	1.80 ± 0.1	1.8 ± 0.09
OND	–35 mV	3.6 ± 0.5	172 ± 5.1	–32.3 ± 3	–51.6 ± 1.9	449.2 ± 35.1	1.6 ± 0.2	1.8 ± 0.0.7
OIND	–35 mV	3.8 ± 0.4	173 ± 4.4	–32 ± 2.4	–51.9 ± 2	435.66 ± 31.9	1.68 ± 0.1	1.8 ± 0.1
Healthy controls	–35 mV	3.5 ± 0.3	171 ± 4.4	–33.1 ± 2.6	–53.5 ± 1.8	455.3 ± 29.5	1.65 ± 0.1	1.8 ± 0.05

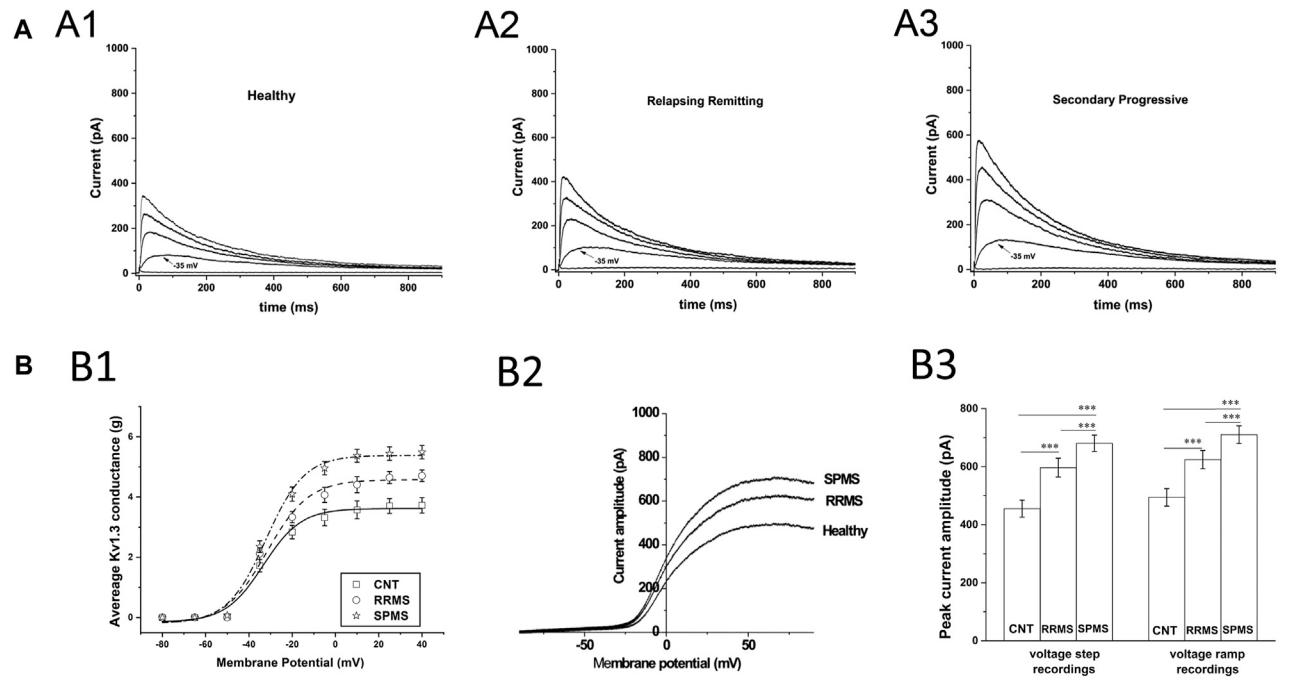

FIGURE 1 | Patch clamp data from T cells of MS patients and healthy controls. **(A)**: Higher current responses in MS T cells. Whole-cell currents from T lymphocytes bathed in extracellular solution of pH 7.4 with their membrane clamped at –90 mV. MS T cells (N = 855) have higher peak K_V1.3 amplitudes than controls (N = 1,258). **(A1–A3):** Representative K_V1.3 currents elicited by 1000-ms depolarizing pulses in 15-mV increments, given every 60 s are displayed at physiologically relevant potentials (–50 to +10 mV) for reasons of clarity. **(B)**: T cell Kv1.3 currents in SPMS have significantly higher mean peak amplitudes than both RRMS and healthy controls. **(B1)**: Increased peak Kv1.3 conductance, in MS patients compared to healthy individuals. Peak current amplitudes in response to voltage step protocols were converted to conductance (g) values, averaged and plotted against the corresponding voltage for SPMS (*), RRMS (○) and healthy controls (□) (g-V curves). The average maximal peak conductance was 5.49 ± 0.22 for SPMS (n = 18 patients, N = 415 cells), 4.7 ± 0.19 for RRMS (n = 20 patients, N = 440 cells) and 372 ± 0.25 for healthy individuals (n = 21, N = 542 cells) ($p < 0.001$). Data shown are average values ±S.E. Plots are fitted to Boltzmann functions. **(B2):** Representative whole-cell currents of a healthy individual, an RRMS patient and a SPMS one, in response to voltage-ramps (–100 to +100 mV). Both RRMS and SPMS T cells have higher peak amplitudes than T cells of their control counterparts, while SPMS T cells present higher peak amplitudes than the RRMS patients **(B3)**: **Left**: Average peak Kv1.3 currents, in response to +40 mV voltage steps, were 680.5 ± 28.4 for SPMS (n = 18 patients, N = 415 cells), 596.7 ± 32.2 for RRMS (n = 20 patients, N = 440 cells) and 455.3 ± 29.5 for healthy controls (n = 21, N = 542 cells) (***: $p < 0.001$). **Right**: Average peak currents in response to voltage ramps were 710.21 ± 29.9 for SPMS (n = 18 patients, N = 1,410 cells), 624.1 ± 31.5 for RRMS (n = 20 patients, N = 1,480 cells) and 494.3 ± 30.2 pA for healthy controls (n = 21, N = 1,510 cells) (***: $p < 0.001$). One way ANOVA with Bonferroni post hoc correction was applied for statistical analysis.

exhibit cumulative inactivation, and their opening is facilitated by alkaline pH (Morton et al., 2005). Thus, we exposed T cells to an alkaline extracellular solution (pH 8.5) to enhance opening of TASK-2 channels, and used a 0 mV holding potential to inactivate all Kv1.3 channels–(Hajdu et al., 2010) without impacting TASK-2 channels (Morton et al., 2005). As seen in **Figure 2A** currents elicited under these conditions had very small amplitude and did not differ between MS patients (11.9 ± 0.48 pA for SPMS n = 12, 12.2 ± 0.53 pA for RRMS n = 14) and healthy controls (11.2 ± 0.6 pA n = 15). These small currents were voltage-independent, non-inactivating, and had a

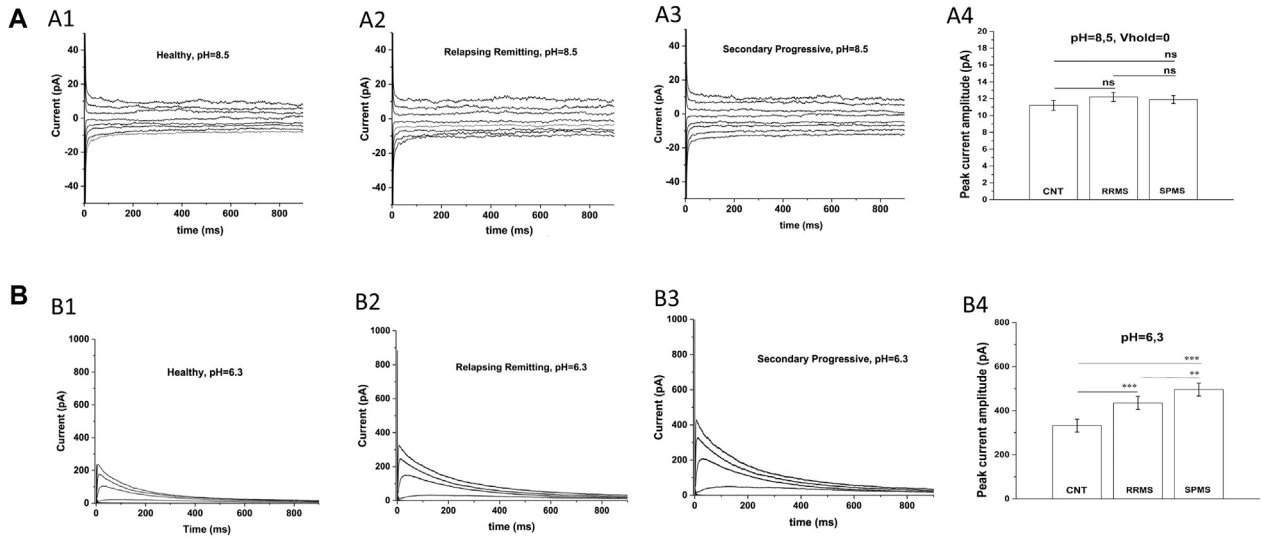

FIGURE 2 | Specific electrophysiological protocols exclude TASK-2 contribution to the increased potassium conductance of MS T lymphocytes. **(A)**: T cells from either MS patients or healthy controls present similar current-responses in alkaline solution at a 0 mV holding potential: Whole-cell currents recorded from T lymphocytes bathed in an alkaline (pH = 8.5) extracellular solution with their membranes clamped at 0 mV. **(A1–A3):** Whole-cell current responses to 15 mV voltage-steps, given every 5 s from T lymphocytes of healthy controls, RRMS and SPMS patients. **(A4):** Average peak currents (at +40 mV) did not differ significantly between groups. Average values ±SE were: 11.9 ± 0,48 pA for SPMS (n = 12, N = 235 cells), 12.2 ± 0,53 pA for RRMS (n = 14, N = 282 cells) and 11.2 pA ± 0,6 for healthy subjects (n = 15, N = 310 cells) (ns: non-significant). Method: One way ANOVA with Bonferroni post hoc correction. **(B)**. T cells of MS patients exhibit higher K^+ currents than controls in acidic extracellular solution: Whole-cell currents recorded from T cells bathed in acidic (pH = 6.3) extracellular medium with their membrane held at −90 mV. $K_V1.3$ currents from T cells of healthy controls, RRMS and SPMS patients elicited by 1000-ms depolarizing pulses in 15-mV increments, given every 60 s (pH = 6.3). **(B1–B3):** Displayed are whole-cell $K_V1.3$ current responses at physiologically relevant potentials, ranging from −50 mV to +10 mV. T cells from MS patients bathed in acidic extracellular conditions present higher current responses than controls. **(B4)**: Peak currents at +40 mV were: 496.06 ± 34.5 for SPMS (n = 12, N = 230 cells), 435.08 ± 32.1 pA for RRMS (n = 12, N = 252 cells) and 332.36 ± 28.9 pA for healthy controls (n = 14, N = 310 cells) (***: $p < 0.001$, **: $p < 0.01$, one-way ANOVA).

reversal potential of 5 mV which is close to the reversal potential of chloride (0 mV) or of non-selective cations (0 mV) rather than potassium (−83.5 mV) (**Figure 2A**); we did not further characterize these currents because it was out of the scope of this investigation. Therefore, under TASK-2 favoring conditions, we were unable to detect any measurable TASK-2 conductance in T cells of either MS patients or healthy individuals. This is in line with previous studies that also did not detect TASK-2 currents in T cells (Hajdu et al., 2010), and reported Kv1.3 and calcium-activated channels KCa3.1 as the only functional potassium channels in human and rat T cells (Chiang et al., 2017).

Next, we recorded currents from T lymphocytes bathed in acidic extracellular solution (pH 6.3), where TASK-2 activation is minimal (Morton et al., 2005) and if present their contribution will be negligible. Currents were elicited from a holding potential of −90 mV in response to membrane depolarizations delivered every 60 s. Under these TASK-2 hindering conditions, T cells exhibited currents with biophysical properties characteristic of Kv1.3 (fast activation, slow inactivation and cumulative inactivation), and with amplitudes significantly higher in MS (496.06 ± 34.5 pA for SPMS n = 12, 435.0811.9 ± 32.1 pA for RRMS n = 12) than control T cells (332.36 ± 28.9 pA n = 14) (**Figure 2B** $p < 0.001$). These results corroborate and support our data obtained with regular extracellular solutions (pH 7.4) and validate the characterization of our currents as *bona fide* Kv1.3. Taken together, our findings indicate that PB T lymphocytes from MS patients express Kv1.3 currents with significantly higher amplitude than PB T cells from controls (680.5 ± 28.4 for SPMS vs 596.7 ± 32.2 for RRMS and 455.3 ± 29.5 for CNTs at pH 7.4).

Kv1.3 Channel Membrane Density is Increased in MS T Lymphocytes

The finding that PB T lymphocytes of MS patients manifest higher Kv1.3 currents could be due to either a larger cell size or an increase in the membrane density of Kv1.3 channels. Based on cell capacitance measurements, T lymphocyte sizes were similar in MS patients (average Cm = 1.67 pF) and healthy controls (average Cm = 1.65 pF). The above capacitance values indicate that recordings were made from resting rather than activated T cells. Furthermore, calculation of the Kv1.3 channel densities/μm^2 of cell surface, as described in the *methods* section, showed that T cells had significantly higher Kv1.3 channel densities in MS, (n = 38, N = 852 cells) compared to healthy individuals (n = 21, N = 540 cells), or patients with OND (n = 16, N = 335 cells), CIS (n = 6, N = 130 cells) and OIND (n = 9, 253 cells) (**Figure 3A1**, $p < 0.001$). The higher Kv1.3 channel density in MS is not because a minority of cells (e.g., activated TEM cells with a $Kv1.3^{high}$ phenotype) expressed high numbers of Kv1.3 channels and skewed the average. Of 855 MS-patient T cells studied with voltage step protocols, 86% had a channel density greater than 2.1 channels/μm^2, whereas only 15% of 1,258 control T cells studied (healthy individuals, OND, OIND, CIS) had a channel density above this cut-off value. Therefore, these results indicate that the majority of

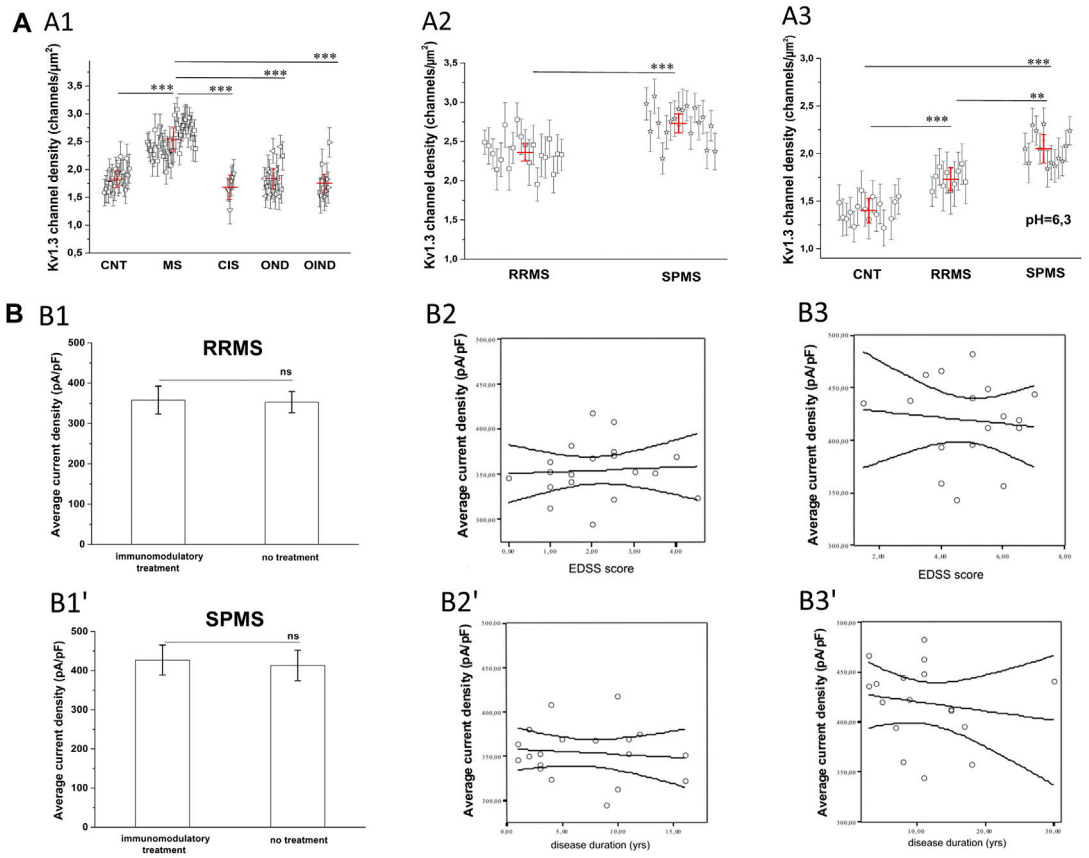

FIGURE 3 | (A): Calculated $K_V1.3$ channel densities per T lymphocyte from whole-cell currents recorded from a holding potential of −90 mV. **(A1):** $K_V1.3$ channel densities in MS patients (n = 38, N = 852 cells) are significantly higher ($p < 0.001$), compared to healthy control subjects (n = 21, N = 540 cells), patients with: clinically isolated Syndrome (CIS) (n = 6, N = 130 cells), other neurological disorders (OND) (n = 16 patients, N = 335 cells), and other inflammatory neurological disorders (OIND) (n = 9 patients, N = 253 cells). Each symbol represents mean values for each individual patient and error bars are standard deviation of the mean. Red horizontal lines with red error bars correspond to the average value ±standard error for each group. Comparisons are shown only for statistically significant differences (***: $p < 0.001$). One way ANOVA with Bonferroni post hoc correction was applied for statistical analysis. **(A2):** Sub-grouping of MS patients showed significantly higher $K_V1.3$ channel densities in Secondary Progressive Multiple Sclerosis (SPMS) (n = 18 patients, N = 415 cells), compared to Relapse Remitting Multiple Sclerosis (RRMS) (n = 20 patients. N = 440 cells). Values shown are mean ± SD for each subject. Red horizontal lines correspond to the average value ±standard error for each group. ($p < 0.001$). (***: $p < 0.001$). **(A3)** In acidic extracellular solution, where TASK-2 activation is negligible, Kv1.3 channel densities are significantly higher in T cells of patients with SPMS (n = 12, N = 230 cells), compared to both RRMS (n = 12, N = 252 cells) and healthy controls (n = 14, N = 310 cells). Individual marks represent mean ± SD for each subject; red horizontal lines and bars represent average ±SE. (***: $p < 0.001$, **: $p < 0,01$). **(B).** Effect of MS severity (MMSE score), duration (years) and immunomodulatory treatment on $K_V1.3$ current density. **(B1-B1′).** $K_V1.3$ density was not affected by immunomodulatory treatment in RRMS [treated: 357.7 ± 34 pA/pF, (n = 14); untreated: 350.2 ± 27 pA/pF, (n = 6),] or SPMS patients [treated: 426.8 ± 38.3 pA/pF (n = 13); untreated: 412.9 ± 39 pA/pF, (n = 5)]. Average values ±SE are shown (ns: non-significant). **(B2–B2′).** In RRMS, $K_V1.3$ current density did not correlate with either EDSS ($r^2 = 0.05$, $p = 0.7$) or disease duration ($r^2 = 0.1$, $p = 0.3$). **(B3-B3′).** In SPMS, correlations were also non-significant for either EDSS ($r^2 = 0.11$, $p = 0.5$) or disease duration ($r^2 = 0.16$, $p = 0.6$).

resting T-cells in MS exhibit an elevated Kv1.3 channel density and suggest that Kv1.3 expression may be a useful biomarker to distinguish MS from other CNS inflammatory disorders.

Sub-grouping of MS patients into relapsing-remitting (RRMS) and secondary progressive (SPMS) disease revealed that T lymphocytes of SPMS patients had significantly higher Kv1.3 current amplitudes (**Figure 1B**, $p < 0.001$) and channel membrane density (**Figure 3A2**, $p < 0.001$) than T lymphocytes of RRMS patients. Similar results were obtained from experiments performed in acidic (6.3) pH, where, as aforementioned, TASK-2 activation is minimal. Under these conditions T lymphocytes from SPMS patients had significantly higher Kv1.3 densities compared to both RRMS patients and healthy controls (**Figure 3A3**).

For both RRMS and SPMS subgroups, there was no significant correlation between Kv1.3 channel density and either immunomodulatory treatment (**Figures 3B1,B1′**), disability or disease duration (**Figures 3B2,B2′,tB3,B3′**). Therefore, increased Kv1.3 expression in T cells is correlated to the subtype of MS rather than any other parameter we tested.

Enhanced Kv1.3 mRNA Expression in T Lymphocytes From MS Patients Compared to Controls

Following the functional studies that showed a specific up-regulation in Kv1.3 current responses in MS, we went on to assess the expression levels of all potassium-channel gene

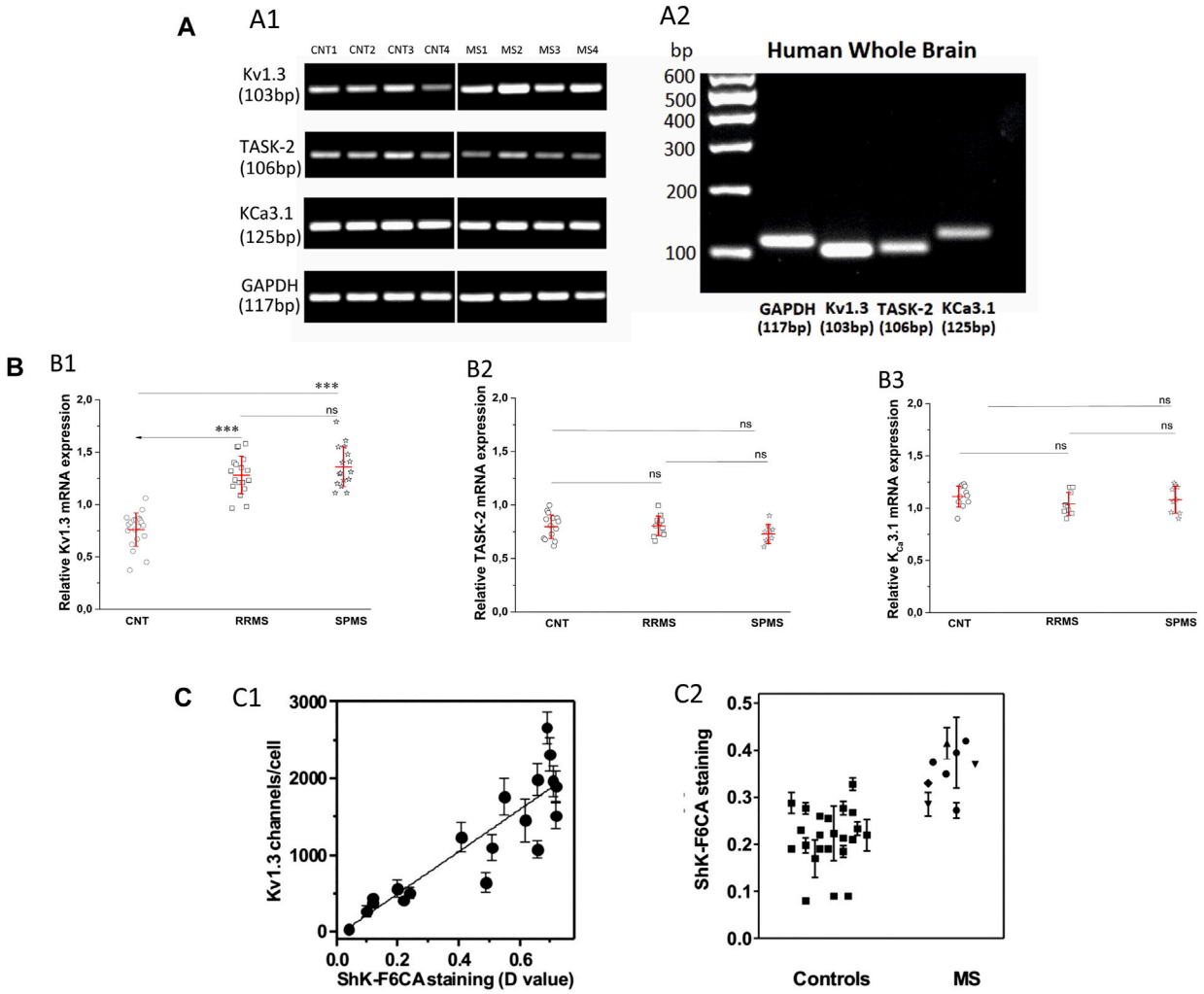

FIGURE 4 | (A). Expression of Kv1.3, TASK-2 and KCa3.1 mRNA in T lymphocytes of patients with multiple sclerosis. **(A1):** Agarose gel image from PCR products of K_V1.3, TASK-2, KCa3.1 and the housekeeping gene glyceraldehyde-3-phosphate dehydrogenase (GAPDH) in T lymphocytes of four healthy control subjects (lanes CNT 1–4) and four patients with multiple sclerosis (lanes MS 1–4). The PCR products demonstrated: a band with a molecular size of 103 bp, corresponding to K_V1.3, a band of 106 bp corresponding to TASK-2, a band of 125 bp corresponding to KCa3.1, and a band of 117 bp corresponding to GAPDH transcripts. MS patients gave K_V1.3 bands of higher intensity (1.32 ± 0.18, n = 34) compared to healthy controls (0.76 ± 0.16, n = 20, $p < 0.001$) and similar intensities for the TASK-2 (controls 0.78 ± 0.12, MS 0.77 ± 0.1) and KCa3.1 (control 1.12 ± 0.14, MS 1.06 ± 0.11) bands in these samples. In the same samples the bands of the housekeeping gene GAPDH had similar intensities. **(A2):** Agarose gel image of the PCR products of GAPDH, Kv1.3, TASK-2 and KCa3.1 amplified from cDNA derived from commercially available human whole brain (HWB) RNA. HWB was used as positive internal control for all the sets of primers we designed. Standard 100 bp ladder testify that the PCR products of GAPDH, Kv1.3, TASK-2 and KCa3.1 obtained by HWB RNA are of the expected size (117, 103, 106, and 125 bp, respectively). **(B)**: Up-regulation of K_V1.3 mRNA in T lymphocytes of patients with multiple sclerosis. **(B1)**: Relative levels of K_V1.3 mRNA, calculated as a ratio to GAPDH in healthy control subjects (n = 20) and patients with either relapsing-remitting (RRMS, n = 18) or secondary progressive multiple sclerosis (SPMS, n = 16). A statistically significant increase of K_V1.3 mRNA expression was observed between either RRMS (1.28 ± 0.18) or SPMS (1.36 ± 0.19) and control subjects (0.76 ± 0.16). (***: $p < 0.001$). **(B2)**: Relative TASK-2 mRNA expression in healthy controls (0.78 ± 0.12, n = 11), RRMS (0.79 ± 0.1, n = 10) and SPMS patients (0.74 ± 0.1, n = 9). **(B3)**: KCa3.1 expression in healthy subjects (1.12 ± 0.14, n = 11), RRMS (1.04 ± 0.11, n = 9) and SPMS (1.08 ± 0.13, n = 9). TASK-2 and KCa3.1 mRNA expression did not differ significantly between controls, RRMS and SPMS (ns: non-significant). All values are mean ± SE. **(C)**. Higher expression of Kv1.3 channels detected by flow cytometry in the peripheral blood T cells of patients with MS. **(C1)**: Kv1.3 channel expression by T lymphocytes was determined in parallel by whole-cell patch clamp (y axis) and by flow cytometry (x axis). R^2 = 0.79. **(C2)**: Kv1.3 expression levels measured by flow cytometry in T lymphocytes isolated from the peripheral blood of healthy controls (squares), and patients with MS. A statistically significant increase of Kv1.3 expression was observed in T cells from MS patients compared to controls (D value = 0.22 ± 0.04 vs 0.37 ± 0.06; $p < 0.001$).

products reported to be expressed in human T cells, namely, Kv1.3, KCa3.1 and TASK-2 in MS patients and control subjects. We performed semi-quantitative PCR using as reference the mRNA of the housekeeping gene GAPDH. As shown in **Figure 4A**, PB T lymphocytes from both MS patients and controls yielded specific band products of the predicted size for all three potassium channels tested. Interestingly, T lymphocytes of MS patients had significantly higher expression levels of Kv1.3 mRNA (mean expression ratio: 1.32 ± 0.18, n = 34) as compared to T lymphocytes of healthy individuals (0.76 ± 0.16, n = 20, $p < 0.001$) (**Figure 4B**). Thus, MS T cells exhibit a parallel increase of Kv1.3 mRNA expression and of the number of functional Kv1.3 channels.

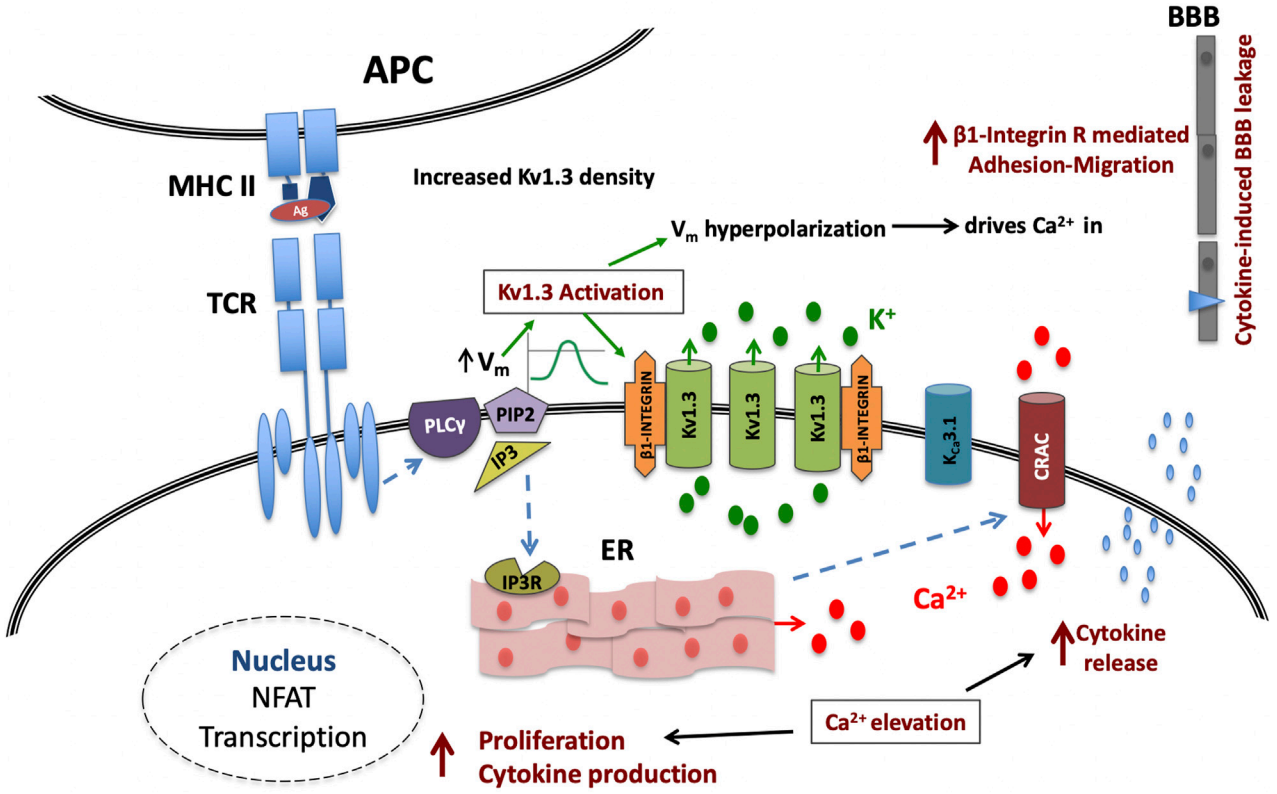

FIGURE 5 | Kv1.3 channel up-regulation enhances signaling in MS T cells. Upon TCR antigenic (Ag) stimulation, the IP3-induced calcium release from the intracellular stores (ER) causes on one hand membrane depolarization (Vm), followed by a Kv1.3 channel-mediated hyperpolarization and on the other, the formation of conductive Calcium Release Activated Calcium (CRAC) channels; in MS-T cells this hyperpolarization will be of increased magnitude due to higher Kv1.3 channel density. This in turn will translate into a stronger than physiological driving force for calcium ions (Ca^{2+}) through CRAC channels and therefore a cytosolic calcium signal of amplified intensity and duration that in turn will potentiate the effectiveness of the immune stimulus, and may even allow sub-threshold stimuli to reach activation threshold, priming T cell activation that otherwise would not. Additionally all calcium-dependent processes that follow the successful activation of MS T cells, such as cytokine production, cytokine secretion and proliferation, will be heightened. Moreover, the immune stimulus-induced Kv1.3 activity in these cells, will increase β1-integrin activation, facilitating their adhesion and cytokine-induced migration into the CNS.

Additionally, Kv1.3 mRNA expression within MS sub-groups was slightly higher in SPMS patients (1.36 ± 0.19, n = 16) compared to those with RRMS (1.28 ± 0.18, n = 18), but the difference did not reach statistical significance (**Figure 4B1**).

We did not detect any significant differences in the expression levels of KCa3.1 (control 1.12 ± 0.14, MS 1,06 ± 0.11) and TASK-2 (controls 0.78 ± 0.12, MS 0.77 ± 0.1) mRNA products (**Figures 4B2,B3**). Therefore, based on our data MS patients present a specific up-regulation in the constitutive expression of the Kv1.3 gene product.

Our data do not support previous findings reporting increased TASK-2 mRNA in MS (Bittner et al., 2010). This discrepancy could reflect differences in the experimental methods and in the set of primers used by the two groups. At this point it is worth mentioning that initially, we tried the same pair of primers for TASK-2 mRNA detection used in the aforementioned study (Bittner et al., 2010); however, in our hands these primers did not yield any detectable products at the expected size neither from mRNA isolated from human T lymphocytes nor from commercially available human brain total mRNA (TAKARA).

Enhanced Levels of $K_V1.3$ Membrane-Protein Expression in a Second MS Cohort

In a cohort of MS patients from North America, cell surface expression of $K_V1.3$ was measured in freshly isolated peripheral blood mononuclear cells using a validated fluorescein-conjugated ShK-F6CA assay. ShK-F6CA blocks $K_V1.3$ with low picomolar affinity and exquisite selectivity by binding to the channel tetramer (Beeton et al., 2003). The intensity of ShK-F6CA staining reflects the number of Kv1.3 tetramers on the cell

surface (Beeton et al., 2003). We found a strong correlation between the mean fluorescent intensity of ShK-F6CA staining with the number of $K_V1.3$ channels/cell determined by whole-cell patch clamp (**Figure 4C1**). Peripheral blood mononuclear cells from North American MS patients expressed higher ShK-F6CA staining than cells from healthy individuals, which is indicative of more cell surface $K_V1.3$ tetramers (**Figure 4C2**, $p < 0.001$).

DISCUSSION

In this study we report that T lymphocytes of MS patients specifically express higher levels of the voltage-gated potassium channel Kv1.3 than their control group counterparts. This Kv1.3 up-regulation in MS is evident at the cell surface protein level, the density of functional channels and at the amount of mRNA.

These results are at odds with an earlier report that presented TASK-2 specific up-regulation in T cells of MS patients (Bittner et al., 2010). Our experiments diminish the possibility of a TASK-2 contribution in our potassium current recordings and fail to show the presence of any detectable functional TASK-2 channels in freshly isolated unsorted resting human T lymphocytes under our experimental conditions that differ in the composition of the recording solutions, the voltage protocols (holding potential, inter-pulse duration) and the use of sorted ($CD4^+$ and $CD8^+$ T cells) vs unsorted T cells. This finding is consistent with other reports that either failed to record TASK-2 currents or report that the only potassium channels in human and rat T cells are Kv1.3 and KCa3.1 (Hajdú et al., 2010; Chiang et al., 2017). Additionally, we show that although TASK-2 mRNA is constitutively expressed in PB T lymphocytes, it is only the Kv1.3 mRNA that is up-regulated in MS. These discrepancies however, may merely reflect differences in the experimental conditions (primers, cycles or enzymes) or the T cell subpopulation tested (MACS-sorted $CD8^+$ PB T cell vs unsorted PB T cells).

Earlier studies have demonstrated the specific presence of myelin auto-reactive T_{EM} cells in the PB of MS patients (Wulff et al., 2003), that when activated acquire a $Kv1.3^{high}$ phenotype. Therefore, it is only just for someone to wonder if in our experiments, recordings from a few $Kv1.3^{high}$ T lymphocytes could have skewed our average data to show increased Kv1.3 channel density in MS. However, according to our data more than 85% of MS T lymphocytes had augmented Kv1.3 current responses; moreover the majority of clamped cells had a small size (1,6 pF), consistent with resting rather than activated T lymphocytes. Therefore, our data support a global increase of Kv1.3 channel density in resting T lymphocytes of MS patients and do not seem to concern a minor subpopulation of these cells because otherwise we would not be able to detect it. This increase goes along with a concomitant amplification in the constitutive levels of Kv1.3 mRNA, suggesting that the up-regulation of Kv1.3 channels in MS is the product of an enhanced gene transcription rather than of a translational or post-translational modification. This could be the result of either genetic or epigenetic factors and warrants further investigation.

The finding of a specific Kv1.3 up-regulation in the PB T lymphocytes of patients with MS, complements a long line of evidence that strongly supports Kv1.3 channel involvement in MS pathophysiology, such as: the presence of $Kv1.3^{high}$ T_{EM} cells in the inflammatory lesions of MS brains (Rus et al., 2005); the association of a Kv1.3 gain-of-function gene polymorphism with MS severity (Lioudyno et al., 2021); the Kv1.3 up-regulation in brains of animals with experimental allergic encephalomyelitis (Bozic et al., 2018); the finding that Kv1.3 pharmacological blockade or Kv1.3 gene-silencing in animal models of MS 1) renders mice resistant to experimental allergic encephalomyelitis (Beeton et al., 2001), 2) decreases demyelination (Murray et al., 2015), and 3) drives T cells toward an immune-regulatory phenotype (Gocke et al., 2012).

The pathophysiological relevance of the increase in the density of active Kv1.3 channels in T lymphocytes of MS patients can only be evaluated if we take into account the role of these channels in T lymphocyte processes that determine the fate and function of these cells. As aforementioned, Kv1.3 are the main potassium channels of T lymphocytes at rest and during the initial steps of the activation process and their functional relevance is underscored by their localization in the immune synapse (Panyi et al., 2004) that fulfills the spatiotemporal requirements for their participation in the activation-signaling network. Activation of Kv1.3 channels generates graded negative membrane potentials proportional to the potassium ions flowing out of the cell. Membrane hyperpolarizations are of crucial biological importance for the activation of T lymphocytes because they provide the necessary negative electromotive force that enables calcium ions to flow into the T lymphocytes through CRAC channels, thus sustaining the cytosolic calcium elevations in order for the activation process to proceed. From the above it becomes evident that the activity of Kv1.3 channels is directly linked to the amount of calcium ions that enter the cell. On the other hand, the activity of Kv1.3 is dictated by the density of functional channels on the plasma membrane and by their opening probability, which is governed by the degree of membrane depolarization. Consequently, similar antigenic stimulations in resting T lymphocytes of the same subset will produce calcium signals of different magnitude and duration when membrane densities of functional Kv1.3 channels vary (**Figure 5**).

Based on the above, the Kv1.3 up-regulated phenotype of T lymphocytes could account for and is consistent with the previously reported enhanced calcium responses (Martino et al., 1998) and T cell hyper-responsiveness in MS. The predicted increase of calcium influx through CRAC channels in MS T cells, is expected to enhance the production of proinflammatory cytokines (e.g. interferon-γ, interleukin-17 and Tumor Necrosis Factor α), known to be associated with MS pathogenesis (Wagner et al., 2020), via calcineurin-NFAT (Nuclear factor of Activated T cells) activation (Gwack et al., 2007); it is also expected to render these cells less dependent on co-stimulatory signals (Markovic-Plese et al., 2001) and more resistant to co-inhibitory ones (Fife and Bluestone, 2008) and therefore to be one of the underlying factors that drive T cell function in MS away from a context-specific responsiveness and immune homeostasis.

Stronger hyper-polarizations following T lymphocyte stimulation in MS, would act as signal enhancers and thus buoy weak stimuli (low affinity antigens, low antigen titters or antigen peptides with low homology to the cognate ones) to reach activation threshold. The propensity for immune activation by the Kv1.3 up-regulation in MS may at least partly explain the presence of activated T cells, especially the myelin-specific ones (Zhang et al., 1994) that characterise this disorder. Moreover, activation of Kv1.3 channels induces β1-integrin receptor activation and promotes T cell adhesion and migration (Levite et al., 2000) and Kv1.3 channels have been shown to modulate T cell motility within inflammatory tissues (Matheu et al., 2008). Thus increased Kv1.3 expression will favor trafficking of MS T cells to inflammatory sites within the CNS, where they may contribute to myelin destruction.

The increased Kv1.3 channel density in MS could negatively interfere with the immune mechanisms responsible for deleting potentially pathogenic T cells from the periphery in order to sustain immune homeostasis and avert autoimmunity. Namely, the CD95/Fas apoptotic pathway has Kv1.3 down-regulation as one of the first steps (Szabo et al., 1996); consequently Kv1.3 up-regulation may confer a degree of resistance to Fas-induced apoptosis in MS T-lymphocytes. Aberrations in this pathway have been linked to autoimmunity and more specifically to MS (Volpe et al., 2016).

From the above it is valid to argue that T lymphocyte Kv1.3 up-regulation in MS may be an important factor in disease pathogenesis. Strikingly, we found significantly higher Kv1.3 channel expression in SPMS compared to RRMS; the underlying cause of this finding cannot be explained by our data and warrants further investigation. It could represent a disease stage-specific enhancement in the functional expression of Kv1.3 channels due to different levels of systemic immune activation; interestingly it has been reported that SPMS T lymphocytes show significantly reduced Fas-mediated apoptosis compared to RRMS (Comi et al., 2000), a finding that could be accounted for by the enhanced Kv1.3 channel expression in SPMS. Alternatively, based on a recent genetic study that as aforementioned, associates a gain-of-function Kv1.3 gene polymorphism to a more aggressive disease course (Lioudyno et al., 2021), one may propose that the higher Kv1.3 expression in the SPMS group could merely reflect a history of more active disease tending to progress to the SPMS phenotype with a higher frequency.

In summary, our study is in line with a body of evidence showing that Kv1.3 channels may be involved in MS and supports the pharmacological inhibition of their activity as a potential treatment for the disease, especially for SPMS, where treatment options are limited. Moreover, the specificity of Kv1.3 up-regulation for MS compared to other neurological disorders with or without inflammation, strongly supports the use of Kv1.3 expression as a peripheral biomarker for the disease.

DATA AVAILABILITY STATEMENT

The original contributions presented in the study are included in the article/Supplementary Material, further inquiries can be directed to the corresponding author.

ETHICS STATEMENT

The studies involving human participants were reviewed and approved by the Scientific and Ethics committee of St Panteleimon General State Hospital of Nikaia. Patients came from either the outpatient department or the neurological clinic of the above Hospital; Informed consent for blood sample collection as well as for clinical and demographic data use was obtained from all participating subjects. Blood samples for the US cohort were collected with IRB approval (Mkhikian et al., 2011, 2: 334. doi: 10.1038/ncomms1333) and banked de-identified. The patients/participants provided their written informed consent to participate in this study.

AUTHOR CONTRIBUTIONS

IM: data acquisition and analysis, drafting of manuscript and figures; IC: data acquisition and analysis, drafting of manuscript and figures; CB: data acquisition and analysis, drafting of manuscript and figures; MG: data acquisition, drafting of manuscript; ER: data acquisition; SA: data analysis; PS: data analysis; MP: design and synthesis of ShK-F6CA for Kv1.3; KC: design of study, drafting of manuscript and figures, CP: conception and design of study on Greek cohort, drafting of manuscript and figures.

FUNDING

MG is co-financed by Greece and the European Union (European Social Fund-ESF) through the Operational Programme «Human Resources Development, Education and Lifelong Learning» in the context of the project "Strengthening Human Resources Research Potential *via* Doctorate Research" (MIS-5000432), implemented by the State Scholarships Foundation (IKY). Studies on the US cohort were supported by NIH grants (NS048252 to KC and MP and AI08226 to MD), and Lee Kong Chian School of Medicine, Nanyang Technological University (NTU) Singapore Start-Up Grant (to KC). Blood samples were kindly provided for the Greek cohort by IM and for the US cohort by Barbara L. Newton and Michael Demetriou (Department of Neurology, University of California, Irvine, California, United States).

REFERENCES

Beeton, C., Wulff, H., Barbaria, J., Clot-Faybesse, O., Pennington, M., Bernard, D., et al. (2001). Selective Blockade of T Lymphocyte K (+) Channels Ameliorates Experimental Autoimmune Encephalomyelitis, a Model for Multiple Sclerosis. *Proc. Natl. Acad. Sci. U S A.* 98, 13942–13947. doi:10.1073/pnas.241497298

Beeton, C., Wulff, H., Singh, S., Botsko, S., Crossley, G., Gutman, G. A., et al. (2003). A Novel Fluorescent Toxin to Detect and Investigate Kv1.3 Channel

Up-Regulation in Chronically Activated T Lymphocytes. *J. Biol. Chem.* 278, 9928–9937. doi:10.1074/jbc.M212868200

Beeton, C., Wulff, H., Standifer, N. E., Azam, P., Mullen, K. M., Pennington, M. W., et al. (2006). Kv1.3 Channels Are a Therapeutic Target for T Cell-Mediated Autoimmune Diseases. *Proc. Natl. Acad. Sci. U S A.* 103 (46), 17414–17419. doi:10.1073/pnas.0605136103

Bittner, S., Bobak, N., Herrmann, A. M., Göbel, K., Meuth, P., Höhn, K. G., et al. (2010). Upregulation of K2P5.1 Potassium Channels in Multiple Sclerosis. *Ann. Neurol.* 68, 58–69. doi:10.1002/ana.22010

Böyum, A. (1968). Isolation of Mononuclear Cells and Granulocytes from Human Blood. Isolation of Monuclear Cells by One Centrifugation, and of Granulocytes by Combining Centrifugation and Sedimentation at 1 G. *Scand. J. Clin. Lab. Invest. Suppl.* 97, 77–89. PMID: 4179068.

Bozic, I., Tesovic, K., Laketa, D., Adzic, M., Jakovljevic, M., Bjelobaba, I., et al. (2018). Voltage Gated Potassium Channel Kv1.3 Is Upregulated on Activated Astrocytes in Experimental Autoimmune Encephalomyelitis. *Neurochem. Res.* 43, 1020–1034. doi:10.1007/s11064-018-2509-8

Cahalan, M. D., Chandy, K. G., DeCoursey, T. E., and Gupta, S. (1985). A Voltage-Gated Potassium Channel in Human T Lymphocytes. *J. Physiol.* 358, 197–237. doi:10.1113/jphysiol.1985.sp015548

Cahalan, M. D., and Chandy, K. G. (2009). The Functional Network of Ion Channels in T Lymphocytes. *Immunol. Rev.* 231, 59–87. doi:10.1111/j.1600-065X.2009.00816.x

Chiang, E. Y., Li, T., Jeet, S., Peng, I., Zhang, J., Lee, W. P., et al. (2017). Potassium Channels Kv1.3 and KCa3.1 Cooperatively and Compensatorily Regulate Antigen-specific Memory T Cell Functions. *Nat. Commun.* 8, 14644. doi:10.1038/ncomms14644

Comi, C., Leone, M., Bonissoni, S., DeFranco, S., Bottarel, F., Mezzatesta, C., et al. (2000). Defective T Cell Fas Function in Patients with Multiple Sclerosis. *Neurology* 55, 921–927. doi:10.1212/wnl.55.7.921

Fife, B. T., and Bluestone, J. A. (2008). Control of Peripheral T-Cell Tolerance and Autoimmunity via the CTLA-4 and PD-1 Pathways. *Immunol. Rev.* 224, 166–182. doi:10.1111/j.1600-065X.2008.00662.x

Gocke, A. R., Lebson, L. A., Grishkan, I. V., Hu, L., Nguyen, H. M., Whartenby, K. A., et al. (2012). Kv1.3 Deletion Biases T Cells toward an Immunoregulatory Phenotype and Renders Mice Resistant to Autoimmune Encephalomyelitis. *J. Immunol.* 188, 5877–5886. doi:10.4049/jimmunol.1103095

Gourraud, P. A., Harbo, H. F., Hauser, S. L., and Baranzini, S. E. (2012). The Genetics of Multiple Sclerosis: an Up-To-Date Review. *Immunol. Rev.* 248, 87–103. doi:10.1111/j.1600-065X.2012.01134.x

Goverman, J. (2009). Autoimmune T Cell Responses in the central Nervous System. *Nat. Rev. Immunol.* 9, 393–407. doi:10.1038/nri2550

Gwack, Y., Feske, S., Srikanth, S., Hogan, P. G., and Rao, A. (2007). Signalling to Transcription: Store-Operated Ca2+ Entry and NFAT Activation in Lymphocytes. *Cell Calcium* 42, 145–156. doi:10.1016/j.ceca.2007.03.007

Hajdú, P., Szilágyi, O., Tóth, A., Krasznai, Z., Pocsai, K., and Panyi, G. (2010). Answer to the "comment on functional consequences of Kv1.3 ion channel rearrangement into the immunological synapse" by Stefan Bittner et al. [Immunol. Lett. 125 (Aug 15 (2)) (2009) 156-157]. *Immunol. Lett.* 129, 47–49. doi:10.1016/j.imlet.2009.12.026

Hille, B. (2001). *Ion Channels of Excitable Membranes*. Sunderland, MA: Sinauer.

Lassmann, H. (2004). Recent Neuropathological Findings in MS--implications for Diagnosis and Therapy. *J. Neurol.* 251, IV2–5. doi:10.1007/s00415-004-1402-3

Levite, M., Cahalon, L., Peretz, A., Hershkoviz, R., and Ariel, A. (2000). Extracellular K(+) and Opening of Voltage-Gated Potassium Channels Activate T Cell Integrin Function: Physical and Functional Association between Kv1.3 Channels and Beta1 Integrins. *J. Exp. Med.* 191 (7), 1167–1176. doi:10.1084/jem.191.7.1167

Lewis, R. S. (2001). Calcium Signaling Mechanisms in T Lymphocytes. *Annu. Rev. Immunol.* 19, 497–521. doi:10.1146/annurev.immunol.19.1.497

Lioudyno, V., Abdurasulova, I., Negoreeva, I., Stoliarov, I., Kudriavtsev, I., Serebryakova, M., et al. (2021). A Common Genetic Variant Rs2821557 in KCNA3 Is Linked to the Severity of Multiple Sclerosis. *J. Neurosci. Res.* 99, 200–208. doi:10.1002/jnr.24596

Lublin, F. D., Reingold, S. C., Cohen, J. A., Cutter, G. R., Soelberg Sørensen, P., Thompson, A. J., et al. (2014). Defining the Clinical Vourse of Multiple Sclerosis: The 2013 Revisions. *Neurology* 83, 278–286. doi:10.1212/WNL.0000000000000560

Malissen, B., and Bongrand, P. (2015). Early T Cell Activation: Integrating Biochemical, Structural, and Biophysical Cues. *Annu. Rev. Immunol.* 33, 539–561. doi:10.1146/annurev-immunol-032414-112158

Markovic-Plese, S., Cortese, I., Wandinger, K. P., McFarland, H. F., and Martin, R. (2001). CD4+CD28- Costimulation-independent T Cells in Multiple Sclerosis. *J. Clin. Invest.* 108, 1185-1194. doi:10.1172/JCI12516

Martino, G., Grohovaz, F., Brambilla, E., Codazzi, F., Consiglio, A., Clementi, E., et al. (1998). Proinflammatory Cytokines Regulate Antigen-independent T-Cell Activation by Two Separate Calcium-Signaling Pathways in Multiple Sclerosis Patients. *Ann. Neurol.* 43, 340–349. doi:10.1002/ana.410430312

Matheu, M. P., Beeton, C., Garcia, A., Chi, V., Rangaraju, S., Safrina, O., et al. (2008). Imaging of Effector Memory T-Cells during a Delayed-type Hypersensitivity Reaction and Suppression by Kv1.3 Channel Block. *Immunity* 29, 602–614. doi:10.1016/j.immuni.2008.07.015

Mkhikian, H., Grigorian, A., Li, C. F., Chen, H. L., Newton, B., Zhou, R. W., et al. (2011). Genetics and the Environment Converge to Dysregulate N-Glycosylation in Multiple Sclerosis. *Nat. Commun.* 2, 334. doi:10.1038/ncomms1333

Morton, M. J., Abohamed, A., Sivaprasadarao, A., and Hunter, M. (2005). Determinants of pH Sensing in the Two-Pore Domain K^+ Channel, TASK-2. *Proc. Natl. Acad. Sci. USA* 102, 16102–16106. doi:10.1007/s00424-002-0901-210.1073/pnas.0506870102

Murray, J. K., Qian, Y. X., Liu, B., Elliott, R., Aral, J., Park, C., et al. (2015). Pharmaceutical Optimization of Peptide Toxins for Ion Channel Targets: Potent, Selective, and Long-Lived Antagonists of Kv1.3. *J. Med. Chem.* 58, 6784–6802. doi:10.1021/acs.jmedchem.5b00495

Panyi, G., Bagdany, M., Bodnar, A., Vamosi, G., Sventezi, G., Jenei, A., et al. (2003). Colocalization and Nonrandom Distribution of Kv1.3 Potassium Channels and CD3 Molecules in the Plasma Membrane of Human T Lymphocytes. *Proc. Natl. Acad. Sci. USA* 100, 2592–2597. doi:10.1073/pnas.0438057100

Panyi, G., Vamosi, G., Bacso, Z., Bagdany, M., Bodnar, A., Varga, Z., et al. (2004). Kv1.3 Potassium Channels Are Localized in the Immunological Synapse Formed between Cytotoxic and Target Cells. *Proc. Natl. Acad. Sci. USA* 101, 1285–1290. doi:10.1073/pnas.0307421100

Poulopoulou, C., Papadopoulou-Daifoti, Z., Hatzimanolis, A., Fragiadaki, K., Polissidis, A., Anderzanova, E., et al. (2008). Glutamate Levels and Activity of the T Cell Voltage-Gated Potassium Kv1.3 Channel in Patients with Systemic Lupus Erythematosus. *Arthritis Rheum.* 58 (5), 1445–1450. doi:10.1002/art.23446

Poulopoulou, C., Davaki, P., Koliaraki, V., Kolovou, D., Markakis, I., and Vassilopoulos, D. (2005b). Reduced Expression of Metabotropic Glutamate Receptor 2 mRNA in T Cells of ALS Patients. *Ann. Neurol.* 58, 946–949. doi:10.1002/ana.20675

Poulopoulou, C., Markakis, I., Davaki, P., Nikolaou, C., Poulopoulos, A., Raptis, E., et al. (2005a). Modulation of Voltage-Gated Potassium Channels in Human T Lymphocytes by Extracellular Glutamate. *Mol. Pharm.* 67, 856–867. doi:10.1124/mol.67.3.856

Rus, H., Pardo, C. A., Hu, L., Darrah, E., Cudrici, C., Niculescu, T., et al. (2005). The Voltage-Gated Potassium Channel Kv1.3 Is Highly Expressed on Inflammatory Infiltrates in Multiple Sclerosis Brain. *Proc. Natl. Acad. Sci. USA* 102, 11094–11099. doi:10.1073/pnas.0501770102

Severson, C., and Hafler, D. A. (2010). T-cells in Multiple Sclerosis. *Results Probl. Cell Differ* 51, 75–98. doi:10.1007/400_2009_12

Szabò, I., Gulbins, E., Apfel, H., Zhang, X., Barth, P., Busch, A. E., et al. (1996). Tyrosine Phosphorylation Dependent Suppression of a Voltage-Gated K^+ Channel in T Lymphocytes upon Fas Stimulation. *J. Biol. Chem.* 271, 20465–20469. doi:10.1074/jbc.271.34.20465

Thompson, A. J., Banwell, B. L., Barkhof, F., Carroll, W. M., Coetzee, T., Comi, g., et al. (2018). Diagnosis of Multiple Sclerosis: 2017 Revisions of the McDonald Criteria. *Lancet Neurol.* 17, 162–173. doi:10.1016/S1474-4422(17)30470-2

Volpe, E., Sambucci, M., Battistini, L., and Borsellino, G. (2016). Fas-Fas Ligand: Checkpoint of T Cell Functions in Multiple Sclerosis. *Front. Immunol.* 7, 382. doi:10.3389/fimmu.2016.00382

Wagner, C. A., Roqué, P. J., and Goverman, J. M. (2020). Pathogenic T Cell Cytokines in Multiple Sclerosis. *J. Exp. Med.* 217, e20190460. doi:10.1084/jem.20190460

Wulff, H., Calabresi, P. A., Allie, R., Yun, S., Pennington, M., Beeton, C., et al. (2003). The Voltage-Gated Kv1.3 K(+) Channel in Effector Memory T-Cells as New Target for MS. *J. Clin. Invest.* 111, 1703–1713. doi:10.1172/JCI16921

Zhang, J., Markovic-Plese, S., Lacet, B., Raus, J., Weiner, H. L., and Hafler, D. A. (1994). Increased Frequency of Interleukin 2-responsive T Cells Specific for Myelin Basic Protein and Proteolipid Protein in Peripheral Blood and Cerebrospinal Fluid of Patients with Multiple Sclerosis. *J. Exp. Med.* 179, 973–984. doi:10.1084/jem.179.3.973

Conflict of Interest: The author MP is employed by AmbioPharm Inc. KC, CB, and MP have a patent "Analogs of ShK toxin and their uses in selective inhibition of Kv1.3 potassium channels" (US patent application 11/663398) licensed to TEKv Therapeutics.

The remaining authors declare that the research was conducted in the absence of any commercial or financial relationships that could be construed as a potential conflict of interest.

Publisher's Note: All claims expressed in this article are solely those of the authors and do not necessarily represent those of their affiliated organizations, or those of the publisher, the editors and the reviewers. Any product that may be evaluated in this article, or claim that may be made by its manufacturer, is not guaranteed or endorsed by the publisher.

frontiers in Pharmacology

ORIGINAL RESEARCH
published: 29 September 2021
doi: 10.3389/fphar.2021.733610

Optimization of *Pichia pastoris* Expression System for High-Level Production of Margatoxin

Muhammad Umair Naseem[1], *Gabor Tajti*[1], *Attila Gaspar*[2], *Tibor G. Szanto*[1], *Jesús Borrego*[1] *and Gyorgy Panyi*[1]*

[1]*Department of Biophysics and Cell Biology, Faculty of Medicine, University of Debrecen, Debrecen, Hungary,* [2]*Department of Inorganic and Analytical Chemistry, Faculty of Science and Technology, Institute of Chemistry, University of Debrecen, Debrecen, Hungary*

Margatoxin (MgTx) is a high-affinity blocker of voltage-gated potassium (Kv) channels. It inhibits Kv1.1–Kv1.3 ion channels in picomolar concentrations. This toxin is widely used to study physiological function of Kv ion channels in various cell types, including immune cells. Isolation of native MgTx in large quantities from scorpion venom is not affordable. Chemical synthesis and recombinant production in *Escherichia coli* need *in vitro* oxidative refolding for proper disulfide bond formation, resulting in a very low yield of peptide production. The *Pichia pastoris* expression system offers an economical approach to overcome all these limitations and gives a higher yield of correctly refolded recombinant peptides. In this study, improved heterologous expression of recombinant MgTx (rMgTx) in *P. pastoris* was obtained by using preferential codons, selecting the hyper-resistant clone against Zeocin, and optimizing the culturing conditions. About 36 ± 4 mg/L of >98% pure His-tagged rMgTx (TrMgTx) was produced, which is a threefold higher yield than has been previously reported. Proteolytic digestion of TrMgTx with factor Xa generated untagged rMgTx (UrMgTx). Both TrMgTx and UrMgTx blocked the Kv1.2 and Kv1.3 currents (patch-clamp) (K_d for Kv1.2 were 64 and 14 pM, and for Kv1.3, 86 and 50 pM, respectively) with comparable potency to the native MgTx. The analysis of the binding kinetics showed that TrMgTx had a lower association rate than UrMgTx for both Kv1.2 and Kv1.3. The dissociation rate of both the analogues was the same for Kv1.3. However, in the case of Kv1.2, TrMgTx showed a much higher dissociation rate with full recovery of the block than UrMgTx. Moreover, in a biological functional assay, both peptides significantly downregulated the expression of early activation markers IL2R and CD40L in activated $CD4^+$ T_{EM} lymphocytes whose activation was Kv1.3 dependent. In conclusion, the authors report that the *Pichia* expression system is a powerful method to produce disulfide-rich peptides, the overexpression of which could be enhanced noticeably through optimization strategies, making it more cost-effective. Since the presence of the His-tag on rMgTx only mildly altered the block equilibrium and binding kinetics, recombinant toxins could be used in ion channel research without removing the tag and could thus reduce the cost and time demand for toxin production.

Keywords: *Pichia pastoris*, patch-clamp, margatoxin, recombinant expression, Kv1.3 blocker, $CD4^+$ T_{EM} cells

OPEN ACCESS

Edited by:
Ildikò Szabò,
University of Padua, Italy

Reviewed by:
Lane Brown,
Washington State University, United States
Roope Mannikko,
University College London, United Kingdom

***Correspondence:**
Gyorgy Panyi
panyi@med.unideb.hu

Specialty section:
This article was submitted to Pharmacology of Ion Channels and Channelopathies, a section of the journal Frontiers in Pharmacology

Received: *30 June 2021*
Accepted: *30 August 2021*
Published: *29 September 2021*

Citation:
Naseem MU, Tajti G, Gaspar A, Szanto TG, Borrego J and Panyi G (2021) Optimization of Pichia pastoris *Expression System for High-Level Production of Margatoxin. Front. Pharmacol. 12:733610. doi: 10.3389/fphar.2021.733610*

INTRODUCTION

Voltage-gated potassium (Kv) channels are present in a variety of cells and tissues where they regulate multiple physiological processes, including cardiac function, neural excitability, muscle contraction, cell proliferation, cell volume control, and hormonal secretion (Coetzee et al., 1999; Giangiacomo et al., 2004). In recent years, it has been shown that modulating the function of Kv channels may have therapeutic potential in cardiac arrhythmia, diabetes, asthma, inflammation, neuronal disorders, and T-cell–mediated autoimmune diseases and anti-tumor immunity (Chandy et al., 2004; Panyi et al., 2006; Jiménez-Vargas et al., 2012; Panyi et al., 2014; Kazama, 2015; Rubaiy, 2016; Yang and Nerbonne, 2016; Hofschröer et al., 2021). Kv1.3 plays a key role in pathogenesis of autoimmune diseases, e.g., multiple sclerosis, rheumatoid arthritis, and type-1 diabetes by triggering the activation and proliferation of T effector memory (T_{EM}) cells (Chandy et al., 2004; Beeton et al., 2011a; Lam and Wulff, 2011; Chi et al., 2012; Toldi et al., 2013; Koshy et al., 2014). Since selective block of Kv1.3 suppresses the proliferation of T_{EM} cells, Kv1.3 has become an attractive immunomodulatory drug target in treating autoimmune diseases. Numerous peptide toxins have been derived over the past few decades from scorpion venom, which target and modulate Kv channel functions. These peptides consist of 20–80 residues and 3–4 conserved disulfide bridges to stabilize their tertiary structures that are responsible for specific interaction with ion channels (Shen et al., 2017; Tajti et al., 2020). Of these, the scorpion toxins from the α-KTx family, e.g., charybdotoxin (α-KTx 1.1), margatoxin (α-KTx 2.2), and Vm24 (α-KTx 23.1), have provided the platform for studying the pharmacological, physiological, and structural characteristics of different subtypes of K^+ channels (Tenenholz et al., 2000; de la Vega et al., 2003; Han et al., 2011; Veytia-Bucheli et al., 2018). Although scorpion toxins inhibit Kv1.3 at nanomolar concentrations, they often show off-target effects by blocking other Kv1.x ion channels (Kalman et al., 1998; Bagdány et al., 2005). Therefore, for therapeutic purposes, peptide engineering is needed to design a peptide toxin with a higher selectivity and potency for Kv1.3. ShK-186 (Dalazatide), one of the engineered analogs of ShK toxin (isolated from sea anemone), is a potent and selective inhibitor of Kv1.3 that is under clinical trials for the treatment of multiple autoimmune disorders (Pennington et al., 2015; Tarcha et al., 2017; Tajti et al., 2020; Wang et al., 2020).

For structure–function relationship studies of engineered peptides and therapeutic applications, a large amount of peptide toxins is needed. Natural crude venom yields a limited amount of peptide toxins that are usually inadequate for biological analysis, while the chemical synthesis offers an expensive approach to produce disulfide-rich peptides and their analogs (Jensen et al., 2009). On the other hand, the heterologous protein expression system is a cost-effective and the most widely used technique to produce large quantities of recombinant proteins. Still, intracellular recombinant expression of eukaryotic origin proteins in bacteria has limitations, such as insoluble expression, a lack of posttranslational modifications, and disulfide bond formation (Rudolph and Lilie, 1996). However, the periplasmic expression or use of engineered *Escherichia coli* strains, which are capable of disulfide bond formation, usually produce refolded soluble proteins, but their yield is very low (Lobstein et al., 2012; Klint et al., 2013). To overcome all these limitations, the *Pichia pastoris* expression system was introduced that provides an efficient and economical approach, and produces heterologous proteins in correctly refolded form with disulfide bridges (White et al., 1994; Anangi et al., 2012). High-level growth in a simple medium, ease of genetic manipulation, and capability of performing posttranslational modifications are the other advantages of this system. Furthermore, the recombinant proteins are secreted directly into the medium with very few endogenous proteins, which simplifies the downstream processing (Macauley-Patrick et al., 2005; Cregg, 2007). The overexpression of heterologous proteins in this system can be enhanced considerably by codon optimization, screening for multiple copy integrant, choosing an efficient promoter, and optimizing fermentation conditions, such as biomass production, pH of the medium, induction duration, and percentage of methanol induction (Macauley-Patrick et al., 2005; Yu et al., 2010; Yu et al., 2013). In comparison to the yeast expression system, production of recombinant proteins in insect cell and animal cell cultures is complicated and expensive (Escoubas et al., 2003).

Margatoxin (MgTx) is a 39-amino-acid peptide toxin isolated from the venom of the scorpion *Centruroides margaritatus*. Its 3D structure consists of an α-helix and three antiparallel β-strands stabilized by three disulfide bonds. This peptide toxin has been widely used for structural and functional characterization of Kv1.x ion channels in various cell types and tissues, as it inhibits Kv1.2 and Kv1.3 ion channels with high potency in picomolar concentrations (Garcia-Calvo et al., 1993; Bartok et al., 2014). Previous studies report the production of recombinant MgTx (rMgTx) in *E. coli* and *P. pastoris* with a yield of 3–4 mg (Garcia-Calvo et al., 1993; Johnson et al., 1994) and 12–15 mg per liter (Anangi et al., 2012), respectively.

In this work, the *P. pastoris* expression system was optimized to achieve a high-level expression of rMgTx. First, biased codon optimization was used to select the clone showing hyper-resistance against the selection marker. The fermentation conditions (pH of the medium, induction time course, and methanol induction) were then optimized to get a high yield (36 mg/L) of the peptide. After purification, the N-terminal His-tag was removed by using factor Xa protease. It was found that both versions (tagged and untagged) of rMgTx inhibited the hKv1.3 and hKv1.2 channels in picomolar concentrations. Both peptides also downregulated IL2R and CD40L expression in activated $CD4^+$ T_{EM} cells through Kv1.3 blockade. Moreover, in this study, the influence of the N-terminal His-tag (additional residues) of rMgTx on binding kinetics to hKv1.3 and hKv1.2 was studied.

MATERIALS AND METHODS

Construction of Plasmid

The amino acid sequence of MgTx was retrieved from the online protein (Uniprot P40755) database. The MgTx gene cassette was designed by placing the 6xHis-tag at the N-terminal to facilitate purification, and factor Xa protease site was introduced in

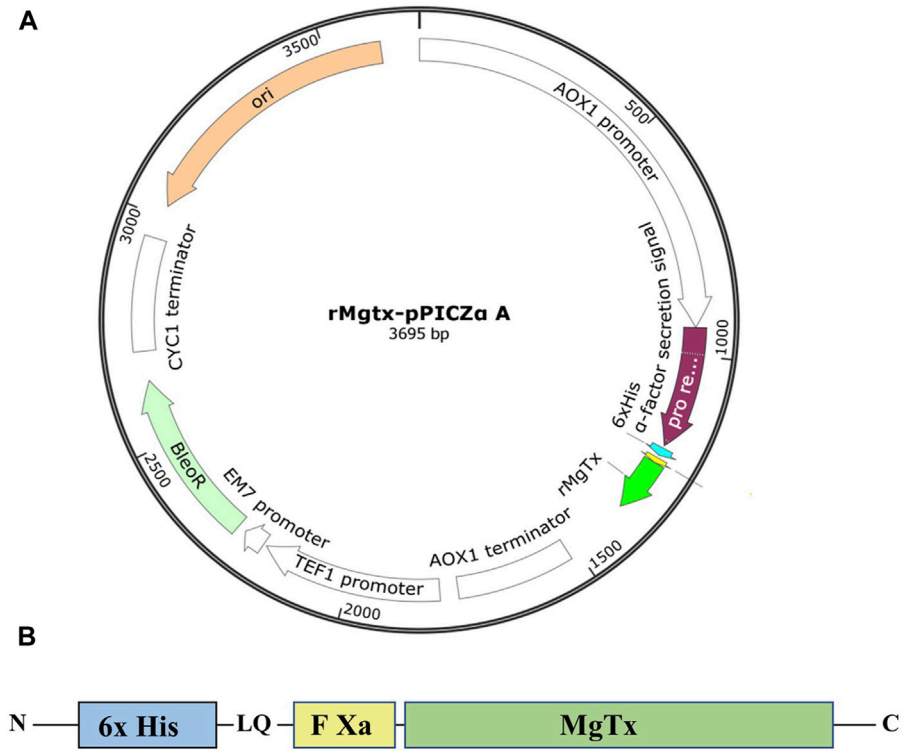

FIGURE 1 | (A) Graphical representation of recombinant plasmid TrMgTx–pPICZαA designed using the SnapGene® tool. **(B)** Schematic demonstration of the TrMgTx cassette.

between them to obtain native N-terminal MgTx, as demonstrated in **Figure 1**. The codon-optimized DNA sequence of this MgTx cassette for *P. pastoris* was generated according to the codon usage database available at www.kazusa.or.jp/codon and synthesized from Integrated DNA Technologies, Belgium. The codon-optimized MgTx cassette was cloned into yeast expression vector pPICZα A (Invitrogen, United States) by using *EcoRI* and *XbaI* restriction sites. In-frame ligation and nucleotide sequence of MgTx was confirmed by DNA sequencing by using plasmid-specific primers and aligning the obtained DNA sequence with the theoretical sequence of MgTx.

Transformation of *Pichia pastoris* X-33 and Selection of Hyper-Resistant Transformants Against Zeocin

The expression plasmid was linearized by digesting with *SacI* endonuclease enzyme and transformed into *P. pastoris* X-33 competent cells using Pichia EasyComp Transformation Kit (Invitrogen, United States), following the protocol specified by the manufacturer. Transformed X-33 cells were spread on YPD agar plate (2% peptone, 1% yeast extract, 2% agar, 2% dextrose, and pH 7.0) containing 100 μg/ml of Zeocin. After 3-day incubation at 28°C, 24 prominent colonies were regrown on YPD plates supplemented with progressively increasing Zeocin 500, 1000, and 2000 μg/ml for the selection of the clone showing hyper-resistance against Zeocin. To confirm the integration of expression construct into the genome of *Pichia* transformants, survived on 2000 μg/ml Zeocin, colony PCR was performed by using plasmid-specific primers.

Time Course Study of MgTx Expression and Optimization of pH of the Medium and Methanol Induction

A selected clone from the YPD plate containing 2000 μg/ml of Zeocin was grown overnight in 5 ml of the YPD medium and diluted the next day to an OD_{600} = 0.2 in 5 ml of BMGY medium (1% yeast extract, 2% peptone, 100 mM potassium phosphate, pH 6.0, 1.34% YNB, 4×10^{-5}% biotin, and 2% glycerol) for biomass production at 30°C with constant shaking (230 rpm) until the OD_{600} reached between 15 and 20 (after 24–36 h). Cells were collected by centrifugation, resuspended in 5 ml of BMMY induction medium (same as BMGY with 0.5% methanol instead of glycerol), and grown for 5 days at 28°C with constant shaking (230 rpm). Absolute methanol (MeOH, 0.5%) was added every 24 h to maintain the induction, except when MeOH concentration dependence of induction was studied. To find the suitable amount of methanol induction, cells were induced with 0.5, 1, and 1.5% MeOH, and for pH optimization, cells were grown in media of different pH, i.e., 5, 6, and 7, without buffering. About 15 μl of the supernatant samples were taken at indicated time points and analyzed on 16% tricine–SDS-PAGE. The amount of His-tagged rMgTx

(TrMgTx) in the gel image was determined by comparing the band intensities with the standards (TrMgTx with known concentration) using Image Lab tool (Bio-Rad). All the experiments were run in triplicates.

Large-Scale Fed-Batch Fermentation and Purification of TrMgTx

Large-scale flask-level production was executed following the optimized conditions as described earlier. The clone with the highest expression level of TrMgTx was inoculated in a 2-L flask containing 250 ml of the BMGY medium, and when the OD_{600} reached between 15 and 20, the cells were shifted to 250 ml of the BMMY induction medium and induced with 0.5% MeOH for 72 h.

Two-step purification was used to efficiently isolate secreted TrMgTx from the culture. The cultured supernatant was collected by high-speed centrifugation, 2× diluted with buffer (50 mM potassium phosphate, pH 7.4), and 60 mM imidazole was added. The filtered supernatant was loaded on pre-equilibrated His-trap column packed with Ni Sepharose™ High Performance affinity media (GE Healthcare, United Kingdom) with a binding buffer (50 mM potassium phosphate, 300 mM NaCl, and pH 7.4) at a flow rate of 3 ml/min using the liquid chromatography (LC) system (Shimadzu, Germany). After washing the column with three column volumes (CVs) of wash buffer (binding buffer + 60 mM imidazole), proteins were eluted by running three CVs of the elution buffer (binding buffer + 500 mM imidazole) and an additional three CVs of 1 M imidazole in isocratic mode. Fractions collected from the affinity column were directly applied on reversed-phase C_{18} semi-prep column (10 mm) × 250 mm, 5 µM bead size, 300 Å pore size, Vydac® 218 TP, HiChrom, United Kingdom) using Prominence HPLC System (Shimadzu, Germany) at a flow rate of 1 ml/min. Then, a linear gradient of 10–30% of Solvent B (0.1% TFA in 95% acetonitrile) in Solvent A (0.1% TFA in deionized distilled water) was run for 30 min. Absorbance was monitored at 230 nm with a PDA detector. The peak fractions were collected manually and tested on 16% tricine–SDS-PAGE. The purity level was judged by reloading the fraction on the reversed-phase C_{18} analytical column and was calculated by the equation: (area under the peak of interest)/(cumulated area under all the peaks) × x100.

SDS-PAGE and Western Blot

16% Tricine–SDS-PAGE was performed as described hitherto (Schägger, 2006). The protein sample was mixed with tricine sample buffer (Bio-Rad) at 1:1, incubated at 95°C for 5 min, and subsequently centrifuged at 10,000 rpm for 30 s before loading. Electrophoresis was carried out at constant 120 V for 90 min. For protein visualization, the gel was stained with Coomassie Brilliant Blue G-250 for 45 min and then destained by using 40% methanol and 10% acetic acid mixture for 2–3 h.

For Western blotting, the resolved proteins were electrotransferred in wet conditions onto a charged Immobilon-P PVDF membrane (Merck, Germany). Non–specific binding of antibodies in the subsequent steps was prevented by membrane blocking with 5% (w/v) skim milk in TBST (50 mM Tris-HCl, pH 7.5, 150 mM NaCl, and 0.1% Tween 20), overnight at 4°C. The washed membrane was probed with mouse anti-histidine monoclonal antibodies conjugated with horseradish peroxidase (Bio-Rad, CA, United States) in TBST (1:2,500) and incubated for 1 h at room temperature. The bands were visualized using Pierce™ enhanced chemiluminescent (ECL) substrate (Thermo Scientific, MA, United States).

Cleavage of His-Tag From TrMgTx

Hexahistidine residues fused at the N-terminal of TrMgTx were cleaved with factor Xa protease (Thermo Scientific, United States Cat# 32,521). About 300 µg of TrMgTx was mixed with factor Xa at an enzyme-to-substrate ratio of 1:100 in TBS buffer (50 mM Tris, 100 mM NaCl, 6 mM $CaCl_2$, pH 8.0) and incubated overnight at 25°C. The next day, the samples treated with or without enzyme were analyzed on 16% tricine/6 M urea–SDS-PAGE. To purify untagged rMgTx (UrMgTx), the cleaved His-tag and undigested peptide fragments were captured by using pre-charged Ni^+ beads, centrifuged at a high speed for 1 min to remove the beads, and the supernatant was loaded on a reversed-phase C_{18} analytical column (4.6 mm × 250 mm, 5 µM bead size, Vydac® 218TP) using the HPLC system (Shimadzu, Germany) and eluted with a linear gradient of 10–30% of Solvent B (0.1% TFA in 95% acetonitrile) in Solvent A (0.1% TFA in deionized distilled water) that was run for 25 min.

Mass Spectrometry Analyses

Mass spectrometric determinations were performed with an ESI-QTOF-MS instrument (maXis II UHR ESI-QTOF MS, Bruker, Bremen, Germany). The mass spectrometer was operated in a positive ionization mode; 0.5 bar nebulizer pressure, 200°C dry gas temperature, 4 L/min dry gas flow rate, 4000 V capillary voltage, 500 V end plate offset, 1 Hz spectra rate, and 500–2,500 m/z mass range were applied. ESI tuning mix (Agilent) calibrant injected after each run enabled internal m/z calibration. Mass spectra were processed and evaluated by Compass Data Analysis version 4.4 (Bruker).

Cells

The human venous blood from anonymized healthy donors was obtained from a blood bank. The peripheral blood mononuclear cells were isolated through Histopaque1077 (Sigma-Aldrich Hungary, Budapest, Hungary) density gradient centrifugation. Cells obtained were resuspended in RPMI 1640 medium containing 10% fetal calf serum (Sigma-Aldrich), 100 µg/ml penicillin, 100 µg/ml streptomycin, and 2 mM_L glutamine, seeded in a 24-well culture plate at a density of $5 x 10^5$cells per ml, and grown in a 5% CO_2 incubator at 37°C for 2–5 days. Phytohemagglutinin A (Sigma-Aldrich) was added in 5, 7, and 10 µg/ml concentrations to the medium to boost the potassium ion channel expression.

CHO cells were transiently transfected with the vector pCMV6-GFP (OriGene Technologies, Germany) encoding the human Kv1.2 ion channel using Lipofectamine 2000 (Invitrogen, Carlsbad, CA), following the manufacturer's protocol, and grown

under the standard conditions as used previously (Bagdány et al., 2005). GFP-positive transfectants were identified with Nikon TE 2000U fluorescence microscope (Nikon, Tokyo, Japan), and currents were recorded after 24 h post transfection.

Electrophysiology

Electrophysiological measurements were performed by using the patch-clamp technique in whole-cell or outside-out patch configuration and voltage clamp mode using the Multiclamp 700B amplifier and Axon Digidata1440 digitizer (Molecular Devices, Sunnyvale, CA). Micropipettes were pulled from GC150F-15 borosilicate capillaries (Harvard Apparatus Kent, United Kingdom), resulting in 3–5 MΩ resistance in the bath solution. The extracellular solution contained 145 mM NaCl, 5 mM KCl, 1 mM $MgCl_2$, 2.5 mM $CaCl_2$, 5.5 mM glucose, and 10 mM HEPES, with a pH of 7.35 and an osmolarity between 302 and 308 mOsM/L. When the toxins were dissolved at different molar concentrations in bath solution, it was supplemented with 0.1 mg/ml of BSA. The pipette filling (intracellular) solution consisted of 140 mM KF, 2 mM $MgCl_2$, 1 mM $CaCl_2$, 10 mM HEPES, and 11 mM EGTA, with a pH of 7.22 and an osmolarity of 295 mOsM/L.

To record the hKv1.3 and hKv1.2 currents, 15- to 200-ms-long depolarization impulses were applied at +50 mV from a holding potential of −120 mV every 15 s. The pClamp 10.1 software package was used to acquire and analyze the measured data. Current traces were low-pass filtered by the analog four-pole Bessel filters of the amplifiers, and the sampling frequency was set at 20 kHz, at least twice that of the filter cutoff frequency. The effect of the toxin at a given molar concentration was calculated as the remaining current fraction (RCF = I/I_0, where I_0 is the peak current in the absence of the toxin and I is the peak current at equilibrium block at a given toxin concentration). The data points on dose–response curves represent the mean of 3–4 individual measurements. The data points were fitted with a three-parameter [inhibition] vs response model, RCF = Bottom + [Top–Bottom)/(1+([toxin]/K_d)], where Top and Bottom values were constrained to 1 and 0, respectively, and [toxin] is the concentration of the toxin. The best fit curve gave K_d of the given toxin.

Analysis of the Binding and Unbinding Kinetics of the Peptides

To examine the effect of additional residues of TrMgTx on binding to the ion channel, the association and dissociation rate constants of both the versions of the toxin were determined for the Kv1.3 channel of the activated human T lymphocytes and the hKv1.2 channel transiently expressed in the CHO cell. Whole-cell currents were recorded after applying the toxin (200 pM for Kv1.3 and 100 pM for Kv1.2) to the extracellular solution until the equilibrium block was achieved (wash-in), and then removed it by perfusing the toxin-free control solution (washout). Peak currents at a time point t [I(t)] were normalized to the peak current in the absence of the toxin [$I_{norm}(t) = I(t)/I_0$], and these were plotted as a function of time. The association time constant (τ_{on}) was determined by fitting the data points during the wash-in procedure in the one-phase decay equation: $I_{norm}(t) = \left((1-RCF)\times e^{-\frac{t}{\tau on}}\right)+RCF$, with the RCF = I/I_0 at the equilibrium block as defined in the Electrophysiology section. The dissociation time constant (τ_{off}) was determined by fitting the following equation to the data points during the washout procedure: $I_{norm}(t) = RCF + \left(1-e^{-\frac{t}{\tau_{off}}}\right)$

The association rate constant (k_{on}) and dissociation rate constant (k_{off}) were calculated from the measured time constants, assuming a simple bimolecular interaction between the channel and toxin, and by using the following equations (Peter et al., 2001), with τ_{on} and τ_{off} defined above, and [toxin] as the toxin concentration:

$$k_{on} = \frac{1-\left(\tau_{on}\times k_{off}\right)}{\tau_{on}\times [toxin]}, k_{off} = \frac{1}{\tau_{off}}.$$

IL2R and CD40L Expression Assay in $CD4^+$ Effector Memory T Lymphocyte

The mononuclear cells were isolated from anonymized healthy donors as described earlier. Prior to $CD4^+$ T_{EM} cells separation, dead cells were removed using the Dead Cell Removal Microbead Kit (Miltenyi Biotec B.V & CO. KG, Bergisch Gladbach, Germany). Untouched $CD4^+$ T_{EM} lymphocytes were purified through magnetic cell sorting (negative selection) with the $CD4^+$ Effector Memory T Cell Isolation Kit (Miltenyi Biotec B.V. & Co. KG, Bergisch Gladbach, Germany) according to the manufacturer's protocol.

For TCR-specific stimulation, anti-human CD3 monoclonal antibodies (clone OKT3, BioLegend, San Diego, CA) were bound to the surface of 24-well cell culture plates at a density of 5 μg/well in phosphate-buffered saline (PBS) overnight at 4°C. Before seeding the cells, the wells were washed twice with PBS to remove the unbound antibodies. The $CD4^+$ T_{EM} cells were divided into four groups: 1) unstimulated, 2) stimulated, 3) stimulated + TrMgTx (8.5 nM), and 4) stimulated + UrMgTx (5 nM). The cells were seeded at a density of 0.5×10^6 cells/ml per well, and when indicated, the cells were preincubated with the toxins for 5 min prior to the stimulation. The plate was incubated at 37°C in 5% CO_2 for 24 h. Each experiment was performed in technical duplicates on three different donors.

For quantifying the extent of T_{EM} cell stimulation, cells were washed with PBS buffer containing 1% of fetal bovine serum (FBS) and stained with fluorescein isothiocyanate (FITC)–labeled anti-human CD154 (CD40L) antibody (clones 24–31, BioLegend, San Diego, CA) and PerCP/Cyanine5.5–labeled anti-human CD25 (IL2R) antibody (clone BC96, BioLegend) at 4°C for 20 min. Cells were washed with the PBS + 1% FBS buffer and resuspended in 150 μl in PBS + 1% FBS. Samples were measured with NovoCyte 3000 RYB flow cytometer (ACEA Bioscience Inc.), FITC and PerCP/Cyanine5.5 were excited by using blue laser (488 nm), and 530/30 nm and 695/40 nm emission filters were used, respectively. Flow cytometry data were analyzed using

FCS Express 6.0 (De Novo Software, Glendale, CA). Briefly, cells were gated on the basis of their FSC and SSC parameters, and then, the histograms corresponding to CD40L and CD25 were plotted as peak-normalized overlays. Mean fluorescent intensities (MFIs) were computed from the histograms and normalized to that of their stimulated (S) but not treated control. The negative (unlabeled) and unstimulated control (US) were always used for comparison.

Statistics

Data analyses and graph generation were performed using the GraphPad Prism software (version 9.1, La Jolla CA, United States). Statistical comparisons were made by using one-way ANOVA with Tukey's test and unpaired *t* test. For all the experiments, data are reported with standard error of mean (SEM).

RESULTS

Transformation of TrMgTx–pPICZαA Recombinant Plasmid Into *P. pastoris* X-33 and Selection of Hyper-Resistant Transformants Against Zeocin

The expression cassette, consisting of six histidines followed by the factor Xa cleavage site and coding DNA sequence of MgTx (**Figure 1B**), was synthesized by using favorable codons for *P. pastoris* and cloned into pPICZαA expression vector under the control of alcohol oxidase I (AOX1) promoter. In-frame ligation to the α-factor secretion signal and nucleotide sequence of the TrMgTx was verified by DNA Sanger sequencing. A schematic illustration of the TrMgTx–pPICZαA recombinant plasmid was created by using the *in silico* SnapGene® cloning tool (**Figure 1A**). The recombinant plasmid was linearized with the *SacI* enzyme and transformed into *Pichia* X-33 competent cells. Following 3 days of incubation at 30°C, more than 40 prominent colonies were observed on the YPD agar plate, containing 100 μg/ml of Zeocin. Hyper-resistant clones against Zeocin were selected by growing the initially chosen colonies on the YPD agar plates augmented with gradually increasing Zeocin to 0.5, 1, and 2 mg/ml (**Supplementary Figure S1**). The transformants that survived against the highest concentration of Zeocin (2 mg/ml) were selected, and colony PCR was performed which confirmed the integration of TrMgTx–pPICZαA plasmid by a single crossover at the 5′ AOX1 locus of the *P. pastoris* genome (**Supplementary Figure S2**).

Overexpression of TrMgTx as a Function of Culturing Time, Methanol Induction, and pH of the Medium

Supernatant samples were collected from the cultures every 24 h post methanol induction for 5 days and were analyzed by tricine–SDS-PAGE. A peptide band of ~6.5 kDa MW was detectable by using R-250 Coomassie Brilliant blue (CBB) after 24 h of methanol induction. This band gradually attained maximal density after 72 h of induction. However, the amount of secreted peptide toxin declined on the fourth and fifth day following induction (**Figures 2A,B**). The molecular mass of TrMgTx estimated from the gel was slightly higher than the predicted mass (5.9 kDa), most likely because of its higher PI value of 9.10. The highest concentration of peptide in the supernatant was 78 ± 7 mg/L after 72 h of induction. This yield was, in all pairwise multiple comparison (Tukey's test), significantly higher than the yield at any other time point ($p < 0.05$).

For optimization of methanol induction, biomass production of a TrMgTx clone was induced with 0.5, 1, and 1.5% MeOH, using a medium of pH 6. The gel scanning assay revealed that the amount of TrMgTx was the largest in the supernatant after inducing with 0.5% methanol for 72 h (71 ± 13 mg/L) (**Figure 2C**). This yield is significantly higher than that of the other two samples induced with 1 and 1.5% MeOH (all pairwise multiple comparison (Tukey's test), $p < 0.05$). Similarly, to find a suitable pH of the medium for improved expression of the peptide, biomass was induced with 0.5% MeOH in a media having pH 5, 6, or 7, or "not adjusted" for 72 h (**Figure 2D**). The supernatant of the culture at pH 6 showed 76 ± 8 mg/L expression of the peptide toxin which is considerably higher than for other samples from cultures with a pH 5 or 7 or "not adjusted" (all pairwise multiple comparison (Tukey's test), $p < 0.05$).

Purification of Tagged Recombinant MgTx

A *Pichia* X-33 clone that produced large amounts of TrMgTx in small cultures was subjected to large-scale fermentation in a medium of pH 6, and the expression was induced with 0.5% methanol for 3 days. The culture medium was centrifuged, filtered through a 0.45-μm membrane to remove cell debris, and then loaded on the Ni^{+} Sepharose column using the LC system as the first step of the two-step purification protocol applied. After removing the unbound proteins, His-tagged peptides were eluted with 0.5 and 1 M imidazole in isocratic mode. A very large peak appeared in the chromatogram with 0.5 M imidazole as compared with the peak obtained with 1 M imidazole, confirming that 0.5 M imidazole removed most of the bonded TrMgTx from the resin (**Figure 3A**). When the collected fractions were analyzed on tricine–SDS-PAGE, a clear and dense band of TrMgTx around ~6.5 kDa was observed in the elution fraction (with 0.5 M imidazole) and a low-intensity band of the same size appeared in the fraction eluted with 1 M imidazole. On the contrary, no such band was observed in the fractions collected during the loading of the supernatant (flow though) and washing of the column (**Figure 3B**), demonstrating that resin had efficiently captured all His-tagged peptides from the cultured supernatant.

To achieve high purity and homogeneity of the recombinantly produced TrMgTx, the partially purified fraction (i.e., eluted by 0.5 mM imidazole, see the Purification of Tagged Recombinant MgTx section for details) was applied on the C_{18} RP-HPLC semi-preparative column (second step of the purification protocol) and eluted with a gradient of 10–30% of acetonitrile in distilled water for 30 min (**Figure 3C**). Tricine–SDS-PAGE analyses of the collected HPLC fractions (**Figure 3D**) showed that a single

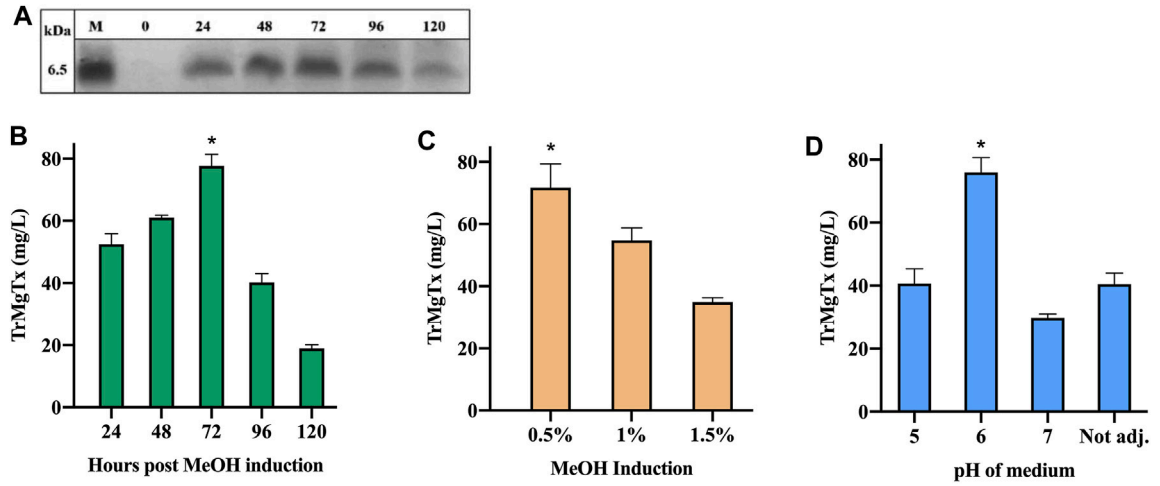

FIGURE 2 | Optimization of TrMgTx expression in shake-flask fermentation. **(A)** 15 µl of supernatant samples were collected at indicated time points and analyzed by using 16% tricine–SDS-PAGE (stained with R-250 CBB). The samples from 24 to 120 h show bands of ~6.5 kDa (close to the estimated MW of TrMgTx). **(B)** Concentration of TrMgTx in supernatant was quantified at the indicated time points by comparing the gel band intensity of TrMgTx with that of the standards by using Image Lab software (Bio-Rad). Expression was induced by 0.5% methanol at pH = 6.0 of the medium. **(C)** Secretion of TrMgTx in culture (at pH 6) induced with different MeOH concentrations for 72 h, peptide concentration was determined as in (**A**). **(D)** TrMgTx expression was determined as in **(A)** when induced with 0.5% MeOH for 72 h at the indicated pH values of the medium. Label "Not adj." means that the pH of the medium was not buffered. Data represent the mean of three independent experiments, where the error bars are SEM. Asterisks indicate significant difference in all pairwise multiple comparison (Tukey's test), $^*p < 0.05$.

band of TrMgTx at ~6.5 kDa MW appeared in the fraction corresponding to the peak eluted at the retention time (R_T) of ~28 min (indicating to peak 2 in the chromatogram shown in **Figure 3C**). The average molecular mass of 5980.86 Da was determined for TrMgTx by ESI-QTOF-MS which is in full agreement with the predicted average mass (5980.96 Da) of the peptide (**Figure 3E**). The quality of the peptide after the two-step purification was assessed by using the anti-His antibody in the Western blot (**Figure 4A**) and HPLC (**Figure 4B**). The Western blot verified the purity and identity of TrMgTx by detecting a single band with anti-His antibodies (**Figure 4A**) of the appropriate size (cf. **Figures 3B,D**). The TrMgTx is more than 98% pure after the two-step purification as assessed by the C_{18} RP-HPLC analytical column (**Figure 4B**). **Table 1** summarizes the purification scheme; on average, a total of 9.1 mg of TrMgTx was produced with 43% net recovery from 250 ml *P. pastoris* culture under optimized conditions.

Recombinant Margatoxin With Native N-Terminal

TrMgTx contains 14 additional N-terminal amino acid residues (EFHHHHHHLQIEGR). This mainly consists of 6x histidines used for affinity purification and the protease cleavage site for factor Xa. Factor Xa protease cleaves the tagged peptides without leaving any extra amino acids at the N-terminal (Waugh, 2011). To get rMgTx with native N-terminal, all the additional residues were removed by digesting the tagged peptide with factor Xa protease overnight. Tricine–SDS-PAGE analyses (**Figure 5A**) revealed that a band of ~4.1 kDa (the MW of native MgTx) was present in the overnight digested sample, confirming the successful removal of additional residues. The UrMgTx was purified using the C_{18} RP-HPLC column after separating the 6xHis fragments with Ni^+ beads. The peak at R_T 21.6 min in the chromatogram (**Figure 5B**) indicates the elution of UrMgTx. The determined average mass (4178.95 Da) of UrMgTx is equivalent to the theoretical mass (4179.018 Da) of native MgTx, proving that there is no extra residue at either terminal of UrMgTx after cleaving the tag (**Figure 5C**).

Effect of Tagged and Untagged Recombinant Margatoxin on hKv1.2 and hKv1.3 Ion Channel

Pharmacological activity of both versions of rMgTx was evaluated by studying their effect on the hKv1.2 and hKv1.3 ion channels. The hKv1.2 current was recorded in CHO cells, which heterologously expressed the hKv1.2 ion channel, and hKv1.3 current was recorded in the human peripheral blood lymphocytes. The stimulation of the hKv1.3 channel expression (activation of isolated mononuclear cells by PHA, see the Materials and Methods section) and recording conditions (no Ca^{2+} in the pipette to elicit Ca^{2+}-activated K^+ channels) guaranteed that the current recorded in these cells is K^+ current through Kv1.3 (Varga et al., 2012; Bartok et al., 2014; Tajti et al., 2021). A custom-built perfusion system was used to apply toxins at a very small perfusion rate of 200 µl/min. The speed and complete solution exchange in the recording chamber at this perfusion rate were tested frequently using fully reversible blockers as a positive control. Around 50% reduction in the peak current upon perfusion of the positive control in concentrations equal to the respective K_d values, i.e., 10 mM

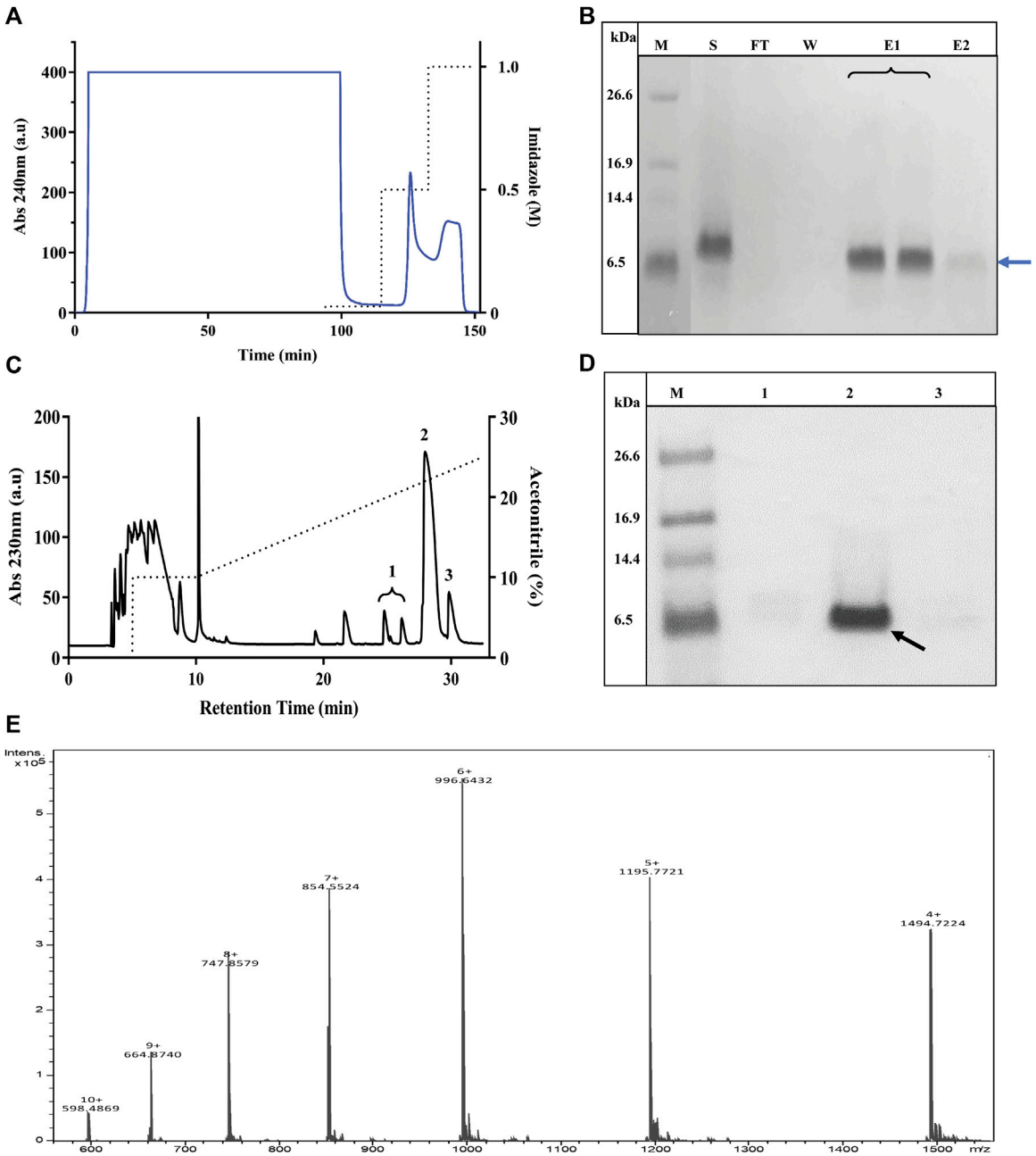

FIGURE 3 | Purification of TrMgTx. **(A)** The chromatogram shows the loading of the supernatant of *P. pastoris* culture (cultured for 72 h, pH 6, induced with 0.5% MeOH) on a Ni^{2+} affinity column and elution with imidazole in isocratic mode. Absorbance was measured at 240 nm (indicated with blue line, left axis) and dotted line denotes the concentration of imidazole in elution buffer (right axis). **(B)** 16% Tricine–SDS-PAGE illustrates the analysis of fractions collected from Ni^{2+} affinity chromatography, where lane labels stand for **M**: low-molecular-weight (LMW) protein marker, **S**: raw (unpurified) supernatant, **FT**: flow through, **W**: wash with washing buffer, **E1**: elution with 0.5 M imidazole, and **E2**: elution with 1 M imidazole. A band at 6.5 kDa position (blue arrow) in lane E1 and E2 represents partially purified TrMgTx. **(C)** RP-HPLC chromatogram of TrMgTx. Partially purified TrMgTx in step 1 **(A,B)** was applied on RP-HPLC C_{18} semi-prep column and eluted with a gradient of 10–30% acetonitrile (shown with dotted line, right axis) over 30 min. Absorbance was recorded at 230 nm (left axis). Numbers indicate the peaks collected. **(D)** 16% Tricine–SDS-PAGE analysis of fractions collected from the RP-HPLC column. Lanes represent **M**: LMW protein marker, **1–3**: fractions from corresponding peaks as indicated in RP-HPLC chromatogram (panel **C**). The band of 6.5 kDa in lane 2 indicated with a black arrow represents purified TrMgTx. **(E)** ESI-QTOF-MS spectrum shows the average mass (5980.86 Da) of purified TrMgTx.

tetraethylammonium for hKv1.3 and 14 nM charybdotoxin for hKv1.2, proved the complete exchange of solution (data not shown).

TrMgTx and UrMgTx at the 200 pM concentration inhibited ~70 and ~80% of the whole-cell hKv1.3 current upon reaching the block equilibrium, respectively.

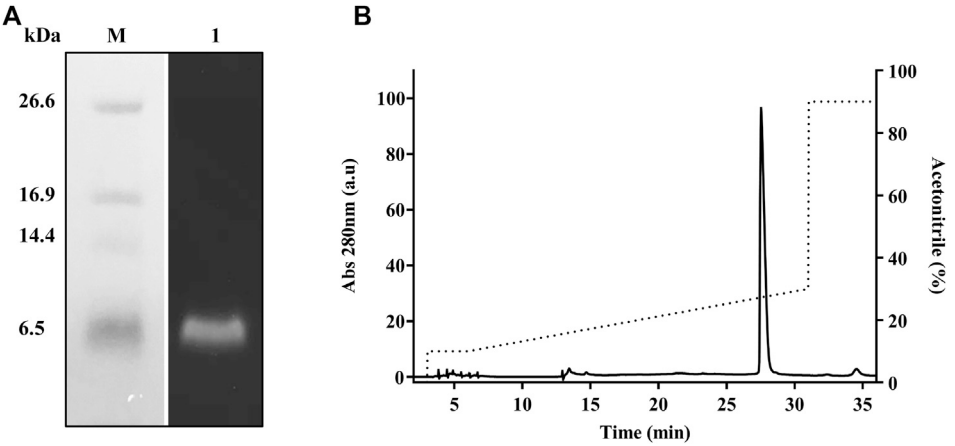

FIGURE 4 | Purity analysis of TrMgTx produced by the two-step purification protocol. **(A)** Western blot of the sample eluted from the RP-HPLC column (**Figures 3C,D**) using HRP conjugated anti-His primary antibodies. **Lane M**: low-molecular-weight protein marker, **lane 1**: TrMgTx after RP-HPLC purification. **(B)** TrMgTx eluted from the RP-HPLC column (**Figures 3C,D**) was loaded on C_{18} analytical column and eluted with a gradient of 10–30% acetonitrile over 25 min (dotted line, right axis). The absorbance was measured at 280 nm (left axis). Single peak indicates TrMgTx. Purity was calculated as [(area under the peak of interest)/(cumulated area under all peaks) × 100] and is shown in **Table 1**.

TABLE 1 | TrMgTx purification scheme.

	Purification Step	Avg. Vol. (ml)	Avg. TrMgTx Concentration (mg/ml)	Avg. Total TrMgTx Amount (mg)	[a]Avg. Net Recovery (%)	Purity (%)
–	Cultured supernatant	246	0.085[b]	20.8	100	–
1	Ni^{2+} affinity chromatography	14.5	1.01[b]	14.7	70.6	–
2	RP-HPLC–	32.6	0.279[c]	9.1	43.2	>98[d]

[a]*Net recovery = TrMgTx acquired after a given step/total TrMgTx in cultured supernatant.*
[b]*Gel scan analysis with Image Lab Software (see **Figure 2** legend).*
[c]*Pierce™ BCA Protein Quantification kit.*
[d]*% Purity was assessed by RP-HPLC (see **Figure 4B**).*

Figures 6A,B show the current traces recorded in the presence and absence of the respective peptide toxins. **Figures 6C,D** demonstrate the development and recovery from the block of the hK1.3 current with TrMgTx and UrMgTx as indicated using the colored bars. In case of hKv1.3, the block equilibrium develops slower for TrMgTx than for UrMgTx upon application of 200 pM of toxin in bath solution, as reported by the time constants (τ_{on}) obtained by fitting a single exponential function to the decay of the peak currents in the presence of the blockers (for TrMgTx τ_{on} = 168 ± 19 s and for UrMgTx τ_{on} = 116 ± 10 s were obtained, n = 4). Almost full recovery of the peak currents was attained upon perfusing the bath medium with toxin-free solution with similar time constants for washout (τ_{off}) for the two peptides (for TrMgTx τ_{off} = 568 ± 84 s and for UrMgTx τ_{off} = 560 ± 28 s were obtained, n = 4). To reveal the impact of additional amino acids at the N-terminal of TrMgTx on the interaction with hKv1.3, blocking parameters k_{on}, k_{off}, and equilibrium dissociation constant K_d were calculated (**Table 2**) from the measured time constant values and plotted on the bar graph in **Figure 6F**. The k_{on} rate of UrMgTx was significantly higher than was for TrMgTx (in unpaired *t test* comparison, $n = 4$, $p < 0.001$); however, the k_{off} rate of the peptides was statistically the same ($p > 0.05$, $n = 4$). The hKv1.3 blocking potency of both tagged and UrMgTx was obtained by determining their k_d values by using dose–response relationships as well. The data points were fitted using a three-parameter [inhibition] vs response equation, and the best fit gave the k_d 50 and 86 pM for UrMgTx and TrMgTx, respectively, as is shown in **Figure 6E**. Based on the dose–response relationship, the tagged version of the toxin, TrMgTx, is slightly less potent for hKv1.3 than the tag-free version of the peptide, UrMgTx.

A similar set of experiments were repeated for the hKv1.2 ion channel expressed in CHO cells. TrMgTx and UrMgTx at 100 pM concentrations blocked about 60 and 90% of the whole-cell current of hK1.2, respectively, as shown by the current traces recorded in the presence and absence of the respective peptide toxins (**Figures 7A,B**). The change in the peak current of hK1.2 upon application and washout of the TrMgTx and UrMgTx (colored bars) is shown in **Figures 7C,D**. Like hKv1.3, the equilibrium block of hKv1.2 with

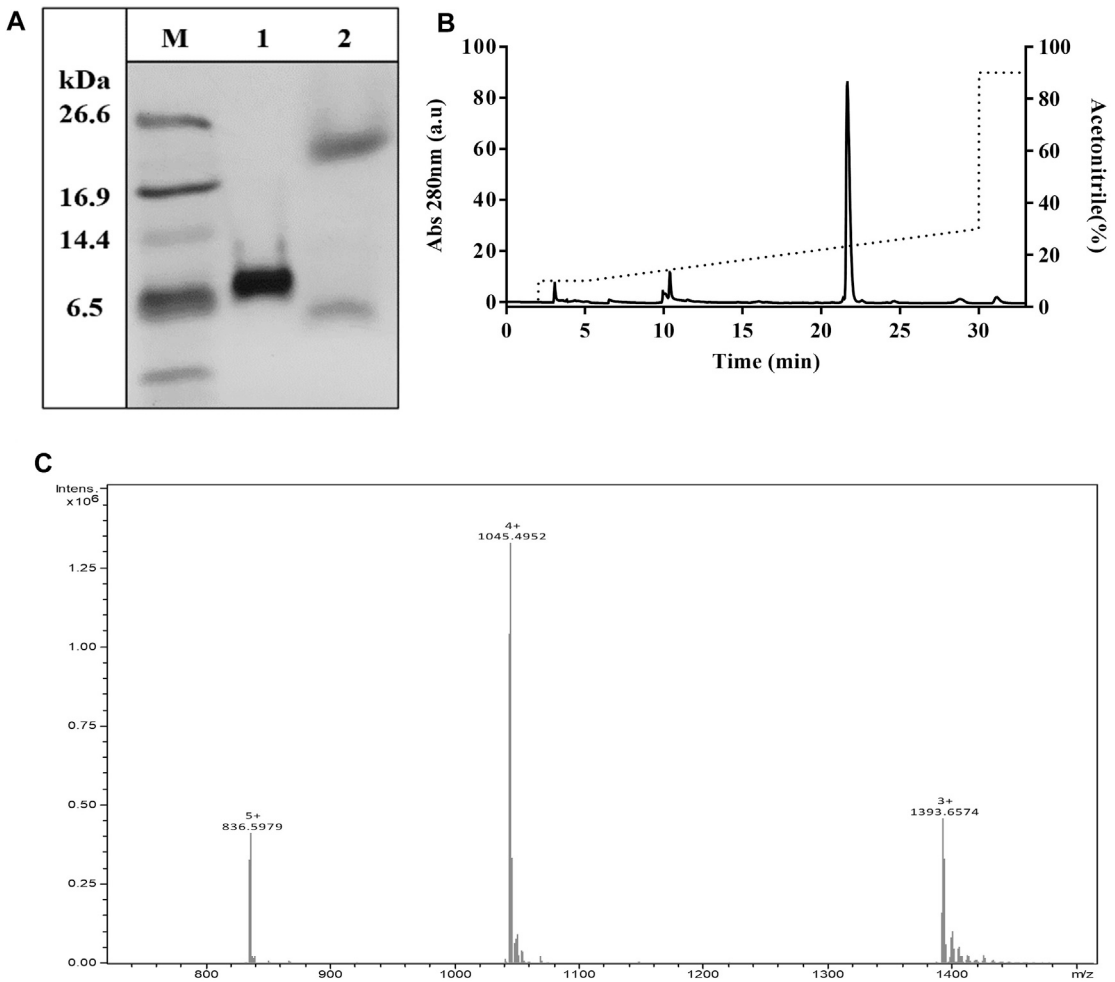

FIGURE 5 | Removal of tag from TrMgTx. **(A)** 16% Tricine–SDS-PAGE analysis of the TrMgTx samples incubated overnight at 25°C without (**lane 1**) and with (**lane 2**) factor Xa protease (at 1:200 enzyme to peptide ratio); **M**: low-molecular-weight protein marker. **(B)** RP-HPLC chromatogram shows the purification of UrMgTx. After separating the His-tag fragments with Ni^{+} beads, the digested sample was loaded on C_{18} column and eluted with a gradient of 10–30% acetonitrile over 25 min. The absorbance was measured at 280 nm (left axis), dotted line shows the acetonitrile gradient (right axis). **(C)** ESI-QTOF-MS spectrum illustrates the average mass (4178.95 Da) of the purified UrMgTx.

TrMgTx developed on a slower time course than with the UrMgTx at identical (100 pM) concentrations (for TrMgTx τ_{on} = 202 ± 2.3 s and for UrMgTx τ_{on} = 191 ± 12 s). Perfusion of the bath with toxin-free solution results in slow but full recovery (τ_{off} = 532 ± 69 s) from the block in case of TrMgTx. On the contrary, in case of UrMgTx, slow and partial recovery (τ_{off} = 1308 ± 351 s) from the block was observed. Blocking parameters k_{on}, k_{off}, and K_d for hKv1.2 were calculated from measured time constant values as given in **Table 2** and plotted on a bar graph (**Figure 7F**). The k_{on} obtained for UrMgTx is slightly higher than that of TrMgTx (unpaired *t test*, n = 3–4, $p < 0.01$); however, the k_{off} rate of UrMgTx is substantially lower than that of TrMgTx (unpaired *t test*, n = 3–4, $p < 0.001$). In the dose–response relationship, the best fit of data points results in K_d = 64 pM for TrMgTx and K_d = 14 pM for UrMgTx (**Figure 7E**). Tagged TrMgTx is nearly fivefold less potent for hKv1.2 than tag-free UrMgTx.

Kv1.3 Inhibition by rMgTx Decreases the Activation of $CD4^{+}$ T_{EM} Cells

Upon T lymphocyte stimulation, the expression of activation markers in the cell membrane, such as IL2R and CD40 ligand, are upregulated. High-affinity blockers of Kv1.3 inhibit the activation and proliferation of human T_{EM} cells through decreasing the driving force for the Ca^{2+} influx (Chandy et al., 2004; Cahalan and Chandy, 2009). In this study, it has been investigated whether recombinantly produced MgTx (with tag or without tag) would affect the expression of IL2R and CD40L, as activation markers in $CD4^{+}$ T_{EM} cells upon TCR ligation for 24 h. The presence of either toxin TrMgTx or UrMgTx (at ~100× concentration of their

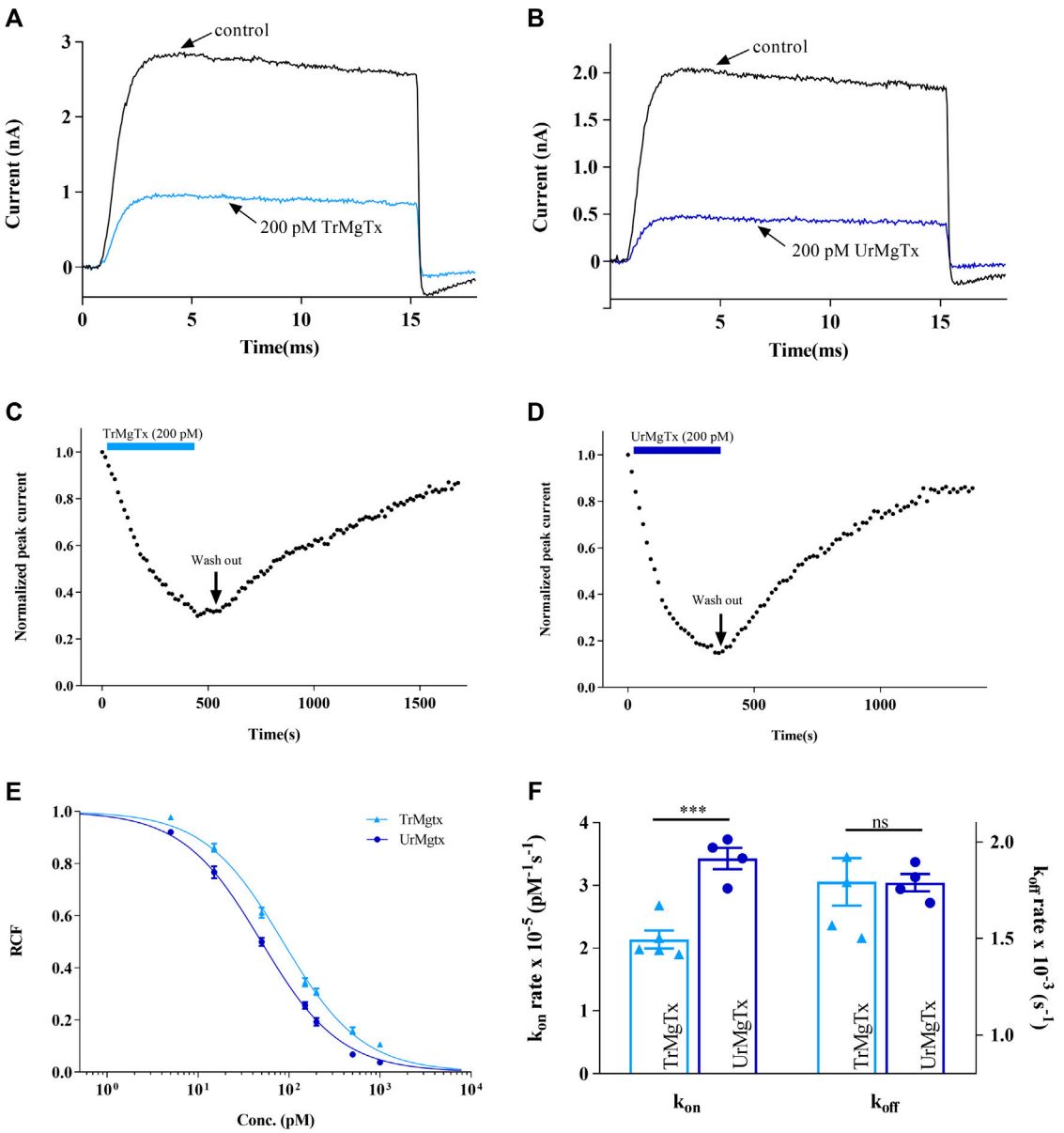

FIGURE 6 | Inhibition of hKv1.3 currents by tagged and untagged recombinant MgTx. **(A,B)** Whole-cell currents through hKv1.3 were evoked from activated human peripheral lymphocytes by depolarization to +50 mV from a holding potential −120 mV for 15 ms duration. Test pulses were applied every 15 s. Representative traces show the K^+ current before the application of toxin (control) and after reaching the equilibrium block in the presence TrMgTx **(A)** or UrMgTx **(B)** at 200 pM concentration (as indicated). **(C,D)** Development of and recovery from the block of hKv1.3 current. Normalized peak currents were measured in whole-cell patch configuration and plotted against time as 200 pM of TrMgTx [**(C)**, light blue bar] or UrMgTx [**(D)**, dark blue bar] was applied to the bath solution. Following block equilibrium, the recording chamber was perfused with toxin-free solution (arrow, washout) to demonstrate reversibility of the block. **(E)** Concentration-dependent block of hKv1.3 by TrMgTx and UrMgTx. The RCF values taken at different toxin concentrations were fitted with a three-parameter (inhibition) vs response model (see the Materials and Methods section for details). The best fit resulted in K_d = 50 pM for UrMgTx and K_d = 86 pM for TrMgTx. Error bar represents SEM and n = 3–4. **(F)** Comparison of block kinetics of TrMgTx and UrMgTx for hKv1.3. Association rate constant k_{on} (left y-axis) and dissociation rate constant k_{off} (right y-axis) were calculated from measured time constants (τ_{on}, τ_{off}) for the development of the block in the presence of 200 pM toxin and the washout (see panel **C**,**D**), assuming a simple bimolecular reaction between the channel and toxin (see the Materials and Methods section for details) and plotted on bar graph. Symbols indicate individual data points (n = 4); bar heights and error bars indicate mean ± SEM. ***p < 0.001, ns = not significant, unpaired t test.

TABLE 2 | Kinetic parameters of rMgTx and Kv channel interaction.

Kv Channel	Toxin	k_{on} ($pM^{-1}s^{-1}$)	k_{off} (sec^{-1})	K_d (pM)
Kv1.3	TrMgTx	2.14E-05	0.00179	83.90
	UrMgTx	3.43E-05	0.00179	52.20
Kv1.2	TrMgTx	3.05E-05	0.00190	62.29
	UrMgTx	4.62E-05	0.00098	15.04

k_{on} and k_{off} were calculated from averaged τ_{on} and τ_{off} values obtained from 3–5 independent experiments (see the Materials and Methods section for details). K_d was determined as k_{off}/k_{on}.

respective K_d values) during the T_{EM} cell stimulation significantly reduced the upregulation of IL2R and CD40L expression. About 8.5 nM of TrMgTx showed ~39% inhibition of IL2R expression and ~36% inhibition of CD40L expression. Similarly, 5 nM of UrMgTx hampered expression of both activation markers by ~45% (**Figures 8A-D**). It is important to note that CD40L expression of the stimulated cells after treatment with either TrMgTx or UrMgTx was comparable to that of unstimulated cells (**Figure 8D**). These results suggest that both TrMgTx and UrMgTx are biologically active peptides; however, TrMgTx has a slightly lesser efficacy than UrMgTx due to the presence of a His-tag at the N-terminus.

DISCUSSION

In this article, an improved production of rMgTx in the *P. pastoris* expression system has been described by optimizing various aspects of the vector and the selection/culturing conditions (pH, methanol induction, and fermentation duration) and confirmed the applicability of the recombinant peptides in electrophysiological and functional assays. Firstly, the coding DNA sequence of MgTx was generated by using preferred codons for *P. pastoris*, and Zeocin (2 mg/ml) hyper-resistant transformants were selected for expression studies. Secondly, upon substantial optimization, a yield of 83 ± 3 mg/L TrMgTx (i.e., His-tagged rMgTx) was obtained in the culture supernatant at pH 6.0 of the culturing medium and 72 h of fermentation following 0.5% methanol induction. Following Ni^{2+} affinity chromatography/RP-HPLC purification, the final yield of 36 ± 4 mg/L TrMgTx was obtained at >98% purity, as confirmed by RP-HPLC, mass spectrometry, and Western blot analysis, using anti-His antibody. Thirdly, to compare the potency of TrMgTx in inhibiting Kv1.2 and Kv1.3 channels with that of the untagged rMgTx (i.e., UrMgTx) having native-like N-terminal, TrMgTx was digested using factor Xa protease, and subsequently purified with RP-HPLC, and the cleavage was confirmed using mass spectrometry. In the electrophysiology assay (patch-clamp), it was shown in this study that TrMgTx is slightly less potent than UrMgTx in inhibition of either Kv1.2 (K_d = 64 vs 14 pM) or Kv1.3 (K_d = 86 vs 50 pM), albeit both peptides displayed picomolar affinity for the channels. The analysis of the association and dissociation kinetics showed that the somewhat lower affinity of TrMgTx for Kv1.2 can be explained by the lower association and increased dissociation rate of the toxin–channel complex as compared with UrMgTx. Fourthly, in a biological functional study, it was shown that both peptides significantly reduced the expression of IL2R and CD40L in activated $CD4^+$ T_{EM} cells at a 100× higher concentration than the K_d values of the respective toxins for Kv1.3.

Scorpion venom–derived peptide toxins have been under the spotlight for the past 2 decades, especially α-KTxs, as they effectively block the Kv1.3 channel in sub-nanomolar concentrations. Therefore, these can be used to treat autoimmune diseases through blockade of upregulated Kv1.3 channel in autoreactive human $CD4^+$ T_{EM} cells (Shen et al., 2017; Tajti et al., 2020). However, selectivity of these peptide toxins for Kv1.3 is still an issue because they block various other subtypes of Kv ion channels with high affinity (Kalman et al., 1998; Bagdány et al., 2005). Consequently, these undesired effects may restrict their use as potential therapeutic drugs. Selectivity of these peptides for Kv1.3 can be enhanced by peptide engineering. One example is the double substituted analog of Anuroctoxin that exhibits more than 16,000-fold selectivity for Kv1.3 over Kv1.2 (as compared with the 10-fold selectivity of the wild-type toxin), while maintaining the affinity towards Kv1.3 (Bartok et al., 2015). Similarly, the Kv1.3 selectivity of HsTx1 over Kv1.1 was improved significantly by R14A substitution (Rashid et al., 2014). In addition, peptide toxins are widely used to investigate the function of Kv1.x ion channels in various cell types *in vivo* as well as *in vitro* (Erdogan et al., 2005; Tubert et al., 2016; Schwartz et al., 2020; Toldi et al., 2020). Obviously, one needs a reliable and economical system to produce an ample amount of these peptide toxins and their analogs to develop them as therapeutic drugs for the treatment of autoimmune disorders and to study the physiological role of ion channels.

The natural resources (e.g., venom glands) provide a very minute quantity of pure wild-type peptides, which is usually insufficient for structural and functional experiments. Since peptide toxins consist of 30–80 amino acids and they maintain their tertiary structure with 3–4 disulfide bonds, chemical synthesis (Jensen et al., 2009) and recombinant production in *E. coli* of such peptides need oxidative refolding and repurification to get the correctly refolded and biological active isomer (Rudolph and Lilie, 1996). Some engineered *E. coli* strains, on the other hand, are capable of disulfide bond formation and refold the peptide (Lobstein et al., 2012; Klint et al., 2013). However, neither chemical synthesis nor *E. coli* recombinant production approaches seem to be efficient to produce a high yield of disulfide-rich peptides. For example, MgTx was previously produced in *E. coli* yielding 3–4 mg/L of functional peptides (Garcia-Calvo et al., 1993). The *P. pastoris* expression system offers an economical and better approach to overcome these limitations and gives higher yields of correctly folded recombinant peptides. This system has many pros as a host for heterologous production of proteins, such as high biomass production in simple medium, ease of genetic manipulation, and capability of performing posttranslational modifications. Additionally, *P. pastoris* secretes the heterologous proteins into medium with very few endogenous proteins which significantly simplifies the downstream processing (Macauley-Patrick et al., 2005; Cregg, 2007). In line with these, Anangi et al. (2012)

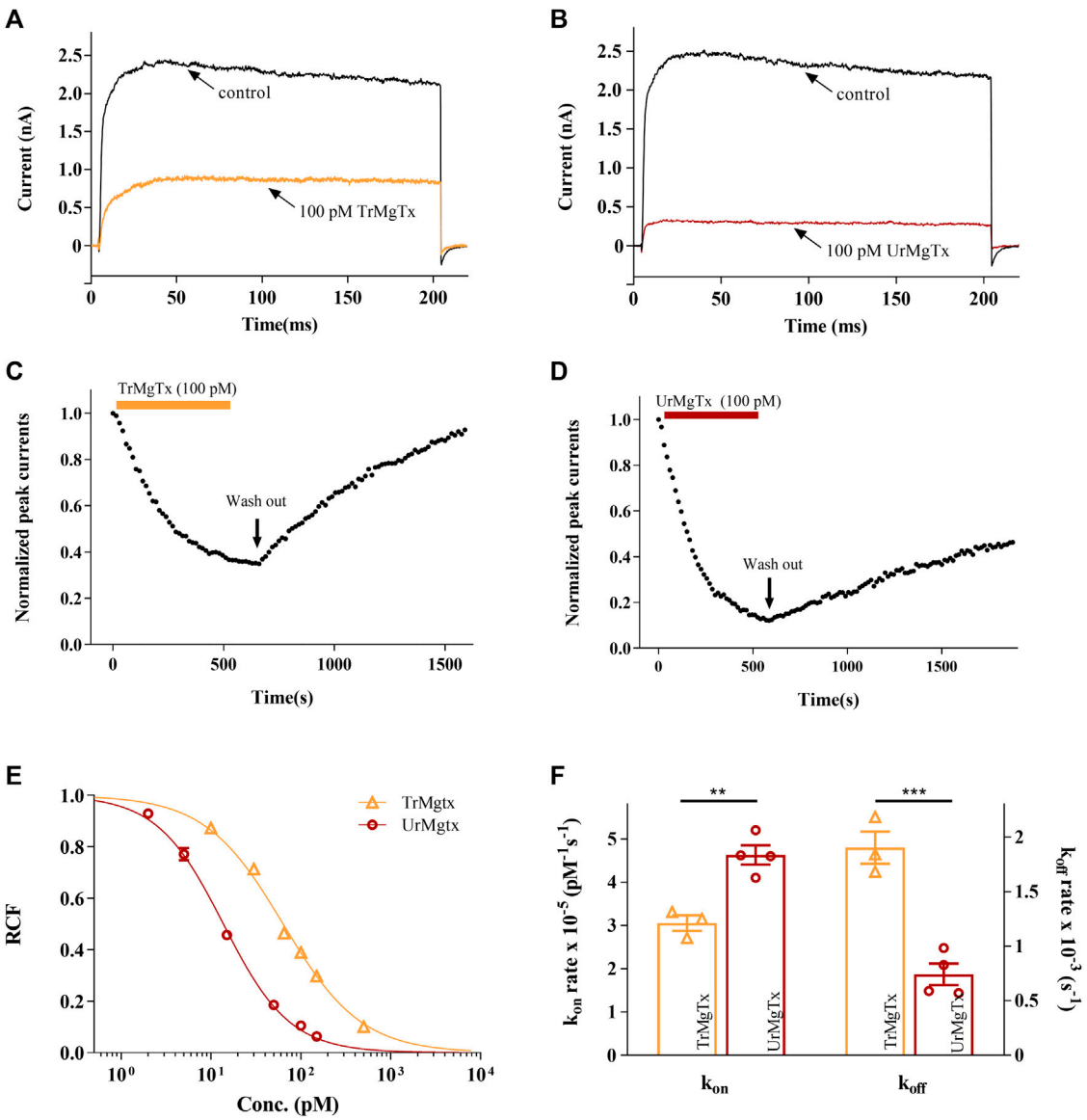

FIGURE 7 | Inhibition of hKv1.2 currents by tagged and untagged recombinant MgTx. **(A,B)** The K^+ currents through hKv1.2 were evoked from transiently transfected CHO cells either in whole-cell or outside-out patch configuration by depolarization to +50 mV from a holding potential −120 mV for 200 ms duration. Test pulses were applied every 15 s. Representative traces show the K^+ current before the application of toxin (control) and after reaching the equilibrium block in the presence TrMgTx **(A)** or UrMgTx **(B)** in 100 pM concentration (as indicated). **(C,D)** Development of and recovery from block of hKv1.2 current. Normalized peak currents were measured in whole-cell patch configuration and plotted against time as 100 pM of either TrMgTx (C, yellow bar) or UrMgTx (D, burgundy bar) was applied to the bath solution. Following block equilibrium, the recording chamber was perfused with toxin-free solution (arrow, washout) to assess reversibility of the block. **(E)** Concentration-dependent block of hKv1.2 by TrMgTx and UrMgTx. The RCF values taken at different toxin concentrations were fitted with a three-parameter (inhibition) vs response model (see the Materials and Methods section for details). The best fit yielded K_d = 14 pM for UrMgTx and K_d = 64 pM for TrMgTx. Error bars represent SEM and n = 3–5. **(F)** Comparison of block kinetics of TrMgTx and UrMgTx for hKv1.2. Association rate constant k_{on} (left y-axis) and dissociation rate constant k_{off} (right y-axis) were calculated from measured time constants (τ_{on}, τ_{off}) for the development of the block in the presence of 100 pM toxin and the washout (see **C** and **D**), assuming a simple bimolecular reaction between the channel and toxin (see the Materials and Methods section for details) and plotted on bar graph. Symbols indicate individual data points (n = 3–4), bar heights and error bars indicate mean ± SEM. $^{**}p < 0.01$, $^{***}p < 0.001$, ns = not significant, unpaired t test comparison.

expressed and purified the His-tagged MgTx and Agitoxin in the *Pichia* expression system with a yield of 12–15 mg/L and 14–18 mg/L, respectively (Anangi et al., 2012).

The expression level of heterologous proteins in *P. pastoris* can be enhanced by adopting various strategies. These include the usage of codon-optimized genes, screening for high-copy

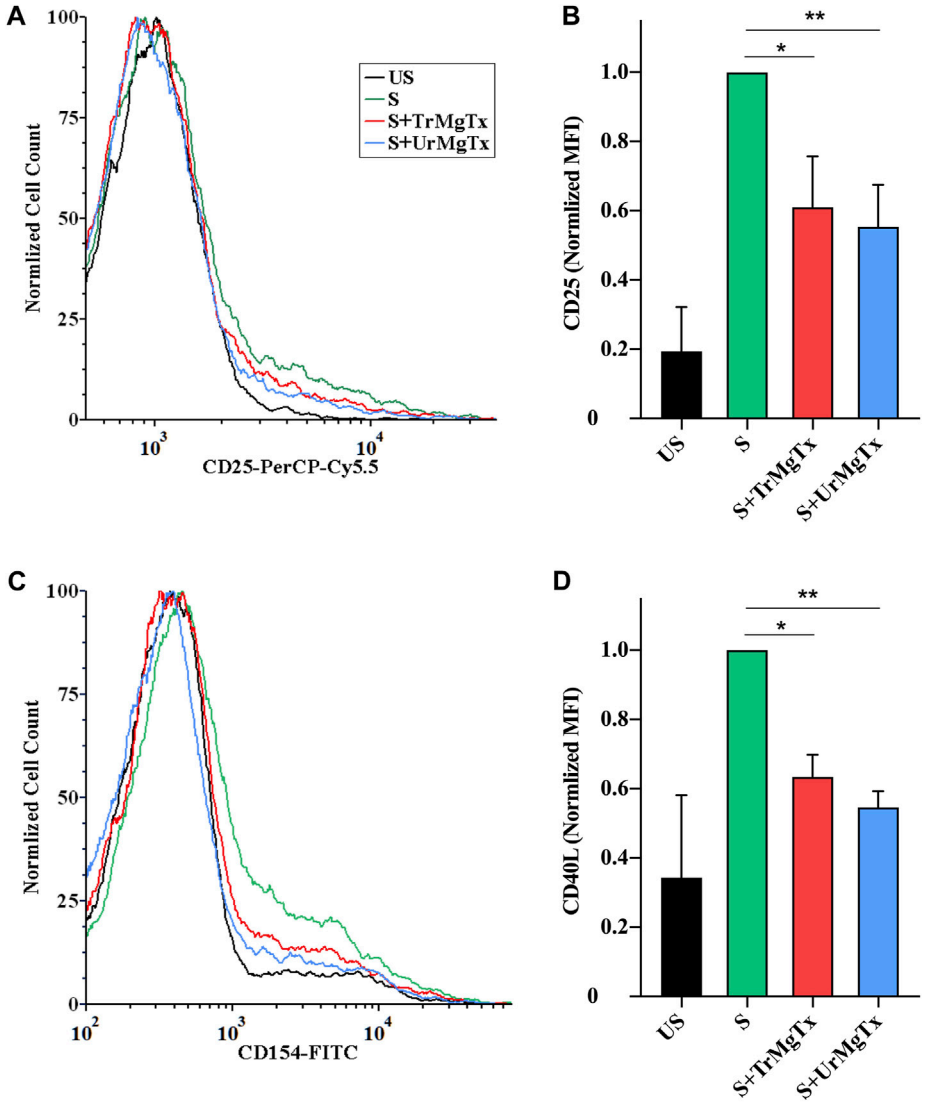

FIGURE 8 | rMgTx decreases the expression of IL2R (CD25) and CD40L. Isolated $CD4^+$ T_{EM} cells were stimulated with anti-human CD3 antibody in the presence or absence of toxins. After 24 h of stimulation, cells were labelled with anti-CD25 (IL2R) **(A,B)** and anti-CD154 (CD40L) antibodies **(C,D)**. Treatment labels: US, unstimulated (black); S, stimulated with anti-human CD3 antibody–coated wells **(**5 μg/well; see the Materials and Methods section for details, green); S + TrMgTx, stimulated in the presence of TrMgTx (8.5 nM, red); S + UrMgTx, stimulated in the presence of UrMgTx (5 nM, blue). **(A,C)** Fluorescence histograms were obtained from T lymphocytes gated based on their FSC and SSC parameters (10,000 events were recorded), and then, histograms corresponding to CD25 or CD154 expression were plotted as peak-normalized overlay. Plots were made using FCS Express 6.0. (**A,C**) has the same color code. **(B,D)** Mean fluorescence intensities (MFI) were determined from the histograms and normalized to that of their stimulated but not treated control (S). Data represent values from three independent experiments (two technical repeats in each) with SEM. Significant differences of IL2R and CD40L expression between the stimulated samples in the absence and presence of toxin is indicated with asterisks (*$p < 0.05$, **$p < 0.01$, all pairwise multiple comparison).

integrant, choice of efficient promoter, and optimization of cell fermentation conditions (Macauley-Patrick et al., 2005; Yu et al., 2010). Previous studies report that the use of codon-optimized gene sequence increases the heterologous protein expression about 1- to 10-fold in *P. pastoris* over the native gene sequence (Yadava and Ockenhouse, 2003; Li et al., 2010; Yu et al., 2013; Wang et al., 2015). For example, codon-optimized glucanase gene from *B. licheniformis* was expressed 10-fold higher compared with the wild-type gene in *P. pastoris* (Teng et al., 2007). To improve the recombinant expression, the codon-biased MgTx gene was generated according to the codon usage table for *P. pastoris* available at www.kazusa.or.jp/codon. Generally, it has also been observed that an increase in the copy number of the expression cassette significantly increases the expression of the target gene (Clare et al., 1991; Vassileva et al., 2001; Mansur et al., 2005; Nordén et al., 2011). Upon transformation into *P. pastoris*, multicopy integration of expression cassette could occur spontaneously at single locus by homologous recombination. In this study, multicopy clones of *P. pastoris* were created by using the post-transformational vector amplification method

described by Sunga et al. (2008). Initially, transformants were selected on low concentration of Zeocin and then subject to progressively increasing higher concentrations (up to 2 mg/ml of Zeocin). Nordén et al. (2011) reported that hyper-resistance against Zeocin was intimately correlated with enhanced expression of foreign proteins in *P. pastoris*. As such, this strategy was followed to select hyper-resistant *P. pastoris* strains.

The expression level of recombinant proteins in *P. pastoris* is a function of several fermentation factors such as biomass production, pH of the medium, methanol induction, dissolved oxygen, and medium types. The influence of these factors on heterologous protein expression in *P. pastoris* varies for each protein (Macauley-Patrick et al., 2005; André et al., 2006; Khatri and Hoffmann, 2006; Minjie and Zhongping, 2013). Thus, in the present study, to achieve maximal expression of rMgTx, first the time course of methanol-induced peptide production was optimized and later the optimal concentration of methanol for induction and the optimal pH of the medium were determined. As a strong methanol-induced promoter, *AOX1* was employed here, and different concentrations of methanol were expected to significantly alter the heterologous protein expressions. Based on various foreign proteins, the suitable methanol concentration ranged between 0.1 and 3% (v/v) (Minjie and Zhongping, 2013). When the biomass was induced with 0.5% methanol in BMMY medium for 72 h, it was found to yield the highest titer of TrMgTx. Similarly, Mu et al. (2008) reported that the highest concentration of basic fibroblast growth factor was obtained at 0.5% (v/v) MeOH and yielded 150 mg/L peptide after 72 h of induction. On the contrary, Zhang et al. (2009) suggested that moderate methanol concentration and induction time to get the maximal expression of inulinases in *P. pastoris* were 1.5% (v/v) and 72 h, respectively. The pH of the medium is also an essential factor to be optimized to improve the titer of heterologous protein in *P. pastoris* because the stability of foreign protein depends on the pH of the culturing medium. *P. pastoris* can grow in a wide pH range of 3.0–7.0, without altering the growth rate drastically; however, the optimal pH varies for different recombinant proteins (Macauley-Patrick et al., 2005; Minjie and Zhongping, 2013). In this study, the highest level of rMgTx expression in culturing medium with pH 6.0 was observed. Likewise, studies have reported that the optimal pH for production of mouse epidermal growth factor, α-amylase, and human serum albumin in *P. pastoris* is pH 6.0 as well (Kobayashi et al., 2000; Park, 2006), whereas the optimal pH for the human growth hormone and insulin-like growth factor-I are 5.0 and 3.0, respectively (Brierley et al., 1994; Çalık et al., 2010). These results indicate that methanol induction and pH, among others, must be optimized for individual proteins. Conclusively, the highest concentration of TrMgTx in the culture medium was 83 ± 3 mg/L when the *P. pastoris* clone was induced under optimized conditions (0.5% MeOH, pH 6.0 for 72 h). The two-step purification strategy exploited in this study resulted in more than 98% pure peptide, albeit the final yield reduced to 36 ± 4 mg of TrMgTx from 1 L of culture. The final yield is threefold higher than previously reported yields for TrMgTx in *P. pastoris* and is 10–12 times higher than the production in *E. coli* (Garcia-Calvo et al., 1993; Johnson et al., 1994; Anangi et al., 2012).

In this pharmacological study using patch-clamp electrophysiology, it has been demonstrated that both versions of recombinantly produced MgTx (tagged and untagged) potently blocked hKv1.3 and hKv1.2 currents. The K_d values of the UrMgTx for hKv1.2 and hKv1.3 channels are in good agreement with the previous data on the native or rMgTx (Garcia-Calvo et al., 1993; Chandy et al., 2004; Bartok et al., 2014). However, the affinity of TrMgTx for both hK1.3 and hK1.2 was slightly less than that for UrMgTx. The reduced affinity of TrMgTx may be related to the additional 14 residues at its N-terminal that may interfere with the interaction of TrMgTx with the pore region of the ion channel. Chang et al. (2015) demonstrated that N-terminally extended analogs of Shk toxin inhibited the hKv1.3 channel with reduced potency as compared with the native peptide toxin.

The kinetics of current block by UrMgTx was consistent with previously reported data for MgTx. In case of hKv1.3, the equilibrium block develops rapidly and is fully recoverable upon washout, whereas the block of hKv1.2 develops relatively slowly and reversibility of the block is limited during the time scale of the whole-cell patch-clamp recording (Bartok et al., 2014). The association rate of TrMgTx, which has the N-terminal His-tag, was ~1.6-fold lower than that of UrMgTx for both hKv1.2 and hKv1.3. The reduced k_{on} rate could be explained by non–diffusion-limited bimolecular toxin–channel interactions described by Escobar et al. (1993) and Peter et al. (2001). In this model, the transition from the toxin–channel encounter complex to the toxin bound state (B) is a rate-limiting step for the block of pores of the channels. This transition may be sensitive to the rearrangement of amino acid side chains, hydrogen-bond formation, and squeezing water molecules and cations out of the extracellular vestibule of the channel to make stable toxin–channel complex (Peter et al., 2001). This process might have been altered by the additional amino acids at the N-terminus of tagged toxin, thereby leading to the decrease in k_{on} observed in this study. On the other hand, the dissociation rate (k_{off}) of TrMgTx was identical to that of UrMgTx for hKv1.3, but k_{off} was much higher for TrMgTx than for UrMgTx in case of hKv1.2. Moreover, the block of Kv1.2 by TrMgTx was fully reversible upon washout that is in clear contrast to UrMgTx. The increased k_{off} might indicate that the presence of the N-terminal tag in TrMgTx creates unfavorable interactions between the channel and the bound peptide, thereby shortening the lifetime of the toxin bound channel (Peter et al., 2001). Although TrMgTx is slightly less potent than UrMgTx with different block kinetics, the TrMgTx can be an excellent tool, as 1) it inhibits hKv1.2 and hKv1.3 in picomolar concentrations, 2) the reversible nature of the block of hKv1.2 might be preferable for the physiological study of ion channels, and 3) the production of TrMgTx does not require proteolytic cleavage of tag and downstream isolation steps, which makes the production straightforward, easy, and cost-efficient. Moreover, the His-tag of TrMgTx can be recognized by anti–His-tag antibodies and can potentially be used to determine the toxin concertation in biological fluids (Borrego et al., *manuscript in preparation*).

Kv1.3 expression is dramatically upregulated in effector memory T (T_{EM}) cells upon activation (Wulff et al., 2003).

Inhibition of Kv1.3 by high-affinity blockers impede the Ca^{+}-dependent response to TCR activation and subsequently cell proliferation (Cahalan and Chandy, 2009). It was demonstrated in this study that the TrMgTx and UrMgTx strongly inhibited the expression of the early activation markers interleukin-2 receptor α (CD25) and CD40 ligand in anti–CD3-activated $CD4^{+}$ T_{EM} lymphocytes, presumably due to the lack of calcineurin activation and the consequent translocation of NFAT to the CD25 and CD40L promoters (Tsytsykova et al., 1996; Schuh et al., 1998). Approximately 100× higher toxin concentrations than the K_d of the respective peptides for Kv1.3 were used in this assay to ensure practically a complete blockade of the Kv1.3 channels. The use of high toxin concentrations is in accordance with previous reports where significantly higher concentrations of Vm24 and Shk were used in biological assays than the K_d of the toxin for Kv1.3 (Beeton et al., 2011a; Veytia-Bucheli et al., 2018). For example, Vm24, which has low picomolar affinity for Kv1.3 (3 pM, Varga et al., 2012) significantly downregulated CD25 and CD40L in T_{EM} lymphocytes at 1 nM concentration (Veytia-Bucheli et al., 2018).

In conclusion, this study reports that the *Pichia* expression system is a powerful method to produce disulfide-rich peptides, and through optimization strategies, overexpression could be enhanced noticeably, making it more cost-effective. rMgTx was produced with a very high yield, as compared with previous reports, by optimizing several factors. The presence of the His-tag on rMgTx was shown to only mildly alter the block equilibrium and binding kinetics for the K^{+} channels. Moreover, both tagged and untagged peptides equipotently reduced the proliferation of $CD4^{+}$ T_{EM} cells. Based on this, tagged rMgTx could be used directly in investigating the role of Kv1.3 and other Kv ion channels in different cells and tissues without removing the tag, thereby reducing the cost and time demand of peptide production.

DATA AVAILABILITY STATEMENT

The raw data supporting the conclusions of this article will be made available by the authors, without undue reservation.

ETHICS STATEMENT

The studies involving human participants were reviewed and approved by the Ethical Committee of the Hungarian Medical Research Council. The patients/participants provided their written informed consent to participate in this study.

AUTHOR CONTRIBUTIONS

MUN: conceptualization, design, experiments, and writing of the first draft. GT: flow cytometry and tools for biological assays. AG: mass spectrometry. TGS: patch-clamp electrophysiology and methods for electrophysiology. JB: recombinant peptide production and peptide purification. GP: conceptualization, design, writing of the final version of the manuscript, and acquisition of funding.

FUNDING

The following grants supported the work: OTKA K119417 (GP), EFOP-3.6.1-16-2016-00022 (MUN, JB, and GP), and GINOP-2.3.2-15-2016-00044 (GP). This work was supported by the Stipendium Hungaricum Scholarship by the Tempus Public Foundation (to MUN).

ACKNOWLEDGMENTS

The authors thank the expert technical assistance of Cecilia Nagy and Adrienn Bagosi.

SUPPLEMENTARY MATERIAL

The Supplementary Material for this article can be found online at: https://www.frontiersin.org/articles/10.3389/fphar.2021.733610/full#supplementary-material

REFERENCES

Anangi, R., Koshy, S., Huq, R., Beeton, C., Chuang, W. J., and King, G. F. (2012). Recombinant Expression of Margatoxin and Agitoxin-2 in Pichia pastoris: an Efficient Method for Production of KV1.3 Channel Blockers. *PLoS One* 7, e52965. doi:10.1371/journal.pone.0052965

André, N., Cherouati, N., Prual, C., Steffan, T., Zeder-Lutz, G., Magnin, T., et al. (2006). Enhancing Functional Production of G Protein-Coupled Receptors in Pichia pastoris to Levels Required for Structural Studies via a Single Expression Screen. *Protein Sci.* 15, 1115–1126. doi:10.1110/ps.062098206

Bagdány, M., Batista, C. V., Valdez-Cruz, N. A., Somodi, S., Rodriguez de la Vega, R. C., Licea, A. F., et al. (2005). Anuroctoxin, a New Scorpion Toxin of the Alpha-KTx 6 Subfamily, Is Highly Selective for Kv1.3 over IKCa1 Ion Channels of Human T Lymphocytes. *Mol. Pharmacol.* 67, 1034–1044. doi:10.1124/mol.104.007187

Bartok, A., Fehér, K., Bodor, A., Rákosi, K., Tóth, G. K., Kövér, K. E., et al. (2015). An Engineered Scorpion Toxin Analogue with Improved Kv1.3 Selectivity Displays Reduced Conformational Flexibility. *Sci. Rep.* 5, 18397. doi:10.1038/srep18397

Bartok, A., Toth, A., Somodi, S., Szanto, T. G., Hajdu, P., Panyi, G., et al. (2014). Margatoxin Is a Non-selective Inhibitor of Human Kv1.3 K+ Channels. *Toxicon* 87, 6–16. doi:10.1016/j.toxicon.2014.05.002

Beeton, C., Pennington, M. W., and Norton, R. S. (2011a). Analogs of the Sea Anemone Potassium Channel Blocker ShK for the Treatment of Autoimmune Diseases. *Inflamm. Allergy Drug Targets* 10, 313–321. doi:10.2174/187152811797200641

Brierley, R. A., Davis, G. R., and Holtz, G. C. (1994). *Production of Insulin-like Growth Factor-1 in Methylotrophic Yeast Cells*. Washington, DC: Google Patents.

Cahalan, M. D., and Chandy, K. G. (2009). The Functional Network of Ion Channels in T Lymphocytes. *Immunol. Rev.* 231, 59–87. doi:10.1111/j.1600-065X.2009.00816.x

Çalık, P., Bayraktar, E., İnankur, B., Soyaslan, E. Ş., Şahin, M., Taşpınar, H., et al. (2010). Influence of pH on Recombinant Human Growth Hormone Production by *Pichia pastoris*. *J. Chem. Tech. Biotechnol.* 85, 1628–1635.

Chandy, K. G., Wulff, H., Beeton, C., Pennington, M., Gutman, G. A., and Cahalan, M. D. (2004). K+ Channels as Targets for Specific Immunomodulation. *Trends Pharmacol. Sci.* 25, 280–289. doi:10.1016/j.tips.2004.03.010

Chang, S. C., Huq, R., Chhabra, S., Beeton, C., Pennington, M. W., Smith, B. J., et al. (2015). N-terminally Extended Analogues of the K^+ Channel Toxin from Stichodactyla Helianthus as Potent and Selective Blockers of the Voltage-Gated Potassium Channel Kv1.3. *FEBS J.* 282, 2247–2259. doi:10.1111/febs.13294

Chi, V., Pennington, M. W., Norton, R. S., Tarcha, E. J., Londono, L. M., Sims-Fahey, B., et al. (2012). Development of a Sea Anemone Toxin as an Immunomodulator for Therapy of Autoimmune Diseases. *Toxicon* 59, 529–546. doi:10.1016/j.toxicon.2011.07.016

Clare, J. J., Rayment, F. B., Ballantine, S. P., Sreekrishna, K., and Romanos, M. A. (1991). High-level Expression of Tetanus Toxin Fragment C in *Pichia pastoris* Strains Containing Multiple Tandem Integrations of the Gene. *Biotechnology (N Y)* 9, 455–460. doi:10.1038/nbt0591-455

Coetzee, W. A., Amarillo, Y., Chiu, J., Chow, A., Lau, D., Mccormack, T., et al. (1999). Molecular Diversity of K+ Channels. *Ann. N. Y Acad. Sci.* 868, 233–285. doi:10.1111/j.1749-6632.1999.tb11293.x

Cregg, J. M. (2007). Introduction: Distinctions between *Pichia pastoris* and Other Expression Systems. *Methods Mol. Biol.* 389, 1–10. doi:10.1007/978-1-59745-456-8_1

Erdogan, A., Schaefer, C. A., Schaefer, M., Luedders, D. W., Stockhausen, F., Abdallah, Y., et al. (2005). Margatoxin Inhibits VEGF-Induced Hyperpolarization, Proliferation and Nitric Oxide Production of Human Endothelial Cells. *J. Vasc. Res.* 42, 368–376. doi:10.1159/000087159

Escobar, L., Root, M. J., and Mackinnon, R. (1993). Influence of Protein Surface Charge on the Bimolecular Kinetics of a Potassium Channel Peptide Inhibitor. *Biochemistry* 32, 6982–6987. doi:10.1021/bi00078a024

Escoubas, P., Bernard, C., Lambeau, G., Lazdunski, M., and Darbon, H. (2003). Recombinant Production and Solution Structure of PcTx1, the Specific Peptide Inhibitor of ASIC1a Proton-Gated Cation Channels. *Protein Sci.* 12, 1332–1343. doi:10.1110/ps.0307003

Garcia-Calvo, M., Leonard, R. J., Novick, J., Stevens, S. P., Schmalhofer, W., Kaczorowski, G. J., et al. (1993). Purification, Characterization, and Biosynthesis of Margatoxin, a Component of *Centruroides margaritatus* Venom that Selectively Inhibits Voltage-dependent Potassium Channels. *J. Biol. Chem.* 268, 18866–18874. doi:10.1016/s0021-9258(17)46707-x

Giangiacomo, K. M., Ceralde, Y., and Mullmann, T. J. (2004). Molecular Basis of Alpha-KTx Specificity. *Toxicon* 43, 877–886. doi:10.1016/j.toxicon.2003.11.029

Han, S., Hu, Y., Zhang, R., Yi, H., Wei, J., Wu, Y., et al. (2011). ImKTx88, a Novel Selective Kv1.3 Channel Blocker Derived from the Scorpion *Isometrus maculates*. *Toxicon* 57, 348–355. doi:10.1016/j.toxicon.2010.12.015

Hofschröer, V., Najder, K., Rugi, M., Bouazzi, R., Cozzolino, M., Arcangeli, A., et al. (2020). Ion Channels Orchestrate Pancreatic Ductal Adenocarcinoma Progression and Therapy. *Front. Pharmacol.* 11, 586599. doi:10.3389/fphar.2020.586599

Jensen, J. E., Durek, T., Alewood, P. F., Adams, D. J., King, G. F., and Rash, L. D. (2009). Chemical Synthesis and Folding of APETx2, a Potent and Selective Inhibitor of Acid Sensing Ion Channel 3. *Toxicon* 54, 56–61. doi:10.1016/j.toxicon.2009.03.014

Jiménez-Vargas, J. M., Restano-Cassulini, R., and Possani, L. D. (2012). Toxin Modulators and Blockers of hERG K(+) Channels. *Toxicon* 60, 492–501. doi:10.1016/j.toxicon.2012.03.024

Johnson, B. A., Stevens, S. P., and Williamson, J. M. (1994). Determination of the Three-Dimensional Structure of Margatoxin by 1H, 13C, 15N Triple-Resonance Nuclear Magnetic Resonance Spectroscopy. *Biochemistry* 33, 15061–15070. doi:10.1021/bi00254a015

Kalman, K., Pennington, M. W., Lanigan, M. D., Nguyen, A., Rauer, H., Mahnir, V., et al. (1998). ShK-Dap22, a Potent Kv1.3-specific Immunosuppressive Polypeptide. *J. Biol. Chem.* 273, 32697–32707. doi:10.1074/jbc.273.49.32697

Kazama, I. (2015). Physiological Significance of Delayed Rectifier K(+) Channels (Kv1.3) Expressed in T Lymphocytes and Their Pathological Significance in Chronic Kidney Disease. *J. Physiol. Sci.* 65, 25–35. doi:10.1007/s12576-014-0331-x

Khatri, N. K., and Hoffmann, F. (2006). Oxygen-limited Control of Methanol Uptake for Improved Production of a Single-Chain Antibody Fragment with Recombinant *Pichia pastoris*. *Appl. Microbiol. Biotechnol.* 72, 492–498. doi:10.1007/s00253-005-0306-1

Klint, J. K., Senff, S., Saez, N. J., Seshadri, R., Lau, H. Y., Bende, N. S., et al. (2013). Production of Recombinant Disulfide-Rich Venom Peptides for Structural and Functional Analysis via Expression in the Periplasm of *E. coli*. *PloS one* 8, e63865. doi:10.1371/journal.pone.0063865

Kobayashi, K., Kuwae, S., Ohya, T., Ohda, T., Ohyama, M., and Tomomitsu, K. (2000). Addition of Oleic Acid Increases Expression of Recombinant Human Serum Albumin by the AOX2 Promoter in *Pichia pastoris*. *J. Biosci. Bioeng.* 89, 479–484. doi:10.1016/s1389-1723(00)89100-8

Koshy, S., Huq, R., Tanner, M. R., Atik, M. A., Porter, P. C., Khan, F. S., et al. (2014). Blocking KV1.3 Channels Inhibits Th2 Lymphocyte Function and Treats a Rat Model of Asthma. *J. Biol. Chem.* 289, 12623–12632. doi:10.1074/jbc.M113.517037

Lam, J., and Wulff, H. (2011). The Lymphocyte Potassium Channels Kv1.3 and KCa3.1 as Targets for Immunosuppression. *Drug Dev. Res.* 72, 573–584. doi:10.1002/ddr.20467

Li, Y., Zhang, B., Chen, X., Chen, Y., and Cao, Y. (2010). Improvement of *Aspergillus sulphureus* Endo-Beta-1,4-Xylanase Expression in *Pichia pastoris* by Codon Optimization and Analysis of the Enzymic Characterization. *Appl. Biochem. Biotechnol.* 160, 1321–1331. doi:10.1007/s12010-009-8621-0

Lobstein, J., Emrich, C. A., Jeans, C., Faulkner, M., Riggs, P., and Berkmen, M. (2012). SHuffle, a Novel *Escherichia coli* Protein Expression Strain Capable of Correctly Folding Disulfide Bonded Proteins in its Cytoplasm. *Microb. Cel Fact* 11, 56. doi:10.1186/1475-2859-11-56

Macauley-Patrick, S., Fazenda, M. L., Mcneil, B., and Harvey, L. M. (2005). Heterologous Protein Production Using the *Pichia pastoris* Expression System. *Yeast* 22, 249–270. doi:10.1002/yea.1208

Mansur, M., Cabello, C., Hernández, L., País, J., Varas, L., Valdés, J., et al. (2005). Multiple Gene Copy Number Enhances Insulin Precursor Secretion in the Yeast *Pichia pastoris*. *Biotechnol. Lett.* 27, 339–345. doi:10.1007/s10529-005-1007-7

Minjie, G., and Zhongping, S. (2013). Process Control and Optimization for Heterologous Protein Production by Methylotrophic *Pichia pastoris*. *Chin. J. Chem. Eng.* 21, 216–226.

Mu, X., Kong, N., Chen, W., Zhang, T., Shen, M., and Yan, W. (2008). High-level Expression, Purification, and Characterization of Recombinant Human Basic Fibroblast Growth Factor in *Pichia pastoris*. *Protein Expr. Purif.* 59, 282–288. doi:10.1016/j.pep.2008.02.009

Nordén, K., Agemark, M., Danielson, J. Å., Alexandersson, E., Kjellbom, P., and Johanson, U. (2011). Increasing Gene Dosage Greatly Enhances Recombinant Expression of Aquaporins in *Pichia pastoris*. *BMC Biotechnol.* 11, 47–12. doi:10.1186/1472-6750-11-47

Panyi, G., Beeton, C., and Felipe, A. (2014). Ion Channels and Anti-cancer Immunity. *Philos. Trans. R. Soc. Lond. B Biol. Sci.* 369, 20130106. doi:10.1098/rstb.2013.0106

Panyi, G., Possani, L. D., Rodríguez de la Vega, R. C., Gáspár, R., and Varga, Z. (2006). K+ Channel Blockers: Novel Tools to Inhibit T Cell Activation Leading to Specific Immunosuppression. *Curr. Pharm. Des.* 12, 2199–2220. doi:10.2174/138161206777585120

Park, E. Y. (2006). Enhanced Production of Mouse α-Amylase by Feeding Combined Nitrogen and Carbon Sources in Fed-Batch Culture of Recombinant *Pichia pastoris*. *Process Biochem.* 41, 390–397.

Pennington, M. W., Chang, S. C., Chauhan, S., Huq, R., Tajhya, R. B., Chhabra, S., et al. (2015). Development of Highly Selective Kv1.3-blocking Peptides Based on the Sea Anemone Peptide ShK. *Mar. Drugs* 13, 529–542. doi:10.3390/md13010529

Péter, M., Jr, Varga, Z., Hajdu, P., Gáspár, R., Jr, Damjanovich, S., Horjales, E., et al. (2001). Effects of Toxins Pi2 and Pi3 on Human T Lymphocyte Kv1.3 Channels: the Role of Glu7 and Lys24. *J. Membr. Biol.* 179, 13–25. doi:10.1007/s002320010033

Rashid, M. H., Huq, R., Tanner, M. R., Chhabra, S., Khoo, K. K., Estrada, R., et al. (2014). A Potent and Kv1.3-selective Analogue of the Scorpion Toxin HsTX1 as a Potential Therapeutic for Autoimmune Diseases. *Sci. Rep.* 4, 4509–9. doi:10.1038/srep04509

Rodríguez de la Vega, R. C., Merino, E., Becerril, B., and Possani, L. D. (2003). Novel Interactions between K+ Channels and Scorpion Toxins. *Trends Pharmacol. Sci.* 24, 222–227. doi:10.1016/S0165-6147(03)00080-4

Rubaiy, H. N. (2016). The Therapeutic Agents that Target ATP-Sensitive Potassium Channels. *Acta Pharm.* 66, 23–34. doi:10.1515/acph-2016-0006

Rudolph, R., and Lilie, H. (1996). *In Vitro* folding of Inclusion Body Proteins. *FASEB J.* 10, 49–56. doi:10.1096/fasebj.10.1.8566547

Schuh, K., Twardzik, T., Kneitz, B., Heyer, J., Schimpl, A., and Serfling, E. (1998). The Interleukin 2 Receptor Alpha chain/CD25 Promoter Is a Target for Nuclear Factor of Activated T Cells. *J. Exp. Med.* 188, 1369–1373. doi:10.1084/jem.188.7.1369

Schwartz, A. B., Kapur, A., Huang, Z., Anangi, R., Spear, J. M., Stagg, S., et al. (2020). Olfactory Bulb-Targeted Quantum Dot (QD) Bioconjugate and Kv1. 3 Blocking Peptide Improve Metabolic Health in Obese Male Mice. *J. Neurochem.* 157, 1876. doi:10.1111/jnc.15200

Shen, B., Cao, Z., Li, W., Sabatier, J. M., and Wu, Y. (2017). Treating Autoimmune Disorders with Venom-Derived Peptides. *Expert Opin. Biol. Ther.* 17, 1065–1075. doi:10.1080/14712598.2017.1346606

Sunga, A. J., Tolstorukov, I., and Cregg, J. M. (2008). Posttransformational Vector Amplification in the Yeast *Pichia pastoris*. *FEMS Yeast Res.* 8, 870–876. doi:10.1111/j.1567-1364.2008.00410.x

Tajti, G., Szanto, T. G., Csoti, A., Racz, G., Evaristo, C., Hajdu, P., et al. (2021). Immunomagnetic Separation Is a Suitable Method for Electrophysiology and Ion Channel Pharmacology Studies on T Cells. *Channels (Austin)* 15, 53–66. doi:10.1080/19336950.2020.1859753

Tajti, G., Wai, D. C. C., Panyi, G., and Norton, R. S. (2020). The Voltage-Gated Potassium Channel KV1.3 as a Therapeutic Target for Venom-Derived Peptides. *Biochem. Pharmacol.* 181, 114146. doi:10.1016/j.bcp.2020.114146

Tarcha, E. J., Olsen, C. M., Probst, P., Peckham, D., Muñoz-Elías, E. J., Kruger, J. G., et al. (2017). Safety and Pharmacodynamics of Dalazatide, a Kv1.3 Channel Inhibitor, in the Treatment of Plaque Psoriasis: A Randomized Phase 1b Trial. *PLoS One* 12, e0180762. doi:10.1371/journal.pone.0180762

Tenenholz, T. C., Klenk, K. C., Matteson, D. R., Blaustein, M. P., and Weber, D. J. (2000). "Structural Determinants of Scorpion Toxin Affinity: The Charybdotoxin (α-KTX) Family of K+-channel Blocking Peptides," in *Reviews of Physiology, Biochemistry and Pharmacology, Volume 140* (Springer), 135–185. doi:10.1007/bfb0035552

Teng, D., Fan, Y., Yang, Y. L., Tian, Z. G., Luo, J., and Wang, J. H. (2007). Codon Optimization of *Bacillus licheniformis* Beta-1,3-1,4-Glucanase Gene and its Expression in Pichia pastoris. *Appl. Microbiol. Biotechnol.* 74, 1074–1083. doi:10.1007/s00253-006-0765-z

Toldi, G., Bajnok, A., Dobi, D., Kaposi, A., Kovács, L., Vásárhelyi, B., et al. (2013). The Effects of Kv1.3 and IKCa1 Potassium Channel Inhibition on Calcium Influx of Human Peripheral T Lymphocytes in Rheumatoid Arthritis. *Immunobiology* 218, 311–316. doi:10.1016/j.imbio.2012.05.013

Toldi, G., Legány, N., Ocsovszki, I., and Balog, A. (2020). Calcium Influx Kinetics and the Characteristics of Potassium Channels in Peripheral T Lymphocytes in Systemic Sclerosis. *Pathobiology* 87, 311–316. doi:10.1159/000509674

Tsytsykova, A. V., Tsitsikov, E. N., and Geha, R. S. (1996). The CD40L Promoter Contains Nuclear Factor of Activated T Cells-Binding Motifs Which Require AP-1 Binding for Activation of Transcription. *J. Biol. Chem.* 271, 3763–3770. doi:10.1074/jbc.271.7.3763

Tubert, C., Taravini, I. R. E., Flores-Barrera, E., Sánchez, G. M., Prost, M. A., Avale, M. E., et al. (2016). Decrease of a Current Mediated by Kv1.3 Channels Causes Striatal Cholinergic Interneuron Hyperexcitability in Experimental Parkinsonism. *Cell Rep* 16, 2749–2762. doi:10.1016/j.celrep.2016.08.016

Varga, Z., Gurrola-Briones, G., Papp, F., Rodríguez de la Vega, R. C., Pedraza-Alva, G., Tajhya, R. B., et al. (2012). Vm24, a Natural Immunosuppressive Peptide, Potently and Selectively Blocks Kv1.3 Potassium Channels of Human T Cells. *Mol. Pharmacol.* 82, 372–382. doi:10.1124/mol.112.078006

Vassileva, A., Chugh, D. A., Swaminathan, S., and Khanna, N. (2001). Expression of Hepatitis B Surface Antigen in the Methylotrophic Yeast *Pichia pastoris* Using the GAP Promoter. *J. Biotechnol.* 88, 21–35. doi:10.1016/s0168-1656(01)00254-1

Veytia-Bucheli, J. I., Jiménez-Vargas, J. M., Melchy-Pérez, E. I., Sandoval-Hernández, M. A., Possani, L. D., and Rosenstein, Y. (2018). Kv1.3 Channel Blockade with the Vm24 Scorpion Toxin Attenuates the CD4+ Effector Memory T Cell Response to TCR Stimulation. *Cell Commun Signal* 16, 45. doi:10.1186/s12964-018-0257-7

Wang, J.-R., Li, Y.-Y., Liu, D.-N., Liu, J.-S., Li, P., Chen, L.-Z., et al. (2015). Codon Optimization Significantly Improves the Expression Level of α-amylase Gene from *Bacillus licheniformis* in *Pichia pastoris*. *Biomed. Research International* 2015, 248680. doi:10.1155/2015/248680

Wang, X., Li, G., Guo, J., Zhang, Z., Zhang, S., Zhu, Y., et al. (2020). Kv1.3 Channel as a Key Therapeutic Target for Neuroinflammatory Diseases: State of the Art and beyond. *Front. Neurosci.* 13, 1393. doi:10.3389/fnins.2019.01393

Waugh, D. S. (2011). An Overview of Enzymatic Reagents for the Removal of Affinity Tags. *Protein Expr. Purif.* 80, 283–293. doi:10.1016/j.pep.2011.08.005

White, C. E., Kempi, N. M., and Komives, E. A. (1994). Expression of Highly Disulfide-Bonded Proteins in *Pichia pastoris*. *Structure* 2, 1003–1005. doi:10.1016/s0969-2126(94)00103-0

Wulff, H., Calabresi, P. A., Allie, R., Yun, S., Pennington, M., Beeton, C., et al. (2003). The Voltage-Gated Kv1.3 K(+) Channel in Effector Memory T Cells as New Target for MS. *J. Clin. Invest.* 111, 1703–1713. doi:10.1172/JCI16921

Yadava, A., and Ockenhouse, C. F. (2003). Effect of Codon Optimization on Expression Levels of a Functionally Folded Malaria Vaccine Candidate in Prokaryotic and Eukaryotic Expression Systems. *Infect. Immun.* 71, 4961–4969. doi:10.1128/iai.71.9.4961-4969.2003

Yang, K. C., and Nerbonne, J. M. (2016). Mechanisms Contributing to Myocardial Potassium Channel Diversity, Regulation and Remodeling. *Trends Cardiovasc. Med.* 26, 209–218. doi:10.1016/j.tcm.2015.07.002

Yu, M., Wen, S., and Tan, T. (2010). Enhancing Production of *Yarrowia lipolytica* Lipase Lip2 in *Pichia pastoris*. *Eng. Life Sci.* 10, 458–464. doi:10.1002/elsc.200900102

Yu, P., Yan, Y., Gu, Q., and Wang, X. (2013). Codon Optimisation Improves the Expression of *Trichoderma viride* Sp. Endochitinase in *Pichia pastoris*. *Sci. Rep.* 3, 3043–3046. doi:10.1038/srep03043

Zhang, T., Gong, F., Peng, Y., and Chi, Z. (2009). Optimization for High-Level Expression of the *Pichia guilliermondii* Recombinant Inulinase in *Pichia pastoris* and Characterization of the Recombinant Inulinase. *Process Biochem.* 44, 1335–1339. doi:10.1016/j.procbio.2009.07.008

Conflict of Interest: The authors declare that the research was conducted in the absence of any commercial or financial relationships that could be construed as a potential conflict of interest.

Publisher's Note: All claims expressed in this article are solely those of the authors and do not necessarily represent those of their affiliated organizations, or those of the publisher, the editors and the reviewers. Any product that may be evaluated in this article, or claim that may be made by its manufacturer, is not guaranteed or endorsed by the publisher.

frontiers in Physiology

REVIEW
published: 08 October 2021
doi: 10.3389/fphys.2021.736681

Modulation of Adaptive Immunity and Viral Infections by Ion Channels

*Karen Bohmwald[1], Nicolás M. S. Gálvez[1], Catalina A. Andrade[1], Valentina P. Mora[1], José T. Muñoz[1], Pablo A. González[1], Claudia A. Riedel[2] and Alexis M. Kalergis[1,3]**

[1] *Departamento de Genética Molecular y Microbiología, Facultad de Ciencias Biológicas, Millennium Institute on Immunology and Immunotherapy, Pontificia Universidad Católica de Chile, Santiago, Chile,* [2] *Departamento de Ciencias Biológicas, Facultad de Ciencias de la Vida, Millennium Institute on Immunology and Immunotherapy, Universidad Andres Bello, Santiago, Chile,* [3] *Departamento de Endocrinología, Facultad de Medicina, Pontificia Universidad Católica de Chile, Santiago, Chile*

Most cellular functions require of ion homeostasis and ion movement. Among others, ion channels play a crucial role in controlling the homeostasis of anions and cations concentration between the extracellular and intracellular compartments. Calcium (Ca^{2+}) is one of the most relevant ions involved in regulating critical functions of immune cells, allowing the appropriate development of immune cell responses against pathogens and tumor cells. Due to the importance of Ca^{2+} in inducing the immune response, some viruses have evolved mechanisms to modulate intracellular Ca^{2+} concentrations and the mobilization of this cation through Ca^{2+} channels to increase their infectivity and to evade the immune system using different mechanisms. For instance, some viral infections require the influx of Ca^{2+} through ionic channels as a first step to enter the cell, as well as their replication and budding. Moreover, through the expression of viral proteins on the surface of infected cells, Ca^{2+} channels function can be altered, enhancing the pathogen evasion of the adaptive immune response. In this article, we review those ion channels and ion transporters that are essential for the function of immune cells. Specifically, cation channels and Ca^{2+} channels in the context of viral infections and their contribution to the modulation of adaptive immune responses.

Keywords: Ca^{2+}, Ca^{2+} channels, T cells, immune response, viral infection

OPEN ACCESS

Edited by:
Barbara Niemeyer, Saarland University, Germany

Reviewed by:
Ossama Kashlan, University of Pittsburgh, United States
Qiu-Xing Jiang, Hauptman-Woodward Medical Research Institute, United States

***Correspondence:**
Alexis M. Kalergis
akalergis@bio.puc.cl;
akalergis@icloud.com

Specialty section:
This article was submitted to Membrane Physiology and Membrane Biophysics, a section of the journal Frontiers in Physiology

Received: *05 July 2021*
Accepted: *10 September 2021*
Published: *08 October 2021*

Citation:
Bohmwald K, Gálvez NMS, Andrade CA, Mora VP, Muñoz JT, González PA, Riedel CA and Kalergis AM (2021) Modulation of Adaptive Immunity and Viral Infections by Ion Channels. Front. Physiol. 12:736681. doi: 10.3389/fphys.2021.736681

Abbreviations: Ca^{2+}, Calcium; Mg^{2+}, Magnesium; Zn^{2+}, Zinc; K^{+}, Potassium; Na^{+}, Sodium; Cl^{-}, Chloride; $HPO4^{2-}$, Phosphate; $HCO3^{-}$, Bicarbonate; CRAC, Ca^{2+} release-activated Ca^{2+} channels; TRP, Transient receptor potential; CFTR, Cystic fibrosis transmembrane conductance regulator; GABA, Gamma-aminobutyric acid; PLCβ, phospholipase Cβ; PIP_2, Phosphatidylinositol 4,5-bisphosphate; IP_3, inositol (1,4,5) trisphosphate; DAG, Diacylglycerol; IP_3R, IP_3 receptor; ER, Endoplasmic reticulum; MAGT1, Magnesium transporter protein 1; DCs, Dendritic cells; STIM1, Stromal interaction molecule 1; pMHC, Peptide-MHC; PMCAs, Plasma membrane Ca^{2+} ATPase pumps; SERCA, Sarco-endoplasmic reticulum Ca^{2+} ATPase; ADP, Adenosine diphosphate; cADPR, cyclic ADP ribose; Panx1, Pannexin 1 hemichannels; TRPM2, TRP cation channel subfamily M member 2; NMDARs, *N*-methyl-D-aspartate receptors; AMPARs, α-amino-3-hydroxy-5-methyl-4-isoxazole propionic acid receptors; cSMACs, Central supramolecular activation clusters; PKC, Protein kinase C; PI3K-C2β, Phosphatidylinositol-3-kinase; NFAT, Nuclear factor of activated T cells; NF-κB, Nuclear factor kappa-light-chain-enhancer of activated B cells; JNK, c-Jun NH_2-terminal kinase; AP-1, Activator protein 1; PKCθ, Protein kinase C theta; IKK, Iκ kinase; CNS, Central nervous system; CID, Combined immunodeficiency; HIV, Human immunodeficiency virus; hRSV, Human respiratory syncytial virus; SARS-CoV2, Severe acute respiratory coronavirus 2; HBV, Hepatitis B virus; HSV, Herpes simplex virus; DHPR, Voltage-sensitive *dihydropyridine* receptor; VPM, Verapamil.

INTRODUCTION

Ion homeostasis must be strictly modulated in cells of the immune system since these charged atoms or molecules play critical roles in several different physiological aspects (Feske et al., 2015; Rubaiy, 2017). Cations are mainly represented by calcium (Ca^{2+}), magnesium (Mg^{2+}), zinc (Zn^{2+}), potassium (K^+), and sodium (Na^+), and anions by chloride (Cl^-), phosphate ($HPO_4{}^{2-}$), and bicarbonate ($HCO3^-$) (Feske et al., 2015; Rubaiy, 2017; Vaeth and Feske, 2018). Na^+, K^+, and Cl^- usually maintain electrical gradients, and these cations contribute to the survival of the cell along with the movement of organelles, while Cl^- concentration plays a role in the movement and the acidification process of organelles (Feske et al., 2012, 2015; Chakraborty et al., 2017; Murray et al., 2017; Rubaiy, 2017; Vaeth and Feske, 2018). Therefore, the mobilization of these charged atoms or molecules across the hydrophobic plasma membrane alters the electrochemical gradient in a localized fashion, inducing conformational changes that will influence the function of membrane proteins on those specific portions of the membrane (Feske et al., 2012, 2015; Chaigne-Delalande and Lenardo, 2014; Rubaiy, 2017; Vaeth and Feske, 2018). Given the relevance of ion channels and transporters in cellular functions, it is expected for immune cells, such as dendritic cells (DCs) and lymphocytes, to express several of these proteins for a specialized regulation of ion transport (**Figure 1**; Feske et al., 2012, 2015; Rubaiy, 2017; Vaeth and Feske, 2018). Overall, these channels are plasma membrane integral proteins that allow ions to transit from one side of the membrane to the other (Di Resta and Becchetti, 2010; Kim, 2014). Usually, cellular channels can be found in an open, resting closed, or inactivated closed state, in line with the physiological conditions and needs of the cell (Di Resta and Becchetti, 2010; Kim, 2014).

Although currently there is not a thorough characterization regarding the modulation of ion channels and transporters in immune cells during infectious diseases, some reports have provided relevant information to understand better the contribution of these molecules during an infection (Cahalan and Chandy, 1997; Panyi et al., 2004; Feske et al., 2012, 2015; RamaKrishnan and Sankaranarayanan, 2016; Vaeth and Feske, 2018). It has been described that both, ion channels and transporters can regulate cation transport and modulate the immune response (Zweifach and Lewis, 1993; Lewis, 2001; Hogan et al., 2010; Feske et al., 2012). The most relevant ion channels and transporters include the Ca^{2+} release-activated Ca^{2+} (CRAC) channels, voltage-gated such as K^+ channel (K_v)1.3 and Ca^{2+}-activated K^+ channel (K_{Ca})3.1, transient receptor potential (TRP) channels, P2X receptors family and pannexin hemichannels, voltage-gated Ca^{2+}, Na^+, and H^+ channels, and Mg^{2+} and Zn^{2+} channels, among others (Zweifach and Lewis, 1993; Lewis, 2001; Schenk et al., 2008; Franchi et al., 2009; Yip et al., 2009; Hogan et al., 2010; Woehrle et al., 2010; Junger, 2011; Feske et al., 2012; Prakriya and Lewis, 2015; **Figure 2**). One of the ion channels that regulates anion transport, and the immune response is the cystic fibrosis transmembrane conductance regulator (CFTR) and gamma-aminobutyric acid (GABA) receptors. In general, Ca^{2+} channel signaling starts with the influx of Ca^{2+} from the extracellular space, which triggers the activation of phospholipase Cβ (PLCβ) and the subsequent cleavage of phosphatidylinositol 4,5-bisphosphate (PIP_2) into inositol (1,4,5) trisphosphate (IP_3) and diacylglycerol (DAG) by PLCγ. After this, the binding of IP_3 with to the IP_3-receptor (IP_3R) on the endoplasmic reticulum (ER) allows the diffusion of Ca^{2+} into the cytoplasm (Clapham, 2007). The following sections will discuss the contribution of ion channels and transporters to the interface between antigen-presenting cells, such as DCs and T cells, an interaction commonly known as immunological synapse. Further, the modulation of these channels during adaptive immune responses, diseases, channelopathies, and viral infections will be discussed.

ION CHANNELS EXPRESSED BY T AND B CELLS

T cells and B cells are the main players of the adaptive immune response and express various ion channels and transporters on their surface (Feske et al., 2012; Netea et al., 2019). These channels can regulate the concentration of different ions inside these cells and modulate their functions (Feske et al., 2012). This section will discuss the ion channels and transporters expressed by these lymphocytes.

Ion Channels Expressed by T Cells

T cells play an essential role at connecting the humoral and cellular arms of adaptive immunity, which is critical to properly response to infections by various pathogens (Jasenosky et al., 2015; Lee et al., 2020). T cells can be classified into two major types: $CD4^+$ T cells that orchestrate the immune response against a specific pathogen, and $CD8^+$ T cells that have cytotoxic properties and can induce the apoptosis of cells infected by a pathogen (Whitacre et al., 2012; Jasenosky et al., 2015). In general, these cells can be recognized for the T cell receptor found on their surface (Whitacre et al., 2012). Additionally, T cells express several ion channels and transporters that modulate the activation of these cells through the influx of Ca^{2+}, Mg^{2+} and Zn^{2+}, or the efflux of K^+ and Cl^- (**Table 1**; Feske, 2013; Feske et al., 2015).

Calcium Channels

CRAC channels contribute significantly to modulating immune cells, particularly the T cells, as these channels are mainly responsible for Ca^{2+} influx, promoting an increase in the concentration of this ion that can be maintained for hours after the initial opening of these channels (Lewis, 2001; Joseph et al., 2014). Ca^{2+} levels modulate the activation, proliferation, and cytokine secretion by T lymphocytes, among other relevant processes (reviewed later; Lewis, 2001). CRAC channels are located on the membrane of T cells and are composed of three proteins, ORAI1, ORAI2, and ORAI3 (Vaeth et al., 2020). CRAC channels are also the main Ca^{2+} channels activated on antigen-presenting cells upon antigen recognition, promoting DCs maturation in a Ca^{2+}-controlled fashion (Prakriya and Lewis, 2015). Usually, Ca^{2+} concentration

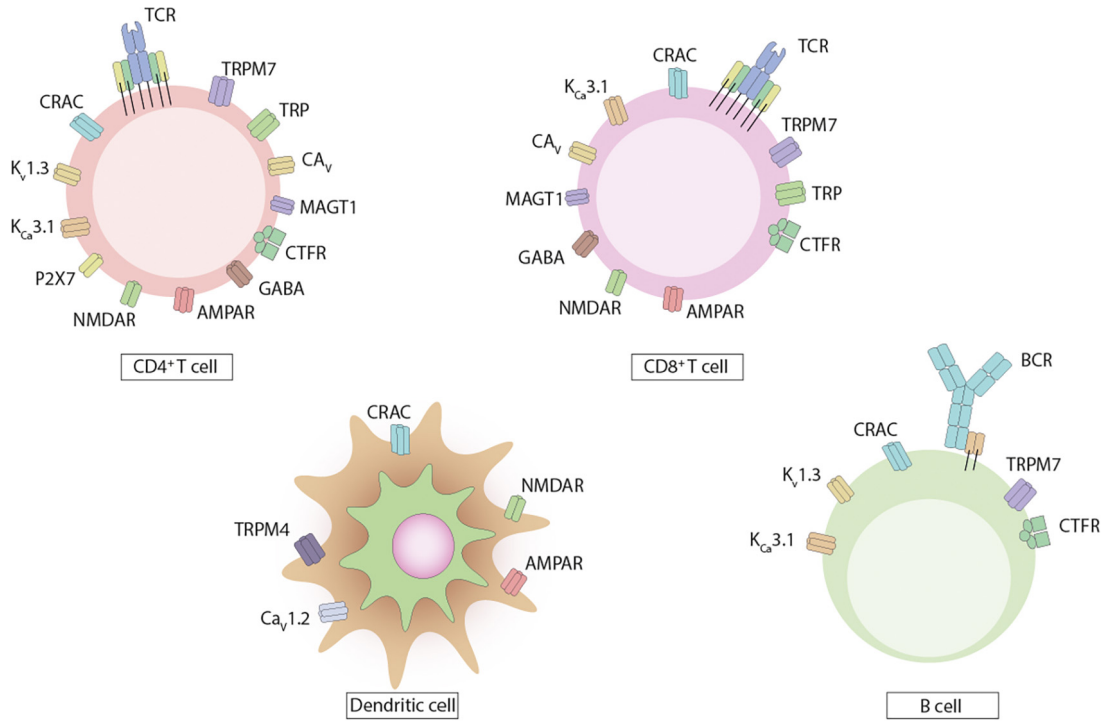

FIGURE 1 | Ion channels and transporters expressed by dendritic cells and lymphocytes. The immune cells express on their surface various types of ion channels and transporters. $CD4^+$ and $CD8^+$ T cells express channels for Ca^{2+}, Mg^{2+}, K^+, and Cl^-, with fewer channels reported on $CD8^+$ T cells. B cells express channels for Ca^{2+}, Mg^{2+}, and K^+. Dendritic cells express Ca^{2+} channels.

in the cytoplasm of resting lymphocytes is close to 50 to 100 nM (**Figure 2**). Upon T cell receptor or B cell receptor engagement, Ca^{2+} concentration in the cytoplasm can reach up to 1 μM (Lewis, 2001; Feske et al., 2012). The mechanisms underlying Ca^{2+} increase after T cell receptor and B cell receptor engagement involves the activation of PLCγ1 or PLCγ2 (Zweifach and Lewis, 1993; Hogan et al., 2003). The production of IP_3 by PLCγ leads to the release of Ca^{2+} from the ER that will stimulate Ca^{2+} influx across the plasma membrane through the store-operated Ca^{2+} entry (Zweifach and Lewis, 1993; Hogan et al., 2010). CRAC channels are responsible for the store-operated Ca^{2+} entry, and they are activated upon binding to the stromal interaction molecule 1 (STIM1) and ORAI 1–3 proteins (Hogan et al., 2010). Notably, the activation of CRAC channels occurs after the ORAI proteins bind to STIM proteins at the ER-plasma membrane junction (ORAI binding site to STIM is located at the carboxyl terminus of the former; Feske et al., 2012; Joseph et al., 2014). Upon binding, STIM proteins sense Ca^{2+} depletion inside the ER, oligomerizing and redistributing toward these junctions where they communicate this Ca^{2+} decrease to CRAC channels (Hogan et al., 2003; Feske et al., 2012). The cytoplasmic domain of STIM1 interacts with the N and C termini in ORAI1, and CRAC channels are activated, leading to the store-operated Ca^{2+} entry (Feske et al., 2012). STIM2, another isoform of STIM proteins, is expressed in lymphocytes and can interact with ORAI1, although with slower kinetics than STIM1 (Feske et al., 2012). Activation of CRAC channels and the store-operated Ca^{2+} entry induction is key for cytokine production because $CD4^+$ and $CD8^+$ T cells from STIM1-deficient mice and ORAI1 cannot secrete cytokines, such as IL-2, IL-4, IL-17, TNF, and IFN-γ (Trebak and Kinet, 2019). In T cells, mitochondria work alongside CRAC channels and interact with them to maintain Ca^{2+} influx and regulate homeostasis (Joseph et al., 2014). After T cell receptor engagement and immunological synapsis formation, mitochondria moves closes to CRAC channels in response to the massive transportation of Ca^{2+}, thus prolonging CRAC activity (Joseph et al., 2014). **Figure 2** describes these events on T cells upon T cell receptor engagement by cognate peptide-MHC (pMHC) complexes on the antigen-presenting cells surface.

The modulation of the Ca^{2+} concentrations inside T cells is also mediated by plasma membrane Ca^{2+} ATPase pumps (PMCAs). During immunological synapsis, PMCAs are in close contact with CRAC channels, which modulates the activity of the ATPase pump. However, PMCAs efflux of Ca^{+2} from the T cell is reduced, to allow mitochondrial control of Ca^{+2} flux (Quintana and Hoth, 2012). PMCAs also promote the activation the sarco-endoplasmic reticulum Ca^{2+} ATPase (SERCA), which removes cytosolic Ca^{2+} into the ER and the mitochondria (Hogan et al., 2003; Korthals et al., 2017). In addition, ryanodine receptor channels also increase the efflux of Ca^{2+} from the ER to the cytoplasm (Fenninger and Jefferies, 2019). These channels are activated by the release of cyclic adenosine diphosphate (ADP) ribose (cADPR) induced upon the store-operated Ca^{2+} entry

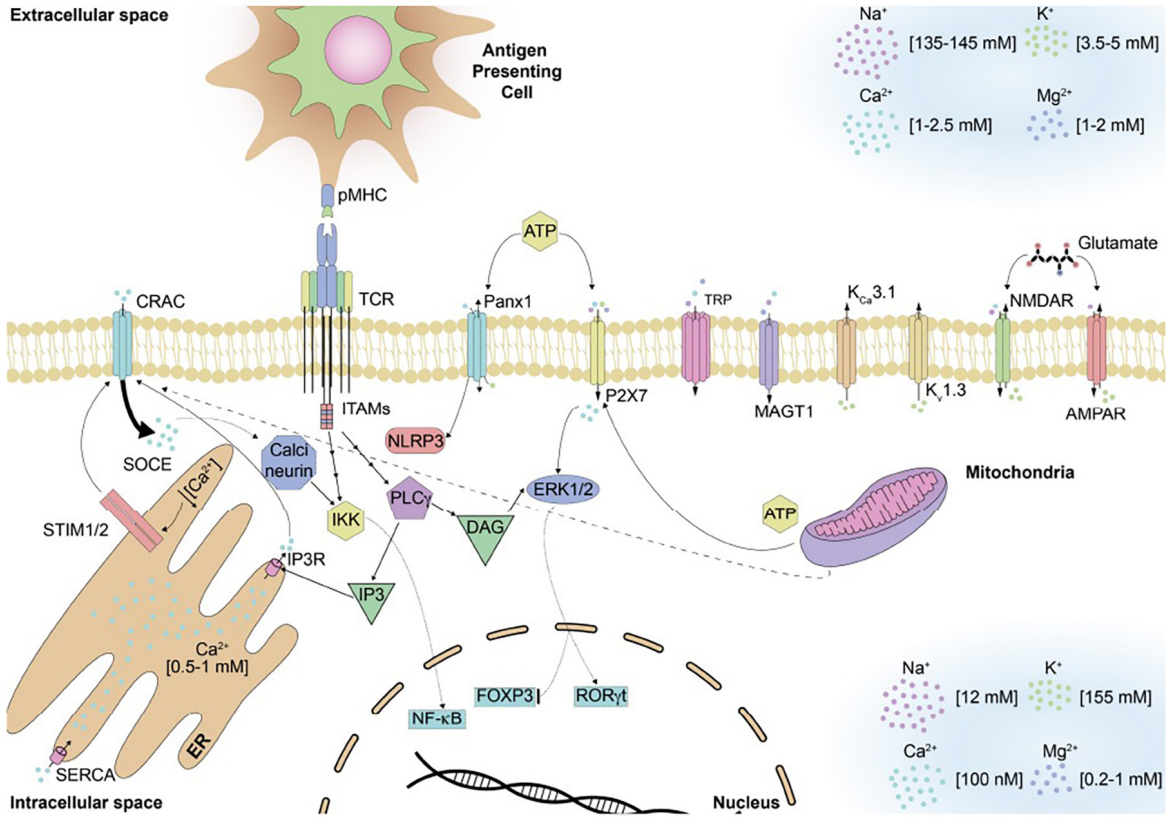

FIGURE 2 | Ion channels and signaling pathways described for T cells. Several channels responsible of regulating the ion homeostasis can be found on the surface of T cells. These channels maintain the different concentrations of ion in the extracellular and intracellular space and are permeable to specific ions. T cell receptor engagement with the pMHC molecule found on antigen presenting cells will induce a signaling cascade that will result on the influx of Ca^{2+} and eventual store-operated Ca^{2+} entry inside of T cells. All these events will result in the activation of different transcription factor that will activate the effector function of T cells.

(Fenninger and Jefferies, 2019). PMCAs are activated after Ca^{2+}-loaded calmodulin binds to their carboxyl terminus (Joseph et al., 2014; Fenninger and Jefferies, 2019). Although PMCAs have a high affinity for Ca^{2+}, they also have low permeability for this cation, which is why they modulate Ca^{2+} concentration at basal levels (Joseph et al., 2014).

The P2X purinoreceptor ion-channel family (and specifically P2X1, P2X2, and P2X7) consists of another group of channels related to immunity and myeloid and lymphoid cell modulation (Junger, 2011). These channels require extracellular ATP for activation and are non-selective for cations, such as Ca^{2+} and Na^{+} (Junger, 2011). P2X7 receptors mainly control complex pathways that modulate Ca^{2+} and Na^{+} influx and K^{+} efflux and are primarily expressed by T lymphocytes and innate immune cells (Yip et al., 2009; Junger, 2011). Activation of P2X7 by ions such as K^{+}, Na^{+}, Ca^{2+}, and Cl^{-} results in significant stimulation of the NLRP3 inflammasome in several innate cells, such as in macrophages and monocytes (Yip et al., 2009; Junger, 2011). Furthermore, NLRP3 oligomerization and inflammasome activation will result in Caspase 1-induced cleavage of pro-IL-1β and pro-IL-18 into their mature forms, IL-1β and IL-18 (Franchi et al., 2009). These cytokines will activate additional signaling pathways to induce inflammation and immune cell function (Franchi et al., 2009). Remarkably, Pannexin 1 hemichannels (Panx1) has been reported to co-localize with P2X7 at the immunological synapsis, (Woehrle et al., 2010). Because Panx1 can release ATP into the extracellular space, it has been suggested that T cells can modulate P2X7 signaling (Woehrle et al., 2010). This modulation can work in an autocrine fashion to amplify gene expression, T cell effector functions, and T cell receptor signals upon pMHC engagement (Schenk et al., 2008; Woehrle et al., 2010; Junger, 2011; **Figure 2**). Activation of the inflammasome and Caspase-1 is also linked to programmed cell death (Martinon et al., 2002; Shi et al., 2017). Gasdermin D is a target of Caspase-1, -4, -5, and -11 and has been identified as a key component of the molecular mechanisms of pyroptosis (Lamkanfi et al., 2008; Shi et al., 2015). Pyroptosis is a cellular phenomenon leading to programmed cell death that increases the presence of inflammatory molecules in the extracellular space, such as IL-1β (Shi et al., 2017), which differs from non-inflammatory cell death triggered by apoptosis (Jorgensen and Miao, 2015). The inflammatory features of pyroptosis include the activation of PRRs and an increased transcription of pro-inflammatory cytokines, which classifies this process as an innate immunity-related mechanism (Jorgensen and Miao, 2015). Gasdermin D is usually found in an inactivated state

TABLE 1 | Role of ion channels expressed by lymphocytes.

Ion to be modulated	Channels	Role in the lymphocytes functioning		References
		T cells	**B cells**	
Ca^{2+}	CRAC	Increment of $[Ca^{2+}]_i$ upon T cell receptor engagement. Participates in the secretion of cytokines.	Increment of $[Ca^{2+}]_i$ upon B cell receptor engagement Modulates the proliferation of B cells. Modulates the secretion of antibodies.	Lewis, 2001; Feske et al., 2012; Prakriya and Lewis, 2015; Trebak and Kinet, 2019
	P2X	Amplifies gene expression, T cell effector functions, and T cell receptor signaling.	Not expressed by this cell type	Schenk et al., 2008; Woehrle et al., 2010; Junger, 2011
	TRP	Enhances T cell receptor stimulation. Regulates differentiation of T cell into Th1 or Th2 profile. Induces proliferation.	Not expressed by this cell type	Weber et al., 2010; Acharya et al., 2021
	Ca_v	Secretion of IL-2. Differentiation of T cells into Th2 profiles. Homeostasis of naïve T cells.	Not expressed by this cell type	Cabral et al., 2010; Omilusik et al., 2011; Fenninger and Jefferies, 2019
Mg^{2+}	TRPM7	Promotes T cell development and maturation.	Might be essential for B cell survival.	Jin et al., 2008; Feske et al., 2012; Brandao et al., 2013
	MagT1	Induces the activation of T cells.	Does not induce the activation of B cells.	Goytain and Quamme, 2005
K^+	K_v	Promotes the central and effector memory phenotypes of T cells.	Promotes the secretion of autoantibodies. Induces proliferation of class-switching memory B cells	Chiang et al., 2017
	K_{Ca}		Unknown role	
Zn^{2+}	ZIP	Unknown role	Unknown role	Feske et al., 2012
Cl^-	CAGA	Inhibition of T cell function and proliferation.	Not expressed by this cell type	Feske et al., 2012
	CFTR	Regulates differentiation profile of T cells.	Activation and proliferation of B cells.	Polverino et al., 2019

and, upon cleavage by the aforementioned Caspases, can act as a pore-forming protein by disrupting the plasma membrane, cell swelling, and lysis, in a pyroptotic fashion (Ding et al., 2016; Liu et al., 2016). Remarkably, increased cytosolic Ca^{2+} leads to increased translocation of GSDMD into the membrane and enhanced LPS-induced pyroptosis, in a PLCγ1-dependent manner (Liu et al., 2020). Therefore, Ca^{2+} contributes to the modulation of programmed cell death.

Transient receptor potential channels were initially described in *Drosophila melanogaster* mutants and constitute a superfamily including 6 subfamilies in humans: TRP canonical (TRCP), TRP vanilloid (TRPV), TRP melastatin (TRPM), TRP ankyrin (TRPA), TRP mulcolipin, and TRP polycystic (Minke and Cook, 2002; Wenning et al., 2011; Feske et al., 2012; Samanta et al., 2018). The most common TRP receptors expressed by T cells are TRPC and TRPM (Parenti et al., 2016; Froghi et al., 2021). TRPC channels are thought to be responsible for Ca^{2+} influx into T cells and are usually associated with PLCγ signaling (Feske et al., 2012). Further studies are required to elucidate if these channels contribute to the store-operated Ca^{2+} entry and T cell activation (Minke and Cook, 2002; Feske et al., 2012). TRP cation channel subfamily M member 2 (TRPM2) channels have been shown to regulate Ca^{2+} in a non-selective fashion in several immune cells (Yamamoto et al., 2010). These channels are regulated by several intracellular factors, mostly related to ADP, such as cADP and cADPR (Yamamoto et al., 2010; Huang et al., 2018). Other molecules, such as hydrogen peroxide, may modulate the permeability and activity of TRPM2 (Yamamoto et al., 2010; Sumoza-Toledo and Penner, 2011; Wenning et al., 2011). Different reports have shown that these channels can enhance T cell receptor stimulation in T cells and inhibit reactive oxygen species production in phagocytic cells (Di et al., 2011; Chung et al., 2015; Syed Mortadza et al., 2015; Morad et al., 2021). Furthermore, this channel can promote the secretion of cytokines such as IL-2, IL-17, and IFN-γ (Melzer et al., 2012). TRPM4, the most studied TRP channels in immune cells, are highly permeable to Na^+ and K^+ and partially to Ca^{2+} (Vennekens and Nilius, 2007). The influx of Ca^{2+} will induce the activation of TRPM4, which will negatively modulate store-operated Ca^{2+} entry and promote Na^+ influx, membrane depolarization, and reduction of Ca^{2+} influx due to stabilizing electrical charges (Vennekens and Nilius, 2007; Feske et al., 2012; Bose et al., 2015). The modulation of Ca^{2+} levels regulates the Th1 and Th2 differentiation of T cells (Weber et al., 2010). Lastly, TRPM8 has been associated to T cell activation, increasing CD25 and CD69 expression and TNF-α secretion (Acharya et al., 2021). Although TRPM8 might not be necessary for T cell activation, inhibition of this channel impairs T cell proliferation (Acharya et al., 2021).

Ca_v channels induce specific Ca^{2+} influx in excitable cells and are divided into three subfamilies, Ca_v1, Ca_v2, and Ca_v3. T cells express only the Ca_v1 first subfamily (Feske et al., 2012, 2015), which comprises $Ca_v1.1$, $Ca_v1.2$, $Ca_v1.3$, $Ca_v1.4$, and the regulatory subunits β3 and β4 (Feske et al., 2012, 2015; Badou et al., 2013). Treatment of Jurkat T cells with a Ca_v channel antagonists reduces IL-2 production (Fenninger and Jefferies, 2019), suggesting the involvement of this channel in the secretion of this cytokine. The upregulation of Ca_v 1.2 and Ca_v 1.3 channels and the differentiation of T cells toward a Th2 profile are also

associated (Cabral et al., 2010). $Ca_v1.2$ activity is also regulated via STIM, as upon inhibition of Ca_v 1.2, the interaction between STIM and ORAI occurs (Badou et al., 2013). The influx of Ca^{2+} generated by Ca_v 1.4 channels modulates the homeostasis of naïve T cells and is important for the generation of T cell responses (Omilusik et al., 2011).

Magnesium Transporters and Channels

Magnesium is another secondary messenger important for modulating the function of T cells, which has been associated with promoting the correct function and development of these cells (Feske et al., 2012). Magnesium transporter protein 1 (MAGT1, an Mg^{2+} transporter) is a highly selective Mg^{2+} channel that is not permeable to other divalent cations such as Ca^{2+}, Zn^{2+}, and Ni^{2+} (**Figure 2**; Goytain and Quamme, 2005; Ravell et al., 2020) and is involved in T cell development and function (Goytain and Quamme, 2005). Notably, MAGT1 will induce PLCγ1 activation and then store-operated Ca^{2+} entry, upon Mg^{2+} influx and T cell receptor stimulation (Ravell et al., 2020). T cells lacking MAGT1 channels exhibit an impaired capacity to be activated upon T cell receptor engagement and show a decreased Ca^{2+} influxes (Li et al., 2011; Brandao et al., 2013).

TRP cation channel subfamily M member 7 is a non-selective Mg^{2+} channel expressed by T cells, permeable also to Ca^{2+} (Bates-Withers et al., 2011; Antunes et al., 2016; Vaeth and Feske, 2018). TRPM7 channels regulate Mg^{2+} concentration and cell homeostasis in the entire organism (Bates-Withers et al., 2011; Antunes et al., 2016; Vaeth and Feske, 2018) and are fundamental for T cell development and maturation (Jin et al., 2008; Feske et al., 2012). The absence of this channel impairs the development of T cells, resulting in $CD4^-$ and $CD8^-$ T cells (Schmitz et al., 2003; Feske et al., 2012). However, it seems that the lack of TRPM7 does not modify the intracellular concentration of Mg^{2+} ($[Mg^{2+}]_i$) in T cells, but rather the primary function of this channel might be related to Ca^{2+} influx (Feske et al., 2012). The translocation of Ca^{2+} or Mg^{2+} into target cell leads to the phosphorylation of molecules involved in the signaling of tyrosine kinases-based receptors, promoting cell differentiation, growth and activation (Zou et al., 2019).

Potassium Channels

The $K_v1.3$ and $K_{Ca}3.1$ channels modulate K^+ homeostasis (Chiang et al., 2017). These channels must control the efflux of K^+, which leads to hyperpolarization of the plasma membrane (Lam and Wulff, 2011; Chiang et al., 2017). These channels inhibit membrane depolarization upon the influx of other cations, such as Mg^{2+} and Ca^{2+} (Lam and Wulff, 2011). The topology of $K_v1.3$ and $K_{Ca}3.1$ is very similar, as they are homotetramers with each subunit exhibiting six transmembrane segments (Di Lucente et al., 2018; Ji et al., 2018). However, these channels differ in the mechanism of activation (Wulff et al., 2009). While $K_v1.3$ is activated upon membrane depolarization leading to K^+ efflux, $K_{Ca}3.1$ activation requires the release of Ca^{2+} and calmodulin. This process leads to repolarization of the plasma membrane upon K^+ efflux and continuous influx of Ca^{2+} (Wulff et al., 2009). Interestingly, these channels are relevant for establishing central and effector memory phenotypes in T cells (Chiang et al., 2017).

Additional Cationic Channels

N-methyl-D-aspartate receptors (NMDARs) and α-amino-3-hydroxy-5-methyl-4-isoxazole propionic acid receptors (AMPARs) are ionotropic glutamate receptors that deserve mention, as they are considered receptors linked to ion channels and are relevant during glutamatergic transmission in the central nervous system (CNS; Traynelis et al., 2010). Glutamate is considered one of the primary excitatory neurotransmitters of the CNS in mammals, and it can interact with ionotropic and metabotropic receptors (Traynelis et al., 2010). NMDARs and AMPARs are, as many of the channels mentioned so far, non-selective cations channels that are mostly permeable to K^+ and Na^+, and to some extent to Ca^{2+} (Traynelis et al., 2010). These receptors will produce excitatory post-synaptic responses upon activation (Fourgeaud et al., 2010; Traynelis et al., 2010; Kahlfuß et al., 2014). These receptors can also be found in several isoforms, depending on the subunit composition (Fourgeaud et al., 2010; Traynelis et al., 2010; Kahlfuß et al., 2014). Recent reports have described that immune cells, such as DCs are sensitive to and can release glutamate (Fourgeaud et al., 2010; Kahlfuß et al., 2014). Further, AMPAR and NMDAR are expressed by some immune cells, suggesting that these receptors can modulate the development, activation, or effector functions of these immune cells (Fourgeaud et al., 2010; Kahlfuß et al., 2014). However, more exhaustive studies are required to better define the contribution of these channels and the associated signaling pathways to the function of T cells and other immune cells.

Additional ion channels can be found on the surface of T cells, such as Zn^{2+} channels -i.e., ZIP3, ZIP6, ZIP8, ZIP10, ZIP14-, but the contribution of these channels to the function of T cells has not been defined (Feske et al., 2012).

Anionic Channels

CFTR is one of the anionic channels expressed by T cells (Feske et al., 2012). CFTR promotes the efflux of Cl^- from the intracellular to the extracellular and its absence on $CD4^+$ T cells induces a Th2 polarization leading to an increase in the secretion of IL-4 (Feske et al., 2012; Polverino et al., 2019). Another Cl^- channel in T cells is GABA receptors, and the activation of this receptor has been described to inhibit the function and proliferation of these cells (Feske et al., 2012). Additionally, the treatment with GABA has prevented the secretion of IL-2 and IFN-γ on $CD8^+$ T cells (Feske et al., 2012). Finally, the LRRC8-A channel has been identified on T cells and shown to be important for T cell development, function and survival (Kumar et al., 2014; Serra et al., 2021).

Ion Channels Expressed by B Cells

B cells can act as professional antigen-presenting cells that can prime T cells and can also differentiate into plasma cells to produce antibodies, which bind to specific antigens of pathogens, promoting their clearance (Whitacre et al., 2012;

Häusser-Kinzel and Weber, 2019). B cells express the B cell receptor on their surface (Whitacre et al., 2012) and several ion channels and transporters that modulate their activation and function, through the influx of Ca^{2+}, Mg^{2+}, and Zn^{2+}, or the efflux of K^+ and Cl^- (Scharenberg et al., 2007; Feske et al., 2015; **Table 1**).

Calcium Channels

Ca^{2+} ions act as a second messenger in B cells and are required for proliferation and antibody secretion (Vig and Kinet, 2009; Feske et al., 2012; Trebak and Kinet, 2019). Ca^{2+} influx in B cells is controlled by CRAC channels, which are activated upon antigen recognition (Feske et al., 2012, 2015). Therefore, CRAC channels contribute to the establishment of immunity against infections, modulating B cell proliferation and antibody secretion by these cells. The lack of ORAI1 in B cells can lead to immunodeficiency and also to autoimmunity (Feske et al., 2012). However, the absence of ORAI1 does not affect B cell development (Mahtani and Treanor, 2019). Autoimmune disorders described in the absence of ORAI1 are associated with inflammation of the CNS (Gauthier et al., 2006; Feske et al., 2012). For instance, multiple sclerosis has been related to reduced production of IL-10 by B cells that have mutations associated with CRAC channels (Gauthier et al., 2006; Feske et al., 2012).

Magnesium Channels

Mg^{2+} is a secondary messenger essential in B cells because the lack of this cation prevents the proliferation of these cells (Feske et al., 2012). TRPM7 is the Mg^{2+} channel described in B cells, responsible for the entry of both Mg^{2+} and Ca^{2+} (Feske et al., 2012, 2015). Even though the role of Mg^{2+} has not been thoroughly studied, it is known that the lack of TRP7M in B cells induces cell death after 24 h, suggesting that the role of Mg^{2+} in B cells might be essential for cell survival (Brandao et al., 2013). The TRP7M might be essential for cell survival since the influx of Mg^{2+} induces the phosphorylation of targets from the signaling pathway involved with the tyrosine kinase-based receptors, leading to cell differentiation, growth and function (Zou et al., 2019). Interestingly, the lack of the channel TRPM7 has been associated with an increase of MAGT1 in B cells (Zou et al., 2019), a phenomenon that has not been described yet for T cells.

Potassium Channels

As seen for T cells, the influx of Ca^{2+} in B cells is highly dependent on the transmembrane electrostatic potential (Feske et al., 2012). K^+ channels control the depolarization of the B cell membrane through the efflux of K^+, and the channels involved in this process are $K_v1.3$ and $K_{ca}3.1$ (Feske et al., 2012, 2015). $K_v1.3$ channels are expressed in proliferating B cells producing autoantibodies and switching to memory B cells (Wulff et al., 2004; Land et al., 2017). Blockade of this channel decreases the release of autoantibodies and has been related to inhibiting the proliferation of class-switched memory B cells (Land et al., 2017). Additionally, it has been suggested that blocking $K_v1.3$ channels might help controlling multiple sclerosis, a disease in which the proliferation of class-switched memory cells is detrimental (Beeton and Chandy, 2005; Feske et al., 2012).

Importantly, although B cells express additional ion channels such as Zn^{2+} channels -i.e., ZIP3, ZIP6, ZIP8, ZIP10, ZIP14, their contribution to B cell function remains unknown (Feske et al., 2015).

Anionic Channels

CFTR is the only Cl^- channel described on the surface of B cells (Feske et al., 2012). Absence of this channel leads to the inhibition of conductance of Cl^-, decreasing B cell activation and proliferation (Polverino et al., 2019). No other anionic channels have been described to be expressed by these cells.

CONTRIBUTION OF ION CHANNELS TO THE IMMUNOLOGICAL SYNAPSE AND OTHER T CELL FUNCTIONS

One of the most relevant processes that initiate an adaptive immune response is the interaction between antigen-presenting cells (particularly DCs) and T cells (González et al., 2007; Carreño et al., 2010, 2011). This interaction requires ions to be mobilized from several compartments and considers the participation of ion channels and transporters (Quintana et al., 2011). The contribution of ion channels and transporters (mainly focused on Ca^{2+}), and the function of these channels during the immunological synapsis and other processes such as T cell activation, proliferation, and differentiation, will be discussed in this section.

Interaction Between Dendritic Cells and T Cells

An immunological synapsis must be established to induce the activation of an adequate adaptive immune response (González et al., 2007; Franchi et al., 2009; Carreño et al., 2010, 2011). Ion channels are needed for the proper maturation of DCs, and several issues can arise when these channels are not working properly. For instance, inhibition of $K_v1.3$ results in an impairment in the expression of maturation markers, MHC-II expression, and secretion of cytokines (RamaKrishnan and Sankaranarayanan, 2016). Impairment of all these characteristics will cause a reduced activation and proliferation of T cells (RamaKrishnan and Sankaranarayanan, 2016). TRPM4 is required for the migration of peripheral DCs into the lymph nodes by activating PLC (Barbet et al., 2008). Therefore, a mutation or deletion of TRPM4 in DCs impairs the assembly of the immunological synapsis in lymph nodes, because DCs fail to reach this organ (Barbet et al., 2008). $Ca_v1.2$ will activate Ryanodine receptors, leading to the expression of MHC-II on the plasma membrane of DCs (Vukcevic et al., 2008). A mutation in the gene encoding for this channel would cause MHC-II not to be expressed on the DC membrane, antigen presentation would not occur, preventing the establishment of the immunological synapsis (RamaKrishnan and Sankaranarayanan, 2016).

Upon establishment of the immunological synapsis, regions known as central supramolecular activation clusters (cSMACs) are formed in the immediate vicinity of the T cell receptor-pMHC complex and concentrate most CD28 and T cell receptor molecules (Grakoui et al., 1999). Surrounding the immunological synapsis, peripheral supramolecular activation clusters emerge, where integrins such as CD2 and different intercellular adhesion molecules are located (Grakoui et al., 1999). At the most peripheric region, distant supramolecular activation clusters are formed, consisting mostly of CD45 and CD43 (Grakoui et al., 1999). One of the main indirect effects of the entry of Ca^{2+} into the T cell is the reorganization of actin on the three SMACs, modulating the intensity and the duration of T cell receptor signaling (Billadeau et al.,2007). After activation of T lymphocytes, there is a release of Ca^{2+} from the ER into the cytoplasm that leads to the activation of CRAC channel (Smith-Garvin et al., 2009). This will induce changes in the membrane potential, inducing the activation of voltage-dependent ion channels, such as $K_v1.3$. This will allow the exit of K^+ to the extracellular space and maintain the T cell membrane potential (Grissmer et al., 1993). The primary function of intracellular Ca^{2+} influx is the mobilization of the centrosome to the cSMAC (Kloc et al., 2014). The centrosome is a cellular organelle that works as the microtubule-organizing center and is spatially close to the Golgi apparatus and several vesicles (Kloc et al., 2014). The mechanism by which the centrosome is mobilized due to Ca^{2+} flux is not entirely clear. Actin interaction with myosin generates a contraction that promotes that the centrosome, along with the Golgi apparatus, move toward the cSMAC (Billadeau et al., 2007). Because the centrosome moves toward the cSMAC, the T cell can release the proper cytokines in a localized and focused way toward the antigen-presenting cells or target cell because microtubule-organizing center carries with it the Golgi and vesicles containing cytokines (Martín-Cófreces et al., 2008; Kloc et al., 2014).

The interaction between DCs and T cells is also modulated by the intracellular concentration of Mg^{2+}, Zn^{2+}, and Ca^{2+} and the activity of ion channels and transporters (Feske et al., 2012; **Figure 2**). These cations can act as second messengers modulating various T cell functions, such as cytotoxicity, differentiation, and cytokine production (Feske et al., 2012). After T cell receptor activation, MAGT1 elicits a specific influx of Mg^{2+}, which activates PLCγ1 and consequently the influx of Ca^{2+} after T cell receptor activation (Feske et al., 2012). The increase in Ca^{2+} in the cytosol after T cell receptor engagement will trigger various signaling pathways leading to the T cell activation and the induction of the immune response in a T cell-dependent manner (Joseph et al., 2014). However, the mechanisms involved in activating the MAGT1 transporter are not clear yet (Feske et al., 2012). **Figure 2** describes the events occurring upon T cell receptor engagement by the cognate pMHC complex, focusing on Ca^{2+} signaling.

After T cell receptor engagement, there is an influx of Ca^{2+} producing a significant increase of intracellular Ca^{2+} concentration (around 50–100 fold increase as compared to resting values; Feske et al., 2012). This phenomenon promotes the activation of transcription factors and signal transduction molecules. Among the different channels that modulate this influx are TRP channels, Ca_v channels, P2X channels, and CRAC channels (Feske et al., 2012). To maintain the electrical gradient necessary for the transportation of this ion, Na^+, Cl^-, and K^+ channels work alongside these Ca^{2+} channels (Feske et al., 2012; Vaeth et al., 2020; **Figure 2**).

T cell receptor engagement leads to the depletion of Ca^{2+} stores within the ER and the phosphorylation of PLCγ (Yang and Jafri, 2020). Although two isoforms of PLCγ have been described, namely PLCγ1 and PLCγ2 (Joseph et al., 2014) T cells mainly express PLCγ1 (Joseph et al., 2014). The activation of a tyrosine kinase promotes the PLCγ1 phosphorylation, and therein, its activation (Vaeth et al., 2020; Yang and Jafri, 2020). PLCγ1 hydrolyzes phosphatidylinositol 4,5-bisphosphate (PIP_2) into DAG and IP_3, molecules that act as second messengers in these cells (Vaeth et al., 2020; Yang and Jafri, 2020). DAG activates the protein kinase C (PKC) and the mitogen-activated protein kinase/extracellular signal-regulated kinase (MAPK/ERK) pathways, while IP_3 binds to IP_3R on the ER membrane. The IP_3R is an ion channel permeable to Ca^{2+}, which causes the release of this cation from this organelle as discussed above, with the ER later being refilled by the SERCA pump to recover original Ca^{2+} levels (Joseph et al., 2014; Vaeth et al., 2020; Yang and Jafri, 2020; **Figure 2**).

Phospholipase Cγ is composed of three SH domains needed to achieve proper phosphorylation of the phospholipase (Joseph et al., 2014). The activation of PLCγ occurs at microclusters in T cells, which are small protein aggregates promoted by the phosphorylation of the ζ-chain of the ZAP-70 protein (Joseph et al., 2014). The events occurring before phosphorylation are related to the activation of the ZAP-70 protein due to the phosphorylation of the immune receptor tyrosine activating motif, which is mediated by the Src family kinases (Joseph et al., 2014). This family of kinases is also in charge of the phosphorylation of NMDAR subunits in hippocampal neurons (Zainullina et al., 2011). Since Src proteins are expressed in both cell types, they might also regulate the activity of NMDAR in T cells (Zainullina et al., 2011). Following antigen stimulation, these receptors regulate T lymphocyte functions and contribute to the Ca^{2+} influx mediated by the store-operated Ca^{2+} entry (Zainullina et al., 2011; Joseph et al., 2014; Fenninger and Jefferies, 2019). Significantly, the activation of PLCγ at microclusters depends on the linker for activation of T cells, the SH domain-containing leukocyte protein of 76 KDa, Vav1, guanine nucleotide exchange factor, c-Cbl, and Itk (Joseph et al., 2014). In summary, PLCγ needs to be phosphorylated to begin the mobilization of Ca^{2+} from the ER Ca^{2+} stores into the cytoplasm, increasing the intracellular Ca^{2+}concentration ($[Ca^{2+}]_i$).

Proliferation of T Cells

As described above, the influx of Ca^{2+} into T cells is dependent on the transmembrane electrostatic potential (Feske et al., 2012). If the transmembrane electrostatic potential is negative, Ca^{2+}

may enter the cell (Feske et al., 2012; Yang and Jafri, 2020). However, the influx of Ca^{2+} promotes a transient depolarization of the membrane, which does not favor ion entry (Feske et al., 2015). K^+ channels contribute significantly to this process because they compensate this depolarization by maintaining a negative voltage in the T cell membrane and even hyperpolarizing it through the efflux of K^+, providing a driving force that allows Ca^{2+} entry through CRAC channels (Fanger et al., 2001; Cahalan and Chandy, 2009; Lam and Wulff, 2011; Feske et al., 2012, 2015; Teisseyre et al., 2019; Yang and Jafri, 2020). There is some controversy about the role that K^+ channels play with regards to Ca^{+2} influx and a clamp in membrane potential caused by the opening of K^+ channels may attenuate Ca^{+2} entry (Cahalan and Chandy, 2009). The movement of ions through membranes depends on various factors, such as the concentration gradient, the membrane potential, and the permeable ions involved (Bowman and Baglioni, 1984). All of these factors can be grouped in the electro-diffusion theory, which is the basis of the Goldman-Hodgkin-Katz equation (Bowman and Baglioni, 1984). There is not much information regarding K^+ efflux and Ca^{+2} influx in T cells, but these two ions have been studied in non-excitable cells (HeLa cells) using a path-clamp measurement to determine membrane potential while stimulating the cell with a femtosecond laser (Ando et al., 2009). One of the main conclusions was that after laser irradiation on HeLa cells, an hyperpolarization of membrane potential correlates with a rise in intracellular Ca^{+2} (Ando et al., 2009). The crucial role that K^+ channels play in the modulation of Ca^{2+} entry through CRAC channels allows its influx and further signaling, promoting the proliferation of T cells.

In T cells, K^+ efflux is controlled by the channels $K_v1.3$, $K_{Ca}3.1$, $K_{2p}3.1$, $K_{2p}5.1$, and $K_{2p}9.1$ (Feske et al., 2015). The two most commonly expressed channels in the membrane of T cells are $K_v1.3$ and $K_{Ca}3.1$ (Feske et al., 2012; Conforti, 2017). Several studies have evaluated the impact of blocking these channels on T cell function and the effects vary depending on the channel that was inhibited (Petho et al., 2016). For example, the simultaneous blockage of the channels $K_v1.3$, $K_{Ca}3.1$, and CRAC can prevent T cell proliferation, while only blocking $K_v1.3$ alters the secretion of cytokines by $CD4^+$ T cells (Petho et al., 2016; Veytia-Bucheli et al., 2018). Interestingly, the activation of $K_{Ca}3.1$ channels in $CD8^+$ T cells modulates their chemotactic activity toward tumor cells, suggesting that the increased activity of this channel might promote $CD8^+$ T cell infiltration (Chimote et al., 2018). Additionally, pharmacological inhibition of both K^+ channels in human $CD4^+$ T cells induces a decrease in IL-2 production (Valle-Reyes et al., 2018). This decrease in IL-2 correlates with the inhibition of T cell proliferation primarily in the early stages of T cell activation (Verheugen et al., 1997).

Naïve T cells express mainly $K_v1.3$ channels, and upon T cell receptor engagement, there is an upregulation and recruitment of $K_{Ca}3.1$ channel into the IS (Feske et al., 2015). Membrane depolarization by the influx of Ca^{2+} is sensed by a set of arginine residues in the transmembrane segment four of these channels, causing conformational changes and their opening. Interestingly, the activation of this channel is also regulated by Lck, PKC ζ, and PKA (Nicolaou et al., 2010; Feske et al., 2012, 2015).

The binding of Ca^{2+} and calmodulin inside T cells activates the K_{Ca} 3.1 channel, as the C terminus of this channel is constitutively linked to calmodulin (Feske et al., 2012). The activation of this channel is also dependent on PKA and the class 2 phosphatidylinositol-3-kinase (PI3K-C2β), which is activated after T cell receptor stimulation (Feske et al., 2012). The activation of PI3K-C2β increases PI_3P levels in the plasma membrane, allowing the histidine kinase nucleoside diphosphate kinase B to activate the K_{Ca} 3.1 channel by phosphorylating histidine 358 in its carboxyl terminus (Feske et al., 2012, 2015). Accordingly, dephosphorylation of PI_3P and K_{Ca} 3.1 inhibits the activity of this channel, T cell proliferation, and Ca^{2+} influx induced by T cell receptor signaling (Feske et al., 2012, 2015). Such an inhibition occurs through the PI_3P phosphatase myotubularin-related protein 6 and the histidine phosphatase phosphohistidine phosphatase-1. K_{Ca} 3.1 channels can also be inhibited through the ubiquitination and inhibition of PI3K-C2β due to the E3 ubiquitin ligase tripartite motif-containing protein 27 (Feske et al., 2012, 2015).

T Cell Polarization

The overall immune response must be tightly regulated to recognize and clear different pathogens. $CD4^+$ T cells are usually in charge of orchestrating this response by polarizing into different Th profiles, with key cytokines secreted by each of these profiles (Gálvez et al., 2021). For instance, while a Th1 polarization induces the secretion of IFN-γ and will be optimal for the clearance of intracellular pathogens, a Th2 response induces the secretion of IL-4 and will be optimal for the clearance of extracellular bacteria and a Th17 response induces the secretion of IL-17 and will be optimal for the clearance of extracellular pathogens, such as parasites (Gálvez et al., 2021). Interestingly, the absence of TRPA1 induces the polarization of T cells into a Th1 profile, increasing the expression of T-bet and IFN-γ (Bertin et al., 2017). The role of ion channels modulating T cell profiles toward a Th2 response has been associated with the upregulation of Ca_v channels mentioned above (Feske et al., 2012). The role of some ion channels during Th17 polarization has been partially described up to date. The entry of Ca^{2+} through the P2 × 7 receptor activates ERK1 or ERK2, which suppresses the transcription of forkhead box P3 and promotes the expression of retinoic acid receptor-related orphan receptor-γt, which induces the polarization of T cells toward a Th17 phenotype, altogether inhibiting the regulatory T cells (T_{reg}) polarization (Feske et al., 2012).

Cytokine Secretion by T Cells

Translocation of different transcription factors, such as the nuclear factor of activated T cells (NFAT) and the nuclear factor kappa-light-chain-enhancer of activated B cells (NF-κB) into the nucleus will induce the transcription of genes encoding for cytokines, such as IL-2 (Vaeth et al., 2020; Yang and Jafri, 2020). Ca^{2+} influx through CRAC channels regulates the serine/threonine phosphatase calcineurin function, which coordinates three main signaling pathways (Vaeth et al., 2020;

Yang and Jafri, 2020). The first pathway is related to NFAT signaling, the second one is associated with NF-κB signaling and the third one is related to the c-Jun NH_2-terminal kinase (JNK) pathway (Vaeth et al., 2020; Yang and Jafri, 2020). For the first pathway, calcineurin dephosphorylates NFAT, specifically the regulatory domain in the N terminal (Hogan et al., 2003). This exposes nuclear localization signals, promoting the translocation of this complex toward the nucleus, eventually inducing the transcription of cytokine genes, such as IL-2 (Joseph et al., 2014; Yang and Jafri, 2020). To activate this particular transcription pathway, T cells need a low and extended intracellular Ca^{2+} influx (Joseph et al., 2014; Yang and Jafri, 2020). Certain distal regulatory elements in NFAT target genes from T cells (mainly enhancers) can be found in cytokine genes, including IL-3, GM-CSF, IL-4, IL-10, and IFN-γ genes (Hogan et al., 2003). It is also important to indicate that NFAT can interact with other transcription factors, such as the activator protein 1 (AP-1) transcription factor, ICER, EGR, and GATA (Hogan et al., 2003). Calcineurin also regulates NF-κB signaling pathway, as an increase in intracellular Ca^{2+} promotes PKCα, which along with protein kinase C theta (PKCθ; previously activated by the co-stimulation of the T cell receptor/CD3 and CD28) co-activates the Iκ kinase (IKK) and phosphorylates IκB (Yang and Jafri, 2020). Phosphorylation induces IκB dissociation from NF-κB, leading to IκB polyubiquitination and degradation by the proteasome (Yang and Jafri, 2020). Therefore, NF-κB is initially retained in the cytoplasm because of the association with the inhibitory IκB protein, but later on, after the dissociation from IκB, free NF-κB translocates into the nucleus and promotes gene transcription (Yang and Jafri, 2020). This mechanism for the activation of gene transcription is called the canonical NF-κB activation pathway (Brasier, 2006). To activate this transcription factor, unlike for NFAT signaling pathway, T cells need a high and short increase in Ca^{2+} ions in the cytoplasm (Joseph et al., 2014; Yang and Jafri, 2020; **Figure 2**). Using Hodgkin's cell lines, seventeen novel genes regulated by NF-κB were described, such as IL-13, MDC, I-309, EMR, CD44, and the transcription factors $STAT5_a$, IRF-1, Spi-B, and LITAF (Brasier, 2006).

Another pathway related to Ca^{2+} influx is the JNK pathway. Activation of c-Jun modulated by PKCθ regulates MAPK cascade of SEK1/MKK4 and phosphorylates JNK (Yang and Jafri, 2020). This will trigger JNK signaling, along with calcineurin, which also activates SEK (Yang and Jafri, 2020). SEK phosphorylates two serine residues in the activation domain of c-Jun, promoting the activation of this protein (Yang and Jafri, 2020). c-Jun, along with c-Fos establishes the AP-1 transcription factor complex, which plays a role in cell growth and IL-2 induction (Avraham et al., 1998; Yang and Jafri, 2020). The activation of JNK can be detected minutes after pMHC- T cell receptor interaction, along with the binding of B7-1 and -2 molecules to the CD28 receptor on T cells. Both signals are needed to strongly activate JNK as they synergize (Avraham et al., 1998).

All this coordinated activation of NFAT, NF-κB, and AP-1 will result in the activation of pathways that will induce the secretion of several cytokines, including IL-2, IL-8, IL-1β, IL-4, IL-6, IFN-γ, and TNF-α (Fiebich et al., 2012). Among all of these cytokines, the secretion of IL-2 is essential because it modulates the differentiation of $CD4^+$ T cells toward a Th2 or Th1 profile while inhibiting Th17 differentiation (Fiebich et al., 2012).

DISEASES ASSOCIATED TO DEFICIENCIES IN ION CHANNELS AND TRANSPORTERS

Diseases associated with ion channels and transporters mutations that change the molecular structure, topology, and functions of these proteins are called channelopathies (Kim, 2014; Schorge, 2018; Vaeth and Feske, 2018). These diseases are commonly caused by mutations in the alpha subunits or the accessory proteins of these channels (Kim, 2014; Schorge, 2018; Vaeth and Feske, 2018). Channelopathies have been linked to CNS diseases (i.e., epilepsy, ataxia, and migraine), heart diseases, lung diseases (i.e., cystic fibrosis), liver disease, and kidney diseases (Kim, 2014; Schorge, 2018; Vaeth and Feske, 2018). Channelopathies can also affect the immune system, causing immune alterations, such as autoimmune diseases or immunodeficiencies (Feske et al., 2015; Vaeth and Feske, 2018). For instance, mutations that abolish the functionality of CRAC channels, by loss of function of the ORAI1 gene or mutations in the STIM1 gene (components of this channel that we will further describe below), are responsible for a syndrome called CRAC channelopathy (Feske, 2010; Lacruz and Feske, 2015). This syndrome will lead to the establishment of combined immunodeficiency (CID), a disease that is directly linked to the absence of store-operated Ca^{2+} entry (Feske, 2010; Lacruz and Feske, 2015). CID patients, unlike severe combined immunodeficiency patients, exhibit normal counts of most immune cells, including T and B cells, and most myeloid populations, while displaying odd numbers of unconventional lymphocytic populations, such as Tregs, iNKT cells, and γδ T cells (Feske, 2010; Lacruz and Feske, 2015). Although low in number, these cell types are fundamental for establishing a proper immune response (La Cava, 2009; Nielsen et al., 2017; Gálvez et al., 2021). During their first years of life, CID infants require transplantation of hematopoietic stem cells to face the different severe diseases they develop due to their lack of these unconventional lymphocytes (Feske, 2010; Lacruz and Feske, 2015; Vaeth and Feske, 2018). These severe diseases will usually be caused by common and less pathogenic microorganisms like *Candida albicans*, *Streptococcus pneumoniae,* and cytomegalovirus (Feske, 2010; Lacruz and Feske, 2015; Vaeth and Feske, 2018). The lack of Tregs can also lead to the development of autoimmune hemolytic anemia, which originated from the presence of autoantibodies (Lian et al., 2018). Other diseases related to mutations in ion channels and transporters have been described, such as X-linked immunodeficiency with magnesium defects, Epstein-Barr virus infections, and neoplastic syndrome, which arise from the loss of function MAGT1 (Li et al., 2011; Ravell et al., 2014). Several other disorders have been described, such as agammaglobulinemia resulting from loss of function of LRRC8A (a Cl^- channel) (Sawada et al., 2003) and transient neonatal zinc deficiency, which significantly impairs the activation of T

cells and is originated by loss of function of ZIP4 (a Zn^{2+} channel) (Dufner-Beattie et al., 2005; Geiser et al., 2012). Additionally, channelopathies not only promote the infection, but it has also been described that viral infections can lead to the alteration of cation channels, such as Ca^{2+}, K^+, and Na^+ (Charlton et al., 2020), creating dysregulation of the concentrations of Ca^{2+} along with other concentrations of cations. Furthermore, the immune response elicited against the infection can induce channelopathies, due to the binding of autoantibodies to IC (Vaeth and Feske, 2018). The proper function of these channels is fundamental for the immune system and the overall organism.

MODULATION OF Ca^{2+} DURING VIRAL INFECTIONS

As described above, Ca^{2+} is essential for numerous functions of cells. Interestingly, viruses can take advantage of this by modulating the intracellular concentration of Ca^{2+} ($[Ca^{2+}]_i$) used in processes such as viral replication (Zhou et al., 2009). During viral infections, there are changes on $[Ca^{2+}]_i$ that favor viral replication or the establishment of persistent infections on target cells, as discussed below (Zhou et al., 2009). In this section, we will describe the mechanisms used by RNA viruses, such as the human immunodeficiency virus (HIV), respiratory syncytial virus (hRSV), severe acute respiratory coronavirus 2 (SARS-CoV2), and DNA viruses, such as hepatitis B virus (HBV), and herpes simplex virus (HSV) to modulate the concentration of Ca^{2+} altering the cellular signaling.

RNA Viruses

Human Immunodeficiency Virus

Human immunodeficiency virus is a relevant virus transmitted through sexual intercourse, blood perfusion, needle sharing, and vertical transmission. This virus belongs to the *Retroviridae* family, and its genome is composed of two positive-sense single-stranded RNA molecules encoding for three polyproteins (Gag, Pol, and Env) and six accessory proteins (Tat, Rev, Nef, Vpr, Vif, and Vpu; Frankel and Young, 1998; German Advisory Committee Blood (Arbeitskreis Blut), 2016; Rossi et al., 2021). The main target of infection of HIV are $CD4^+$ cells and CCR5- or CXCR4-positive cells, including DCs, macrophages, T helper cells, monocytes, microglia, and astrocytes (German Advisory Committee Blood (Arbeitskreis Blut), 2016; Rossi et al., 2021). Like other viruses, HIV modulates $[Ca^{2+}]$ and Ca^{2+}-dependent channels during different stages of infection, including replication, assembly, budding, and also during immune response evasion (German Advisory Committee Blood (Arbeitskreis Blut), 2016; Chen et al., 2019). It has been described that HIV proteins have a role in Ca^{2+} modulation. Both HIV proteins gp120 and Tat can increase $[Ca^{2+}]_i$ by modulating Ca^{2+} channels in several cell types, such as immune cells, astrocytes, neurons, and epithelial cells (Zocchi et al., 1998; Contreras et al., 2005; Zhou et al., 2009; Hu, 2016; Cai et al., 2020). In normal conditions, DCs need the Ca^{2+} mobilization for several function such as the engulfment of apoptotic bodies and antigen presentation (Poggi et al., 1998). Accordingly, the voltage-sensitive *dihydropyridine* receptor (DHPR) L-type calcium channel expressed in human monocyte-derived DCs (mo-DCs) plays an essential role in Ca^{2+} mobilization. This function was demonstrated by the use of nifedipine (NFP) which inhibit the DPHR function, affecting Ca^{2+} mobilization and engulfment of apoptotic bodies by mo-DCs (**Figure 3**; Poggi et al., 1998). The same phenomenon was observed when mo-DCs were stimulated with HIV Tat protein, which suggests that this protein can interact with DHPR, prevent the entry of Ca^{2+} into the cells, and affect essential functions, such as apoptotic body engulfment and IL-12 secretion (Poggi et al., 1998).

Moreover, human NK cells express a functional phenylethylamine-sensitive (PAA) L-type calcium channel, which when blocked with verapamil (VPM; L-type calcium channel antagonist) the Ca^{2+} influx from the extracellular media, the tumor cell killing function was affected (Zocchi et al., 1998). The interaction between human NK cells and HIV Tat protein induces a decrease of Ca^{2+} influx, promoting the inhibition of Ca^{2+}-dependent functions, such as NK cell cytotoxicity, as seen with VPM (Zocchi et al., 1998). Like other immune cells, human monocytes stimulated with Tat can mobilize Ca^{2+} from the extracellular media (Contreras et al., 2005). Additionally, human monocytes and other immune cells express a functional DHPR in the cellular membrane surface, which has an essential role in cytokine secretion (Contreras et al., 2005). HIV Tat protein uses DHPR to induce the Ca^{2+} mobilization, promoting the induction of TNF-α production by human monocytes during infections (**Figure 3**; Contreras et al., 2005).

On the other hand, because HIV can induce neurotoxicity, using a recombinant HIV gp120 protein in primary human cultures of astrocytes and neurons has been shown to increase $[Ca^{2+}]_i$, which occurs first in astrocytes and then in neurons, and also that NMDARs may mediate this effect in both cells types (Holden et al., 1999). Only in neurons there exists participation of the L-type calcium channel, as astrocytes do not express it. These results suggest that gp120 can modulate $[Ca^{2+}]$ influx through Ca^{2+} channels and NMDARs, promoting neurotoxicity (Holden et al., 1999).

Another important HIV protein is Nef, which induces T cell activation, which is necessary for viral replication in these cells and promotes hyperactivation in the absence of CD28 ligation (Manninen and Saksela, 2002; Fenard et al., 2005). In Jurkat cells, HIV Nef can induce an increase of Ca^{2+}, mediated by the interaction with IP_3R (Manninen and Saksela, 2002; Zhou et al., 2009). Furthermore, it has been described that Nef is found in lipid rafts, which are recruited into the IS space minutes after T cell receptor engagement (**Figure 3**; Fenard et al., 2005). Besides, HIV Nef can impair the formation of Ca^{2+} domains after T cell receptor engagement, suggesting that this viral protein can control the cellular distribution of Ca^{2+} levels, allowing hyperactivation, which implies a spontaneous T cells proliferation, including the expression of the T cells activation antigens and increased cytokines secretion, among other changes (**Figure 3**; Ott et al., 1997; Fenard et al., 2005).

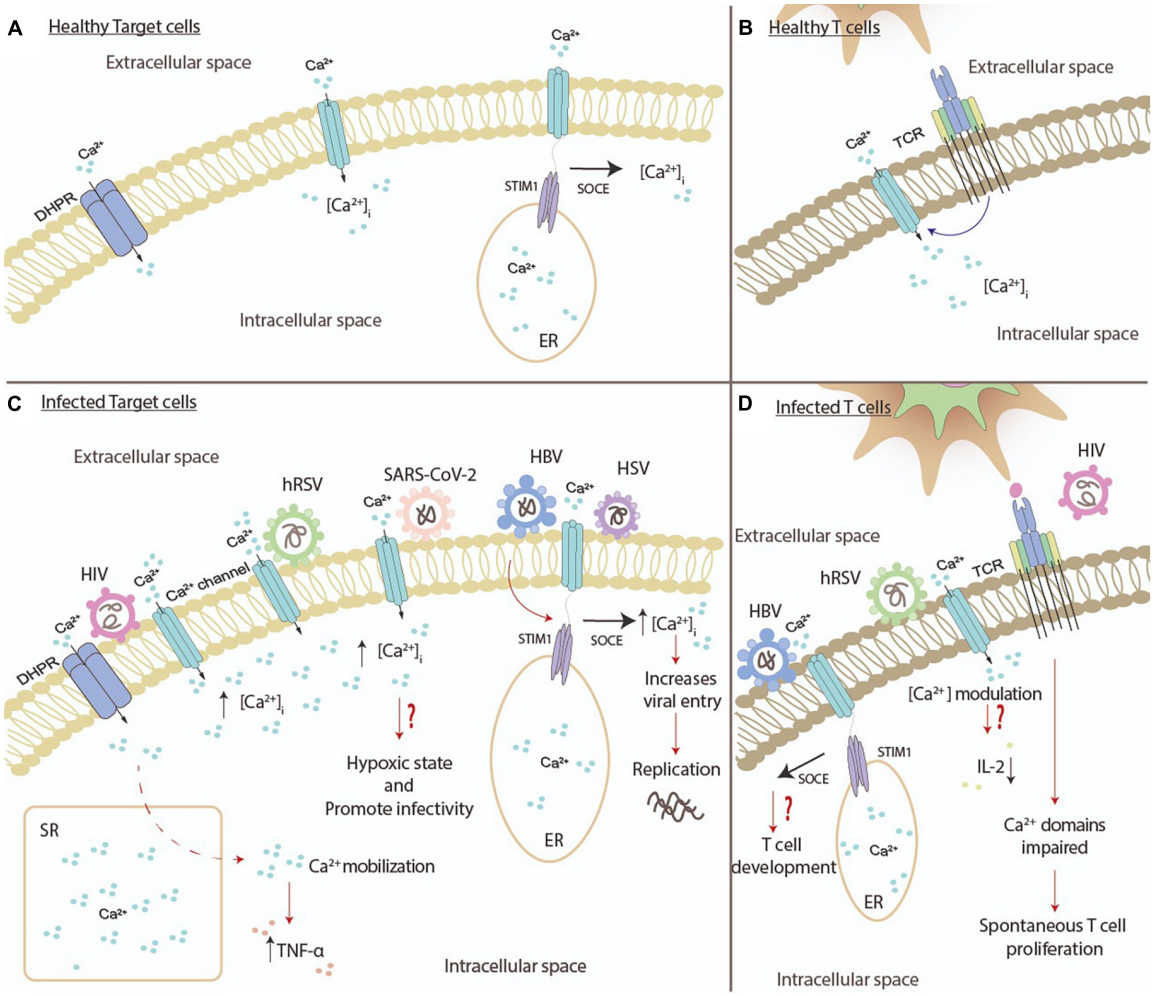

FIGURE 3 | Viral pathogens modify biological processes on immune cells by increasing the Ca^{2+}. **(A)** During normal conditions, various immune cells, such as dendritic cells, monocytes, macrophages, and neutrophils, regulate their concentrations of intracellular Ca^{2+}. The activation of dihydropyridine receptor (DHPR) and Ca^{2+} channels promote the entry of Ca^{2+} into the cells. The interaction between the CRAC channel and STIM1 promotes the movement of Ca^{2+} into the cytosol. **(B)** During normal conditions, T cells regulate their concentrations of intracellular Ca^{2+} through the activation of the T cell receptor (TCR). **(C)** Different viruses can modulate different processes in various immune cells. The human immunodeficiency virus (HIV) can increase the Ca2+ concentration through the modulation of Ca^{2+} channels, and the activation of DHPR promotes the mobilization of Ca^{2+} that leads to the secretion of TNF-α. The human respiratory syncytial virus (hRSV) promotes the increase of Ca^{2+} as well. SARS-CoV-2 might be causing a hypoxic state and increase the infectivity of the virus through the increase Ca^{2+} concentration. The hepatitis B virus (HBV) and herpes simplex virus (HSV) can increase the concentration of intracellular Ca^{2+} through the interaction between the CRAC channel and STIM1. **(D)** RNA viruses can modulate different processes in T cells. HIV proteins activate the T cell receptor (TCR), and as a result, it impairs the domains of Ca^{2+}, leading to spontaneous T cell proliferation. hRSV induces the influx of Ca^{2+} into T cells, which might decrease the secretion of IL-2. As for DNA viruses, such as HBV, the interaction between the CRAC channel and STIM1 might modulate the development of T cells.

Human Respiratory Syncytial Virus

One of the most prevalent viral agents that causes acute lower tract respiratory infections in infants under 2 years old, as wells as immunocompromised and elderly individuals, is hRSV (Tabor et al., 2021). Human RSV is an enveloped, negative-sense single-strand RNA virus that belongs to the *Pneumoviridae* family. This virus encodes for eleven proteins, including three in the virion surface (F, G, and SH) and four proteins found inside the viral structure (N, L, P, and M2.1; Collins et al., 2013; Cui et al., 2016). Decades ago, it was described that syncytia formation, characteristic of hRSV infection, in HEp-2 cells requires the presence of Ca^{2+} (Shahrabadi and Lee, 1988). Later, using a genetically-encoded Ca^{2+} indicator strategy in hRSV-infected MA104 cells, observing increases of $[Ca^{2+}]_i$ and Ca^{2+} influx during cell fusions (**Figure 3**; Perry et al., 2015). Ca^{2+} concentrations increased first in the cytoplasm and then in the ER, and a rapid increase of Ca^{2+} influx before cell death was observed (Perry et al., 2015). Accordingly, the results suggest that hRSV may modulate Ca^{2+} levels. Additionally, hRSV infection requires the host Ca^{2+} pump SPCA1 located in the *trans*-Golgi network. A deficiency of SPCA1 has a relevant impact on hRSV spread and alters the susceptibility of the cells to infection,

corroborating the crucial role of Ca^{2+} (Hoffmann et al., 2017). Additionally, hRSV infection of human epithelial cells, such as BEAS-2B, has been shown to increase upon expression of TRPV1, which is implicated in asthma predisposition (Omar et al., 2017; Harford et al., 2018). With regards to the ability of hRSV to modulate ions, it is known that the SH protein is a viroporin that forms pentameric cation-selective ion channel at the surface of the infected cells, allowing the entry of Na^+ and K^+ and promoting the activation of the NLRP3 inflammasome (Gan et al., 2012; Triantafilou et al., 2013).

As described above, the modulation of $[Ca^{2+}]_i$ through the expression or the function of ion channel and pumps by hRSV can affect the immune response. It is known that hRSV can impair immunological synapsis by recruiting the N protein to the surface of the infected DCs (Gonzalez et al., 2008; Céspedes et al., 2014). Moreover, recent evidence shows that hRSV can infect human T cells ($CD4^+$ and $CD8^+$) and decrease IL-2 production, which may explain the absence of a long-lasting protective immunity (**Figure 3**; Raiden et al., 2017). Regarding the relevance of Ca^{2+} for hRSV infection, currently, there are no studies evaluating whether hRSV infection can modulate $[Ca^{2+}]_i$ or Ca^{2+} signaling pathways in infected DCs or T cells.

Severe Acute Respiratory Coronavirus 2

The newly described coronavirus SARS-CoV-2 is the causative agent of an unprecedented pandemic in the last 100 years. This virus is an enveloped particle with a single-strand positive-sense RNA that encodes four structural proteins (S, E, M, and N) and sixteen non-structural proteins (nsp1-16; McClenaghan et al., 2020; Wang et al., 2020). Patients admitted to hospitals show low serum Ca^{2+}, which is currently a severity indicator (Zhou et al., 2020). Moreover, it has been described that SARS-CoV-2 infection induces hypoxia in epithelial cells and innate immune cells (Serebrovska et al., 2020; Danta, 2021), and in a hypoxic state, there is an increase in $[Ca^{2+}]_i$, mediated by CRAC channels (**Figure 3**; Gusarova et al., 2011; Danta, 2021). Previously, it was described that SARS-CoV and MERS- CoV could alter Ca^{2+} concentration, which induced the viral entry into target cells, promoting viral fusion and, therein, increase their infectivity (Millet and Whittaker, 2018; Straus et al., 2020b). Furthermore, it was reported that the E protein of SARS-CoV is a viroporin that, like the hRSV SH protein, forms a pentameric ion channel that shows higher selectivity for Ca^{2+} than Na^+ and K^+ (Nieto-Torres et al., 2015). Indeed, the IC formed by the E protein can transport the Ca^{2+}, which allows the subsequent activation of the NLRP3 inflammasome (Nieto-Torres et al., 2015). The SARS-CoV2-E (2-E) protein also forms an ion channel permeable to cations such as K^+, Na^+, and Ca^{2+} and causes cell death (Xia et al., 2020). Moreover, the 2-E protein by itself can induce the secretion of pro-inflammatory cytokines by macrophages (Xia et al., 2020).

The relevance of the Ca^{2+} channel for SARS-CoV-2 infection has been observed in Vero E6 and Calu-3 cells, and the use of calcium channels blockers, such as amlodipine, felodipine, and nifedipine, has been studied (Straus et al., 2020a). These Ca^{2+} channels blockers act by inhibiting the L-type Ca^{2+} channel, modulating viral entry into the cells, and viral replication, thus being a promising and potential therapeutic alternative for SARS-CoV-2 infection (Straus et al., 2020a). Although the main cellular targets for SARS-CoV-2 infection are epithelial cells, immune cells such as neutrophils, monocytes, and T cells are also susceptible to infection (Borsa and Mazet, 2020; Pontelli et al., 2020). How SARS-CoV-2 can modulate Ca^{2+} flux or interact with ion channels in infected immune cells remains to be elucidated.

DNA Viruses

Hepatitis B Virus

Hepatitis B virus infection is a common cause of hepatic pathologies, such as hepatitis, cirrhosis, and hepatocellular cancer, which are public health problems worldwide (Hou et al., 2005; Liang, 2009). This virus is transmitted by contact with infected body fluids, such as blood (Hou et al., 2005). HBV is a small DNA enveloped virus with an icosahedral nucleocapsid that belongs to the *Hepadnaviradae* family (Venkatakrishnan and Zlotnick, 2016). This virus encodes for three envelop proteins (L, M, and S) and for the preCore, core, pol, and X (HBx; Seeger and Mason, 2015). Like other viruses, HBV modulates Ca^{2+} concentration to promote viral replication in hepatocytes. Remarkably, the HBx protein has been implicated in Ca^{2+} modulation and signaling (Bouchard et al., 2001; Casciano et al., 2017). In this context, it has been reported that HBx exerts effects on intracellular stored Ca^{2+}, where it induces signal transduction pathways to allow HBV replication (Bouchard et al., 2001). Accordingly, HBx, not only by itself but in an HBV replication context, can interact with mitochondria and probably through the modulation of the mitochondrial permeability transition pore, control $[Ca^{2+}]_i$ influx (McClain et al., 2007). Data obtained from rat primary hepatocytes showed that HBx could increase $[Ca^{2+}]_i$ altering IP_3-linked Ca^{2+} responses and modulate Ca^{2+} influx through the store-operated Ca^{2+} channels, which is necessary for HBV replication (**Figure 3**; Casciano et al., 2017). Furthermore, in HEK 293 cells, the interaction between HBx and ORAI1 is essential to maintain active the store-operated Ca^{2+} entry (Yao et al., 2018). According to this, the co-localization of HBx with ORAI1 suggests an upregulation of the STIM1-ORAI1 complex that modulates store-operated Ca^{2+}channels positively, especially when Ca^{2+} concentrations are low, to induce an intracellular influx (**Figure 3**; Yao et al., 2018).

Hepatitis B virus can infect and replicate in PBMCs, including T cells, affecting the immune response against this virus (Yan et al., 2016). As described early, for the development and function of T cells and DCs, the role of store-operated Ca^{2+} entry is crucial for establishing the immunological synapsis (**Figure 3**; Oh-Hora, 2009; Félix et al., 2013). However, there are no studies that evaluate the role of HBx in immune cells.

Herpes Simplex Viruses

One of the most ubiquitous human infections in the mucocutaneous tissue is caused by herpes simplex viruses type 1 and type 2 (HSV-1 and HSV-2) (He et al., 2020). HSVs belong to the *Herpesviradae* family and have a linear double-stranded DNA genome packaged in an icosahedral capsid that is enveloped. The envelope has numerous proteins, and the

virus encodes twelve different glycoproteins (gB, gC, gD, gE, gG, gH, gI, gJ, gK, gL, gM, and gN; Karasneh and Shukla, 2011; Retamal-Díaz et al., 2016; Madavaraju et al., 2021). HSVs can infect several cell types, including epithelial cells, fibroblasts, neurons, and DCs (Koelle et al., 1993; Karasneh and Shukla, 2011; Retamal-Díaz et al., 2016; Marcocci et al., 2020).

Herpes simplex viruses infection of epithelial cell lines induces a transient increase in $[Ca^{2+}]_i$, mediated by the ER and Ca^{2+} influx from extracellular space (**Figure 3**; Cheshenko et al., 2003). Additionally, IP_3-sensitive Ca^{2+} stores, probably available through the opening of Ca^{2+} channels in the ER membrane, help HSV enter the cell. On the other hand, the chelation of Ca^{2+} and pharmacological inhibition of IP_3R impairs viral infection (Cheshenko et al., 2003). ND7/23 cells (sensory-like neurons) express the $Ca_v3.2$ T-type Ca^{2+} channel that regulates the excitability of neurons. Significantly, the expression of this channel is reduced by HSV-1 infection, which depends on viral replication and protein synthesis (Zhang et al., 2019). HSV-2 infection in HeLa cells promotes an extracellular Ca^{2+} influx, which can be blocked by the use of Ca^{2+} channels blockers and, therein, suppresses viral infection. T-type, but not L-type Ca^{2+} channel, impact HSV-2 infection, as proven by the use of Ca^{2+} channels blockers (Ding et al., 2021). Regarding the effects of HSV-1 on immune cells, it has been reported that these cells express the herpesvirus entry mediator, which is a receptor for the HSV-1 gD, allowing viral entry into DCs and activated T cells (La et al., 2002). Besides, it is known that HSV infection of DCs can modulate the maturation and their capacity of activating T cells, and also cause DC death (Jones et al., 2003; Bosnjak et al., 2005; Retamal-Díaz et al., 2016), but there is no data to date regarding Ca^{2+} modulation and the role of Ca^{2+} channels involved in this process. On the other hand, T cell proliferation can be modulated by the HSV-1 gD protein (Bosnjak et al., 2005). Additionally, HSV infection of T cells, in which gB, gD, gH, and gL are necessary for viral entry, or contact with HSV-infected cells, such as fibroblasts, can impair T cell receptor-mediated activation by altering Ca^{2+} mobilization that is required for the T cell receptor signaling (Koelle et al., 1993; Sloan et al., 2006; Cao et al., 2008). The effects of HSV infection over Ca^{2+} channels in immune cells remains poorly understood and requires more studies to explore the potential development of new therapeutic strategies that target these components.

CONCLUSION

In all cell types, ion balance is crucial to maintain normal physiology and functions. In this context, ion channels play critical roles in controlling ion homeostasis. One of the most relevant ions is Ca^{2+}, which acts as a second messenger, and is crucial for eliciting a proper immune response against pathogens. Immune cells, such as T cells, express a wide variety of ions channels on their surface, including four types of Ca^{2+} channels CRAC, TRP, Ca_v, and P2X (Feske, 2013; Feske et al., 2015). These channels are implicated in the proliferation, activation, and cytotoxicity of T cells, all crucial mechanisms for the adaptive immune response. It has been described that loss-of-function mutations in Ca^{2+} channel genes affect their function on immune cells, provoking combined immunodeficiency and increasing the susceptibility to infections (Vaeth and Feske, 2018). Importantly, viruses also need Ca^{2+} mobilization for entry, replication, and budding (Zhou et al., 2009).

Moreover, viruses such as HIV, hRSV, SARS-CoV2, HBV, and HSV, among others, have proteins that can interfere with the normal function of Ca^{2+} channels to increase $[Ca^{2+}]_i$ and enhance their infectivity in target cells (Zhou et al., 2009). Viral modulation of Ca^{2+} channels expressed in immune cells allows viruses to impair the immune responses as an evasion mechanism (Fenard et al., 2005; Sloan et al., 2006). Despite this knowledge, further insights into the associated mechanism, the impact of using Ca^{2+} channels blockers, and their effects on viral infections are still required.

AUTHOR CONTRIBUTIONS

All authors listed have made a substantial, direct and intellectual contribution to the work, and approved it for publication.

FUNDING

This work was supported by the Millennium Institute of Immunology and Immunotherapy (P09/016-F, ICN09_016, AK); CORFO grant #13CTI-21526/P4 and P5; ANID/FONDECYT grants #3180570 (KB); #1190830 (AK), #1191300 (CR), #1190864 (PG); ANID scholarship #21190183 (NG) and #21210662 (CA); and Biomedical Research Consortium CTU06 (AK). COPEC-UC2019.R.1169. COPEC-UC2020.E.1. Regional Government of Antofagasta through the Innovation Fund for Competitiveness FIC-R 2017 (BIP Code: 30488811-0). AK is a Helen C. Levitt Visiting Professor at the Department of Microbiology and Immunology of the University of Iowa.

REFERENCES

Acharya, T. K., Tiwari, A., Majhi, R. K., and Goswami, C. (2021). Trpm8 channel augments T-cell activation and proliferation/. *Cell Biol. Int.* 45, 198–210. doi: 10.1002/cbin.11483

Ando, J., Smith, N. I., Fujita, K., and Kawata, S. (2009). Photogeneration of membrane potential hyperpolarization and depolarization in non-excitable cells. *Eur. Biophys. J.* 38, 255–262. doi: 10.1007/s00249-008-0397-6

Antunes, T. T., Callera, G. E., He, Y., Yogi, A., Ryazanov, A. G., Ryazanova, L. V., et al. (2016). Transient receptor potential melastatin 7 cation channel kinase: new player in angiotensin II-induced hypertension. *Hypertens* 67, 763–773. doi: 10.1161/HYPERTENSIONAHA.115.07021

Avraham, A., Jung, S., Samuels, Y., Seger, R., and Ben-Neriah, Y. (1998). Co-stimulation-dependent activation of a JNK-kinase in T lymphocytes. *Eur. J. Immunol.* 28, 2320–2330. doi: 10.1002/(SICI)1521-4141(199808)28:08<2320::AID-IMMU2320>3.0.CO;2-K

Badou, A., Jha, M. K., Matza, D., and Flavell, R. A. (2013). Emerging roles of L-type voltage-gated and other calcium channels in T lymphocytes. *Front. Immunol.* 4:243. doi: 10.3389/fimmu.2013.00243

Barbet, G., Demion, M., Moura, I. C., Serafini, N., Léger, T., Vrtovsnik, F., et al. (2008). The calcium-activated nonselective cation channel TRPM4 is essential for the migration but not the maturation of dendritic cells. *Nat. Immunol.* 9, 1148–1156. doi: 10.1038/ni.1648

Bates-Withers, C., Sah, R., and Clapham, D. E. (2011). TRPM7, the Mg(2+) inhibited channel and kinase. *Adv. Exp. Med. Biol.* 704, 173–183.

Beeton, C., and Chandy, K. G. (2005). Potassium channels, memory T cells, and multiple sclerosis. *Neuroscientist* 11, 550–562. doi: 10.1177/1073858405278016

Bertin, S., Aoki-Nonaka, Y., Lee, J., de Jong, P. R., Kim, P., Han, T., et al. (2017). The TRPA1 ion channel is expressed in CD4+ T cells and restrains T-cell-mediated colitis through inhibition of TRPV1. *Gut* 66, 1584–1596. doi: 10.1136/gutjnl-2015-310710

Billadeau, D. D., Nolz, J. C., and Gomez, T. S. (2007). Regulation of T-cell activation by the cytoskeleton. *Nat. Rev. Immunol.* 7, 131–143. doi: 10.1038/nri2021

Borsa, M., and Mazet, J. M. (2020). Attacking the defence: SARS-CoV-2 can infect immune cells. *Nat. Rev. Immunol.* 20:592. doi: 10.1038/s41577-020-00439-1

Bose, T., Cieślar-Pobuda, A., and Wiechec, E. (2015). Role of ion channels in regulating Ca2+ homeostasis during the interplay between immune and cancer cells. *Cell Death Dis.* 6:e1648. doi: 10.1038/cddis.2015.23

Bosnjak, L., Miranda-Saksena, M., Koelle, D. M., Boadle, R. A., Jones, C. A., and Cunningham, A. L. (2005). Herpes simplex virus infection of human dendritic cells induces apoptosis and allows cross-presentation via uninfected dendritic cells. *J. Immunol.* 174, 2220–2227. doi: 10.4049/jimmunol.174.4.2220

Bouchard, M. J., Wang, L. H., and Schneider, R. J. (2001). Calcium signaling by HBx protein in hepatitis B virus DNA replication. *Science* 294, 2376–2378. doi: 10.1126/science.294.5550.2376

Bowman, C. L., and Baglioni, A. (1984). Application of the Goldman-Hodgkin-Katz current equation to membrane current-voltage data. *J. Theor. Biol.* 108, 1–29. doi: 10.1016/S0022-5193(84)80165-4

Brandao, K., Deason-Towne, F., Perraud, A.-L., and Schmitz, C. (2013). The role of Mg2+ in immune cells. *Immunol. Res.* 55, 261–269. doi: 10.1007/s12026-012-8371-x

Brasier, A. R. (2006). The NF-κ κ B regulatory network κ B. *Cardiovasc. Toxicol.* 6, 111–130. doi: 10.1385/CT:6:2:111

Cabral, M. D., Paulet, P. E., Robert, V., Gomes, B., Renoud, M. L., Savignac, M., et al. (2010). Knocking down Cav1 calcium channels implicated in Th2 cell activation prevents experimental asthma. *Am. J. Respir. Crit. Care Med.* 181, 1310–1317. doi: 10.1164/rccm.200907-1166OC

Cahalan, M. D., and Chandy, K. G. (1997). Ion channels in the immune system as targets for immunosuppression. *Curr. Opin. Biotechnol.* 8, 749–756. doi: 10.1016/S0958-1669(97)80130-9

Cahalan, M. D., and Chandy, K. G. (2009). The functional network of ion channels in T lymphocytes. *Immunol. Rev.* 231, 59–87. doi: 10.1111/j.1600-065X.2009.00816.x

Cai, S., Tuohy, P., Ma, C., Kitamura, N., Gomez, K., Zhou, Y., et al. (2020). A modulator of the low-voltage-activated T-type calcium channel that reverses HIV glycoprotein 120-, paclitaxel-, and spinal nerve ligation-induced peripheral neuropathies. *Pain* 161, 2551–2570. doi: 10.1097/j.pain.0000000000001955

Cao, Y.-J., Li, Y.-P., Zhang, Y.-C., and Zhang, C.-Z. (2008). T cell receptor signaling pathways: new targets for herpes simplex virus. *Virol. Sin.* 23, 429–437. doi: 10.1007/s12250-008-3000-5

Carreño, L. J., González, P. A., Bueno, S. M., Riedel, C. A., and Kalergis, A. M. (2011). Modulation of the dendritic cell-T-cell synapse to promote pathogen immunity and prevent autoimmunity. *Immunotherapy* 3, 6–11. doi: 10.2217/imt.11.38

Carreño, L. J., Riquelme, E. M., González, P. A., Espagnolle, N., Riedel, C. A., Valitutti, S., et al. (2010). T-cell antagonism by short half-life pMHC ligands can be mediated by an efficient trapping of T-cell polarization toward the APC. *Proc. Natl. Acad. Sci. U. S. A.* 107, 210–215. doi: 10.1073/pnas.0911258107

Casciano, J. C., Duchemin, N. J., Lamontagne, R. J., Steel, L. F., and Bouchard, M. J. (2017). Hepatitis B virus modulates store-operated calcium entry to enhance viral replication in primary hepatocytes. *PLoS One* 12:e0168328. doi: 10.1371/journal.pone.0168328

Céspedes, P. F., Bueno, S. M., Ramírez, B. A., Gomez, R. S., Riquelme, S. A., Palavecino, C. E., et al. (2014). Surface expression of the hRSV nucleoprotein impairs immunological synapse formation with T cells. *Proc. Natl. Acad. Sci. U. S. A.* 111, E3214–E3223. doi: 10.1073/pnas.1400760111

Chaigne-Delalande, B., and Lenardo, M. J. (2014). Divalent cation signaling in immune cells. *Trends Immunol.* 35, 332–344. doi: 10.1016/j.it.2014.05.001

Chakraborty, K., Leung, K. H., and Krishnan, Y. (2017). High lumenal chloride in the lysosome is critical for lysosome function. *Elife* 6:e28862. doi: 10.7554/eLife.28862.026

Charlton, F. W., Pearson, H. M., Hover, S., Lippiat, J. D., Fontana, J., Barr, J. N., et al. (2020). Ion channels as therapeutic targets for viral infections: further discoveries and future perspectives. *Viruses* 12:844. doi: 10.3390/v12080844

Chen, X., Cao, R., and Zhong, W. (2019). Host calcium channels and pumps in viral infections. *Cells* 9:94. doi: 10.3390/cells9010094

Cheshenko, N., Del Rosario, B., Woda, C., Marcellino, D., Satlin, L. M., and Herold, B. C. (2003). Herpes simplex virus triggers activation of calcium-signaling pathways. *J. Cell Biol.* 163, 283–293. doi: 10.1083/jcb.200301084

Chiang, E. Y., Li, T., Jeet, S., Peng, I., Zhang, J., Lee, W. P., et al. (2017). Potassium channels Kv1.3 and KCa3.1 cooperatively and compensatorily regulate antigen-specific memory T cell functions. *Nat. Commun.* 8:14644. doi: 10.1038/ncomms14644

Chimote, A. A., Balajthy, A., Arnold, M. J., Newton, H. S., Hajdu, P., Qualtieri, J., et al. (2018). A defect in KCa3.1 channel activity limits the ability of CD8+ T cells from cancer patients to infiltrate an adenosine-rich microenvironment. *Sci. Signal.* 11:aaq1616. doi: 10.1126/scisignal.aaq1616

Chung, M.-K., Asgar, J., Lee, J., Shim, M. S., Dumler, C., and Ro, J. Y. (2015). The role of TRPM2 in hydrogen peroxide-induced expression of inflammatory cytokine and chemokine in rat trigeminal ganglia. *Neuroscience* 297, 160–169. doi: 10.1016/j.neuroscience.2015.03.067

Clapham, D. E. (2007). Calcium signaling. *Cell* 131, 1047–1058. doi: 10.1016/j.cell.2007.11.028

Collins, P. L., Fearns, R., and Graham, B. S. (2013). Respiratory syncytial virus: virology, reverse genetics, and pathogenesis of disease. *Curr. Top. Microbiol. Immunol.* 372, 3–38. doi: 10.1007/978-3-642-38919-1_1

Conforti, L. (2017). Potassium channels of T lymphocytes take center stage in the fight against cancer. *J. Immunother. Cancer* 5, 1–3. doi: 10.1186/s40425-016-0202-5

Contreras, X., Bennasser, Y., Chazal, N., Moreau, M., Leclerc, C., Tkaczuk, J., et al. (2005). Human immunodeficiency virus type 1 Tat protein induces an intracellular calcium increase in human monocytes that requires DHP receptors: involvement in TNF-alpha production. *Virology* 332, 316–328. doi: 10.1016/j.virol.2004.11.032

Cui, R., Wang, Y., Wang, L., Li, G., Lan, K., Altmeyer, R., et al. (2016). Cyclopiazonic acid, an inhibitor of calcium-dependent ATPases with antiviral activity against human respiratory syncytial virus. *Antivir. Res.* 132, 38–45. doi: 10.1016/j.antiviral.2016.05.010

Danta, C. C. (2021). SARS-CoV-2, hypoxia, and calcium signaling: the consequences and therapeutic options. *ACS Pharmacol. Transl. Sci.* 4, 400–402. doi: 10.1021/acsptsci.0c00219

Di Lucente, J., Nguyen, H. M., Wulff, H., Jin, L.-W., and Maezawa, I. (2018). The voltage-gated potassium channel Kv1.3 is required for microglial pro-inflammatory activation *in vivo*. *Glia* 66, 1881–1895. doi: 10.1002/glia.23457

Di Resta, C., and Becchetti, A. (2010). Introduction to ion channels. *Adv. Exp. Med. Biol.* 674, 9–21. doi: 10.1007/978-1-4419-6066-5_2

Di, A., Gao, X.-P., Qian, F., Kawamura, T., Han, J., Hecquet, C., et al. (2011). The redox-sensitive cation channel TRPM2 modulates phagocyte ROS production and inflammation. *Nat. Immunol.* 13, 29–34. doi: 10.1038/ni.2171

Ding, J., Wang, K., Liu, W., She, Y., Sun, Q., Shi, J., et al. (2016). Pore-forming activity and structural autoinhibition of the gasdermin family. *Nature* 535, 111–116. doi: 10.1038/nature18590

Ding, L., Jiang, P., Xu, X., Lu, W., Yang, C., Li, L., et al. (2021). T-type calcium channels blockers inhibit HSV-2 infection at the late stage of genome replication. *Eur. J. Pharmacol.* 892:173782. doi: 10.1016/j.ejphar.2020.173782

Dufner-Beattie, J., Huang, Z. L., Geiser, J., Xu, W., and Andrews, G. K. (2005). Generation and characterization of mice lacking the zinc uptake transporter ZIP3. *Mol. Cell. Biol.* 25, 5607–5615. doi: 10.1128/MCB.25.13.5607-5615.2005

Fanger, C. M., Rauer, H., Neben, A. L., Miller, M. J., Rauer, H., Wulff, H., et al. (2001). Calcium-activated potassium channels sustain calcium signaling in T

lymphocytes. Selective blockers and manipulated channel expression levels. *J. Biol. Chem.* 276, 12249–12256. doi: 10.1074/jbc.M011342200

Félix, R., Crottès, D., Delalande, A., Fauconnier, J., Lebranchu, Y., Le Guennec, J.-Y., et al. (2013). The Orai-1 and STIM-1 complex controls human dendritic cell maturation. *PLoS One* 8:e61595. doi: 10.1371/journal.pone.0061595

Fenard, D., Yonemoto, W., de Noronha, C., Cavrois, M., Williams, S. A., and Greene, W. C. (2005). Nef is physically recruited into the immunological synapse and potentiates T cell activation early after TCR engagement. *J. Immunol.* 175, 6050–6057. doi: 10.4049/jimmunol.175.9.6050

Fenninger, F., and Jefferies, W. A. (2019). What's bred in the bone: calcium channels in lymphocytes. *J. Immunol.* 202, 1021–1030. doi: 10.4049/jimmunol.1800837

Feske, S. (2010). CRAC channelopathies. *Pflugers Arch.* 460, 417–435. doi: 10.1007/s00424-009-0777-5

Feske, S. (2013). Ca2+ influx in T cells: how many Ca2+ channels? *Front. Immunol.* 4:99. doi: 10.3389/fimmu.2013.00099

Feske, S., Skolnik, E. Y., and Prakriya, M. (2012). Ion channels and transporters in lymphocyte function and immunity. *Nat. Rev. Immunol.* 12, 532–547. doi: 10.1038/nri3233

Feske, S., Wulff, H., and Skolnik, E. Y. (2015). Ion channels in innate and adaptive immunity. *Annu. Rev. Immunol.* 33, 291–353. doi: 10.1146/annurev-immunol-032414-112212

Fiebich, B. L., Collado, J. A., Stratz, C., Valina, C., Hochholzer, W., Muñoz, E., et al. (2012). Pseudoephedrine inhibits T-cell activation by targeting NF-κB, NFAT and AP-1 signaling pathways. *Immunopharmacol. Immunotoxicol.* 34, 98–106. doi: 10.3109/08923973.2011.582118

Fourgeaud, L., Davenport, C. M., Tyler, C. M., Cheng, T. T., Spencer, M. B., and Boulanger, L. M. (2010). MHC class I modulates NMDA receptor function and AMPA receptor trafficking. *Proc. Natl. Acad. Sci. U. S. A.* 107, 22278–22283. doi: 10.1073/pnas.0914064107

Franchi, L., Eigenbrod, T., Muñoz-Planillo, R., and Nuñez, G. (2009). The inflammasome: a caspase-1-activation platform that regulates immune responses and disease pathogenesis. *Nat. Immunol.* 10, 241–273. doi: 10.1038/ni.1703

Frankel, A. D., and Young, J. A. T. (1998). HIV-1: fifteen proteins and an RNA. *Annu. Rev. Biochem.* 67, 1–25. doi: 10.1146/annurev.biochem.67.1.1

Froghi, S., Grant, C. R., Tandon, R., Quaglia, A., Davidson, B., and Fuller, B. (2021). New insights on the role of TRP channels in calcium signalling and immunomodulation: review of pathways and implications for clinical practice. *Clin. Rev. Allergy Immunol.* 60, 271–292. doi: 10.1007/s12016-020-08824-3

Gálvez, N. M. S., Bohmwald, K., Pacheco, G. A., Andrade, C. A., Carreño, L. J., and Kalergis, A. M. (2021). Type I natural killer T cells as key regulators of the immune response to infectious diseases. *Clin. Microbiol. Rev.* 34:e232-20. doi: 10.1128/CMR.00232-20

Gan, S. W., Tan, E., Lin, X., Yu, D., Wang, J., Tan, G. M. Y., et al. (2012). The small hydrophobic protein of the human respiratory syncytial virus forms pentameric ion channels. *J. Biol. Chem.* 287, 24671–24689. doi: 10.1074/jbc.M111.332791

Gauthier, S. A., Glanz, B. I., Mandel, M., and Weiner, H. L. (2006). A model for the comprehensive investigation of a chronic autoimmune disease: the multiple sclerosis CLIMB study. *Autoimmun. Rev.* 5, 532–536. doi: 10.1016/j.autrev.2006.02.012

Geiser, J., Venken, K. J. T., De Lisle, R. C., and Andrews, G. K. (2012). A mouse model of acrodermatitis enteropathica: loss of intestine zinc transporter ZIP4 (Slc39a4) disrupts the stem cell niche and intestine integrity. *PLoS Genet.* 8:e1002766. doi: 10.1371/journal.pgen.1002766

German Advisory Committee Blood (Arbeitskreis Blut) (2016). Human immunodeficiency virus (HIV). *Transfus. Med. Hemother.* 43, 203–222. doi: 10.1159/000445852

González, P. A., Carreño, L. J., Figueroa, C. A., and Kalergis, A. M. (2007). Modulation of immunological synapse by membrane-bound and soluble ligands. *Cytokine Growth Factor Rev.* 18, 19–31. doi: 10.1016/j.cytogfr.2007.01.003

Gonzalez, P. A., Prado, C. E., Leiva, E. D., Carreno, L. J., Bueno, S. M., Riedel, C. A., et al. (2008). Respiratory syncytial virus impairs T cell activation by preventing synapse assembly with dendritic cells. *Proc. Natl. Acad. Sci. U S A.* 105, 14999–15004. doi: 10.1073/pnas.0802555105

Goytain, A., and Quamme, G. A. (2005). Identification and characterization of a novel mammalian Mg2+ transporter with channel-like properties. *BMC Genom.* 6:48. doi: 10.1186/1471-2164-6-48

Grakoui, A., Bromley, S. K., Sumen, C., Davis, M. M., Shaw, A. S., Allen, P. M., et al. (1999). The immunological synapse: a molecular machine controlling T cell activation. *Science* 285, 221–227. doi: 10.1126/science.285.5425.221

Grissmer, S., Nguyen, A. N., and Cahalan, M. D. (1993). Calcium-activated potassium channels in resting and activated human T lymphocytes: expression levels, calcium dependence, ion selectivity, and pharmacology. *J. Gen. Physiol.* 102, 601–630. doi: 10.1085/jgp.102.4.601

Gusarova, G. A., Trejo, H. E., Dada, L. A., Briva, A., Welch, L. C., Hamanaka, R. B., et al. (2011). Hypoxia leads to Na,K-ATPase downregulation via Ca(2+) release-activated Ca(2+) channels and AMPK activation. *Mol. Cell. Biol.* 31, 3546–3556. doi: 10.1128/MCB.05114-11

Harford, T. J., Rezaee, F., Scheraga, R. G., Olman, M. A., and Piedimonte, G. (2018). Asthma predisposition and respiratory syncytial virus infection modulate transient receptor potential vanilloid 1 function in children's airways. *J. Allergy Clin. Immunol.* 141, 414–416.e4. doi: 10.1016/j.jaci.2017.07.015

Häusser-Kinzel, S., and Weber, M. S. (2019). The role of B cells and antibodies in multiple sclerosis, neuromyelitis optica, and related disorders. *Front. Immunol.* 10:201. doi: 10.3389/fimmu.2019.00201

He, D., Mao, A., Li, Y., Tam, S., Zheng, Y., Yao, X., et al. (2020). TRPC1 participates in the HSV-1 infection process by facilitating viral entry. *Sci. Adv.* 6:eaaz3367. doi: 10.1126/sciadv.aaz3367

Hoffmann, H.-H., Schneider, W. M., Blomen, V. A., Scull, M. A., Hovnanian, A., Brummelkamp, T. R., et al. (2017). Diverse viruses require the calcium transporter SPCA1 for maturation and spread. *Cell Host Microbe* 22, 460–470.e5. doi: 10.1016/j.chom.2017.09.002

Hogan, P. G., Chen, L., Nardone, J., and Rao, A. (2003). Transcriptional regulation by calcium, calcineurin, and NFAT. *Genes Dev.* 17, 2205–2232. doi: 10.1101/gad.1102703

Hogan, P. G., Lewis, R. S., and Rao, A. (2010). Molecular basis of calcium signaling in lymphocytes: STIM and ORAI. *Annu. Rev. Immunol.* 28, 491–533. doi: 10.1146/annurev.immunol.021908.132550

Holden, C. P., Haughey, N. J., Nath, A., and Geiger, J. D. (1999). Role of Na+/H+ exchangers, excitatory amino acid receptors and voltage-operated Ca2+ channels in human immunodeficiency virus type 1 gp120-mediated increases in intracellular Ca2+ in human neurons and astrocytes. *Neuroscience* 91, 1369–1378. doi: 10.1016/S0306-4522(98)00714-3

Hou, J., Liu, Z., and Gu, F. (2005). Epidemiology and prevention of hepatitis B virus infection. *Int. J. Med. Sci.* 2, 50–57. doi: 10.7150/ijms.2.50

Hu, X.-T. (2016). HIV-1 tat-mediated calcium dysregulation and neuronal dysfunction in vulnerable brain regions. *Curr. Drug Targets* 17, 4–14. doi: 10.2174/1389450116666150531162212

Huang, Y., Winkler, P. A., Sun, W., Lü, W., and Du, J. (2018). Architecture of the TRPM2 channel and its activation mechanism by ADP-ribose and calcium. *Nature* 562, 145–163. doi: 10.1038/s41586-018-0558-4

Jasenosky, L. D., Scriba, T. J., Hanekom, W. A., and Goldfeld, A. E. (2015). T cells and adaptive immunity to *Mycobacterium tuberculosis* in humans. *Immunol. Rev.* 264, 74–87. doi: 10.1111/imr.12274

Ji, T., Corbalán-García, S., and Hubbard, S. R. (2018). Crystal structure of the C-terminal four-helix bundle of the potassium channel KCa3.1. *PLoS One* 13:e0199942. doi: 10.1371/journal.pone.0199942

Jin, J., Desai, B. N., Navarro, B., Donovan, A., Andrews, N. C., and Clapham, D. E. (2008). Deletion of Trpm7 disrupts embryonic development and thymopoiesis without altering Mg2+ homeostasis. *Science* 322, 756–760. doi: 10.1126/science.1163493

Jones, C. A., Fernandez, M., Herc, K., Bosnjak, L., Miranda-Saksena, M., Boadle, R. A., et al. (2003). Herpes simplex virus Type 2 induces rapid cell death and functional impairment of murine dendritic cells *in vitro*. *J. Virol.* 77, 11139–11149. doi: 10.1128/JVI.77.20.11139-11149.2003

Jorgensen, I., and Miao, E. A. (2015). Pyroptotic cell death defends against intracellular pathogens. *Immunol. Rev.* 265, 130–142. doi: 10.1111/imr.12287

Joseph, N., Reicher, B., and Barda-Saad, M. (2014). The calcium feedback loop and T cell activation: how cytoskeleton networks control intracellular calcium flux. *Biochim. Biophys. Acta* 1838, 557–568. doi: 10.1016/j.bbamem.2013.07.009

Junger, W. G. (2011). Immune cell regulation by autocrine purinergic signalling. *Nat. Rev. Immunol.* 11, 201–212. doi: 10.1038/nri2938

Kahlfuß, S., Simma, N., Mankiewicz, J., Bose, T., Lowinus, T., Klein-Hessling, S., et al. (2014). Immunosuppression by N-methyl-D-aspartate receptor

antagonists is mediated through inhibition of Kv1.3 and KCa3.1 channels in T cells. *Mol. Cell Biol.* 34, 820–831. doi: 10.1128/MCB.01273-13

Karasneh, G. A., and Shukla, D. (2011). Herpes simplex virus infects most cell types *in vitro*: clues to its success. *Virol. J.* 8, 1–11. doi: 10.1186/1743-422X-8-481

Kim, J.-B. (2014). Channelopathies. *Korean J. Pediatr.* 57, 1–18. doi: 10.3345/kjp.2014.57.1.1

Kloc, M., Kubiak, J. Z., Li, X. C., and Ghobrial, R. M. (2014). The newly found functions of MTOC in immunological response. *J. Leukoc. Biol.* 95, 417–430. doi: 10.1189/jlb.0813468

Koelle, D. M., Tigges, M. A., Burke, R. L., Symington, F. W., Riddell, S. R., Abbo, H., et al. (1993). Herpes simplex virus infection of human fibroblasts and keratinocytes inhibits recognition by cloned CD8+ cytotoxic T lymphocytes. *J. Clin. Invest.* 91, 961–968. doi: 10.1172/JCI116317

Korthals, M., Langnaese, K., Smalla, K.-H., Kähne, T., Herrera-Molina, R., Handschuh, J., et al. (2017). A complex of neuroplastin and plasma membrane Ca2+ ATPase controls T cell activation. *Sci. Rep.* 71, 1–13. doi: 10.1038/s41598-017-08519-4

Kumar, L., Chou, J., Yee, C. S. K., Borzutzky, A., Vollmann, E. H., Andrian, U. H., et al. (2014). Leucine-rich repeat containing 8A (LRRC8A) is essential for T lymphocyte development and function. *J. Exp. Med.* 211:929. doi: 10.1084/jem.20131379

La Cava, A. (2009). Natural tregs and autoimmunity. *Front. Biosci.* 14, 333–343 doi: 10.2741/3247

La, S., Kim, J., Kwon, B. S., and Kwon, B. (2002). Herpes simplex virus type 1 glycoprotein D inhibits t-cell proliferation. *Mol. Cells* 14, 398–403.

Lacruz, R. S., and Feske, S. (2015). Diseases caused by mutations in ORAI1 and STIM1. *Ann. N. Y. Acad. Sci.* 1356, 45–79. doi: 10.1111/nyas.12938

Lam, J., and Wulff, H. (2011). The lymphocyte potassium channels Kv1.3 and KCa3.1 as targets for immunosuppression. *Drug Dev. Res.* 72, 573–584. doi: 10.1002/ddr.20467

Lamkanfi, M., Kanneganti, T.-D., Van Damme, P., Vanden Berghe, T., Vanoverberghe, I., Vandekerckhove, J., et al. (2008). Targeted peptidecentric proteomics reveals caspase-7 as a substrate of the caspase-1 inflammasomes. *Mol. Cell. Proteomics* 7, 2350–2363. doi: 10.1074/mcp.M800132-MCP200

Land, J., Lintermans, L. L., Stegeman, C. A., Muñoz-Elías, E. J., Tarcha, E. J., Iadonato, S. P., et al. (2017). Kv1.3 channel blockade modulates the effector function of B cells in granulomatosis with polyangiitis. *Front. Immunol.* 8:1205. doi: 10.3389/fimmu.2017.01205

Lee, H. G., Cho, M. Z., and Choi, J. M. (2020). Bystander CD4+ T cells: crossroads between innate and adaptive immunity. *Exp. Mol. Med.* 52, 1255–1263. doi: 10.1038/s12276-020-00486-7

Lewis, R. S. (2001). Calcium signaling mechanisms in T lymphocytes. *Annu. Rev. Immunol.* 19, 497–521. doi: 10.1146/annurev.immunol.19.1.497

Li, F.-Y., Chaigne-Delalande, B., Kanellopoulou, C., Davis, J. C., Matthews, H. F., Douek, D. C., et al. (2011). Second messenger role for Mg2+ revealed by human T-cell immunodeficiency. *Nature* 475, 471–476. doi: 10.1038/nature10246

Lian, J., Cuk, M., Kahlfuss, S., Kozhaya, L., Vaeth, M., Rieux-Laucat, F., et al. (2018). ORAI1 mutations abolishing store-operated Ca2+ entry cause anhidrotic ectodermal dysplasia with immunodeficiency. *J. Allergy Clin. Immunol.* 142, 1297–1310.e11. doi: 10.1016/j.jaci.2017.10.031

Liang, T. J. (2009). Hepatitis B: the virus and disease. *Hepatology* 49:S13 doi: 10.1002/hep.22881

Liu, H., Tang, D., Zhou, X., Yang, X., and Chen, A. F. (2020). PhospholipaseCγ1/calcium-dependent membranous localization of Gsdmd-N drives endothelial pyroptosis, contributing to lipopolysaccharide-induced fatal outcome. *Am. J. Physiol. Heart Circ. Physiol.* 319, H1482–H1495. doi: 10.1152/ajpheart.00731.2019

Liu, X., Zhang, Z., Ruan, J., Pan, Y., Magupalli, V. G., Wu, H., et al. (2016). Inflammasome-activated gasdermin D causes pyroptosis by forming membrane pores. *Nature* 535, 153–158. doi: 10.1038/nature18629

Madavaraju, K., Koganti, R., Volety, I., Yadavalli, T., and Shukla, D. (2021). Herpes simplex virus cell entry mechanisms: an update. *Front. Cell. Infect. Microbiol.* 10:852. doi: 10.3389/fcimb.2020.617578

Mahtani, T., and Treanor, B. (2019). Beyond the CRAC: diversification of ion signaling in B cells. *Immunol. Rev.* 291, 104–122. doi: 10.1111/imr.12770

Manninen, A., and Saksela, K. (2002). HIV-1 Nef interacts with inositol trisphosphate receptor to activate calcium signaling in T cells. *J. Exp. Med.* 195, 1023–1032. doi: 10.1084/jem.20012039

Marcocci, M. E., Napoletani, G., Protto, V., Kolesova, O., Piacentini, R., Li Puma, D. D., et al. (2020). Herpes simplex Virus-1 in the brain: the dark side of a sneaky infection. *Trends Microbiol.* 28, 808–820. doi: 10.1016/j.tim.2020.03.003

Martín-Cófreces, N. B., Robles-Valero, J., Cabrero, J. R., Mittelbrunn, M., Gordón-Alonso, M., Sung, C. H., et al. (2008). MTOC translocation modulates IS formation and controls sustained T cell signaling. *J. Cell Biol.* 182, 951–962. doi: 10.1083/jcb.200801014

Martinon, F., Burns, K., and Tschopp, J. (2002). The inflammasome: a molecular platform triggering activation of inflammatory caspases and processing of proIL-beta. *Mol. Cell* 10, 417–426. doi: 10.1016/S1097-2765(02)00599-3

McClain, S. L., Clippinger, A. J., Lizzano, R., and Bouchard, M. J. (2007). Hepatitis B virus replication is associated with an HBx-dependent mitochondrion-regulated increase in cytosolic calcium levels. *J. Virol.* 81, 12061–12065. doi: 10.1128/JVI.00740-07

McClenaghan, C., Hanson, A., Lee, S. J., and Nichols, C. G. (2020). Coronavirus proteins as ion channels: current and potential research. *Front. Immunol.* 11:2651. doi: 10.3389/fimmu.2020.573339

Melzer, N., Hicking, G., Göbel, K., and Wiendl, H. (2012). TRPM2 cation channels modulate T cell effector functions and contribute to autoimmune CNS inflammation. *PLoS One* 7:e47617. doi: 10.1371/journal.pone.0047617

Millet, J. K., and Whittaker, G. R. (2018). Physiological and molecular triggers for SARS-CoV membrane fusion and entry into host cells. *Virology* 517, 3–8. doi: 10.1016/j.virol.2017.12.015

Minke, B., and Cook, B. (2002). TRP channel proteins and signal transduction. *Physiol. Rev.* 82, 429–472. doi: 10.1152/physrev.00001.2002

Morad, H., Luqman, S., Tan, C.-H., Swann, V., and McNaughton, P. A. (2021). TRPM2 ion channels steer neutrophils towards a source of hydrogen peroxide. *Sci. Rep.* 11:9339. doi: 10.1038/s41598-021-88224-5

Murray, J. W., Yin, D., and Wolkoff, A. W. (2017). Reduction of organelle motility by removal of potassium and other solutes. *PLoS One* 12:e0184898. doi: 10.1371/JOURNAL.PONE.0184898

Netea, M. G., Schlitzer, A., Placek, K., Joosten, L. A. B., and Schultze, J. L. (2019). Innate and adaptive immune memory: an evolutionary continuum in the host's response to pathogens. *Cell Host Microbe* 25, 13–26. doi: 10.1016/j.chom.2018.12.006

Nicolaou, S. A., Neumeier, L., Takimoto, K., Lee, S. M., Duncan, H. J., Kant, S. K., et al. (2010). Differential calcium signaling and Kv1.3 trafficking to the immunological synapse in systemic lupus erythematosus. *Cell Calcium* 47, 19–28. doi: 10.1016/j.ceca.2009.11.001

Nielsen, M. M., Witherden, D. A., and Havran, W. L. (2017). γδ T cells in homeostasis and host defence of epithelial barrier tissues. *Nat. Rev. Immunol.* 17, 733–745. doi: 10.1038/nri.2017.101

Nieto-Torres, J. L., Verdiá-Báguena, C., Jimenez-Guardeño, J. M., Regla-Nava, J. A., Castaño-Rodriguez, C., Fernandez-Delgado, R., et al. (2015). Severe acute respiratory syndrome coronavirus E protein transports calcium ions and activates the NLRP3 inflammasome. *Virology* 485, 330–339. doi: 10.1016/j.virol.2015.08.010

Oh-Hora, M. (2009). Calcium signaling in the development and function of T-lineage cells. *Immunol. Rev.* 231, 210–224. doi: 10.1111/j.1600-065X.2009.00819.x

Omar, S., Clarke, R., Abdullah, H., Brady, C., Corry, J., Winter, H., et al. (2017). Respiratory virus infection up-regulates TRPV1, TRPA1 and ASICS3 receptors on airway cells. *PLoS One* 12:e0171681. doi: 10.1371/journal.pone.0171681

Omilusik, K., Priatel, J. J., Chen, X., Wang, Y. T., Xu, H., Choi, K. B., et al. (2011). The CaV1.4 calcium channel is a critical regulator of T cell receptor signaling and naive T Cell Homeostasis. *Immunity* 35, 349–360. doi: 10.1016/j.immuni.2011.07.011

Ott, M., Emiliani, S., Van Lint, C., Herbein, G., Lovett, J., Chirmule, N., et al. (1997). Immune hyperactivation of HIV-1-infected T cells mediated by Tat and the CD28 pathway. *Science* 275, 1481–1485. doi: 10.1126/science.275.5305.1481

Panyi, G., Varga, Z., and Gáspár, R. (2004). Ion channels and lymphocyte activation. *Immunol. Lett.* 92, 55–66. doi: 10.1016/j.imlet.2003.11.020

Parenti, A., De Logu, F., Geppetti, P., and Benemei, S. (2016). What is the evidence for the role of TRP channels in inflammatory and immune cells? *Br. J. Pharmacol.* 173, 953–969. doi: 10.1111/bph.13392

Perry, J. L., Ramachandran, N. K., Utama, B., and Hyser, J. M. (2015). Use of genetically-encoded calcium indicators for live cell calcium imaging and localization in virus-infected cells. *Methods* 90, 28–38. doi: 10.1016/j.ymeth.2015.09.004

Petho, Z., Balajthy, A., Bartok, A., Bene, K., Somodi, S., Szilagyi, O., et al. (2016). The anti-proliferative effect of cation channel blockers in T lymphocytes depends on the strength of mitogenic stimulation. *Immunol. Lett.* 171, 60–69. doi: 10.1016/j.imlet.2016.02.003

Poggi, A., Rubartelli, A., and Raffaella Zocchi, M. (1998). Involvement of dihydropyridine-sensitive calcium channels in human dendritic cell function competition bY HIV-1 Tat. *J. Biol. Chem.* 273, 7205–7209. doi: 10.1074/jbc.273.13.7205

Polverino, F., Lu, B., Quintero, J. R., Vargas, S. O., Patel, A. S., Owen, C. A., et al. (2019). CFTR regulates B cell activation and lymphoid follicle development. *Respir. Res.* 20:133. doi: 10.1186/s12931-019-1103-1

Pontelli, M. C., Castro, I. A., Martins, R. B., Veras, F. P., Serra, L., La, et al. (2020). Infection of human lymphomononuclear cells by SARS-CoV-2. *bioRxiv [preprint]* doi: 10.1101/2020.07.28.225912

Prakriya, M., and Lewis, R. S. (2015). Store-operated calcium channels. *Physiol. Rev.* 95, 1383–1436. doi: 10.1152/physrev.00020.2014

Quintana, A., and Hoth, M. (2012). Mitochondrial dynamics and their impact on T cell function. *Cell Calcium* 52, 57–63. doi: 10.1016/j.ceca.2012.02.005

Quintana, A., Pasche, M., Junker, C., Al-Ansary, D., Rieger, H., Kummerow, C., et al. (2011). Calcium microdomains at the immunological synapse: how ORAI channels, mitochondria and calcium pumps generate local calcium signals for efficient T-cell activation. *EMBO J.* 30, 3895–3912. doi: 10.1038/emboj.2011.289

Raiden, S., Sananez, I., Remes-Lenicov, F., Pandolfi, J., Romero, C., De Lillo, L., et al. (2017). Respiratory syncytial virus (RSV) infects CD4+ T cells: frequency of circulating CD4+ RSV+ T cells as a marker of disease severity in young children. *J. Infect. Dis.* 215, 1049–1058. doi: 10.1093/infdis/jix070

RamaKrishnan, A. M., and Sankaranarayanan, K. (2016). Understanding autoimmunity: the ion channel perspective. *Autoimmun. Rev.* 15, 585–620. doi: 10.1016/j.autrev.2016.02.004

Ravell, J. C., Chauvin, S. D., He, T., and Lenardo, M. (2020). An update on XMEN disease. *J. Clin. Immunol.* 40, 671–681. doi: 10.1007/s10875-020-00790-x

Ravell, J., Chaigne-Delalande, B., and Lenardo, M. (2014). X-linked immunodeficiency with magnesium defect, epstein-barr virus infection, and neoplasia disease: a combined immune deficiency with magnesium defect. *Curr. Opin. Pediatr.* 26, 713–719. doi: 10.1097/MOP.0000000000000156

Retamal-Díaz, A. R., Tognarelli, E., Kalergis, A. M., Bueno, S. M., and González, P. A. (2016). *Immune Evasion by Herpes Simplex Viruses, Herpesviridae, Jozsef Ongradi, IntechOpen.* doi: 10.5772/64128 Available online at: https://www.intechopen.com/chapters/51597

Rossi, E., Meuser, M. E., Cunanan, C. J., and Cocklin, S. (2021). Structure, function, and interactions of the hiv-1 capsid protein. *Life* 11, 1–25. doi: 10.3390/life11020100

Rubaiy, H. N. (2017). A short guide to electrophysiology and ion channels. *J. Pharm. Pharm. Sci.* 20, 48–67. doi: 10.18433/J32P6R

Samanta, A., Hughes, T. E. T., and Moiseenkova-Bell, V. Y. (2018). Transient receptor potential (TRP) channels. *Subcell. Biochem.* 87:1416. doi: 10.1007/978-981-10-7757-9_6

Sawada, A., Takihara, Y., Kim, J. Y., Matsuda-Hashii, Y., Tokimasa, S., Fujisaki, H., et al. (2003). A congenital mutation of the novel gene LRRC8 causes agammaglobulinemia in humans. *J. Clin. Invest.* 112, 1707–1713. doi: 10.1172/JCI18937

Scharenberg, A. M., Humphries, L. A., and Rawlings, D. J. (2007). Calcium signalling and cell-fate choice in B cells. *Nat. Rev. Immunol.* 7, 778–789. doi: 10.1038/nri2172

Schenk, U., Westendorf, A. M., Radaelli, E., Casati, A., Ferro, M., Fumagalli, M., et al. (2008). Purinergic control of T cell activation by ATP released through pannexin-1 hemichannels. *Sci. Signal.* 1:ra6. doi: 10.1126/scisignal.1160583

Schmitz, C., Perraud, A.-L., Johnson, C. O., Inabe, K., Smith, M. K., Penner, R., et al. (2003). Regulation of vertebrate cellular Mg2+ homeostasis by TRPM7. *Cell* 114, 191–200. doi: 10.1016/S0092-8674(03)00556-7

Schorge, S. (2018). Channelopathies go above and beyond the channels. *Neuropharmacology* 132, 1–2. doi: 10.1016/j.neuropharm.2018.02.011

Seeger, C., and Mason, W. S. (2015). Molecular biology of hepatitis B virus infection. *Virology* 479–480, 672–686. doi: 10.1016/j.virol.2015.02.031

Serebrovska, Z. O., Chong, E. Y., Serebrovska, T. V., Tumanovska, L. V., and Xi, L. (2020). Hypoxia, HIF-1α, and COVID-19: from pathogenic factors to potential therapeutic targets. *Acta Pharmacol. Sin.* 41, 1539–1546. doi: 10.1038/s41401-020-00554-8

Serra, S. A., Stojakovic, P., Amat, R., Rubio-Moscardo, F., Latorre, P., Seisenbacher, G., et al. (2021). LRRC8A-containing chloride channel is crucial for cell volume recovery and survival under hypertonic conditions. *Proc. Natl. Acad. Sci.* 118:e2025013118. doi: 10.1073/pnas.2025013118

Shahrabadi, M. S., and Lee, P. W. (1988). Calcium requirement for syncytium formation in HEp-2 cells by respiratory syncytial virus. *J. Clin. Microbiol.* 26, 139–141. doi: 10.1128/jcm.26.1.139-141.1988

Shi, J., Gao, W., and Shao, F. (2017). Pyroptosis: gasdermin-mediated programmed necrotic cell death. *Trends Biochem. Sci.* 42, 245–254. doi: 10.1016/j.tibs.2016.10.004

Shi, J., Zhao, Y., Wang, K., Shi, X., Wang, Y., Huang, H., et al. (2015). Cleavage of GSDMD by inflammatory caspases determines pyroptotic cell death. *Nature* 526, 660–665. doi: 10.1038/nature15514

Sloan, D. D., Han, J.-Y., Sandifer, T. K., Stewart, M., Hinz, A. J., Yoon, M., et al. (2006). Inhibition of TCR signaling by herpes simplex virus. *J. Immunol.* 176, 1825–1833. doi: 10.4049/jimmunol.176.3.1825

Smith-Garvin, J. E., Koretzky, G. A., and Jordan, M. S. (2009). T cell activation. *Annu. Rev. Immunol.* 27, 591–619. doi: 10.1146/annurev.immunol.021908.132706

Straus, M. R., Bidon, M., Tang, T., Whittaker, G. R., and Daniel, S. (2020a). FDA approved calcium channel blockers inhibit SARS-CoV-2 infectivity in epithelial lung cells. *bioRxiv [Preprint]* doi: 10.1101/2020.07.21.214577

Straus, M. R., Tang, T., Lai, A. L., Flegel, A., Bidon, M., Freed, J. H., et al. (2020b). Ca 2+ ions promote fusion of middle east respiratory syndrome coronavirus with host cells and increase infectivity. *J. Virol.* 94, 426–446. doi: 10.1128/JVI.00426-20

Sumoza-Toledo, A., and Penner, R. (2011). TRPM2: a multifunctional ion channel for calcium signalling. *J. Physiol.* 589, 1515–1525. doi: 10.1113/jphysiol.2010.201855

Syed Mortadza, S. A., Wang, L., Li, D., and Jiang, L.-H. (2015). TRPM2 channel-mediated ROS-sensitive Ca(2+) signaling mechanisms in immune cells. *Front. Immunol.* 6:407. doi: 10.3389/fimmu.2015.00407

Tabor, D. E., Fernandes, F., Langedijk, A. C., Wilkins, D., Lebbink, R. J., Tovchigrechko, A., et al. (2021). Global molecular epidemiology of respiratory syncytial virus from the 2017-2018 INFORM-RSV study. *J. Clin. Microbiol.* 59:e1828-20. doi: 10.1128/JCM.01828-20

Teisseyre, A., Palko-Labuz, A., Sroda-Pomianek, K., and Michalak, K. (2019). Voltage-gated potassium channel Kv1.3 as a target in therapy of cancer. *Front. Oncol.* 9:933. doi: 10.3389/fonc.2019.00933

Traynelis, S. F., Wollmuth, L. P., McBain, C. J., Menniti, F. S., Vance, K. M., Ogden, K. K., et al. (2010). Glutamate receptor ion channels: structure, regulation, and function. *Pharmacol. Rev.* 62, 405–496. doi: 10.1124/pr.109.002451

Trebak, M., and Kinet, J.-P. (2019). Calcium signalling in T cells. *Nat. Rev. Immunol.* 19, 154–169. doi: 10.1038/s41577-018-0110-7

Triantafilou, K., Kar, S., Vakakis, E., Kotecha, S., and Triantafilou, M. (2013). Human respiratory syncytial virus viroporin SH: a viral recognition pathway used by the host to signal inflammasome activation. *Thorax* 68, 66–75. doi: 10.1136/thoraxjnl-2012-202182

Vaeth, M., and Feske, S. (2018). Ion channelopathies of the immune system. *Curr. Opin. Immunol.* 52, 39–50. doi: 10.1016/j.coi.2018.03.021

Vaeth, M., Kahlfuss, S., and Feske, S. (2020). CRAC channels and calcium signaling in T cell-mediated immunity. *Trends Immunol.* 41, 878–901. doi: 10.1016/j.it.2020.06.012

Valle-Reyes, S., Valencia-Cruz, G., Liñan-Rico, L., Pottosin, I., and Dobrovinskaya, O. (2018). Differential activity of voltage- and Ca2+-dependent potassium channels in leukemic T cell lines: Jurkat cells represent an exceptional case. *Front. Physiol.* 9:499 doi: 10.3389/fphys.2018.00499

Venkatakrishnan, B., and Zlotnick, A. (2016). The structural biology of hepatitis B virus: form and function. *Annu. Rev. Virol.* 3, 429–451. doi: 10.1146/annurev-virology-110615-042238

Vennekens, R., and Nilius, B. (2007). Insights into TRPM4 function, regulation and physiological role. *Handb. Exp. Pharmacol.* 179, 269–285. doi: 10.1007/978-3-540-34891-7_16

Verheugen, J. A. H., Le Deist, F., Devignot, V., and Korn, H. (1997). Enhancement of calcium signaling and proliferation responses in activated human T lymphocytes. *Cell Calcium* 21, 1–17. doi: 10.1016/S0143-4160(97)90092-0

Veytia-Bucheli, J. I., Jiménez-Vargas, J. M., Melchy-Pérez, E. I., Sandoval-Hernández, M. A., Possani, L. D., and Rosenstein, Y. (2018). Kv1.3 channel blockade with the Vm24 scorpion toxin attenuates the CD4+ effector memory T cell response to TCR stimulation. *Cell Commun. Signal.* 16:45. doi: 10.1186/s12964-018-0257-7

Vig, M., and Kinet, J.-P. (2009). Calcium signaling in immune cells. *Nat. Immunol.* 10, 21–27. doi: 10.1038/ni.f.220

Vukcevic, M., Spagnoli, G. C., Iezzi, G., Zorzato, F., and Treves, S. (2008). Ryanodine receptor activation by Cav1.2 is involved in dendritic cell major histocompatibility complex class II surface expression. *J. Biol. Chem.* 283, 34913–34922. doi: 10.1074/jbc.M804472200

Wang, M.-Y., Zhao, R., Gao, L.-J., Gao, X.-F., Wang, D.-P., and Cao, J.-M. (2020). SARS-CoV-2: structure, biology, and structure-based therapeutics development. *Front. Cell. Infect. Microbiol.* 10:587269. doi: 10.3389/fcimb.2020.587269

Weber, K. S., Hildner, K., Murphy, K. M., and Allen, P. M. (2010). Trpm4 differentially regulates Th1 and Th2 function by altering calcium signaling and NFAT localization. *J. Immunol.* 185, 2836–2846. doi: 10.4049/jimmunol.1000880

Wenning, A. S., Neblung, K., Strauss, B., Wolfs, M.-J., Sappok, A., Hoth, M., et al. (2011). TRP expression pattern and the functional importance of TRPC3 in primary human T-cells. *Biochim. Biophys. Acta* 1813, 412–423. doi: 10.1016/j.bbamcr.2010.12.022

Whitacre, J. M., Lin, J., and Harding, A. (2012). T cell adaptive immunity proceeds through environment-induced adaptation from the exposure of cryptic genetic variation. *Front. Genet.* 3:5. doi: 10.3389/fgene.2012.00005

Woehrle, T., Yip, L., Elkhal, A., Sumi, Y., Chen, Y., Yao, Y., et al. (2010). Pannexin-1 hemichannel-mediated ATP release together with P2X1 and P2X4 receptors regulate T-cell activation at the immune synapse. *Blood* 116, 3475–3484. doi: 10.1182/blood-2010-04-277707

Wulff, H., Castle, N. A., and Pardo, L. A. (2009). Voltage-gated potassium channels as therapeutic targets. *Nat. Rev. Drug Discov.* 8, 982–1001. doi: 10.1038/nrd2983

Wulff, H., Knaus, H.-G., Pennington, M., and Chandy, K. G. (2004). K + channel expression during B cell differentiation: implications for immunomodulation and autoimmunity. *J. Immunol.* 173, 776–786. doi: 10.4049/jimmunol.173.2.776

Xia, B., Shen, X., He, Y., Pan, X., Wang, Y., Yang, F., et al. (2020). SARS-CoV-2 envelope protein causes acute respiratory distress syndrome (ARDS)-like pathological damage and constitutes an antiviral target. *bioRxiv [Preprint]* doi: 10.1101/2020.06.27.174953

Yamamoto, S., Takahashi, N., and Mori, Y. (2010). Chemical physiology of oxidative stress-activated TRPM2 and TRPC5 channels. *Prog. Biophys. Mol. Biol.* 103, 18–27. doi: 10.1016/j.pbiomolbio.2010.05.005

Yan, Q., Lan, Y.-H., Huang, Y.-X., Fan, R.-S., Liu, L., Song, S.-P., et al. (2016). Hepatitis B virus replication is upregulated in proliferated peripheral blood lymphocytes. *Mol. Med. Rep.* 13, 3581–3587. doi: 10.3892/mmr.2016.4973

Yang, P.-C. C., and Jafri, M. S. (2020). Ca2+ signaling in T lymphocytes: the interplay of the endoplasmic reticulum, mitochondria, membrane potential, and CRAC channels on transcription factor activation. *Heliyon* 6:e03526. doi: 10.1016/j.heliyon.2020.e03526

Yao, J.-H., Liu, Z.-J., Yi, J.-H., Wang, J., and Liu, Y.-N. (2018). Hepatitis B virus X protein upregulates intracellular calcium signaling by binding C-terminal of Orail protein. *Curr. Med. Sci.* 38, 26–34. doi: 10.1007/s11596-018-1843-z

Yip, L., Woehrle, T., Corriden, R., Hirsh, M., Chen, Y., Inoue, Y., et al. (2009). Autocrine regulation of T-cell activation by ATP release and P2X7 receptors. *FASEB J.* 23, 1685–1693. doi: 10.1096/fj.08-126458

Zainullina, L. F., Yamidanov, R. S., Vakhitov, V. A., and Vakhitova, Y. V. (2011). NMDA receptors as a possible component of store-operated Ca 2+ entry in human T-lymphocytes. *Biochemistry* 76, 1220–1226. doi: 10.1134/S0006297911110034

Zhang, Q., Hsia, S. C., and Martin-Caraballo, M. (2019). Regulation of T-type Ca2+ channel expression by interleukin-6 in sensory-like ND7/23 cells post-herpes simplex virus (HSV-1) infection. *J. Neurochem.* 151, 238–254. doi: 10.1111/jnc.14697

Zhou, X., Chen, D., Wang, L., Zhao, Y., Wei, L., Chen, Z., et al. (2020). Low serum calcium: a new, important indicator of COVID-19 patients from mild/moderate to severe/critical. *Biosci. Rep.* doi: 10.1042/BSR20202690 Online ahead of print.

Zhou, Y., Frey, T. K., and Yang, J. J. (2009). Viral calciomics: interplays between Ca2+ and virus. *Cell Calcium* 46, 1–17. doi: 10.1016/j.ceca.2009.05.005

Zocchi, M. R., Rubartelli, A., Morgavi, P., and Poggi, A. (1998). HIV-1 tat inhibits human natural killer cell function by blocking L-type calcium channels. *J. Immunol.* 161, 2938–2943.

Zou, Z.-G., Rios, F. J., Montezano, A. C., and Touyz, R. M. (2019). TRPM7, magnesium, and signaling. *Int. J. Mol. Sci.* 20:1877. doi: 10.3390/ijms20081877

Zweifach, A., and Lewis, R. S. (1993). Mitogen-regulated Ca2+ current of T lymphocytes is activated by depletion of intracellular Ca2+ stores. *Proc. Natl. Acad. Sci. U. S. A.* 90, 6295–6299. doi: 10.1073/pnas.90.13.6295

Conflict of Interest: The authors declare that the research was conducted in the absence of any commercial or financial relationships that could be construed as a potential conflict of interest.

Publisher's Note: All claims expressed in this article are solely those of the authors and do not necessarily represent those of their affiliated organizations, or those of the publisher, the editors and the reviewers. Any product that may be evaluated in this article, or claim that may be made by its manufacturer, is not guaranteed or endorsed by the publisher.

frontiers in Physiology

ORIGINAL RESEARCH
published: 18 October 2021
doi: 10.3389/fphys.2021.727549

NSAIDs Naproxen, Ibuprofen, Salicylate, and Aspirin Inhibit TRPM7 Channels by Cytosolic Acidification

*Rikki Chokshi, Orville Bennett, Tetyana Zhelay and J. Ashot Kozak**

Department of Neuroscience, Cell Biology and Physiology, Boonshoft School of Medicine, College of Science and Mathematics, Wright State University, Dayton, OH, United States

Non-steroidal anti-inflammatory drugs (NSAIDs) are used for relieving pain and inflammation accompanying numerous disease states. The primary therapeutic mechanism of these widely used drugs is the inhibition of cyclooxygenase 1 and 2 (COX1, 2) enzymes that catalyze the conversion of arachidonic acid into prostaglandins. At higher doses, NSAIDs are used for prevention of certain types of cancer and as experimental treatments for Alzheimer's disease. In the immune system, various NSAIDs have been reported to influence neutrophil function and lymphocyte proliferation, and affect ion channels and cellular calcium homeostasis. Transient receptor potential melastatin 7 (TRPM7) cation channels are highly expressed in T lymphocytes and are inhibited by Mg^{2+}, acidic pH, and polyamines. Here, we report a novel effect of naproxen, ibuprofen, salicylate, and acetylsalicylate on TRPM7. At concentrations of 3–30 mM, they reversibly inhibited TRPM7 channel currents. By measuring intracellular pH with the ratiometric indicator BCECF, we found that at 300 μM to 30 mM, these NSAIDs reversibly acidified the cytoplasm in a concentration-dependent manner, and propose that TRPM7 channel inhibition is a consequence of cytosolic acidification, rather than direct. NSAID inhibition of TRPM7 channels was slow, voltage-independent, and displayed use-dependence, increasing in potency upon repeated drug applications. The extent of channel inhibition by salicylate strongly depended on cellular $PI(4,5)P_2$ levels, as revealed when this phospholipid was depleted with voltage-sensitive lipid phosphatase (VSP). Salicylate inhibited heterologously expressed wildtype TRPM7 channels but not the S1107R variant, which is insensitive to cytosolic pH, Mg^{2+}, and $PI(4,5)P_2$ depletion. NSAID-induced acidification was also observed in Schneider 2 cells from *Drosophila*, an organism that lacks orthologous COX genes, suggesting that this effect is unrelated to COX enzyme activity. A 24-h exposure to 300 μM–10 mM naproxen resulted in a concentration-dependent reduction in cell viability. In addition to TRPM7, the described NSAID effect would be expected to apply to other ion channels and transporters sensitive to intracellular pH.

Keywords: cation channel, acidification, pH, lymphocyte, phosphoinositide, analgesic, magnesium

OPEN ACCESS

Edited by:
Ildikò Szabò,
University of Padua, Italy

Reviewed by:
Craig Doupnik,
USF Health Morsani College of Medicine, United States
Fan Yang,
Zhejiang University, China

****Correspondence:***
J. Ashot Kozak
juliusz.kozak@wright.edu

Specialty section:
This article was submitted to Membrane Physiology and Membrane Biophysics, a section of the journal Frontiers in Physiology

Received: *18 June 2021*
Accepted: *10 September 2021*
Published: *18 October 2021*

Citation:
Chokshi R, Bennett O, Zhelay T and Kozak JA (2021) NSAIDs Naproxen, Ibuprofen, Salicylate, and Aspirin Inhibit TRPM7 Channels by Cytosolic Acidification. Front. Physiol. 12:727549. doi: 10.3389/fphys.2021.727549

INTRODUCTION

Non-steroidal anti-inflammatory drugs (NSAIDs) are widely used as medication for mild and moderate pain in diseases such as rheumatoid arthritis, spondyloarthropathies and gout (Rider and Jordan, 2010; Firth, 2012). The mechanism of their analgesic action is the inhibition of cyclooxygenase enzymes COX1 and COX2, which catalyze the production of prostaglandins responsible for the pain and inflammation symptoms (Vane, 1971; Fitzpatrick, 2004; Burke et al., 2006). NSAIDs, therefore, exert their therapeutic effects by markedly reducing the production of prostaglandins. The original NSAIDs were nonselective inhibitors of COX enzymes and were followed by compounds specific for COX2, the COX enzyme inducible by inflammation in macrophages, monocytes, and other cell types (Burke et al., 2006). Adverse effects of nonselective NSAIDs include peptic ulcer disease, gastrointestinal bleeding, aseptic meningitis, hyperkalemia, urticaria/angioedema, and aspirin-exacerbated respiratory disease (AERD), and are thought to be mediated by the constitutively active COX-1 enzyme (Berges-Gimeno et al., 2002; Woessner, 2003; Kong et al., 2007). High doses of aspirin and salicylate (millimolar range) have long been known to cause tinnitus, hearing loss and cochlea degeneration (Wei et al., 2010; Namikawa et al., 2017).

Over the years, it has become clear that COX enzymes are not the only target of NSAIDs (Tegeder et al., 2001; Bishay et al., 2010). Moreover, in addition to their widespread use as pain relievers, NSAIDs treat numerous other conditions. Several lines of evidence suggest that NSAIDs can be useful in Alzheimer's disease (AD) by reducing inflammation in the brain (Lim et al., 2000; McGeer and McGeer, 2001b; Aisen et al., 2003; Trepanier and Milgram, 2010), and were found to decrease the incidence of AD in more than a dozen epidemiological studies (McGeer and McGeer, 2001a). NSAIDs have also been reported to reduce colon cancer in animal models of this disease, and the mechanisms may involve reduced proliferation and increased apoptosis of cancer cells (Shiff et al., 1995, 1996; Shiff and Rigas, 1999; Villalobos et al., 2017). Importantly, the beneficial effects of NSAIDs in these diseases were found at doses substantially higher than necessary to inhibit COX enzymes (Tegeder et al., 2001; Schonthal, 2010).

NSAIDs inhibit several ion channels independently of their COX-targeting effects. ASIC (acid-sensing ion channel), Nav1 (voltage-gated sodium channel), TRPV1, and TRPA1, channels involved in peripheral nociception, are inhibited by NSAIDs, which possibly contributes to their analgesic action (Voilley, 2004; Park et al., 2007; Wang et al., 2012; Nozadze et al., 2016; Tsagareli et al., 2018). ATP-sensitive potassium channels (Kir6.2) in pancreatic β cells are inhibited by meclofenamic acid resulting in elevated intracellular calcium and insulin secretion (Li et al., 2007). *Drosophila* and rat voltage-gated potassium channels (Kv2) were directly inhibited by celecoxib (active ingredient of Celebrex) at micromolar concentrations, causing low beating rate and arrhythmia in cultured cardiomyocytes and reducing spontaneous firing in retinal neurons (Frolov et al., 2008a,b).

TRPM7 is a dual ion channel/protein kinase, highly expressed in cells of the immune system such as T and B lymphocytes, basophils, mast cells, macrophages and microglia (Kozak et al., 2002; Jiang et al., 2003; Chokshi et al., 2012b; Freichel et al., 2012; Huang et al., 2014; Kaitsuka et al., 2014; Krishnamoorthy et al., 2018). TRPM7 channels conduct cations and are unique in that they require depletion of cytosolic Mg^{2+} for opening (Hermosura et al., 2002; Kozak et al., 2002; Prakriya and Lewis, 2002). In whole-cell patch clamp, it takes several minutes of internal perfusion of metal chelators to achieve full activation of TRPM7 currents. Conversely, inclusion of 300 μM and higher concentrations of Mg^{2+} in internal solutions will prevent current development (Chokshi et al., 2012a). We recently discovered that in intact cells TRPM7 channel activation and inhibition can be achieved by prolonged exposure of cells to low (micromolar) and high (millimolar) external [Mg^{2+}], respectively (Mellott et al., 2020). In addition to Mg^{2+}, other metal ions, polyamines and protons, are also inhibitory (Kozak and Cahalan, 2003; Kozak et al., 2005; Chokshi et al., 2012b; Zhelay et al., 2018). Channel inhibition by Mg^{2+} and protons does not depend on the kinase activity (Kozak et al., 2005; Matsushita et al., 2005; Beesetty et al., 2021). TRPM7 channels have been implicated in cellular and body Mg^{2+} homeostasis (Zou et al., 2019). TRPM7 channel activity is required for Mg^{2+} entry in T cells; however, the mechanism of Mg^{2+} permeation is not fully elucidated (Deason-Towne et al., 2011; Chubanov et al., 2018; Mellott et al., 2020).

Naproxen, ibuprofen, and salicylates belong to the aryl propionic acid derivative group. We previously reported that TRPM7 channels are inhibited reversibly by propionate (Kozak et al., 2005). The mechanism of this effect is cytosolic acidification; accordingly, in the presence of divalent cations, TRPM7 channels are inhibited by acidic pH with pH_{50} of 6.3 (Chokshi et al., 2012b). The inhibition reflects interference with channel stimulation by the phospholipid $PI(4,5)P_2$ (PIP_2) present in the plasma membrane (Kozak et al., 2005; Zhelay et al., 2018). Moreover, serine 1,107 substitutions with bulkier residues in TRPM7 greatly diminished inhibition by protons, Mg^{2+}, and polyamines while increasing its sensitivity to the agonist PIP_2 (Zhelay et al., 2018).

Here, we have characterized the effects of NSAIDs acetylsalicylate, salicylate, naproxen, and ibuprofen on TRPM7 channels. We found that these drugs potently inhibit the native TRPM7 currents in Jurkat T cells. At 3–30 mM the inhibition was reversible with a slow onset and offset, requiring several minutes. Repeated applications of the drugs in the same cell resulted in progressively stronger reduction in the current, showing use-dependence or sensitization. Single-cell pH measurements showed that the drugs acidified the Jurkat cytosol, and this effect was concentration-dependent. Long-term exposure to naproxen reduced cell viability to a greater extent than salicylate. Depletion of PIP_2 in HEK293 cells by expressing *Ciona* voltage-sensitive lipid phosphatase (CiVSP) resulted in significantly stronger channel inhibition by salicylate. Moreover,

Abbreviations: TRP, Transient receptor potential; PIP_2, Phosphatidylinositol 4,5-bisphosphate; VSP, Voltage-sensitive phosphatase; BCECF, 2',7'-Bis-(2-carboxyethyl)-5-(and-6)-carboxyfluorescein; EGTA, Ethylene glycol-bis(2-aminoethylether)-N,N,N',N'-tetraacetic acid; COX, Cyclooxygenase; HEPES, 4-(2-Hydroxyethyl)-1-piperazineethanesulfonic acid.

salicylate inhibited heterologously expressed wildtype TRPM7 channels but not the pH and Mg^{2+}-insensitive variant S1107R. Based on these findings, we propose that the mechanism of TRPM7 channel inhibition by NSAIDs is acidification and interference with channel-PIP_2 interactions. In *Drosophila* S2 cells which lack COX enzyme orthologs, we found a similar acidification induced by NSAIDs, demonstrating that COX enzymes are not involved in this process.

MATERIALS AND METHODS

Cell Culture and Transfection

Human leukemic Jurkat T lymphocytes and human embryonic kidney (HEK293) cells were kept in a CO_2 incubator (Thermo Scientific, Fairlawn, NJ, United States and Forma Scientific, Marietta, OH, United States) at 37°C and grown in RPMI-1640 (Lonza, Wakersville, MD, United States) supplemented with glutamine, 10% fetal bovine serum (FBS; BioWest, Riverside, MO, United States), and penicillin/streptomycin (Thermo; Chokshi et al., 2012b; Zhelay et al., 2018). Jurkat T cells were passaged by diluting the cell suspension in the complete culture medium, and HEK293 cells were passaged using Cellstripper non-enzymatic cell dissociation solution (Mediatech, Manassas, VA, United States). HEK cells were transfected with pEGFP-TRPM7, pEGFP-TRPM7 S1107R, pIRES2-EGFP CiVSP, and pIRES2-EGFP CiVSP C363S plasmids using TransIT-LT1 transfection reagent (Mirus Bio, Madison, WI, United States) as previously described in detail (Zhelay et al., 2018). Electrophysiological recordings were made 1–2 days after transfection. Successfully transfected cells were identified by their GFP fluorescence. *Drosophila* Schneider 2 (S2) cells from Drosophila Genomics Resource Center (Bloomington, IN, United States) were maintained at room temperature and grown in Schneider's insect medium (Lonza) supplemented with 10% fetal bovine serum (Cherbas and Cherbas, 2007). For passaging, cells were mechanically lifted and diluted in fresh culture medium before re-plating.

Patch-Clamp Electrophysiology

Patch-clamp recordings in the whole-cell configuration were performed as previously described (Kozak and Cahalan, 2003; Chokshi et al., 2012b; Zhelay et al., 2018). Briefly, monovalent TRPM7 currents were evoked using a Mg^{2+}-free pipette solution which contained (in mM): 112 Cs or K glutamate, 8 NaCl, 0.09 $CaCl_2$, 12 EGTA, 1 HEPES, and pH 7.3. In some experiments, 250 μM $MgCl_2$ was added to this solution, yielding free [Mg^{2+}] of 134 μM as estimated by Webmaxc.[1] Extracellular (bath) solution was composed of (in mM) 140 Cs or Na aspartate, 3 CsCl, 4 HEDTA, 10 HEPES, and pH 7.3. In divalent metal-free (DVF) external solutions, TRPM7 current–voltage (I–V) relation becomes semi-linear (Kozak et al., 2002), reversing close to 0 mV. Recordings were made using the computer-driven EPC-10 patch-clamp amplifier (HEKA Elektronik, Lambrecht, Germany) and PatchMaster (v. 2.6) software. Instantaneous I–V relations were obtained from command voltage ramps of 211 ms duration spanning −100 mV or −85 mV to +85 mV applied every 2.5 or 1.5 s (Chokshi et al., 2012b). Currents were sampled at 5 kHz and low-pass filtered at 2.9 kHz. Current amplitudes usually reached a maximum 3–5 min after break-in (Chokshi et al., 2012b). Naproxen sodium, ibuprofen sodium, salicylic acid, and acetylsalicylic acid (Sigma-Aldrich, St. Louis, MO, United States and Acros Organics, Geel, Belgium) were dissolved freshly in the extracellular solution and the pH measured on the day of experiment. Osmolalities of the drug-containing solutions were adjusted by reducing cesium/sodium aspartate concentrations accordingly and measured with a freezing point depression osmometer (Precision Systems, Natick, MA, United States). Both the control and drug-containing external solutions had equal concentrations of permeant monovalent cations (Cs^+ and Na^+). The patch pipettes were manufactured on a DMZ-Universal (Zeitz Instruments, Martinsried, Germany) and P-1000 (Sutter Instrument, Novato, CA, United States) horizontal pullers from borosilicate glass capillaries (Warner Instruments, Hamden, CT, United States) and fire-polished on a MF-830 microforge (Narishige, Tokyo, Japan). Drug-containing solutions were applied to the recording chamber using gravity-fed rapid perfusion systems SB-77 (Warner Instruments, Hamden, CT, United States) and ValveLink 8.2 (AutoMate Scientific, Berkeley, CA, United States), respectively, or slow bath perfusion. All drugs were tested with slow and rapid perfusion, yielding indistinguishable results. Data were analyzed and plotted using Origin (v. 8 and 2016) software (OriginLab, Northampton, MA, United States). Patch clamp experiments were performed at room temperature. Student's two-sample t test was used for determining statistical significance.

Single-Cell pH Measurement

For intracellular pH imaging experiments, 35-mm glass-bottom imaging chambers were used with solution volume of ~1 ml. Cells were seeded on these chambers and incubated in 2 μM BCECF-AM (Invitrogen, Carlsbad, CA, United States) containing buffer for ~45 min at room temperature (Chokshi et al., 2012a). The fluorescent dye-containing solution was aspirated and replaced with normal external solution composed of (in mM): 2 $CaCl_2$, 4.5 KCl, 140 NaCl, 10 HEPES-Na^+, 10 glucose, and pH 7.3. The imaging chamber with attached cells was then mounted on the movable stage of an inverted microscope (Olympus, Tokyo, Japan). Ratiometric imaging was performed by illuminating cells in a selected field every 12 s at 490 and 440 nm using a Lambda 10B shutter and filter wheel (Sutter). Fluorescence was measured at 510 nm. The light source was a 175 W Xenon lamp (QED, Lexington, KY, United States). Images were taken and processed with Pixelfly CCD camera (PCO. Imaging, Kelheim, Germany) and InCytIM 2 software (Intracellular Imaging, Cincinnati, OH, United States). Emitted light intensities averaged for individual cells in the imaging field were plotted against time using Origin. Solutions in the imaging chamber were exchanged with a syringe-driven plastic tubing perfusion system. Typically, at least 20 ml of each solution was perfused through the ~1 ml volume chamber to ensure a

[1]https://somapp.ucdmc.ucdavis.edu/pharmacology/bers/maxchelator/webmaxc/webmaxcS.htm

complete solution exchange. The high [K^+] solution contained 130 mM KCl, 20 mM NaCl, 1 mM $CaCl_2$, 0.5 mM $MgSO_4$, 1 mM NaH_2PO_4, 10 mM HEPES, and 5 mM glucose. Nigericin (Calbiochem, La Jolla, CA, United States) was added to this solution at 2–10 μM. The ratio value was taken at time points where pH_i had achieved a steady value. Experiments were performed at room temperature.

Cytotoxicity Assay

For estimating drug cytotoxicity, Jurkat T cells were maintained in T25 cell culture flasks in RPMI-1640 containing glutamine and 25 mM HEPES (Hyclone, Logan, UT, United States) supplemented with 10% FBS and penicillin/streptomycin. NSAID powder was added on the day of experiment to yield the indicated final concentrations (**Supplementary Figure S1**), and cells were collected after 24-h incubation in a CO_2 incubator at 37°C. Cell viability was measured by trypan blue exclusion using a Vi-CELL automated cell counter (Beckman Coulter, Brea, CA, United States) as previously described in detail (Gibson et al., 2016; Mellott et al., 2020). For each concentration of the drug, the experiment was repeated with three different groups of cells.

RESULTS

NSAIDs Naproxen, Salicylic Acid, Acetylsalicylic Acid, and Ibuprofen Reversibly Inhibit Native TRPM7 Channels in Jurkat T Lymphocytes

We tested naproxen, ibuprofen, salicylic acid, and acetylsalicylic acid for their ability to inhibit the endogenous TRPM7 channel current in Jurkat T lymphocytes. As described in Materials and Methods, we allowed several minutes of Mg^{2+} depletion for the TRPM7 current to develop to full extent before applying the drugs.

Application of naproxen-Na^+ at concentrations of 3, 10, and 30 mM reproducibly inhibited TRPM7 currents. **Figures 1A–C** show the effect of 3, 10, and 30 mM naproxen on the I–V relation of the monovalent TRPM7 current in three representative Jurkat T lymphocytes. The current magnitude was reduced by 3 mM (A), 10 mM (B), and 30 mM (C) naproxen in a voltage-independent manner. In **Figures 1D–F**, the time courses of inhibition by the indicated concentration of naproxen are shown. We used low concentrations of pH buffer HEPES in these recordings (see below). The onset of inhibition was slow,

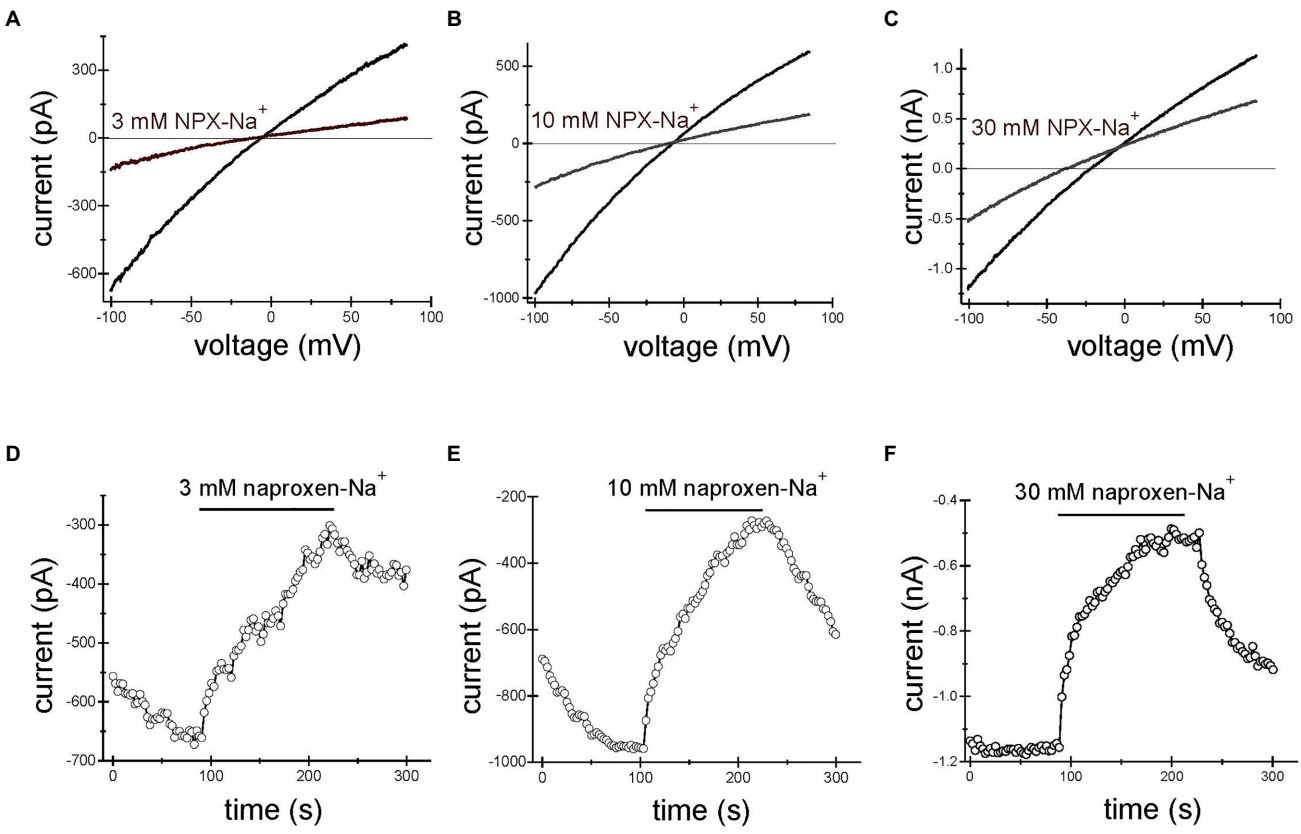

FIGURE 1 | Naproxen-Na^+ inhibits TRPM7 current. TRPM7 monovalent I–V relations in the absence and presence of 3 mM **(A)**, 10 mM **(B)** and 30 mM **(C)** naproxen. **(D–F)** Depict the time courses of inhibition by 3 mM **(D)**, 10 mM **(E)**, and 30 mM **(F)** naproxen. The presence of drug is indicated by horizontal bars. Inward current amplitude was measured at −100 mV and plotted against time. Representative whole cell patch-clamp recordings from $n = 10$ **(A,D)**, $n = 8$ **(B,E)**, and $n = 4$ **(C,F)** Jurkat T cells. Here and in **Figures 2, 3**, the drug was applied multiple times. The initial current development after break-in is not shown. The internal and external solutions were K^+ and Na^+ based, respectively.

reaching a steady state in approximately 2 min. Washout of drug effect was equally slow (**Figures 1D–F**). In most cells, this inhibition was reversible (**Figures 1D–F**), but in some cells at higher concentrations, inhibition could not be reversed even after prolonged washing, presumably because the TRPM7 channels had run down (Kozak et al., 2002; Chokshi et al., 2012b).

Figures 2, 3 show the effects of 3, 10 mM ibuprofen-Na^+ and salicylate in Jurkat cells. Similar to naproxen, these drugs reversibly inhibited native TRPM7 currents. The extent of current inhibition varied greatly from cell to cell showing no apparent dependence on concentration of the drug. Adding Mg^{2+} to the internal solution appeared to facilitate current inhibition (**Figure 3E**). Moreover, repeated application of the same concentration of drug resulted in more robust inhibition (see below).

NSAIDs Naproxen, Ibuprofen, and Salicylate Acidify the Cytoplasm

Since intracellular acidic pH potently and reversibly inhibits TRPM7 channels (Kozak et al., 2005; Chokshi et al., 2012b; Zhelay et al., 2018), and the NSAIDs in question are weak acids, we hypothesized that at relevant concentrations (Jung and Schwartz, 1994; Huntjens et al., 2006; Capone et al., 2007b), NSAIDs acidify the cell cytoplasm and inhibit the channels indirectly, by exposing them to lower pH from inside. We previously found that 2-APB inhibits TRPM7 channels by acidifying the cytoplasm (Chokshi et al., 2012a).

Naproxen

We loaded Jurkat T cells with the fluorescent dye BCECF for pH measurement as described in detail in Materials and Methods and (O'Connor and Silver, 2007; Chokshi et al., 2012a). **Figure 4A** shows single-cell pH_i time course during sequential exposure to 300 µM, 1 mM and 3 mM naproxen. Increasing drug concentration resulted in progressively more acidic cytoplasmic pH. In order to estimate the actual intracellular pH values achieved in the presence of each naproxen concentration, we performed calibration experiments by bathing the cells in high K^+ (130 mM) solutions of known pH containing H^+/K^+ antiporter nigericin (Negulescu and Machen, 1990; Bowser et al., 1999). In **Figure 4B**, the cells were first incubated in normal (low K^+, high Na^+) solution at pH 7.3 to collect baseline ratiometric measurements. The

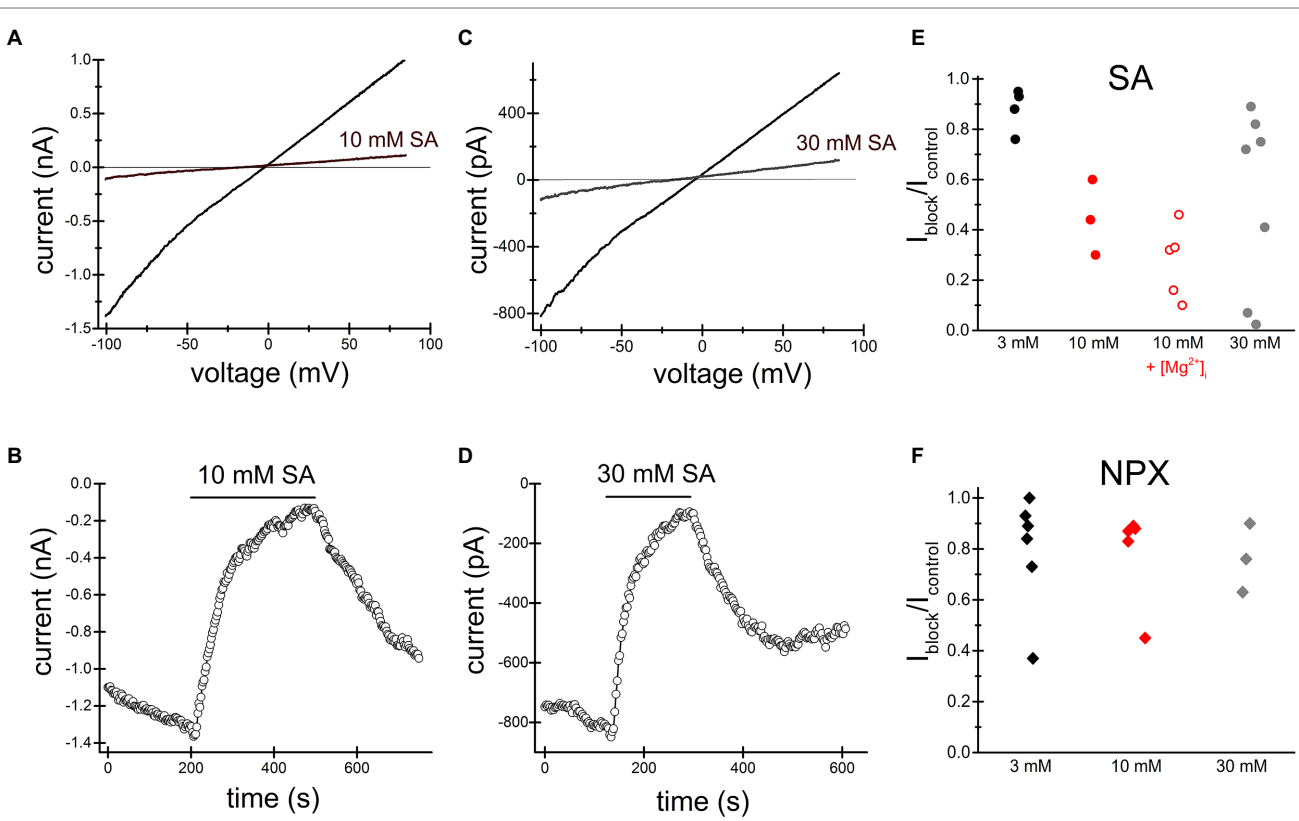

FIGURE 2 | Salicylate inhibits TRPM7 current. Summary of naproxen and salicylate inhibition of TRPM7 current at various concentrations. TRPM7 monovalent I–V relations obtained in the absence and presence of 10 mM **(A)** and 30 mM **(C)** salicylate. **(B,D)** show the corresponding time course of salicylate inhibition. Representative recordings from $n = 3$ **(A,B)** and $n = 9$ **(C,D)** Jurkat T cells. Third **(A,B)** and fourth **(C,D)** drug applications are depicted. **(E)** Summary of salicylate effects on TRPM7 current at 3, 10, and 30 mM. Each symbol represents the ratio of current amplitude after inhibition (I_{block}) to current amplitude before drug application ($I_{control}$) in one cell. The internal solution contained 1 mM HEPES. In cells represented by empty red circles, the internal solution was supplemented with 250 µM $MgCl_2$ (free $[Mg^{2+}] = 134$ µM). **(F)** Summary of naproxen effects on TRPM7 current at 3, 10, and 30 mM. The internal solution contained 1 mM HEPES and no added Mg^{2+}. In **(E,F)** responses to the second application of the drug are plotted.

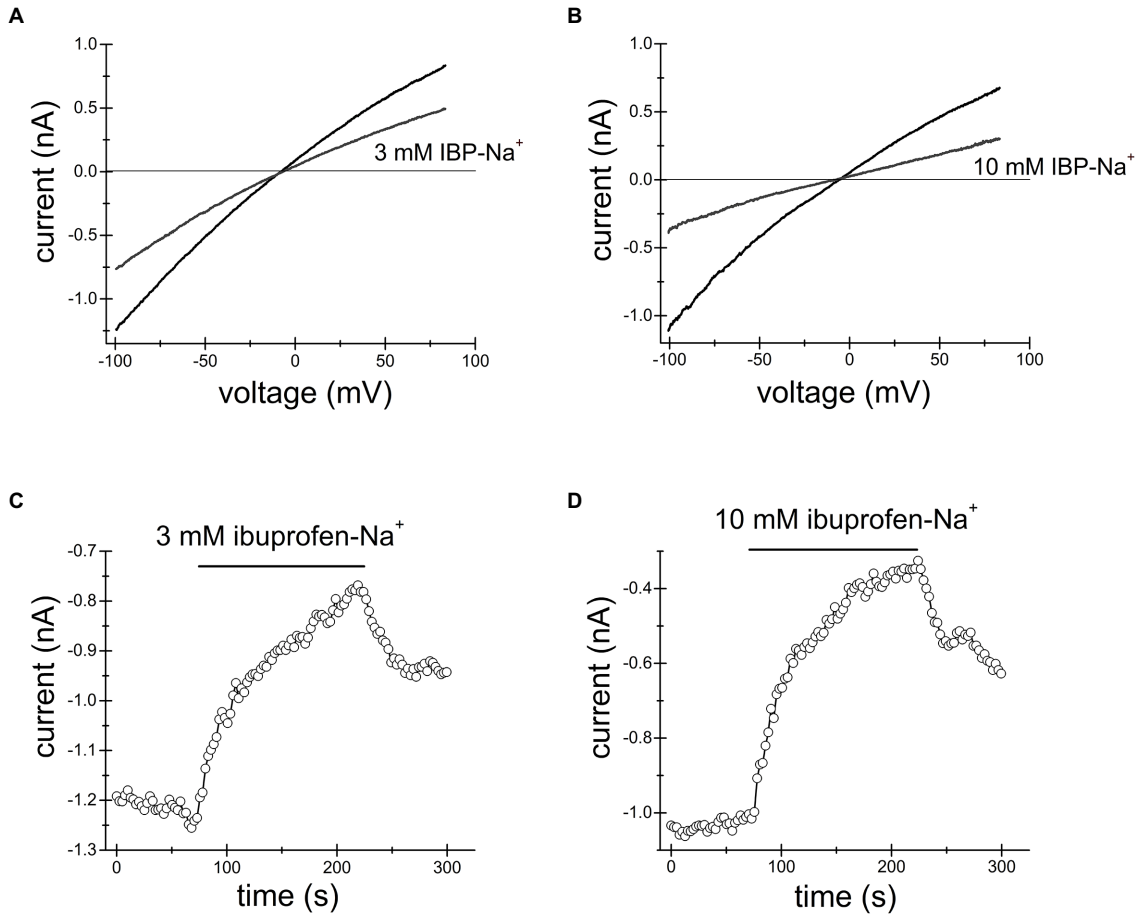

FIGURE 3 | Ibuprofen-Na^+ inhibits TRPM7 current. TRPM7 monovalent I–V relations obtained in the absence and presence of 3 mM **(A)** and 10 mM **(B)** ibuprofen. **(C,D)** show the time course of ibuprofen effect in the same cells. Current amplitudes were measured at −100 mV and plotted against time. Representative recordings from $n = 7$ **(A,C)** and $n = 3$ **(B,D)** Jurkat T cells.

bathing solution was then switched to high K^+ solutions at pH 6.7, 7.0, and 7.3, with nigericin, and corresponding ratio changes were recorded. pH 6.7 in the presence of nigericin resulted in a slow drop in ratiometric signal reaching a plateau in approximately 5 min. As expected, pH 7.0 and pH 7.3 solutions brought the ratiometric signals to higher values. In **Figure 4C**, the calibration curve generated from measurements in **Figure 4B** is shown: average ratio values at steady state (squares) were plotted against extracellular pH and could be fitted with a linear equation. We superimposed the ratio values obtained at steady state in **Figure 4A** for naproxen concentrations of 300 µM, 1 mM, and 3 mM on the calibration line (circles). We obtained cytoplasmic pH values of 7.94, 7.56, and 7.28, respectively, for these concentrations of the drug. Thus, we find that naproxen, at therapeutically relevant concentrations, acidifies Jurkat T cell cytoplasm in a concentration-dependent manner.

Ibuprofen

We proceeded to measure pH changes induced by commonly used NSAID drug ibuprofen in Jurkat T cells. In the experiment shown in **Figure 4D** BCECF loaded cells were incubated in normal external solution with addition of increasing concentrations of ibuprofen. **Figure 4D** shows that ibuprofen reduced the ratiometric signal in a dose-dependent manner at 300 µM, 1 mM, and 3 mM. Reductions in ratiometric signal were reversed upon washout (2 Ca bar). We performed calibration experiments similar to **Figure 4B** and superimposed the steady-state ratio measurements from **Figure 4D** on the calibration line obtaining values of 7.59, 7.38, and 7.14 for 300 µM, 1 mM, and 3 mM ibuprofen, respectively. We find that like naproxen, ibuprofen significantly acidifies Jurkat T cell cytoplasm concentration-dependently and that the effect is reversible.

Salicylate

In experiments similar to **Figures 4A–F**, we tested the effect of salicylate on cytosolic pH. Addition of salicylic acid at 300 µM, 1 mM, and 3 mM concentrations reduced the cell pH to 7.47, 7.34, and 7.10, respectively (**Figures 4G–I**). Similar to naproxen and ibuprofen, salicylate acidified Jurkat T cells in a concentration-dependent manner. Interestingly, there was no significant recovery from acidification in the presence of these drugs (**Figure 4**).

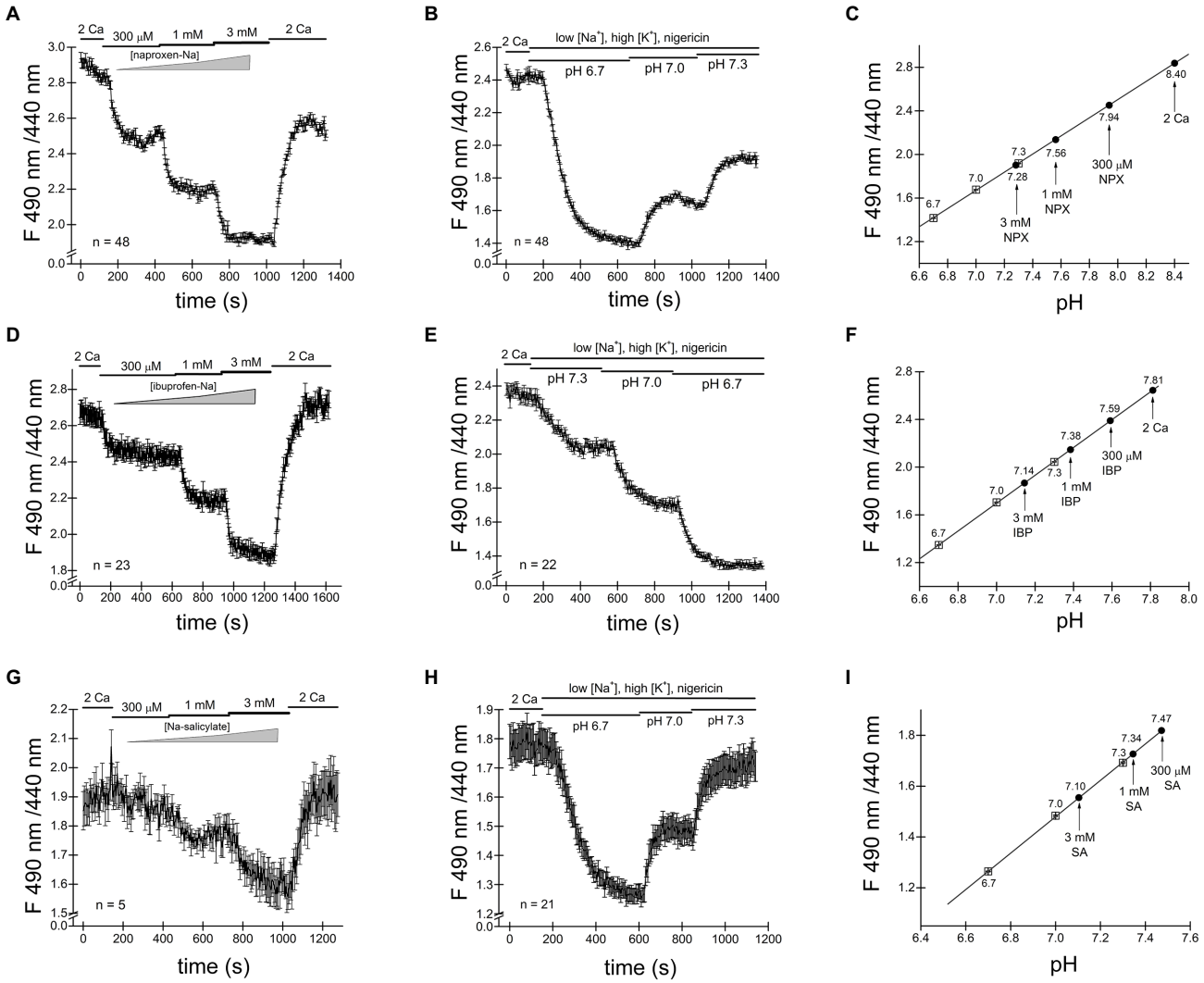

FIGURE 4 | Cytosolic acidification induced by naproxen, ibuprofen and salicylate. Fluorescence ratiometric pH measurements were performed in Jurkat T cells loaded with BCECF dye and superfused with the indicated concentrations of naproxen **(A)**. Naproxen-induced acidification was reversed upon washout (2 Ca bar). **(B)** Calibration experiment was performed by exposing the cells to low Na^+/high K^+ solution containing 5 μM nigericin at three different extracellular pH values (6.7, 7.0, and 7.3). **(C)** Calibration curve constructed from measurement means taken at steady state in **(B)**. The line is a linear fit. Mean steady state fluorescence ratios in the presence of naproxen from (**A**; indicated by vertical arrows) are superimposed on the calibration curve to determine the corresponding cellular pH. **(D,G)** Ratiometric BCECF measurements for ibuprofen and salicylate were performed as in **(A–C)**. Ibuprofen and salicylate dose-dependently and reversibly acidified the Jurkat T cell cytoplasm. Data points in **(A,B,D,E,G,H)** represent means±SEM obtained from measurements performed in groups of cells. **(F,I)** Calibration curves generated from **(D,E)**, and **(G,H)**, respectively, as in **(C)**.

In the course of these experiments, we noticed that the resting pH values between various groups of Jurkat T cells varied greatly. In **Figure 4C**, for example, the initial pH appears to be alkaline, close to 8.4. In cells shown in **Figure 4F**, the resting pH is close to 7.81 and in **Figure 4I**, it is 7.47. The nature of this variability in cytosolic pH between various batches of cells is not known and necessitated calibration in the same group of cells exposed to drugs. Based on our intracellular pH measurements, we conclude that the substantial cytosolic acidification caused by NSAIDs tested can explain inhibition of TRPM7 channels observed in patch-clamp electrophysiology. The cell-to-cell variability of resting pH_i may explain the variability in channel inhibition (see above).

Does the NSAID Effect Involve the COX Pathway?

Ibuprofen, naproxen and salicylic acid are thought to involve a reversible inhibition of COX enzymes by binding non-covalently (Burke et al., 2006). As shown in **Figures 1–4**, both TRPM7 channel inhibition and cytosolic acidification are reversible upon removal of the drug, and therefore may involve COX enzyme activity. Acetylsalicylic acid (aspirin), on the other hand, inhibits these enzymes irreversibly, by acetylation. We, therefore, tested acetylsalicylate for its ability to acidify the cytosol. **Figures 5A,B** shows that similar to naproxen ibuprofen and salicylate, acetylsalicylate-Na^+ reversibly inhibited TRPM7 channels and

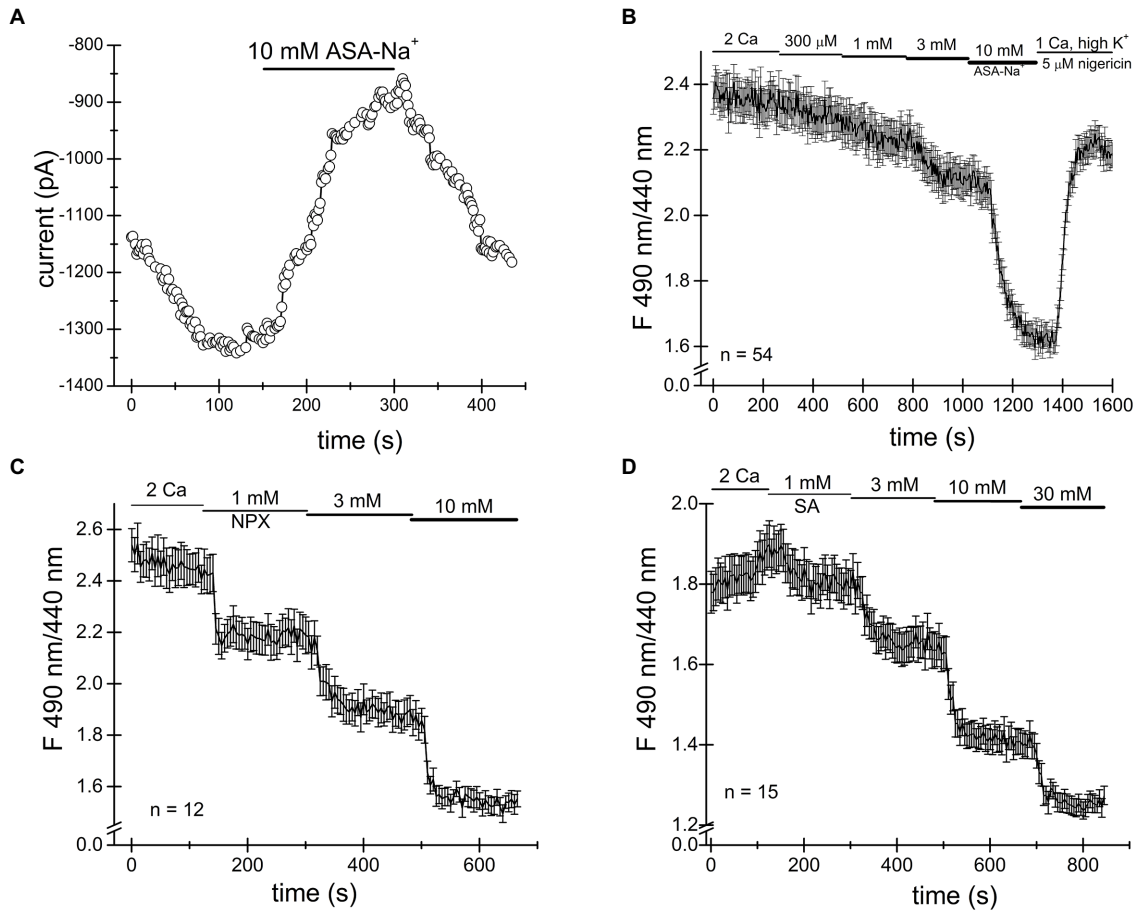

FIGURE 5 | Cytosolic acidification caused by NSAIDs does not require COX enzymes. **(A)** Acetylsalicylate inhibits TRPM7 current in Jurkat T cells reversibly. **(B)** Acidification in Jurkat T cells induced by acetylsalicylate is reversible. Naproxen **(C)** and ibuprofen **(D)** acidify *Drosophila* S2 cells.

acidified the cytosolic pH in a concentration-dependent manner. Acidification was reversed upon washout. Acetylsalicylate acetylates a serine in COX-1 and 2 in the active site of the enzyme. Since it stands out among other NSAIDs for the irreversibility of its COX inhibition, reversibility of channel acidification and channel inhibition strongly suggests that NSAID effect on cytosolic pH is independent of their effect on COX enzymes.

It has been reported that *Drosophila* genome lacks orthologs of mammalian COX enzymes and TRPM7 channel/kinase (Manning et al., 2002; Frolov et al., 2008b). In order to further test whether the NSAID acidifying effect on cytosol requires COX enzymes, we performed intracellular pH measurements in *Drosophila* S2 cells. As shown in **Figures 5C,D**, we find that naproxen and salicylate elicited reversible acidifications of the cytoplasm, qualitatively similar to their effect in Jurkat T cells. This experiment confirmed that neither COX enzymes nor, apparently, TRPM7 are required for the acidification caused by these NSAIDs.

Salicylate and Naproxen Inhibition of TRPM7 Current Depends on PIP_2 Levels

The inhibition of TRPM7 channels by cytosolic Mg^{2+}, polyamines, and protons is indirect and involves the electrostatic screening/sequestration of phosphoinositide PIP_2 (Kozak et al., 2005; Chokshi et al., 2012c; Zhelay et al., 2018). PIP_2 is a necessary cofactor of TRPM7 and other TRP channels (reviewed in Suh and Hille, 2008; Rohacs, 2014). The voltage-sensitive lipid phosphatase (VSP) from Ciona is a convenient tool for depleting phosphoinositides in intact cells (Yudin et al., 2021). We showed previously that depletion of PIP_2 by overexpressing VSP mimicked inhibition of TRPM7 by cytosolic cations (Zhelay et al., 2018). Specifically, inhibition by acidic pH and 2-APB, a TRPM7 blocker which acidifies the cytosol, was strengthened in PIP_2-depleted cells (Chokshi et al., 2012a; Zhelay et al., 2018). In order to examine if TRPM7 channel inhibition by NSAIDs occurs by a similar mechanism, we measured salicylate and naproxen effects on the native TRPM7 current in HEK cells transfected with WT and C363S VSP. HEK cells possess substantial TRPM7 channel activity (Chokshi et al., 2012b). Ten millimolar salicylate and naproxen effect in cells expressing the inactive VSP mutant was very small (**Figure 6**). By contrast, both drugs inhibited TRPM7 currents completely in PIP_2 depleted cells (**Figure 6**). It should be noted that in WT VSP expressing cells, drug washout could not be observed (**Figures 6D,F**), likely because of increased current rundown

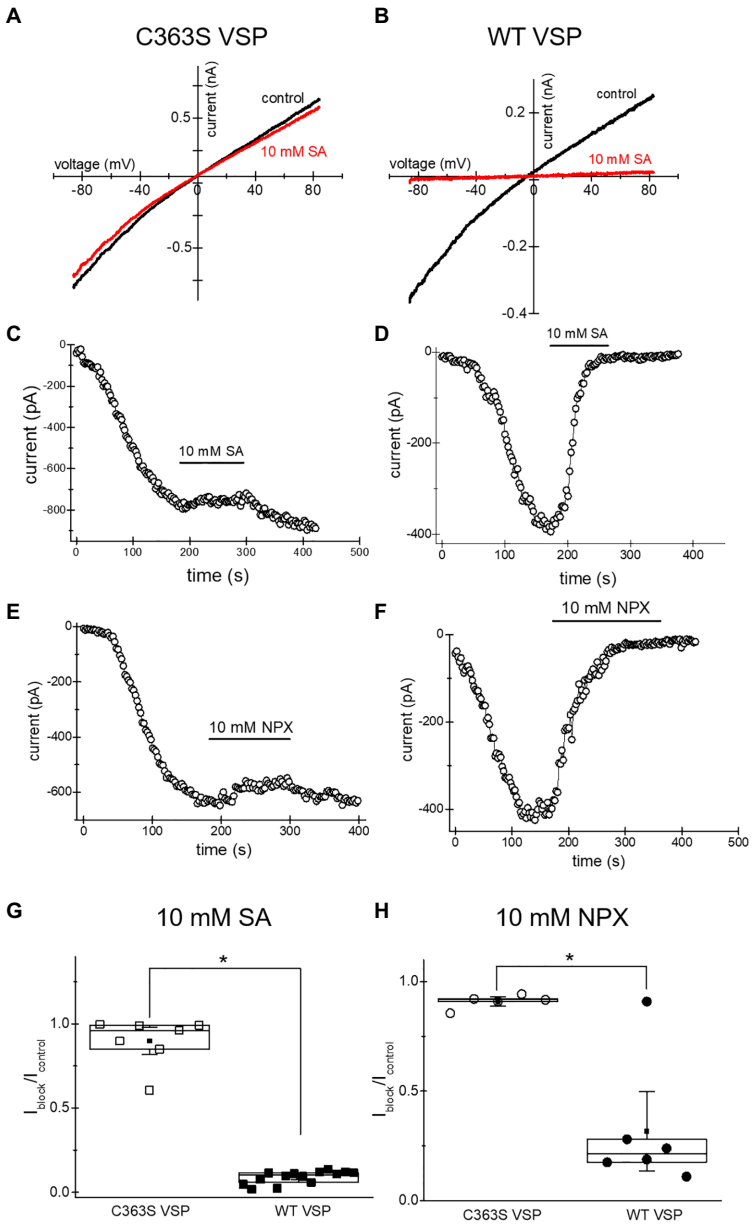

FIGURE 6 | Salicylate effect on TRPM7 current in HEK293 cells expressing WT CiVSP and its inactive C363S variant. **(A,B)** Endogenous TRPM7 monovalent I–V relations in the absence and presence of 10 mM salicylate. HEK293 cells were transfected with C363S VSP **(A)** and WT VSP **(B)**. **(C,D)** Time courses of 10 mM salicylate effect in HEK cells expressing C363S and WT VSP. **(E,F)** Time courses of 10 mM naproxen effect in HEK cells overexpressing C363S and WT VSP. **(G,H)** $I_{block}/I_{control}$ ratios measured for 10 mM salicylate **(G)** and 10 mM naproxen **(H)**. Current amplitude was measured at the 40th **(G)** and 35th **(H)** ramp during drug application (I_{block}) and divided by the amplitude immediately before drug application ($I_{control}$). The current amplitudes were measured at −85 mV. The internal and external recording solutions were Cs^+ based. *$p < 0.05$, Student's two-sample t test.

(Zhelay et al., 2018). These experiments strongly suggested that NSAID-induced TRPM7 current inhibition depends on cellular PIP_2 levels, as found previously for 2-APB.

Use-Dependence (Sensitization) of Channel Inhibition

Next, we investigated NSAID effects when applied repeatedly. Such drug application protocols with washout steps between them could mimic the situation *in vivo*, where the patient takes the drug several times daily and the effective concentrations of NSAID in the blood vary depending on proximity to the time of drug intake. **Figure 7A** shows a representative graph where 30 mM salicylate was repeatedly applied. Inhibition was progressively more pronounced for every application. At the same time, the current was running down (amplitude of current after drug washout is smaller than before its application; see Kozak et al., 2005 for a detailed discussion of rundown).

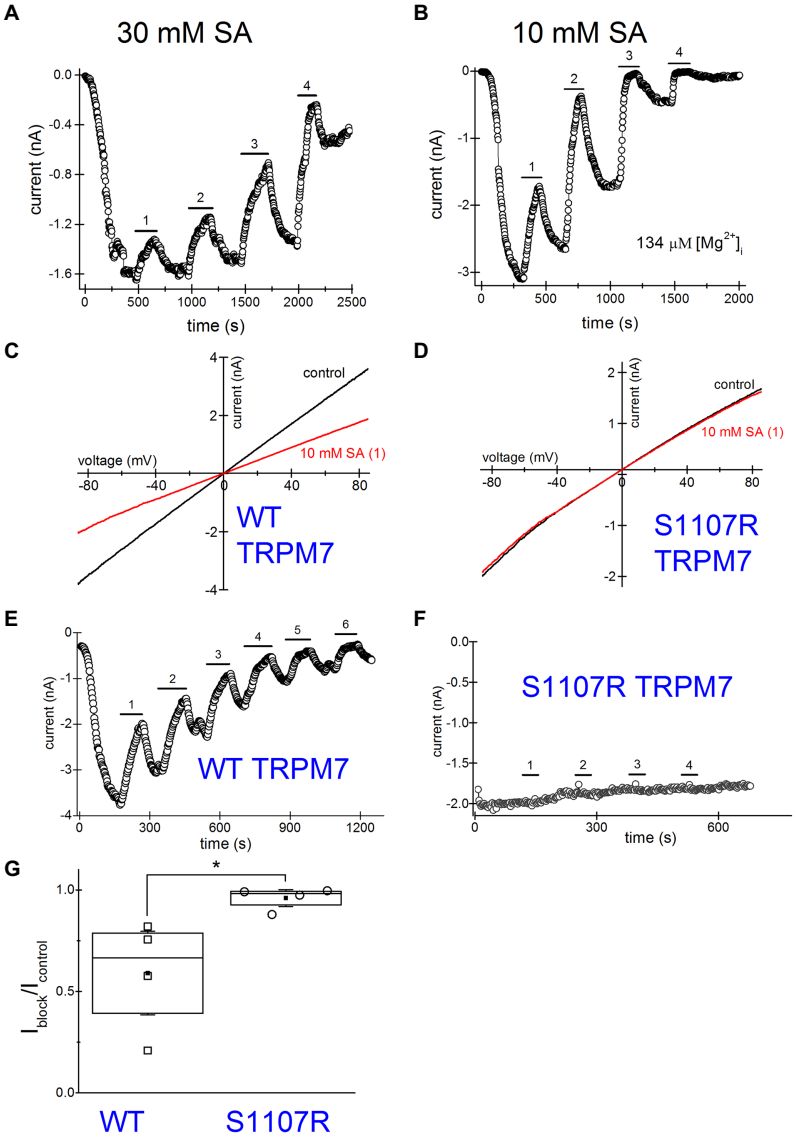

FIGURE 7 | Increased inhibition of TRPM7 current revealed by multiple applications of salicylate. Salicylate effect on WT and S1107R TRPM7. **(A)** Effect of repeated application of 30 mM salicylate on the native TRPM7 current in Jurkat T cells. The internal solution contained no added Mg^{2+}. **(B)** Repeated application of 10 mM salicylate in a Jurkat T cell. The internal solution contained 134 μM free [Mg^{2+}]. **(C,D)** I–V relations obtained in the absence and presence of 10 mM salicylate (first application) in HEK293 cells expressing WT **(C)** and S1107R **(D)** mTRPM7. **(E,F)** The time course of repeated salicylate applications in the same experiments as **(C,D)**, respectively. **(G)** Fraction of current block by 10 mM salicylate of WT and S1107R mutant mTRPM7 channels during second application of the drug (see **E,F**). Current amplitude was measured at the 30th ramp during drug application (I_{block}) and divided by the amplitude immediately before drug application ($I_{control}$). The current amplitudes were measured at −85 mV. The internal and external recording solutions were Cs^+ based. *$p < 0.05$, Student's pairwise t test.

TRPM7 is strongly dependent on intracellular free Mg^{2+} being inhibited by this ion with a double dose–response relationship with IC_{50} values of 10 μM and 165 μM (Chokshi et al., 2012b). Despite this, the majority of Jurkat T cells exhibit some degree of TRPM7 channel preactivation even without prior Mg^{2+} depletion (Chokshi et al., 2012b; Zhelay et al., 2018). This was observed in other cell types as well (Kozak and Cahalan, 2003). We performed a series of experiments with pipette solutions containing 134 μM free [Mg^{2+}]. Our goal was to compare NSAID inhibition in the presence and absence of intracellular Mg^{2+}, since normally in intact T cells free Mg^{2+} concentration is close to 1 mM (Rink et al., 1982; Ng et al., 1991). **Figure 7B** shows repeated application of 10 mM salicylate with intracellular Mg^{2+} present. The main difference from **Figure 7A** was the increased speed of inhibition and rundown with Mg^{2+} inside. The current completely ran down in ~30 min. Because of the fast rundown, it was impossible to completely reverse the inhibition. Also, it was difficult to assess the extent of block at third or fourth applications as it was already maximal but clearly, the second application of the drug was almost

twofold more potent than the first one. These experiments suggested that use-dependence of NSAID effect is increased with Mg^{2+} inside, which was reminiscent of inhibition by propionate (Zhelay et al., 2018). In conclusion, both the extent of inhibition by NSAIDs and the speed of action demonstrate strong use-dependence.

We reasoned that increased inhibition during repeated application of NSAIDs could potentially be due to increased acidification caused by repeated application of these drugs. To test this possibility, we set out to compare the pH_i during repeated application of the drugs. As shown in **Supplementary Figure S1A**, ibuprofen was applied repeatedly to Jurkat T cells loaded with BCECF dye and corresponding pH-dependent fluorescence signal measured. The degree of acidification caused by this drug appeared similar for each application. This experiment demonstrates that the use-dependence of TRPM7 inhibition discussed in **Figures 7A,B** cannot be explained by greater acidification with repeated drug applications but must have a different underlying mechanism. This mechanism might be PIP_2-dependent, as we found for propionate and 2-APB (Zhelay et al., 2018).

Salicylate Effect on WT and S1107R Mutant TRM7 Channels

Several Ser1107 substitutions in TRPM7 result in significantly reduced sensitivity to Mg^{2+}, acidic pH, and polyamines as well as PIP_2 depletion (Hofmann et al., 2014; Zhelay et al., 2018). If TRPM7 channel inhibition by NSAIDs is a consequence of cytosolic acidification, then TRPM7 S1107R mutant, which is less pH-sensitive, would be less sensitive to NSAID inhibition as well. In order to investigate this question, we compared salicylate effects on heterologously expressed WT and S1107R TRPM7 channels in HEK293 cells. We observed a robust and reversible inhibition of WT TRPM7 currents (**Figures 7C,D**), whereas S1107R variant was not inhibited (**Figures 7D,F,G**). We conclude from these experiments that NSAID inhibition of TRPM7 channels reflects the interference of acidic pH with PIP_2-channel interactions. In agreement with this, 30 mM salicylate inhibition of TRPM7 channels was relieved by application of 15 mM NH_4^+, which alkalinizes the cytosol ($n = 3$, data not shown). Interestingly, the endogenous current in HEK cells was significantly less sensitive to salicylate (**Figures 6A,C**) than the overexpressed TRPM7 channels in the same cell type (**Figures 7C,E**). This difference may be due to the dependence on TRPM7 kinase resting pH in HEK cells. We recently showed that in murine macrophages isolated from TRPM7 K1646R kinase-dead mice, the pH is more alkaline than in WT, suggesting that kinase activity may make pH_i more acidic (Beesetty et al., 2021). WT TRPM7 overexpressing HEK cells also respond readily to acidification in propionate and 2-APB (Zhelay et al., 2018). Although we have not tested NSAIDs directly in mammalian macrophages, they are likely to acidify the cytoplasm as is the case in *Drosophila S2* macrophages (**Figure 5**), leading to suppressed phagocytosis. Further investigations will be required to explain the difference between native and overexpressed TRPM7 current sensitivity to NSAIDs.

DISCUSSION

The present study was undertaken to characterize the effects of several common NSAIDs ibuprofen, naproxen, salicylate, and acetylsalicylate on TRPM7 channels. These drugs reversibly inhibited both native (Jurkat T cells) and recombinant TRPM7 at concentrations of 3 mM and higher (**Figures 1–3, 5**, **7**). The onset of inhibition was slow, taking several minutes, and voltage-independent, making it unlikely that these drugs interact directly with the ion permeation pathway (**Figures 1–3, 5**, **7**). In agreement with this, TRPM7 channels with the S1107R substitution in the intracellular portion (Zhelay et al., 2018) were insensitive to salicylate (**Figures 7D,F,G**). TRPM7 current reduction was readily reversible upon removal of the drug (**Figures 1–3, 5**, **7**). At concentrations of 300 μM and above, these NSAIDs potently and dose-dependently acidified the cytoplasm of Jurkat T cells (**Figures 4, 5**). Similar to channel inhibition, the onset of acidification was also slow. Since TRPM7 channels are inhibited by acidic pH (Chokshi et al., 2012b), cytosolic acidification is likely responsible for NSAID-mediated inhibition of these channels. Previously, we demonstrated that 2-APB, a widely used TRPM7 blocker, inhibits TRPM7 channels by the same mechanism (Chokshi et al., 2012a; Zhelay et al., 2018). In Jurkat T cells, TRPM7 pH_{50} is close to 7.1 in the absence of external divalent cations (RC and JAK, unpublished observations). In view of this, pH of ~7.0 would be sufficient to inhibit TRPM7 currents substantially. It should also be noted that pH dependence of TRPM7 channel activity is not constant but can vary with PIP_2 levels in the cell (Zhelay et al., 2018).

The observation that TRPM7 current reduction by acetylsalicylic acid (aspirin) was fully reversible at 10 mM (seen in three out of four cells tested, **Figure 5**), suggested that COX enzyme inactivation did not underlie this effect, since unlike other NSAIDs, aspirin binds and covalently modifies COX enzymes (Fitzpatrick, 2004). Furthermore, we tested the drugs in S2 cells, a *Drosophila* macrophage-like cell line (Abrams et al., 1992), lacking both COX and TRPM7 orthologs. Cytosolic acidifications were elicited in these cells by naproxen and salicylate (**Figure 5**), demonstrating that neither COX enzyme inhibition nor presence of TRPM7 protein is required for the pH effect.

What are some likely consequences of acidification and TRPM7 channel inhibition? As a non-selective cation conductance, TRPM7 channel activity is expected to push the T-cell membrane potential toward 0 mV (Chokshi et al., 2012b; Mason et al., 2012). A depolarization would be expected to diminish Ca^{2+} influx, curtailing the long-lasting Ca^{2+} elevations necessary for T-cell activation and clonal expansion (Feske et al., 2012). Ca^{2+} enters the activated T cell primarily through store-operated Ca^{2+}-release activated Ca^{2+} (CRAC) channels (e.g., Lioudyno et al., 2008). In human erythroleukemia cells, Mg^{2+}-inhibited cation (MIC) channels, likely TRPM7, participate in setting the membrane potential (Mason et al., 2012). Similarly, TRPM7 channels would be expected to depolarize T cells. The T-cell membrane potential is primarily determined by potassium-selective conductances (Feske et al., 2012; Papp et al., 2020). However, significant pre-activated TRPM7 currents can be measured in Jurkat T cells even without prior depletion of Mg^{2+} (Chokshi et al., 2012b) and would likely participate

in moving the membrane potential away from K^+ equilibrium potential. Depolarized T-cell membranes reduce Ca^{2+} entry and consequently diminish the activation of nuclear factor of activated T cells (NFAT) transcription factors, responsible for governing many gene expression events in T-cell activation and proliferation (Feske et al., 2012; Yeh and Parekh, 2017). For a related cation channel TRPM4, its genetic suppression in Jurkat T cells resulted in increased Ca^{2+} entry and IL2 production (Launay et al., 2004). Pharmacological blockade of TRPM7 channels resulted in increased IL2 receptor expression and higher number of regulatory T cells in mice (Mendu et al., 2020). Based on these examples, the inhibition of TRPM7 channels by NSAIDs would be expected to increase Ca^{2+} influx, NFAT activation, IL2 secretion and T-cell proliferation. It remains to be determined, however, what the overall NSAID effect on the membrane potential is, given that other pH-sensitive conductances, such as Kv1.3, are likely to be affected (Deutsch and Lee, 1989). In this context, it is noteworthy that pharmacological inhibition of Kv1.3 has been explored as immunomodulatory therapy for various disease states (e.g., Beeton et al., 2001; Schmalhofer et al., 2002; Rangaraju et al., 2009). In the final analysis, the action of NSAIDs on T-cell membrane potential and calcium signaling will depend on the interplay between activity of various channels and their relative pH sensitivity as well as the effects of NSAIDs on Ca^{2+} metabolism reported previously (e.g., Weiss et al., 2001; Chen et al., 2010; Villalonga et al., 2010; Munoz et al., 2011).

During repeated applications of the drugs, the inhibitory effect on TRPM7 currents increased in potency, what we refer to as use-dependence (**Figures 7A,B,E**). Repeated treatment of intact cells with NSAIDs, however, did not result in progressively more cytoplasmic acidification and, therefore, could not explain the use-dependence of channel blockade (**Supplementary Figure S1**). TRPM7 channels are inhibited by Mg^{2+} in a use-dependent fashion: applications of the same concentration of Mg^{2+} to inside-out patches resulted in progressively more potent inhibition, a form of sensitization to Mg^{2+} (Chokshi et al., 2012c). This use-dependence of Mg^{2+} inhibition was similar to what was observed with propionate (Zhelay et al., 2018), and we explain it by gradual depletion of PIP_2 from channel vicinity and increased potency of cations in disrupting PIP_2-channel interactions. In agreement with this, propionate-induced channel inhibition showed use-dependence only in whole-cell, which favors PIP_2 loss but not in perforated-patch recording configuration, which preserves PIP_2 (Zhelay et al., 2018). The extent of channel inhibition was drastically increased in cells depleted of PIP_2 by VSP expression (**Figure 6**). S1107R TRPM7 channels, which are less sensitive to inhibition by protons, were insensitive to salicylate, confirming that cytosolic acidification is responsible for the observed current inhibition (**Figure 7**; Zhelay et al., 2018). Whether the extent of cytosolic acidification depends on the levels of PIP_2 in the cell membrane remains to be examined.

In T cells, significant PIP_2 depletion can occur during T cell receptor (TCR) engagement, when phospholipase C gamma is activated and hydrolyzes PIP_2 (Kane et al., 2000). The increasing potency of block with repeated application may be relevant for long-term administration of these drugs, prescribed in gout and rheumatoid arthritis (Rider and Jordan, 2010) and for specific NSAIDs with long pharmacokinetic half-life, such as naproxen (Sugar et al., 2019). In AERD, where long-term aspirin regiments are assigned to patients as a desensitization therapy (Williams and Woessner, 2008), the use-dependence of NSAID effects may also become significant.

In the present study, we confined our analysis to NSAID inhibition of TRPM7 channels in the absence of extracellular divalent cations (Ca^{2+} and Mg^{2+}). In their presence, addition of NSAIDs resulted in a reduction in tonic voltage-dependent block by divalent cations and change in the I–V relation due to the chelating action of these weak acids (data not shown; Kozak et al., 2002; Kozak and Cahalan, 2003).

We found that significant cytosolic acidification was evident at concentrations of NSAIDs lower than those required for TRPM7 channel inhibition. Thus, at 300 μM and 1 mM, cytosolic acidification was observed, but the channel activity was not inhibited at these concentrations. An important difference between these assays, however, was that in whole-cell patch clamp we used 1 mM internal HEPES buffer which is not present in intact cells during pH measurement. The presence of HEPES, as well as weak acid glutamate, would be expected to counteract (buffer) cytosolic acidifications induced by NSAIDs. It is likely therefore, that in an intact cell, TRPM7 channels would be inhibited by lower NSAIDs concentrations, routinely achieved in blood plasma under NSAID regiments (Jung and Schwartz, 1994; Huntjens et al., 2006; Capone et al., 2007a,b). It is also likely that other ion channels sensitive to cytosolic acidification, such as TRPM3, Kir4.1, and connexins would be affected by these drugs (Pethő et al., 2020).

The focus of this study is on the acute and not long-term effects of NSAIDs on cellular pH. We also tested long-term naproxen and salicylate exposure on Jurkat T-cell viability and found that at concentrations sufficient to inhibit TRPM7, there was a significant cytotoxicity over a 24-h time period. Thus, at 3 mM, the mean cell viability dropped to ~70% and at 10 mM, to ~50% (**Supplementary Figure S1B**). By contrast, 10 mM salicylate effect was modest, reaching ~85% viability (**Supplementary Figure S1C**). It has been reported that naproxen at 0.1–0.4 mM interfered with proliferation of seal lymphocytes without causing apoptosis (Kleinert et al., 2018). Further experiments will be required to elucidate if long-term NSAID cytotoxicity and immunotoxicity are due to acidification or other mechanisms.

DATA AVAILABILITY STATEMENT

The raw data supporting the conclusions of this article will be made available by the authors, without undue reservation.

AUTHOR CONTRIBUTIONS

RC, OB, and TZ performed the experiments and analyzed the data. JK conceived the study, designed the experiments, and wrote and edited the manuscript. All authors contributed to the article and approved the submitted version.

FUNDING

This work was funded by grants 1R15AI090613, 1R01AI114804, and 1R21AI144337 from the National Institute of Allergy and Infectious Diseases (to JK).

ACKNOWLEDGMENTS

We thank Masayuki Matsushita for providing the wildtype pEGFP-mTRPM7 plasmid, Siham Hourani and Shreya Jitendrakumar Patel for excellent technical assistance, and Mark M. Rich and Jananie Rockwood for useful comments on an earlier version of the manuscript. Wildtype and C363S mutant Ciona VSP plasmids in pIRES2-EGFP vector were the kind gift of Yasushi Okamura, Osaka University, Japan.

SUPPLEMENTARY MATERIAL

The Supplementary Material for this article can be found online at: https://www.frontiersin.org/articles/10.3389/fphys.2021.727549/full#supplementary-material

Supplementary Figure S1 | Effect of repeated application of ibuprofen on the degree of acidification. Effects of naproxen and salicylate on cell viability. **(A)** 10 mM ibuprofen-Na^+ was applied to BCECF-loaded Jurkat T cells three times sequentially followed by washes. There was no change in the extent of acidification (F 490 nm / 440 nm) during repeated application of the drug. **(B)** Jurkat T-cell viability was measured after a 24-hour incubation in the absence (control) or presence of 0.3, 3 and 10 mM naproxen-Na^+. Each bar represents the percentage of cells (mean, SEM) which excluded trypan blue dye. **(C)** Mean Jurkat T-cell viability after a 24-hour incubation in the absence and presence of 0.3, 3 and 10 mM salicylate. Asterisks in **(B)** and **(C)** indicate significant differences compared to the control (Student's paired t test).

REFERENCES

Abrams, J. M., Lux, A., Steller, H., and Krieger, M. (1992). Macrophages in *Drosophila* embryos and L2 cells exhibit scavenger receptor-mediated endocytosis. *Proc. Natl. Acad. Sci. U. S. A.* 89, 10375–10379.

Aisen, P. S., Schafer, K. A., Grundman, M., Pfeiffer, E., Sano, M., Davis, K. L., et al. (2003). Effects of rofecoxib or naproxen vs placebo on Alzheimer disease progression: a randomized controlled trial. *JAMA* 289, 2819–2826. doi: 10.1001/jama.289.21.2819

Beesetty, P., Rockwood, J., Kaitsuka, T., Zhelay, T., Hourani, S., Matsushita, M., et al. (2021). Phagocytic activity of splenic macrophages is enhanced and accompanied by cytosolic alkalinization in TRPM7 kinase-dead mice. *FEBS J.* 288, 3585–3601. doi: 10.1111/febs.15683

Beeton, C., Barbaria, J., Giraud, P., Devaux, J., Benoliel, A. M., Gola, M., et al. (2001). Selective blocking of voltage-gated K^+ channels improves experimental autoimmune encephalomyelitis and inhibits T cell activation. *J. Immunol.* 166, 936–944. doi: 10.4049/jimmunol.166.2.936

Berges-Gimeno, M. P., Simon, R. A., and Stevenson, D. D. (2002). The natural history and clinical characteristics of aspirin-exacerbated respiratory disease. *Ann. Allergy Asthma Immunol.* 89, 474–478. doi: 10.1016/S1081-1206(10)62084-4

Bishay, P., Schmidt, H., Marian, C., Haussler, A., Wijnvoord, N., Ziebell, S., et al. (2010). R-flurbiprofen reduces neuropathic pain in rodents by restoring endogenous cannabinoids. *PLoS One* 5:e10628. doi: 10.1371/journal.pone.0010628

Bowser, D. N., Cody, S. H., Dubbin, P. N., and Williams, D. A. (1999). "Introducing and calibrating fluorescent probes in cells and organelles," in *Fluorescent and Luminescent Probes for Biological Activity. 2nd Edn.* ed. W. T. Mason (San Diego, London, Boston, New York, Sydney, Tokyo, Toronto: Academic Press), 65–81.

Burke, A., Smyth, E. M., and Fitzgerald, G. A. (2006). "Analgesic-antypyretic agents; pharmacotherapy of gout," in *The Pharmacological Basis of Therapeutics. 11th Edn.* ed. L. L. Brunton (New York, Chicago, San Francisco: McGraw-Hill), 671–715.

Capone, M. L., Tacconelli, S., Di Francesco, L., Sacchetti, A., Sciulli, M. G., and Patrignani, P. (2007a). Pharmacodynamic of cyclooxygenase inhibitors in humans. *Prostaglandins Other Lipid Mediat.* 82, 85–94. doi: 10.1016/j.prostaglandins.2006.05.019

Capone, M. L., Tacconelli, S., Sciulli, M. G., Anzellotti, P., Di Francesco, L., Merciaro, G., et al. (2007b). Human pharmacology of naproxen sodium. *J. Pharmacol. Exp. Ther.* 322, 453–460. doi: 10.1124/jpet.107.122283

Chen, S. T., Thomas, S., Gaffney, K. J., Louie, S. G., Petasis, N. A., and Schonthal, A. H. (2010). Cytotoxic effects of celecoxib on Raji lymphoma cells correlate with aggravated endoplasmic reticulum stress but not with inhibition of cyclooxygenase-2. *Leuk. Res.* 34, 250–253. doi: 10.1016/j.leukres.2009.09.028

Cherbas, L., and Cherbas, P. (2007). Drosophila cell culture and transformation. *CSH Protoc.* 2007:pdb.top6. doi: 10.1101/pdb.top6

Chokshi, R., Fruasaha, P., and Kozak, J. A. (2012a). 2-Aminoethyl diphenyl borinate (2-APB) inhibits TRPM7 channels through an intracellular acidification mechanism. *Channels* 6, 362–369. doi: 10.4161/chan.21628

Chokshi, R., Matsushita, M., and Kozak, J. A. (2012b). Detailed examination of Mg^{2+} and pH sensitivity of human TRPM7 channels. *Am. J. Phys. Cell Phys.* 302, C1004–C1011. doi: 10.1152/ajpcell.00422.2011

Chokshi, R., Matsushita, M., and Kozak, J. A. (2012c). Sensitivity of TRPM7 channels to Mg^{2+} characterized in cell-free patches of Jurkat T lymphocytes. *Am. J. Phys. Cell Phys.* 302, C1642–C1651. doi: 10.1152/ajpcell.00037.2012

Chubanov, V., Mittermeier, L., and Gudermann, T. (2018). Role of kinase-coupled TRP channels in mineral homeostasis. *Pharmacol. Ther.* 184, 159–176. doi: 10.1016/j.pharmthera.2017.11.003

Deason-Towne, F., Perraud, A. L., and Schmitz, C. (2011). The Mg^{2+} transporter MagT1 partially rescues cell growth and Mg^{2+} uptake in cells lacking the channel-kinase TRPM7. *FEBS Lett.* 585, 2275–2278. doi: 10.1016/j.febslet.2011.05.052

Deutsch, C., and Lee, S. C. (1989). Modulation of K^+ currents in human lymphocytes by pH. *J. Physiol.* 413, 399–413. doi: 10.1113/jphysiol.1989.sp017660

Feske, S., Skolnik, E. Y., and Prakriya, M. (2012). Ion channels and transporters in lymphocyte function and immunity. *Nat. Rev. Immunol.* 12, 532–547. doi: 10.1038/nri3233

Firth, J. (2012). Rheumatoid arthritis: treating to target with disease-modifying drugs. *Br. J. Nurs.* 20, 1240–1245. doi: 10.12968/bjon.2011.20.19.1240

Fitzpatrick, F. A. (2004). Cyclooxygenase enzymes: regulation and function. *Curr. Pharm. Des.* 10, 577–588. doi: 10.2174/1381612043453144

Freichel, M., Almering, J., and Tsvilovskyy, V. (2012). The role of TRP proteins in mast cells. *Front. Immunol.* 3:150. doi: 10.3389/fimmu.2012.00150

Frolov, R. V., Berim, I. G., and Singh, S. (2008a). Inhibition of delayed rectifier potassium channels and induction of arrhythmia: a novel effect of celecoxib and the mechanism underlying it. *J. Biol. Chem.* 283, 1518–1524. doi: 10.1074/jbc.M708100200

Frolov, R. V., Slaughter, M. M., and Singh, S. (2008b). Effects of celecoxib on ionic currents and spontaneous firing in rat retinal neurons. *Neuroscience* 154, 1525–1532. doi: 10.1016/j.neuroscience.2008.05.004

Gibson, J. N., Beesetty, P., Sulentic, C., and Kozak, J. A. (2016). Rapid quantification of mitogen-induced blastogenesis in T lymphocytes for identifying immunomodulatory drugs. *J. Vis. Exp.* 118:55212. doi: 10.3791/55212

Hermosura, M. C., Monteilh-Zoller, M. K., Scharenberg, A. M., Penner, R., and Fleig, A. (2002). Dissociation of the store-operated calcium current I(CRAC) and the mg-nucleotide-regulated metal ion current MagNuM. *J. Physiol.* 539, 445–458. doi: 10.1113/jphysiol.2001.013361

Hofmann, T., Schafer, S., Linseisen, M., Sytik, L., Gudermann, T., and Chubanov, V. (2014). Activation of TRPM7 channels by small molecules under physiological conditions. *Pflugers Arch. Eur. J. Physiol.* 466, 2177–2189. doi: 10.1007/s00424-014-1488-0

Huang, L., Ng, N. M., Chen, M., Lin, X., Tang, T., Cheng, H., et al. (2014). Inhibition of TRPM7 channels reduces degranulation and release of cytokines in rat bone marrow-derived mast cells. *Int. J. Mol. Sci.* 15, 11817–11831. doi: 10.3390/ijms150711817

Huntjens, D. R., Spalding, D. J., Danhof, M., and Della Pasqua, O. E. (2006). Correlation between in vitro and in vivo concentration-effect relationships of naproxen in rats and healthy volunteers. *Br. J. Pharmacol.* 148, 396–404. doi: 10.1038/sj.bjp.0706737

Jiang, X., Newell, E. W., and Schlichter, L. C. (2003). Regulation of a TRPM7-like current in rat brain microglia. *J. Biol. Chem.* 278, 42867–42876. doi: 10.1074/jbc.M304487200

Jung, D., and Schwartz, K. E. (1994). Steady-state pharmacokinetics of enteric-coated naproxen tablets compared with standard naproxen tablets. *Clin. Ther.* 16, 923–929.

Kaitsuka, T., Katagiri, C., Beesetty, P., Nakamura, K., Hourani, S., Tomizawa, K., et al. (2014). Inactivation of TRPM7 kinase activity does not impair its channel function in mice. *Sci. Rep.* 4:5718. doi: 10.1038/srep05718

Kane, L. P., Lin, J., and Weiss, A. (2000). Signal transduction by the TCR for antigen. *Curr. Opin. Immunol.* 12, 242–249. doi: 10.1016/S0952-7915(00)00083-2

Kleinert, C., Lacaze, E., Fortier, M., Hammill, M., De Guise, S., and Fournier, M. (2018). T lymphocyte-proliferative responses of harbor seal (Phoca vitulina) peripheral blood mononuclear cells (PBMCs) exposed to pharmaceuticals in vitro. *Mar. Pollut. Bull.* 127, 225–234. doi: 10.1016/j.marpolbul.2017.12.001

Kong, J. S., Teuber, S. S., and Gershwin, M. E. (2007). Aspirin and nonsteroidal anti-inflammatory drug hypersensitivity. *Clin. Rev. Allergy Immunol.* 32, 97–110. doi: 10.1007/BF02686086

Kozak, J. A., and Cahalan, M. D. (2003). MIC channels are inhibited by internal divalent cations but not ATP. *Biophys. J.* 84, 922–927. doi: 10.1016/S0006-3495(03)74909-1

Kozak, J. A., Kerschbaum, H. H., and Cahalan, M. D. (2002). Distinct properties of CRAC and MIC channels in RBL cells. *J. Gen. Physiol.* 120, 221–235. doi: 10.1085/jgp.20028601

Kozak, J. A., Matsushita, M., Nairn, A. C., and Cahalan, M. D. (2005). Charge screening by internal pH and polyvalent cations as a mechanism for activation, inhibition, and rundown of TRPM7/MIC channels. *J. Gen. Physiol.* 126, 499–514. doi: 10.1085/jgp.200509324

Krishnamoorthy, M., Buhari, F. H. M., Zhao, T., Brauer, P. M., Burrows, K., Cao, E. Y., et al. (2018). The ion channel TRPM7 is required for B cell lymphopoiesis. *Sci. Signal.* 11:eaan2693. doi: 10.1126/scisignal.aan2693

Launay, P., Cheng, H., Srivatsan, S., Penner, R., Fleig, A., and Kinet, J. P. (2004). TRPM4 regulates calcium oscillations after T cell activation. *Science* 306, 1374–1377. doi: 10.1126/science.1098845

Li, J., Zhang, N., Ye, B., Ju, W., Orser, B., Fox, J. E., et al. (2007). Non-steroidal anti-inflammatory drugs increase insulin release from beta cells by inhibiting ATP-sensitive potassium channels. *Br. J. Pharmacol.* 151, 483–493. doi: 10.1038/sj.bjp.0707259

Lim, G. P., Yang, F., Chu, T., Chen, P., Beech, W., Teter, B., et al. (2000). Ibuprofen suppresses plaque pathology and inflammation in a mouse model for Alzheimer's disease. *J. Neurosci.* 20, 5709–5714. doi: 10.1523/JNEUROSCI.20-15-05709.2000

Lioudyno, M. I., Kozak, J. A., Penna, A., Safrina, O., Zhang, S. L., Sen, D., et al. (2008). Orai1 and STIM1 move to the immunological synapse and are up-regulated during T cell activation. *Proc. Natl. Acad. Sci. U. S. A.* 105, 2011–2016. doi: 10.1073/pnas.0706122105

Manning, G., Plowman, G. D., Hunter, T., and Sudarsanam, S. (2002). Evolution of protein kinase signaling from yeast to man. *Trends Biochem. Sci.* 27, 514–520. doi: 10.1016/S0968-0004(02)02179-5

Mason, M. J., Schaffner, C., Floto, R. A., and Teo, Q. A. (2012). Constitutive expression of a Mg^{2+}–inhibited K^+ current and a TRPM7-like current in human erythroleukemia cells. *Am. J. Physiol. Cell Physiol.* 302, C853–C867. doi: 10.1152/ajpcell.00071.2011

Matsushita, M., Kozak, J. A., Shimizu, Y., Mclachlin, D. T., Yamaguchi, H., Wei, F. Y., et al. (2005). Channel function is dissociated from the intrinsic kinase activity and autophosphorylation of TRPM7/ChaK1. *J. Biol. Chem.* 280, 20793–20803. doi: 10.1074/jbc.M413671200

Mcgeer, E. G., and Mcgeer, P. L. (2001a). Chronic inflammation in Alzheimer's disease offers therapeutic opportunities. *Expert. Rev. Neurother.* 1, 53–60. doi: 10.1586/14737175.1.1.53

Mcgeer, P. L., and Mcgeer, E. G. (2001b). Inflammation, autotoxicity and Alzheimer disease. *Neurobiol. Aging* 22, 799–809. doi: 10.1016/s0197-4580(01)00289-5

Mellott, A., Rockwood, J., Zhelay, T., Luu, C. T., Kaitsuka, T., and Kozak, J. A. (2020). TRPM7 channel activity in Jurkat T lymphocytes during magnesium depletion and loading: implications for divalent metal entry and cytotoxicity. *Pflugers Arch. Eur. J. Physiol.* 472, 1589–1606. doi: 10.1007/s00424-020-02457-3

Mendu, S. K., Stremska, M. E., Schappe, M. S., Moser, E. K., Krupa, J. K., Rogers, J. S., et al. (2020). Targeting the ion channel TRPM7 promotes the thymic development of regulatory T cells by promoting IL-2 signaling. *Sci. Signal.* 13:eabb0619. doi: 10.1126/scisignal.abb0619

Munoz, E., Valero, R. A., Quintana, A., Hoth, M., Nunez, L., and Villalobos, C. (2011). Nonsteroidal anti-inflammatory drugs inhibit vascular smooth muscle cell proliferation by enabling the Ca2+−dependent inactivation of calcium release-activated calcium/orai channels normally prevented by mitochondria. *J. Biol. Chem.* 286, 16186–16196. doi: 10.1074/jbc.M110.198952

Namikawa, M., Sano, A., and Tateno, T. (2017). Salicylate-induced suppression of electrically driven activity in brain slices from the auditory cortex of aging mice. *Front. Aging Neurosci.* 9:395. doi: 10.3389/fnagi.2017.00395

Negulescu, P. A., and Machen, T. E. (1990). Intracellular ion activities and membrane transport in parietal cells measured with fluorescent dyes. *Methods Enzymol.* 192, 38–81.

Ng, L. L., Davies, J. E., and Garrido, M. C. (1991). Intracellular free magnesium in human lymphocytes and the response to lectins. *Clin. Sci.* 80, 539–547. doi: 10.1042/cs0800539

Nozadze, I., Tsiklauri, N., Gurtskaia, G., and Tsagareli, M. G. (2016). NSAIDs attenuate hyperalgesia induced by TRP channel activation. *Data Brief* 6, 668–673. doi: 10.1016/j.dib.2015.12.055

O'Connor, N., and Silver, R. B. (2007). Ratio imaging: practical considerations for measuring intracellular Ca2+ and pH in living cells. *Methods Cell Biol.* 81, 415–433. doi: 10.1016/S0091-679X(06)81019-8

Papp, F., Hajdu, P., Tajti, G., Toth, A., Nagy, E., Fazekas, Z., et al. (2020). Periodic membrane potential and Ca(2+) oscillations in T cells forming an immune synapse. *Int. J. Mol. Sci.* 21:1568. doi: 10.3390/ijms21051568

Park, S. Y., Kim, T. H., Kim, H. I., Shin, Y. K., Lee, C. S., Park, M., et al. (2007). Celecoxib inhibits Na+ currents in rat dorsal root ganglion neurons. *Brain Res.* 1148, 53–61. doi: 10.1016/j.brainres.2007.02.023

Pethő, Z., Najder, K., Carvalho, T., Mcmorrow, R., Todesca, L. M., Rugi, M., et al. (2020). pH-channeling in cancer: how pH-dependence of cation channels shapes cancer pathophysiology. *Cancers* 12:2484. doi: 10.3390/cancers12092484

Prakriya, M., and Lewis, R. S. (2002). Separation and characterization of currents through store-operated CRAC channels and Mg(2+)-inhibited cation (MIC) channels. *J. Gen. Physiol.* 119, 487–507. doi: 10.1085/jgp.20028551

Rangaraju, S., Chi, V., Pennington, M. W., and Chandy, K. G. (2009). Kv1.3 potassium channels as a therapeutic target in multiple sclerosis. *Expert Opin. Ther. Targets* 13, 909–924. doi: 10.1517/14728220903018957

Rider, T. G., and Jordan, K. M. (2010). The modern management of gout. *Rheumatology (Oxford)* 49, 5–14. doi: 10.1093/rheumatology/kep306

Rink, T. J., Tsien, R. Y., and Pozzan, T. (1982). Cytoplasmic pH and free Mg^{2+} in lymphocytes. *J. Cell Biol.* 95, 189–196. doi: 10.1083/jcb.95.1.189

Rohacs, T. (2014). Phosphoinositide regulation of TRP channels. *Handb. Exp. Pharmacol.* 223, 1143–1176. doi: 10.1007/978-3-319-05161-1_18

Schmalhofer, W. A., Bao, J., Mcmanus, O. B., Green, B., Matyskiela, M., Wunderler, D., et al. (2002). Identification of a new class of inhibitors of the voltage-gated potassium channel, Kv1.3, with immunosuppressant properties. *Biochemistry* 41, 7781–7794. doi: 10.1021/bi025722c

Schonthal, A. H. (2010). Exploiting cyclooxygenase-(in)dependent properties of COX-2 inhibitors for malignant glioma therapy. *Anti Cancer Agents Med. Chem.* 10, 450–461. doi: 10.2174/1871520611009060450

Shiff, S. J., Koutsos, M. I., Qiao, L., and Rigas, B. (1996). Nonsteroidal antiinflammatory drugs inhibit the proliferation of colon adenocarcinoma cells: effects on cell cycle and apoptosis. *Exp. Cell Res.* 222, 179–188. doi: 10.1006/excr.1996.0023

Shiff, S. J., Qiao, L., Tsai, L. L., and Rigas, B. (1995). Sulindac sulfide, an aspirin-like compound, inhibits proliferation, causes cell cycle quiescence, and induces apoptosis in HT-29 colon adenocarcinoma cells. *J. Clin. Invest.* 96, 491–503. doi: 10.1172/JCI118060

Shiff, S. J., and Rigas, B. (1999). Aspirin for cancer. *Nat. Med.* 5, 1348–1349. doi: 10.1038/70909

Sugar, D., Francombe, D., da Silva, T., Adams, R., and Hutchings, S. (2019). Bioequivalence of 2 naproxen sodium tablet formulations in healthy male and female volunteers. *Curr. Ther. Res. Clin. Exp.* 90, 33–38. doi: 10.1016/j.curtheres.2019.01.004

Suh, B. C., and Hille, B. (2008). PIP2 is a necessary cofactor for ion channel function: how and why? *Annu. Rev. Biophys.* 37, 175–195. doi: 10.1146/annurev.biophys.37.032807.125859

Tegeder, I., Pfeilschifter, J., and Geisslinger, G. (2001). Cyclooxygenase-independent actions of cyclooxygenase inhibitors. *FASEB J.* 15, 2057–2072. doi: 10.1096/fj.01-0390rev

Trepanier, C. H., and Milgram, N. W. (2010). Neuroinflammation in Alzheimer's disease: are NSAIDs and selective COX-2 inhibitors the next line of therapy? *J. Alzheimers Dis.* 21, 1089–1099. doi: 10.3233/JAD-2010-090667

Tsagareli, M. G., Nozadze, I., Tsiklauri, N., and Gurtskaia, G. (2018). Non-steroidal anti-inflammatory drugs attenuate agonist-evoked activation of transient receptor potential channels. *Biomed. Pharmacother.* 97, 745–751. doi: 10.1016/j.biopha.2017.10.131

Vane, J. R. (1971). Inhibition of prostaglandin synthesis as a mechanism of action for aspirin-like drugs. *Nat. New Biol.* 231, 232–235. doi: 10.1038/newbio231232a0

Villalobos, C., Sobradillo, D., Hernandez-Morales, M., and Nunez, L. (2017). Calcium remodeling in colorectal cancer. *Biochim. Biophys. Acta Mol. Cell Res.* 1864, 843–849. doi: 10.1016/j.bbamcr.2017.01.005

Villalonga, N., David, M., Bielanska, J., Gonzalez, T., Parra, D., Soler, C., et al. (2010). Immunomodulatory effects of diclofenac in leukocytes through the targeting of Kv1.3 voltage-dependent potassium channels. *Biochem. Pharmacol.* 80, 858–866. doi: 10.1016/j.bcp.2010.05.012

Voilley, N. (2004). Acid-sensing ion channels (ASICs): new targets for the analgesic effects of non-steroid anti-inflammatory drugs (NSAIDs). *Curr. Drug Targets Inflamm. Allergy* 3, 71–79. doi: 10.2174/1568010043483980

Wang, W., Ye, S. D., Zhou, K. Q., Wu, L. M., and Huang, Y. N. (2012). High doses of salicylate and aspirin are inhibitory on acid-sensing ion channels and protective against acidosis-induced neuronal injury in the rat cortical neuron. *J. Neurosci. Res.* 90, 267–277. doi: 10.1002/jnr.22742

Wei, L., Ding, D., and Salvi, R. (2010). Salicylate-induced degeneration of cochlea spiral ganglion neurons-apoptosis signaling. *Neuroscience* 168, 288–299. doi: 10.1016/j.neuroscience.2010.03.015

Weiss, H., Amberger, A., Widschwendter, M., Margreiter, R., Ofner, D., and Dietl, P. (2001). Inhibition of store-operated calcium entry contributes to the anti-proliferative effect of non-steroidal anti-inflammatory drugs in human colon cancer cells. *Int. J. Cancer* 92, 877–882. doi: 10.1002/ijc.1280

Williams, A. N., and Woessner, K. M. (2008). The clinical effectiveness of aspirin desensitization in chronic rhinosinusitis. *Curr. Allergy Asthma Rep.* 8, 245–252. doi: 10.1007/s11882-008-0041-7

Woessner, K. M. (2003). Crossreacting drugs and chemicals. *Clin. Rev. Allergy Immunol.* 24, 149–158. doi: 10.1385/CRIAI:24:2:149

Yeh, Y. C., and Parekh, A. B. (2017). "CRAC channels and Ca(2+)-dependent gene expression," in *Calcium Entry Channels in Non-excitable Cells*. eds. J. A. Kozak and J. W. Putney (Boca Raton, FL: Taylor & Francis), 93–106.

Yudin, Y., Liu, L., Nagwekar, J., and Rohacs, T. (2021). Methods to study phosphoinositide regulation of ion channels. *Methods Enzymol.* 652, 49–79. doi: 10.1016/bs.mie.2021.01.025

Zhelay, T., Wieczerzak, K. B., Beesetty, P., Alter, G. M., Matsushita, M., and Kozak, J. A. (2018). Depletion of plasma membrane-associated phosphoinositides mimics inhibition of TRPM7 channels by cytosolic Mg(2+), spermine, and pH. *J. Biol. Chem.* 293, 18151–18167. doi: 10.1074/jbc.RA118.004066

Zou, Z. G., Rios, F. J., Montezano, A. C., and Touyz, R. M. (2019). TRPM7, magnesium, and signaling. *Int. J. Mol. Sci.* 20:1877. doi: 10.3390/ijms20081877

Conflict of Interest: The authors declare that the research was conducted in the absence of any commercial or financial relationships that could be construed as a potential conflict of interest.

Publisher's Note: All claims expressed in this article are solely those of the authors and do not necessarily represent those of their affiliated organizations, or those of the publisher, the editors and the reviewers. Any product that may be evaluated in this article, or claim that may be made by its manufacturer, is not guaranteed or endorsed by the publisher.

frontiers in Physiology

ORIGINAL RESEARCH
published: 26 November 2021
doi: 10.3389/fphys.2021.728625

Excessive Accumulation of Intracellular Ca^{2+} After Acute Exercise Potentiated Impairment of T-cell Function

*Renyi Liu[1,2], Karsten Krüger[2], Christian Pilat[2], Wei Fan[3], Yu Xiao[3], Michael Seimetz[4], Robert Ringseis[5], Eveline Baumgart-Vogt[3], Klaus Eder[5], Norbert Weissmann[4] and Frank Christoph Mooren[6]**

[1]Department of Physical Education, China University of Geosciences (Wuhan), Wuhan, China, [2]Department of Exercise Physiology and Sports Therapy, Institute of Sports Science, Justus-Liebig-University Giessen, Giessen, Germany, [3]Institute for Anatomy and Cell Biology II, Justus-Liebig-University Giessen, Giessen, Germany, [4]Excellence Cluster Cardio-Pulmonary Institute (CPI), Universities of Giessen and Marburg Lung Center (UGMLC), Member of the German Lung Center (DZL), Justus-Liebig-University Giessen, Giessen, Germany, [5]Institute of Animal Nutrition and Nutrition Physiology, Justus-Liebig-University Giessen, Giessen, Germany, [6]Department of Rehabilitation Sciences, Faculty of Health, University of Witten/Herdecke, Witten, Germany

OPEN ACCESS

Edited by:
Ildikò Szabò,
University of Padua, Italy

Reviewed by:
Ameet A. Chimote,
University of Cincinnati,
United States
Olivier Dellis,
Institut National de la Santé et de la Recherche Médicale (INSERM),
France

***Correspondence:**
Frank Christoph Mooren
frank.mooren@uni-wh.de

Specialty section:
This article was submitted to Membrane Physiology and Membrane Biophysics, a section of the journal Frontiers in Physiology

Received: 21 June 2021
Accepted: 18 October 2021
Published: 26 November 2021

Citation:
Liu R, Krüger K, Pilat C, Fan W, Xiao Y, Seimetz M, Ringseis R, Baumgart-Vogt E, Eder K, Weissmann N and Mooren FC (2021) Excessive Accumulation of Intracellular Ca^{2+} After Acute Exercise Potentiated Impairment of T-cell Function. Front. Physiol. 12:728625. doi: 10.3389/fphys.2021.728625

Ca^{2+} is an important intracellular second messenger known to regulate several cellular functions. This research aimed to investigate the mechanisms of exercise-induced immunosuppression by measuring intracellular calcium levels, Ca^{2+}-regulating gene expression, and agonist-evoked proliferation of murine splenic T lymphocytes. Mice were randomly assigned to the control, sedentary group (C), and three experimental groups, which performed a single bout of intensive and exhaustive treadmill exercise. Murine splenic lymphocytes were separated by density-gradient centrifugation immediately (E0), 3 h (E3), and 24 h after exercise (E24). Fura-2/AM was used to monitor cytoplasmic free Ca^{2+} concentration in living cells. The combined method of carboxyfluorescein diacetate succinimidyl ester (CFSE) labeling and flow cytometry was used for the detection of T cell proliferation. The transcriptional level of Ca^{2+}-regulating genes was quantified by using qPCR. Both basal intracellular Ca^{2+} levels and agonist (ConA, OKT3, or thapsigargin)-induced Ca^{2+} transients were significantly elevated at E3 group ($p < 0.05$ vs. control). However, mitogen-induced cell proliferation was significantly decreased at E3 group ($p < 0.05$ vs. control). In parallel, the transcriptional level of plasma membrane Ca^{2+}-ATPases (PMCA), sarco/endoplasmic reticulum Ca^{2+}-ATPases (SERCA), TRPC1, and P2X7 was significantly downregulated, and the transcriptional level of IP_3R2 and RyR2 was significantly upregulated in E3 ($p < 0.01$ vs. control). In summary, this study demonstrated that acute exercise affected intracellular calcium homeostasis, most likely by enhancing transmembrane Ca^{2+} influx into cells and by reducing expression of Ca^{2+}-ATPases such as PMCA and SERCA. However, altered Ca^{2+} signals were not transduced into an enhanced T cell proliferation suggesting other pathways to be responsible for the transient exercise-associated immunosuppression.

Keywords: acute exercise, Fura-2(AM), intracellular Ca^{2+}, calcium homeostasis, cell proliferation, calcium channels

INTRODUCTION

Exercise can enhance marked transient physiological changes and has a profound influence on the human immune function. There are a number of studies showing that the effects of acute exhaustive exercise seem to be detrimental, while regular, moderate-intensity physical activity can improve immune defense functions. There is evidence that the transient "open-window" of immunosuppression might exist in the recovery from strenuous exercise as indicated by an impaired immunity around 3–72 h after exercise when athletes seem to be more susceptible to infections. However, this consensus meaning has been disagreed recently due to novel findings demonstrating that exercise stimulates T cell redistribution within organs and tissues, enhances mobilization of hematopoietic stem cells as a result of apoptotic T cells, and reverses T cell immunosenescence (Simpson et al., 2020). Therefore, the effect of a single bout of intensive exercise on immune function remains a controversial topic, and the investigation of underlying molecular mechanisms seems to be a helpful approach to enhance our current understanding.

Ca^{2+} is a key second messenger in the network of cellular signal transduction, which participates in many physiological and pathological processes. The stress of exercise may influence the intracellular Ca^{2+} dynamics of lymphocytes. By using Fura-2 AM dual-wavelength detection technology, our previous work reported that long-term physical training had a significant effect on intracellular calcium signal transduction of lymphocytes in mice (Liu et al., 2017). Since alterations of calcium metabolism have been shown to be involved in some abnormal immune responses, we hypothesized that the mechanisms of acute exercise-induced immunosuppression involve abnormalities in intracellular calcium handling. In order to test this hypothesis, this research examined the effects of acute exercise on intracellular free calcium ion concentrations under basal and agonist-stimulated conditions, the expression of Ca^{2+}-handling factors, and changes of T cell function.

MATERIALS AND METHODS

Animals

In this study, we used a total of 60, 12-week-old male CD1 Swiss mice, weighing (28.0 ± 3.2 g), which were fed in the animal facilities at the Department of Sports Medicine of University of Münster and Justus-Liebig University (Germany), and kept under controlled conditions of temperature and humidity. This specie and model were chosen for being a homogeneous line of mice. Mice were housed collectively (4–6 per cage) and fed tap standard rodent diet and water at will, with a standard 12 h day-night cycle. All procedures were performed following the approval of the local Animal Care and Use Committee. We exert our effort to minimize animal pain and discomfort, and this experiment was performed in accordance with the ARRIVE guidelines.

Treadmill Incremental Test and Exercise Protocol

Animals were adapted to exercise for 1 week before the exercise test, aiming to minimize the stress induced by the equipment. Each animal underwent an incremental exercise test to exhaustion to measure individual maximal oxygen uptake (VO_2max) and the fastest speed as our group previously described (Kruger et al., 2009). After a 5-min warm-up at 0.20 m/s, the running speed was elevated by 0.05 m/s every 3 min until exhaustion. The animals were randomly divided into in four groups, five in each group. The animals in the control group had exposure to the noise of treadmill and allowed to freely run on a treadmill without effort, while the animals of the exercise groups were submitted a single bout of exercise of 80% VO_2max workload until exhaustion, which were anesthetized and killed immediately (E0), 3 h (E3), and 24 h (E24) after exercise for spleen removal.

Preparation of Lymphocytes From Murine Spleens

After the animals were anaesthetized and killed by cervical dislocation, their spleens were separated under aseptic conditions and placed on a 100-μm-pore size nylon mesh (BD Falcon™ Cell Strainer, BD Biosciences, Heidelberg, Germany). And the mesh was put into a culture dish, which PBS was poured into. The spleen was gently squeezed with a 2-ml syringe plunger to generate single cell suspensions. Biocoll separating solution (Biochrom, Berlin, Germany) was used, and lymphocytes are stratified after density gradient centrifugation as our group described before (Liu et al., 2017). The white band of lymphocytes was removed after centrifugation and washed two times by centrifugation in Hanks' Balance Salt Solution (HBSS) containing 5% heat-inactivated fetal calf serum (FCS; Gibco, Darmstadt, Germany). The cell suspension in RPMI1640 containing 10% FCS was prepared to be measured. Cell viability (98%) was quantified by the Trypan blue exclusion assay, whereas purity (95%) was verified by a flow cytometry (EPICS XL Beckman Coulter, Fullerton, CA, United States) in the forward/sideward scatter mode. Moreover, the percentage of T cells in the remaining mixed lymphocyte population was determined to be about 85% by labeling with anti-CD3 antibody as described recently (Krüger et al., 2008). The number of cells was then counted by using a semiautomated hematology analyzer (F-820, Sysmex, Norderstedt, Germany).

Determination of Cytosolic-Free Calcium

Intracellular Ca^{2+} level was assessed by the fluorescence intensity ratio of the calcium probe Fura-2 AM (Molecular Probes Inc., Eugene, OR, United States) as described our previous study (Liu et al., 2017). Briefly, the cells were loaded with 5 μl/ml Fura-2 AM stock (1 mM in DMSO) in 0.8 mM Ca^{2+}-containing solution (140 mM NaCl, 3 mM KCl, 0.4 mM Na_2HPO_4, 10 mM HEPES, 5 mM glucose, and 1 mM $MgCl_2$, and 0.8 mM $CaCl_2$ with pH 7.4). The fluorescence intensities were measured in the dual wavelength ratio mode in a spectrofluorometer (Deltascan; PTI, Canada) at 340 and 380 nm (excitation filters) and 510 nm (emission filter). According to the equation of Grynkiewicz et al. (1985), $[Ca^{2+}]i$ was calculated as follows: $[Ca^{2+}]i = (R\text{-}R\text{min})/(R\text{max}\text{-}R) \times Kd \times F$, with a Kd of Fura-2 for calcium of 220 nM, and where R is the ratio of fluorescence of the sample at 340 and 380 nm. Rmax and Rmin are the ratios for Fura-2 at these wavelengths in the presence of

saturating Ca^{2+} (after application of 10 mM digitonin) and during Ca^{2+}-free conditions (after addition of EGTA, 10 mM final concentration), respectively, and F is the ratio of fluorescence intensity at 380 nm during Ca^{2+}-free conditions to the fluorescence intensity at 380 nm during Ca^{2+}-saturating conditions. To remove the free fura-2 AM, cells loaded with the dye were washed two times with PBS solution. The maximum peak and plateau level of the agonist-induced $[Ca^{2+}]_i$ transient was quantified after the addition of mitogen, concanavalin A (Con A; Sigma Aldrich, St. Louis, United States), the anti-CD3 antibodies (OKT3; Janssen-Cilag, Neuss, Germany), or thapsigargin (TG; Sigma Aldrich, St. Louis, United States). To estimate intracellular Ca^{2+} release and extracellular Ca^{2+} influx, experiments were performed either in absence or in presence of 0.8 mmol/l Ca^{2+} in the measurement medium. For experiments performed in the absence of extracellular calcium, $CaCl_2$ was replaced by 1 mM EGTA in the buffer. The addition of Ca^{2+} allowed measuring transmembrane Ca^{2+} influx.

Mn^{2+}-Quenching Experiments

Bivalent cation, Mn^{2+} and Ca^{2+}, can share common entry channels in cell membrane (Sage et al., 1989), and the former can bind to intracellular Fura-2 (Fura-2-acetoxymethyl ester), with a stronger chemical attraction than the latter and to quench the fluorescence. The decrease in fluorescence of Fura-2 can reflect extracellular Mn^{2+} influx into cells. The determination of Ca^{2+} entry can be quantified the Mn^{2+}-quenching technique (Ferreira et al., 2009). The Mn^{2+}-quenching experiments were carried out by using the same equipment as that for intracellular Ca^{2+} measurements as described above. In the experiments, we used 4 mM Mn^{2+} in the measurement buffer which corresponds to more than twice extracellular Ca^{2+} concentration. The fluorescence was excited at the isosbestic point at 360 nm, and emission was monitored at 510 nm. The rate of Mn^{2+} entry can be obtained from the slope of the fluorescence intensity curve with time. The rate of Mn^{2+}-quenching is shown by the slope of the tangent against a quenching curve after the addition of stimulant. The basal rate of Mn^{2+}-quenching can be determined by measuring "slopes 1" of the initial Fura-2 fluorescence decline, while the rate of fluorescence intensity decreases after the addition of TG (="slope 2"). Therefore, Δslope was regarded as an index to access the rate of fluorescence quenching by extracellular Mn^{2+} influx into cells.

In vitro Stimulation and Proliferation Assays

Lymphocytes were prepared as described above, and cell proliferation was monitored using the cell tracker dye carboxyfluorescein diacetate succinimidyl ester (CFSE, Molecular Probes, Eugene, OR, United States) according to the standard procedure provided by Quah and Parish (2010). Briefly, cells were stained with CFSE dye at 5 μM concentrations and loaded at 37°C for 10 min, and the reaction was terminated by using PBS with 10% (v/v) heat-inactivated FCS. After washing, cells were resuspended in Dulbecco's modified eagle medium (DMEM, PAA Laboratories, Pasching, Austria) with 10% (v/v) heat-inactivated FCS, 50 mg/ml streptomycin, and 50 U/ml penicillin. And the cells were seeded at a density of 2×10^6 cells/per culture dish and then left to incubate at 37°C in a humidified 5% CO_2 atmosphere with additional doses of 2.5 μg/ml Con A or PHA (Sigma-Aldrich, St.Louis, MO, United States). After 72 h of incubation, cells were harvested, stained with anti-CD3-PE antibody (Immunotools, Friesoythe, Germany). Data analysis was performed using a flow cytometer with FlowJo software (Version X; TreeStar, Ashland, OR, United States). AUC is defined as the area under the curve enclosed by the coordinate axis, of which the x-axis indicates cellular generations, and the y-axis shows the percentage of cells in each generation. △AUC as an index was used to evaluate cell proliferative ability.

Quantitative Real-Time PCR

Murine CD3+ T cells were purified directly from splenic cells using an EasySep™ Mouse T Cell Isolation Kit (StemCell Technologies, Vancouver, CA, United States) based on magnetic bead separation technique according to manufactures' instructions. Total RNA was extracted from T lymphocytes using the RNA isolation kit (RNeasy Mini Kit, Qiagen, Hilden, Germany), and a UV-Vis spectrophotometer (ND-1000, Nano-Drop Technologies, Rockland, United States) was used to determine the quantity and purity of the extracted RNA. To remove possible DNA contamination, on-column DNase digestion was applied by using the RNase-free DNase set (Qiagen, Hilden, Germany) in the context of RNA isolation. cDNA was subsequently synthesized by using a cDNA synthesis kit (high-capacity cDNA reverse transcription kit, Applied Biosystems) from RNA samples according to the manufacturer's protocol. cDNA was obtained by on a PCR thermal cycler (T100, Bio-Rad Laboratories, Munich, Germany), and the product was used for qPCR. To determine mRNA expression in T cells, PCR was performed by using the iQ SYBR Green Supermix (Bio-Rad Laboratories, Munich, Germany), and an iCycler (Bio-Rad Laboratories, Munich, Germany) was applied to quantify the amplification products. The PCR primers used are listed in **Table 1**. The reaction conditions were as follows: 1 cycle at 95°C for 3 min, 42 cycles at 95°C for 15 s (denaturation), 61°C for 30 s (annealing), and 72°C for 30 s (elongation). The transcriptional level was normalized to the mRNA expression of housekeeping gene, β-actin. The results were calculated using the $2^{-\Delta(\Delta Ct)}$ method and expressed as fold change in comparison with controls.

Statistical Analysis

Data are expressed as means ± SEM. Shapiro–Wilk's test revealed that data were normally distributed; thus, statistical analysis was performed using one-way ANOVA for comparison between groups. $p < 0.05$ was set as statistical significance. SPSS 20.0 software was used throughout.

RESULTS

Effect of Acute Exercise on Basal Intracellular Ca^{2+} Level and Agonist-Induced Ca^{2+} Transients

In the control group, basal $[Ca^{2+}]_i$ of T cells was determined to be 45.5 ± 5.1 nM. Immediately after exercise, the resting

TABLE 1 | List of primers for quantitative PCR.

Gene	Symbol	Forward primer (5'-3')	Reverse primer (5'-3')
Stromal interaction molecule 1	STIM1	TGAAGAGTCTACCGAAGCAGA	AGGTGCTATGTTTCACTGTTGG
ORAI calcium release-activated calcium modulator 1	ORAI1	AACGAGCACTCGATGCAGG	GGGTAGTCATGGTCTGTGTCC
ORAI calcium release-activated calcium modulator 2	ORAI2	GACCAAGTACCAGTACCCTCA	GCAAACAGATGCACGGCTAC
Inositol 1,4,5-triphosphate receptor 2	IP3R2	CCTCGCCTACCACATCACC	TCACCACTCTCACTATGTCGT
ATPase, Ca^{2+} transporting, cardiac muscle, slow twitch 2	SERCA2	GAGAACGCTCACACAAAGACC	ACTGCTCAATCACAAGTTCCAG
ATPase, Ca^{2+} transporting, plasma membrane	PMCA1	TGAAGGAGCTGCGATCCTCTT	CTGTTCCTGCTCAATTCGACT
Ryanodine receptor 2, cardiac	RYR2	ATTATGAAGGTGGTGCCGTATCA	TTCCACTCCACGCGACTCTTA
Purinergic receptor P2X, ligand-gated ion channel, 7	P2X7	GCACCGTCAAGTGGGTCTT	CAGGCTCTTTCCGCTGGTA
Transient receptor potential cation channel, subfamily C, member 1	TRPC1	ATCATCGGCCAAAACGATCAT	GCAGCTAAAATAACAGGTGCGA
Transient receptor potential cation channel, subfamily M, member 5	TRPM5	CCTCCGTGCTTTTTGAACTCC	CATAGCCAAAGGTCGTTCCTC
Transient receptor potential cation channel, subfamily V, member 4	TRPV4	AAACCTGCGTATGAAGTTCCAG	CCGTAGTCGAACAAGGAATCCA
Transient receptor potential cation channel, subfamily V, member 6	TRPV6	GACCAGACACCTGTAAAGGAAC	AGACACAGCACATGGTAAAGC
Calcium channel, voltage-dependent, R type, alpha 1E subunit	Cav2.3	AAGACCCCAATGTCTCGAAGA	TGGAAGATGAACCCTAGAGCC
Mitochondrial calcium uptake 1	MCU	CTTAACACCCTTTCTGCGTTGG	AGCATCAATCTTCGTTTGGTCT
ATPase, Ca^{2+} transporting, type 2C, member 1	ATP2C1	ATTGTGTGCGTGAAGGAAAACT	AAATAAGCGTAAGTCCGCAGG
Calmodulin 1	Calm1	CAGCGCACAACGCAGGT	TTCAGCAATCTGCTCTTCAGTCAG
Potassium channel, subfamily K, member 5	Kcnk5	TCTTCATCGTGTGGGGTGTCC	ATAGGGCGTGGTAGTTGGCAC
Heat shock protein 1A	HSPa1a	CATCCTGATGGGGGACAAGT	GTGGAGTTGCGCTTGATGAG
β-actin	Actb	GTGACGTTGACATCCGTAAAGA	GCCGGACTCATCGTACTCC

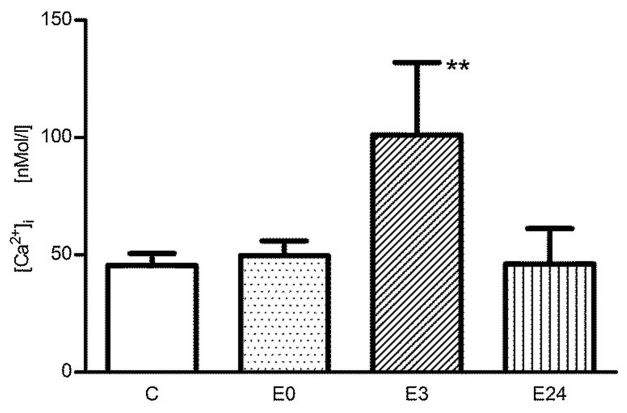

FIGURE 1 | The change of basal $[Ca^{2+}]_i$ of murine splenic T lymphocytes in the control group (C), immediately after (E0), 3 h after (E3), and 24 h (E24) after acute exercise. Data are presented as means ± SEM. $^{**}p < 0.01$ vs. control.

$[Ca^{2+}]_i$ was 49.7 ± 6.2 nM, and no significant change was observed ($p > 0.01$ vs. control, $n = 5$). After 3 h of post-exercise recovery, the resting $[Ca^{2+}]_i$ was highly significantly increased to 101.0 ± 30.9 nM ($p < 0.01$ vs. control, $n = 5$), and the resting intracellular calcium level 24 h after exercise (E24) was 46.0 ± 15.2 nM and unchanged to pre-exercise conditions ($p > 0.01$ vs. control, $n = 5$; **Figure 1**).

Next, cells were stimulated with different agonists known to affect intracellular Ca^{2+} concentrations such as Con A and anti-CD3 antibody (OKT3). Representative tracings of intracellular Ca^{2+} signal after the administration of Con A in calcium containing or Ca^{2+}-free buffer are shown in **Figures 2A,B**, respectively. The stimulant induced a biphasic intracellular Ca^{2+} transient with a peak and a plateau phase in calcium containing buffer. After addition of Con A, a significant absolute and net increase ($=\Delta[Ca^{2+}]_I$) of intracellular Ca^{2+} concentration ($[Ca^{2+}]_i$) in the E3 group could be observed during both peak (**Figures 2C,D**) and plateau phase (**Figures 2E,F**; $p < 0.05$ vs. control, $n = 5$). In **Figures 2G,H**, the measurement was performed in the presence of Ca^{2+}-free buffer. After an initial resting phase of 100 s (=time 1), Con A was added (=time 2) followed by administration of $CaCl_2$ (=time 3). By subtracting mean concentrations at time 1 from time 2 and at time 2 from time 3, the resulting differences should indicate Ca^{2+} release from intracellular stores (stage 1) and transmembrane Ca^{2+} influx (stage 2), respectively. After the administration of Con A, intracellular Ca^{2+} release wasnot affected in the E3 group ($p > 0.05$ vs. control, $n = 5$), while an improved transmembrane Ca^{2+} influx into cells could be observed ($p < 0.05$ vs. control, $n = 5$). Further stimulations were performed only up to 3 h after exercise.

After stimulation with the anti-CD3 antibody (OKT-3), the representative tracings of intracellular Ca^{2+} signals in calcium

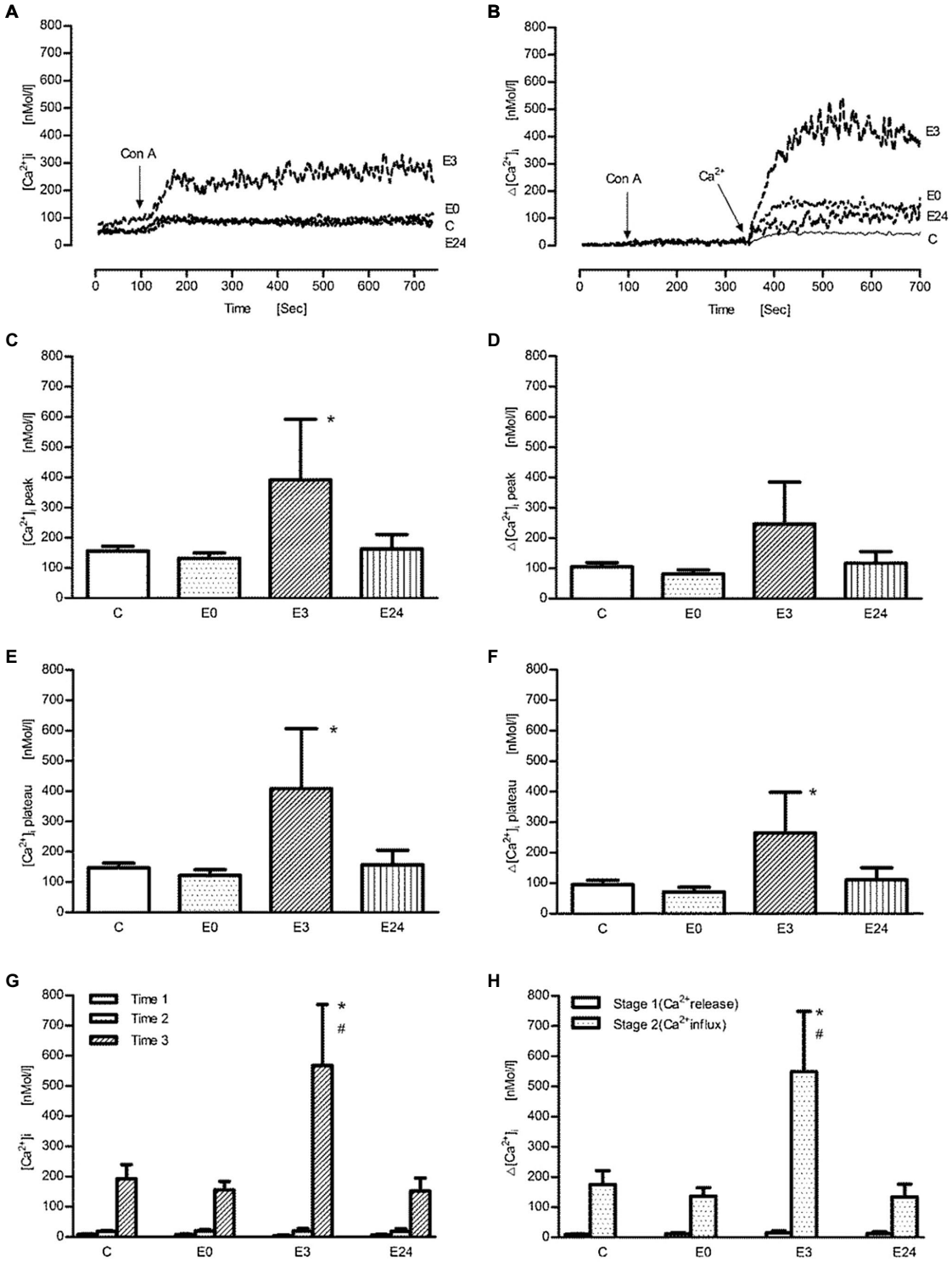

FIGURE 2 | The effect of acute exercise on Con A-induced change of $[Ca^{2+}]$ of murine splenic lymphocytes at the different time points after exercise. **(A,B)** The representative tracings of Con A-induced change of intracellular Ca^{2+} signal in the calcium buffer and the Ca^{2+}-free buffer, respectively; arrow shows when Con A (at 100 s) or Ca^{2+} (at 350 s) were applied; tracing C, the control group; tracings E0, E3, and E24 indicate the exercise groups with cell isolation at time points after, 3 h, and 24 h after exercise. **(C–H)** Bar chart diagrams summarizing the results of the entire groups. **(C–F)** The experiments were performed in the Ca^{2+} buffer; $[Ca^{2+}]_i$ and $\Delta[Ca^{2+}]_i$ were referred to as absolute $[Ca^{2+}]_i$ and net $[Ca^{2+}]_i$ after the addition of Con A, respectively, and were presented separately for peak and plateau phase. **(G,H)** The measurements were performed in Ca^{2+}-free buffer; Time 1: initial resting period, Time 2: addition of Con A, and Time 3: addition of $CaCl_2$; the calculated $\Delta[Ca^{2+}]_i$ levels of stage 1 and stage 2 indicate Ca^{2+} release from ER and transmembrane Ca^{2+} influx from extracellular space, respectively. Data are presented as means ± SEM ($n = 5$). * means $p < 0.05$ vs. control; # means $p < 0.05$ vs. E0.

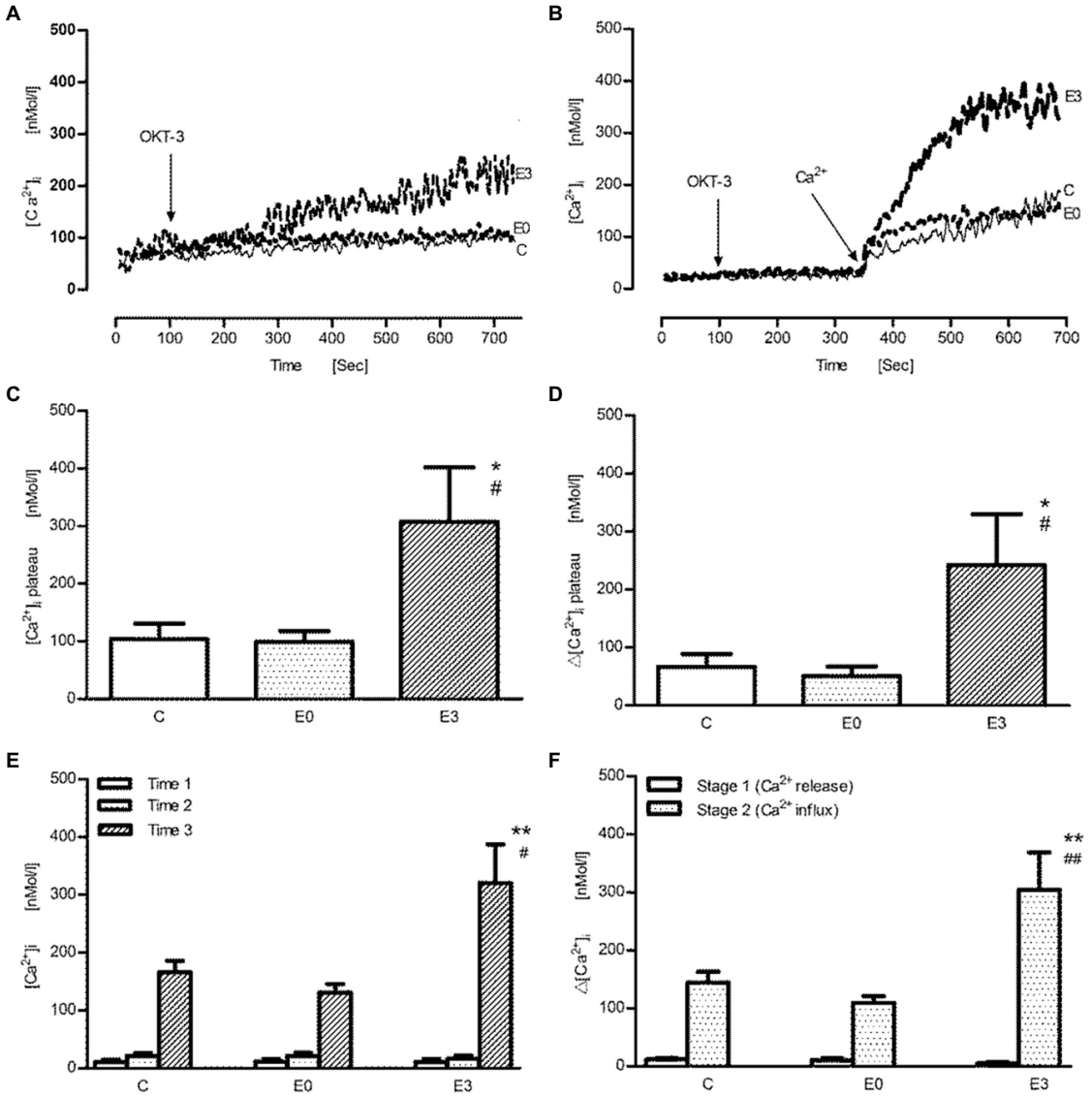

FIGURE 3 | The effect of acute exercise on OKT3-induced change of $[Ca^{2+}]_i$ of murine splenic lymphocytes at the different time points after exercise. **(A,B)** The representative tracings of OKT3-induced change of intracellular Ca^{2+} signal in the calcium buffer and the Ca^{2+}-free buffer, respectively; arrow shows when OKT3 (at 100 s) and Ca^{2+} were applied (at 350 s); tracing C, the control group; tracing E0, and E3 indicate the exercise groups with cell isolation at time points after and 3 h after exercise. **(C–F)** Bar chart diagrams summarize the results of the entire group. **(C,D)** The measurement was performed in the Ca^{2+} buffer; $[Ca^{2+}]_i$ plateau and $\Delta[Ca^{2+}]_i$ plateau were referred to as absolute $[Ca^{2+}]_i$ and net $[Ca^{2+}]_i$ during the plateau phase after stimulation with OKT3, respectively. **(E,F)** The measurement was performed in the Ca^{2+}-free buffer; after the initiative scanning for time 1, OKT3 was added into the buffer for time 2. Next, calcium was administrated for time 3; the calculated $\Delta[Ca^{2+}]_i$ levels of stage 1 and stage 2 indicate Ca^{2+} release from ER and transmembrane Ca^{2+} influx from extracellular space, respectively. Data are presented as means ± SEM ($n = 5$). $^{*}p < 0.05$ or $^{**}p < 0.01$ vs. control, $^{\#}p < 0.05$ or $^{\#\#}p < 0.01$ vs. E0 ($n = 5$).

containing or Ca^{2+}-free buffer are shown in **Figures 3A,B**, respectively. In contrast to stimulation with Con A, a monophasic response after OKT-3 was found making an analysis of peak and plateau values quite impossible. The pattern of exercise effects on anti-CD3 induced Ca^{2+} transients, however, was similar to Con A. In **Figures 3C,D**, using 20 μg/ml OKT-3, a significant increase of absolute and net $[Ca^{2+}]_i$ was found in the E3 group ($p < 0.05$ vs. control, $n = 5$). When cells were suspended first in Ca^{2+}-free solution followed by addition of OKT3, the release of intracellular Ca^{2+} wasnot changed significantly in the E3 group ($p > 0.05$ vs. control, $n = 5$). Upon addition of Ca^{2+}, an improved transmembrane Ca^{2+} influx was shown after exercise ($p < 0.01$ vs. control, $n = 5$; **Figures 3E,F**).

Finally, thapsigargin (TG), an inhibitor of sarco-endoplasmic Ca^{2+}-ATPase, was used. After application of TG in the Ca^{2+}-free buffer, a similar release of Ca^{2+} from intracellular stores could be observed suggesting an identical load of intracellular calcium stores. However, after addition of Ca^{2+} into the extracellular medium, an enhanced Ca^{2+} influx signal was found in the E3 group suggesting an improved entry of extracellular calcium ($p < 0.05$ vs. control,

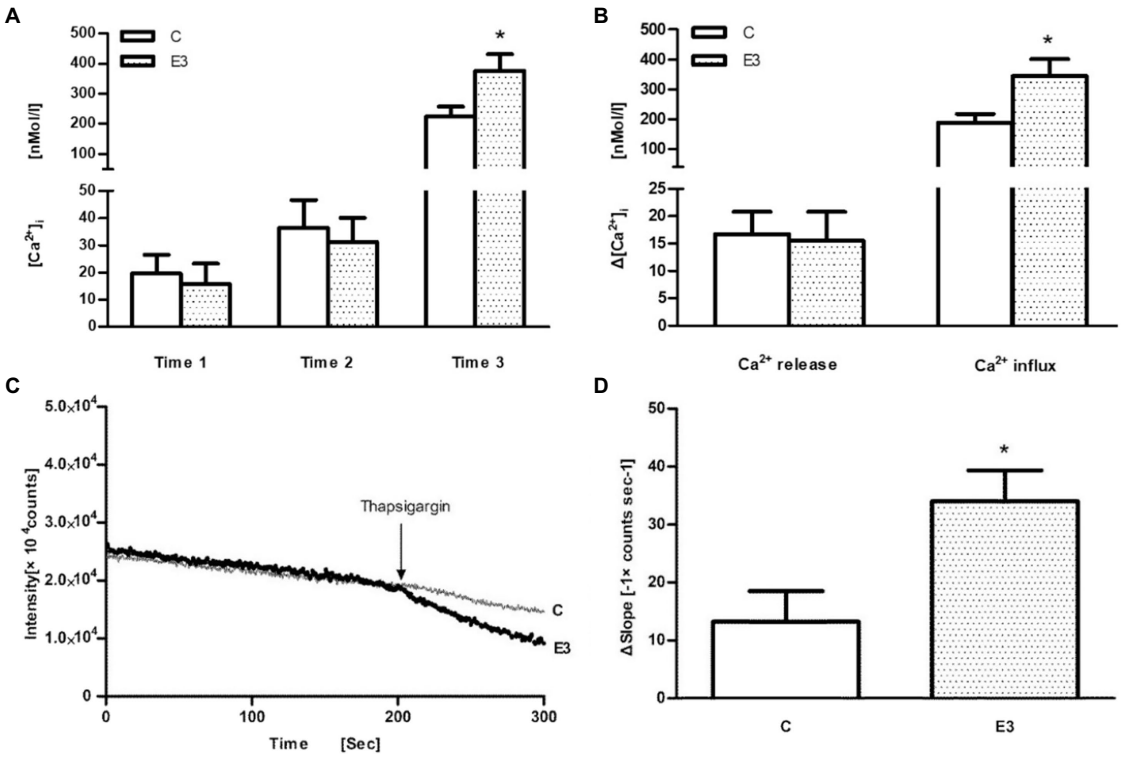

FIGURE 4 | The effect of acute exercise on TG-induced change of $[Ca^{2+}]_i$ and Mn^{2+} influx in murine splenic lymphocytes. C: the control group; E3: the exercise group with cell isolation 3 h after exercise. **(A)** Measurement of $[Ca^{2+}]_i$ initially under Ca^{2+}-free buffer (=time 1), application of TG (=time 2), and addition of $CaCl_2$ (=time 3); **(B)** Ca^{2+} release was quantified by the differences of levels between time 2 and time 1, whereas Ca^{2+} influx was quantified by the differences of levels between time 3 and time 2. **(C)** Representative tracings of the manganese influx measurements of the E3 group (heavy dotted line) and C group (light continuous line). **(D)** The bar chart diagrams show that transmembrane Mn^{2+} influx into cells after the addition of TG was statistically elevated in E3. Data are presented as means ± SEM ($n = 5$). *$p < 0.05$ vs. control ($n = 5$).

$n = 5$; in **Figures 4A,B**). The calcium transients after TG stimulation were monophasic in nature (not biphasic as after Con A stimulation) and were analyzed therefore as single values.

Effect of Acute Exercise in Transmembrane Mn^{2+} Influxes Into Cells

In order to confirm an exercise-associated enhanced Ca^{2+} entry, we used the Mn^{2+}-quenching technique. As shown schematically in **Figure 4C**, the fluorescence intensity at a wavelength of 360 nM continuously decreased after addition of Mn^{2+}. After the application of TG, we observed a larger deflection of the Fura-2 fluorescence quenching in the E3 group (bold line) compared to control group (light line), which indicates an enhanced transmembrane Mn^{2+} influx into cells after exercise ($p < 0.05$ vs. control, $n = 5$), as shown in **Figure 4D**.

Effect of Acute Exercise in Expression of Ca^{2+}-Regulating Genes

As shown in **Figure 5**, the transcription levels of cellular calcium ATPase (PMCA1, SERCA3) and ion channels (TRPC1, P2X7) were statistically reduced, while the transcription levels of internal Ca^{2+} release channels (IP3R2, RYR2) were significantly enhanced in the E3 group compared to control group ($p < 0.05/p < 0.01$ vs. control, $n = 5$). The transcription level of ion channel, TRPM5, was significantly reduced, while transcription levels of intracellular Ca^{2+}-regulating factors, IP3R2, ATP2C1, Cav2.3, and Kcnk5, were significantly increased in the E24 group compared to control group ($p < 0.05/p < 0.01/p < 0.001$ vs. control, $n = 5$). The transcription levels of TRPC1 and Cav2.3 were significantly increased, while the transcription levels of intracellular Ca^{2+}-regulating genes, TRPV6 and Hspa1a, were statistically reduced in the E24 group compared to E3 group ($p < 0.05/p < 0.01$ vs. the E3 group, $n = 5$).

Effect of Acute Exercise in T Cell Proliferation

A single acute bout of exhaustive exercise significantly reduced the mitogen-induced cell proliferation of T cells in the E3 group compared to control group ($p < 0.05/p < 0.001$ vs. control, $n = 5$). The effect could be observed for both PHA and ConA, as shown in **Figure 6**.

DISCUSSION

The major findings of this study were that a single bout of intensive exercise caused reversible increases of both basal and

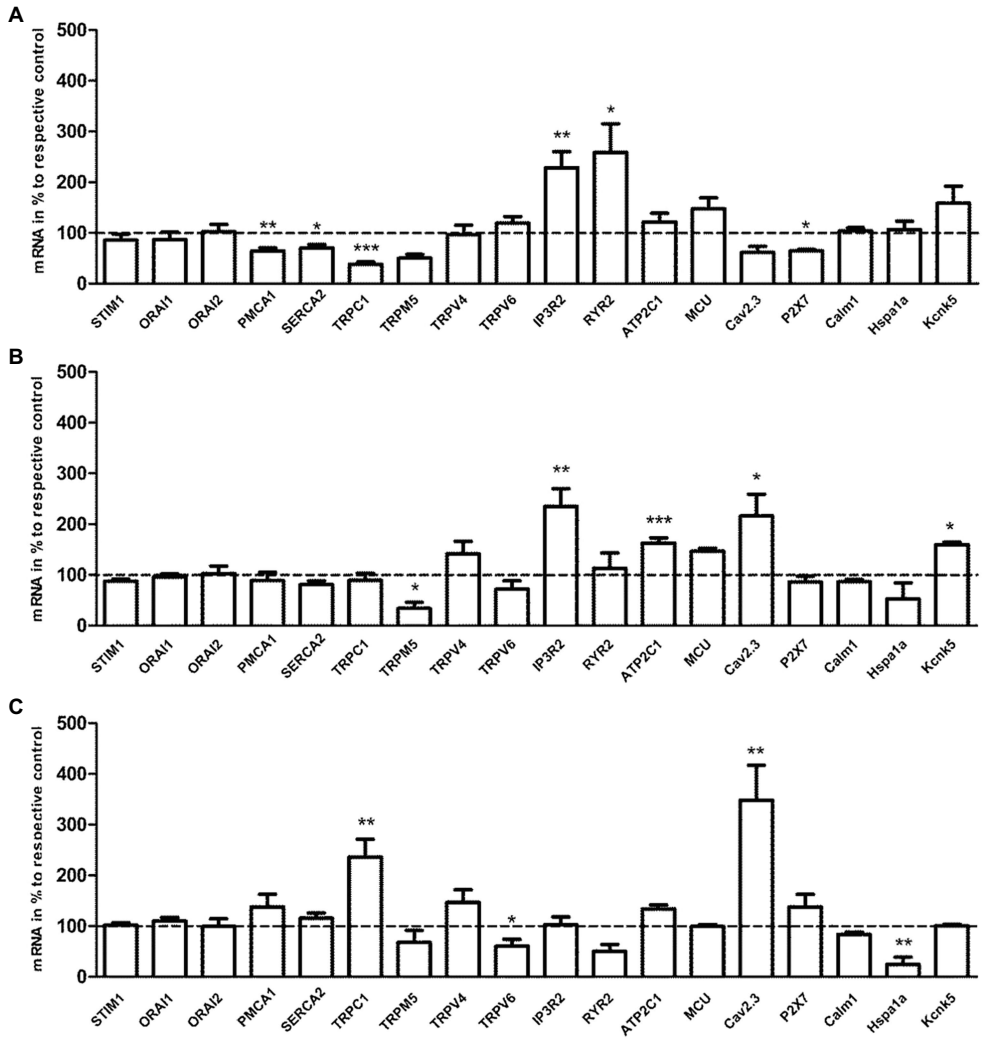

FIGURE 5 | The effects of acute exercise in transcriptional level of Ca^{2+}-regulating genes of murine splenic T lymphocytes. **(A)** mRNA expression of the E3 group vs. the control. **(B)** mRNA expression of the E24 group vs. the control. **(C)** mRNA expression of the E24 group vs. the E3 group. The transcription level of Ca^{2+}-regulating genes was normalized to the housekeeping gene, β-actin mRNA. Note that columns and error bars represent (mRNA in % to respective control ±SEM); $^{*}p<0.05$, $^{**}p<0.01$, $^{***}p<0.001$ ($n=5$).

agonist-induced intracellular Ca^{2+} concentrations during the early post-exercise recovery period. These changes could be related to an enhanced transmembrane Ca^{2+} influx but not to an altered load of intracellular calcium stores. However, enhanced Ca^{2+} transients were not transduced into an improved T cell function as indicated by an impaired cell proliferation suggesting the involvement of other intracellular signaling pathways.

The enhanced resting $[Ca^{2+}]_i$ after acute exercise might be the results of various underlying mechanisms. Exercise stress might damage cell membranes directly by mechanical stress as shown for foot-strike hemolysis during long distance running (Fazal et al., 2017). Changes in cell membrane integrity might result also from enhanced lipid peroxidation due to enhanced exercise-associated oxidative stress. Likewise, previous data from our group have proved that intracellular Ca^{2+} of lymphocytes was affected transiently by acute exercise in humans (Mooren et al., 2001). However, membrane damage seems to be unlikely in the actual case as it should occur very early during and after exercise. The delayed alteration of resting $[Ca^{2+}]_i$ (=3 h post-exercise) in the current study points to another, more likely regulatory processes. The determination of Ca^{2+}-handling proteins mRNA showed a significant reduced expression of both the plasma membrane Ca^{2+}-ATPases (PMCA) and sarco/endoplasmic reticulum Ca^{2+}-ATPases (SERCA). Ca^{2+}-ATPase maintains the global basal free Ca^{2+} levels actively on the expense of ATP in order to transport free calcium ion against its electrochemical gradient either out of cells or into intracellular Ca^{2+} stores. The decreased expression of Ca^{2+}-ATPases could mean a decreased enzyme activity and an impaired ability to regulate intracellular Ca^{2+} levels. The reduced Ca^{2+}-ATPase expression and function should therefore result in a cytoplasmic Ca^{2+} buildup as a result of a new balance

between Ca^{2+} increasing and decreasing processes. Previous studies showed also that the impairment in Ca^{2+} homeostasis just due to one of the Ca^{2+} extruding pathway is enough to interfere with calcium homeostasis and cell function. Therefore, defective Ca^{2+} extrusion due to decreased PMCA expression was responsible for an enhanced cell apoptosis (Pellegrini et al., 2007).

Azenabor and Hoffman-Goetz (2000) found that exhaustive exercise caused the increase of intracellular Ca^{2+} levels in murine thymocytes, and there was a continuous influx of Ca^{2+} after exercise when cells were monitored in Ca^{2+} rich medium. Intracellular Ca^{2+} level actually is the result of a mutual balance among Ca^{2+}-increasing, Ca^{2+}-decreasing, and Ca^{2+}-buffering mechanisms (Mooren and Kinne, 1998). Exercise is obviously able to transiently disturb the balance among the Ca^{2+}-regulating mechanisms in resting cells, which was fully reversible 24 h after exercise. Beside the calcium handling machinery, however, other signaling pathways might be responsible for the dysregulation of basal $[Ca^{2+}]i$ after exercise. There is evidence that an activation of the transcription factor nuclear factor of activated T cells (NFAT), a key regulator of T cell activation, is followed by increased basal Ca^{2+} levels (Martinez et al., 2015).

Next, acute exercise was followed also by enhanced agonist-induced intracellular Ca^{2+} dynamics independent of the stimulant used (Con A, OKT3, and TG). In order to discriminate between the contribution of Ca^{2+} release from intracellular pools such as endoplasmic reticulum and Ca^{2+} influx *via* transmembrane Ca^{2+} channels such as store-operated calcium entry (SOCE), a unique plasma membrane Ca^{2+} entry mechanism, experiments were performed under Ca^{2+}-free conditions. CRAC channels, which are formed by ORAI1-3, are the major SOCE channels in T cells; other channels, such as transient receptor potential (TRP) and voltage-dependent calcium (Cav) channels, also can participate in SOCE (Hoth, 2016). However, at least the voltage-gated Ca^{2+} (Cav) channels are less characterized in T cells. The results suggest that after exercise the transmembrane Ca^{2+} influx into T cells is the major factor for the altered Ca^{2+} signals. Likewise, thapsigargin (TG) by inhibiting the SERCA pumps releases similar amounts of Ca^{2+} from intracellular Ca^{2+} pools suggesting that their load wasnot affected by exercise. Furthermore, the Fura-2-quenching experiments using Mn^{2+} as a surrogate permeable bivalent cation for Ca^{2+} after application of TG support that intensive exercise could improve the transmembrane Ca^{2+} entry during the early (3 h) post-exercise recovery period. The capacity of extracellular Ca^{2+} influx is thereby directly proportional to the ER store depletion (Zweifach and Lewis, 1996). The linearity of the capacity to deplete ER Ca^{2+} stores to determine the subsequent degree and timing of influx could offer an explanation for that the experiments performed in the calcium medium evoked a lower Ca^{2+} entry than those in the Ca^{2+}-free medium. Another explanation might be the nonlinear response of the fluorescent dye especially during/after Ca^{2+}-depleted conditions.

A challenging question is how alterations of Ca^{2+}-handling factors fit with the changed Ca^{2+} transients. The downregulated expression of Ca^{2+}-extruding pumps should delay Ca^{2+} extrusion resulting in enhanced Ca^{2+} transients as observed. The individual contribution of the Ca^{2+}-ATPase is exquisitely coordinated in T cells in time and space in order to effectively modulate intracellular Ca^{2+} dynamics upon activation. PMCA has previously been shown to functionally associate with SOCE channels (Bautista et al., 2002). Thus, Ca^{2+} entry pathways such as TRPC1 and P2X7 have been downregulated as well. The role of purinergic ionotropic P2X7R in T cells has been studied in mice; the activation requires millimolar concentrations of its ligand ATP, which can induce the influx of Ca^{2+}/Na^{+} and the efflux of K^{+} (Foster et al., 2013). The expression of the TRPV4, a Ca^{2+}-permeable nonselective ion channel that is sensitive to variations of body temperature has been shown to be affected by chronic exercise in a tissue dependent manner (Chen et al., 2015). However, acute exercise as used in the actual study did not affect its expression in T cells. It might be speculated that the decreased expression of some transmembrane Ca^{2+} channels serves as a protective mechanism to prevent a further intracellular Ca^{2+} overload. In contrast, the enhanced expression of both IP3R2 and RYR2 receptors had no effects on the calcium load of intracellular stores, but it may have an amplifying effect during agonist induced Ca^{2+} transients. In T cells, Ca^{2+} release from the ER is mediated by binding of IP3 to IP_3R and is further modulated by RyR (Dadsetan et al., 2008). For a proper function, SOCE requires the assembly of ER-located STIM proteins with the plasma membrane channels which occurs within distinct regions in the cell that have been termed as endoplasmic reticulum (ER)–plasma membrane (PM) junctions. The PM and ER are in close proximity to each other within this region, which allows STIM1 in the ER to interact with and activate either ORAI1 or TRPC1 in the plasma membrane (Subedi et al., 2017). Higher expression of intracellular Ca^{2+} release channels might therefore modulate Ca^{2+} permeability and enhance transmembrane Ca^{2+} influx despite lower expression of Ca^{2+} entry pathways. Compared to our recent publication about the effects of regular long-term exercise training on T cell and Ca^{2+} signaling, similarities and dichotomies were found. Exercise training had no effect on the expression of Ca^{2+} extruding pumps from both cell membrane and intracellular stores. Ca^{2+} channel proteins from cell membrane and intracellular stores, such as ORAI1, IP3R2, TRPM5, TRPC1, and TRPV4 Ca2.3 were broadly downregulated (Liu et al., 2017). In contrast, acute exercise induced upregulation of some Ca^{2+} channels such as the intracellular channels IP3R2 and RYR2 and some transmembrane Ca^{2+} channels like Cav2.3 and TRPC1 suggesting a differential regulation of Ca^{2+} signaling in T cells by acute and chronic exercise. The enhanced expression of Cav2.3 occurred delayed 24 h after exercise without any influence on cellular Ca^{2+} signals. Recently, the Cav2.3 gene was shown to be upregulated in pregnancy and type 1 diabetes indicating a shift in immunological status under these conditions (Bhandage et al., 2018).

What might be the exercise-associated condition which modulates transiently intracellular calcium? Previous work has demonstrated that levels of oxidative stress are increased after intensive bouts of exercise (Kruger et al., 2009). Moreover, it has been well documented that free radicals are able to modulate the activity of many Ca^{2+}-handling proteins (Gorlach et al., 2015),

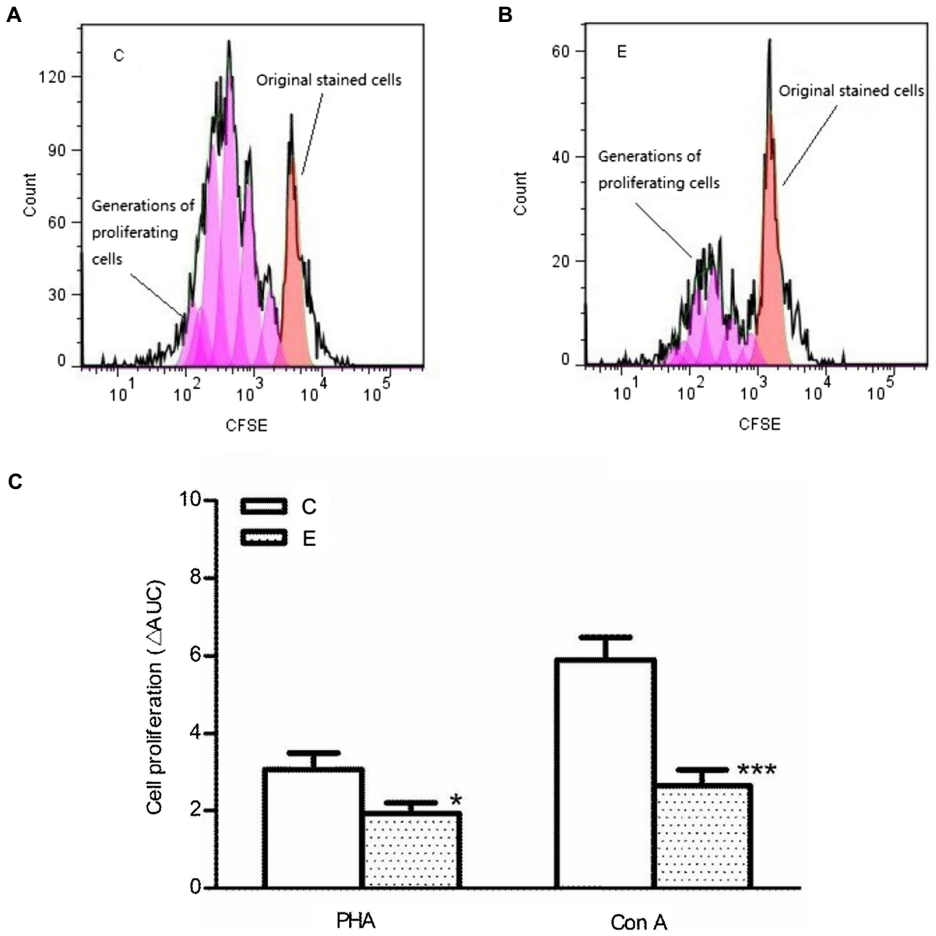

FIGURE 6 | Effects of acute exercise on proliferative capacity of lymphocytes. **(A,B)** CFSE proliferation profile; **(C)** statistical analysis of cell proliferation. E, the exercise mice, which were killed 3 h after exercise; C, the control group; Con A: concanavalin A; PHA: phytohemagglutinin. Data are presented as mean ± SEM, $^{*}p < 0.05$, $^{***}p < 0.001$ vs. control ($n = 5$).

which may result in changed capacitative Ca^{2+} entry and finally in intracellular Ca^{2+} overload. The function of PMCA can be altered by an enhanced lipid peroxidation (Kako et al., 1988; Ohta et al., 1989), and SERCA is highly susceptible to oxidative damage, which can lead to a decrease of SERCA activity and then result in elevation of intracellular Ca^{2+} level (Antipenko and Kirchberger, 1997; Squier and Bigelow, 2000). On the other hand, the elevation of cytosolic Ca^{2+} level can activate the mitochondrial Ca^{2+} uniporter (MCU) that induces mitochondrial Ca^{2+} uptake, an event that drives mitochondrial respiration thereby causing the generation of further free radicals, which may amplify the cellular oxidative stress. A Ca^{2+} overload in mitochondrial matrix causes the opening of the permeability transition pore (PTP) followed by a collapse of mitochondrial potential, mitochondrial swelling and release of cell death inducing agents (Gherardi et al., 2020). Such sequence finally leads to apoptotic cell death, which recently was described to be induced after exhaustive exercise (Kruger et al., 2009).

Finally, acute exhaustive exercise can modulate the ability of T cell proliferation. Many studies have shown that an acute bout of strenuous exercise is followed by reduced immune cells functions in humans and mice (Randall Simpson et al., 1989; Mazzeo et al., 1998; Potteiger et al., 2001). The results of this study confirmed these results in the murine model by demonstrating a reduced proliferative response of splenic lymphocytes to mitogens. However, after acute exercise, the increased intracellular Ca^{2+} signals were not transferred into an enhanced cellular function contrary to our recent findings after chronic exercise training. Chronic moderate exercise elevated basal Ca^{2+} level and agonist-induced Ca^{2+} influx, which was followed by an improved lymphocyte proliferation (Liu et al., 2017). These contrary findings suggest that after acute exercise the usual stimulus–response relationship is broken at least for cell proliferation as one of several T cell functions. One reason might be that exercise induces alterations of spatial and temporal Ca^{2+} patterns such as calcium oscillations, which could not be recognized using the actual technical approach. The increasing $[Ca^{2+}]_i$ *per se* is not enough to trigger cell proliferation (Silberman et al., 2005). The Ca^{2+} signaling promotes cellular proliferation depending on the amplitude

of increase, frequency of oscillations, the duration and nature of change, and the location of cytosolic Ca^{2+} responses (Monteith et al., 2007; Brini and Carafoli, 2009). On the other hand, cellular proliferation ability is controlled also by other signaling pathways than $[Ca^{2+}]_i$, such as transcription factors like cAMP response element-binding protein (CREB), AP-1, and NFAT (Dolmetsch et al., 1998; Martinez et al., 2015; Shin et al., 2019). T cells show hyporesponsive states during conditions of persistent stimulation, referred to as cellular exhaustion. There is evidence that such a hypo-response does not affect all cellular functions to the same degree. Moreover, impaired cellular proliferation occurs despite preserved intracellular Ca^{2+} signaling (Agnellini et al., 2007). NFAT could be identified as a major factor responsible for promoting exhaustion of activated T cells (Martinez et al., 2015). Further studies should therefore focus on the exercise-dependent regulation of cellular transcription factors. Another limitation of the current study includes the investigation of cell suspensions and not single cells. The latter approach would enable the detection of individual calcium signals and patterns and the use of the patch clamp technique for electrophysiological measurements. With the development of molecular biology cloning technology, we have gradually learned that there are great similarities of molecular signatures between humans and animals, but there are also certain differences. Although it is tempting to extrapolate results from one species to another, doing such without assessing the differences of the various ion channels, such as calcium and potassium channels, in different species brings risks, as translation is not always that simple (Tanner and Beeton, 2018).

Thus, taken together, our findings demonstrated that acute exercise affects intracellular calcium homeostasis during resting and stimulated conditions in murine T cells. The changed calcium levels result from an enhanced transmembrane Ca^{2+} influx into cells and an altered expression of cellular Ca^{2+} ATPases such as PMCA and SERCA as well as intracellular Ca^{2+} release channels such as IP3R and RyR. However, the alterations of Ca^{2+} signaling could not be related to the inhibition of cell proliferation in T cells making further studies on the role of additional signaling pathways such as transcription factor activation necessary.

DATA AVAILABILITY STATEMENT

The original contributions presented in the study are included in the article/supplementary material, further inquiries can be directed to the corresponding author.

ETHICS STATEMENT

The animal study was reviewed and approved by the Animal Care and Use Committee of Giessen University.

AUTHOR CONTRIBUTIONS

All authors have made substantial contributions to the conception or design of the work or the acquisition, analysis, or interpretation of data for the work, drafted the work or revised it critically for important intellectual content, approved the final version to be published, and agreed to be accountable for all aspects of the work in ensuring that questions related to the accuracy or integrity of any part of the work are appropriately investigated and resolved. All authors contributed to the article and approved the submitted version.

REFERENCES

Agnellini, P., Wolint, P., Rehr, M., Cahenzli, J., Karrer, U., and Oxenius, A. (2007). Impaired NFAT nuclear translocation results in split exhaustion of virus-specific CD8+ T cell functions during chronic viral infection. *Proc. Natl. Acad. Sci. U. S. A.* 104, 4565–4570. doi: 10.1073/pnas.0610335104

Antipenko, A. Y., and Kirchberger, M. A. (1997). Membrane phosphorylation protects the cardiac sarcoplasmic reticulum Ca^{2+}-ATPase against chlorinated oxidants in vitro. *Cardiovasc. Res.* 36, 67–77. doi: 10.1016/S0008-6363(97)00183-1

Azenabor, A. A., and Hoffman-Goetz, L. (2000). Effect of exhaustive exercise on membrane estradiol concentration, intracellular calcium, and oxidative damage in mouse thymic lymphocytes. *Free Radic. Biol. Med.* 28, 84–90. doi: 10.1016/S0891-5849(99)00209-9

Bautista, D. M., Hoth, M., and Lewis, R. S. (2002). Enhancement of calcium signalling dynamics and stability by delayed modulation of the plasma-membrane calcium-ATPase in human T cells. *J. Physiol.* 541, 877–894. doi: 10.1113/jphysiol.2001.016154

Bhandage, A. K., Jin, Z., Korol, S. V., Tafreshiha, A. S., Gohel, P., Hellgren, C., et al. (2018). Expression of calcium release-activated and voltage-gated calcium channels genes in peripheral blood mononuclear cells is altered in pregnancy and in type 1 diabetes. *PLoS One* 13:e0208981. doi: 10.1371/journal.pone.0208981

Brini, M., and Carafoli, E. (2009). Calcium pumps in health and disease. *Physiol. Rev.* 89, 1341–1378. doi: 10.1152/physrev.00032.2008

Chen, N., Cheng, J., Zhou, L., Lei, T., Chen, L., Shen, Q., et al. (2015). Effects of treadmill running and rutin on lipolytic signaling pathways and TRPV4 protein expression in the adipose tissue of diet-induced obese mice. *J. Physiol. Biochem.* 71, 733–742. doi: 10.1007/s13105-015-0437-5

Dadsetan, S., Zakharova, L., Molinski, T. F., and Fomina, A. F. (2008). Store-operated Ca^{2+} influx causes Ca^{2+} release from the intracellular Ca^{2+} channels that is required for T cell activation. *J. Biol. Chem.* 283, 12512–12519. doi: 10.1074/jbc.M709330200

Dolmetsch, R. E., Xu, K., and Lewis, R. S. (1998). Calcium oscillations increase the efficiency and specificity of gene expression. *Nature* 392, 933–936. doi: 10.1038/31960

Fazal, A. A., Whittemore, M. S., and Degeorge, K. C. (2017). Foot-strike haemolysis in an ultramarathon runner. *BMJ Case Rep.* 2017:bcr2017220661. doi: 10.1136/bcr-2017-220661

Ferreira, V. M., Gomes, T. S., Reis, L. A., Ferreira, A. T., Razvickas, C. V., Schor, N., et al. (2009). Receptor-induced dilatation in the systemic and intrarenal adaptation to pregnancy in rats. *PLoS One* 4:e4845. doi: 10.1371/journal.pone.0004845

Foster, J. G., Carter, E., Kilty, I., Mackenzie, A. B., and Ward, S. G. (2013). Mitochondrial superoxide generation enhances P2X7R-mediated loss of cell surface CD62L on naive human CD4+ T lymphocytes. *J. Immunol.* 190, 1551–1559. doi: 10.4049/jimmunol.1201510

Gherardi, G., Monticelli, H., Rizzuto, R., and Mammucari, C. (2020). The mitochondrial Ca^{2+} uptake and the fine-tuning of aerobic metabolism. *Front. Physiol.* 11:554904. doi: 10.3389/fphys.2020.554904

Gorlach, A., Bertram, K., Hudecova, S., and Krizanova, O. (2015). Calcium and ROS: A mutual interplay. *Redox Biol.* 6, 260–271. doi: 10.1016/j.redox.2015.08.010

Grynkiewicz, G., Poenie, M., and Tsien, R. Y. (1985). A new generation of Ca^{2+} indicators with greatly improved fluorescence properties. *J. Biol. Chem.* 260, 3440–3450. doi: 10.1016/S0021-9258(19)83641-4

Hoth, M. (2016). CRAC channels, calcium, and cancer in light of the driver and passenger concept. *Biochim. Biophys. Acta* 1863, 1408–1417. doi: 10.1016/j.bbamcr.2015.12.009

Kako, K., Kato, M., Matsuoka, T., and Mustapha, A. (1988). Depression of membrane-bound Na^+-K^+-ATPase activity induced by free radicals and by ischemia of kidney. *Am. J. Phys.* 254, C330–C337. doi: 10.1152/ajpcell.1988.254.2.C330

Kruger, K., Frost, S., Most, E., Volker, K., Pallauf, J., and Mooren, F. C. (2009). Exercise affects tissue lymphocyte apoptosis via redox-sensitive and Fas-dependent signaling pathways. *Am. J. Phys. Regul. Integr. Comp. Phys.* 296, R1518–R1527. doi: 10.1152/ajpregu.90994.2008

Krüger, K., Lechtermann, A., Fobker, M., Völker, K., and Mooren, F. C. (2008). Exercise-induced redistribution of T lymphocytes is regulated by adrenergic mechanisms. *Brain Behav. Immun.* 22, 324–338. doi: 10.1016/j.bbi.2007.08.008

Liu, R., Fan, W., Kruger, K., Xiao, Y. U., Pilat, C., Seimetz, M., et al. (2017). Exercise affects T-cell function by modifying intracellular calcium homeostasis. *Med. Sci. Sports Exerc.* 49, 29–39. doi: 10.1249/MSS.0000000000001080

Martinez, G. J., Pereira, R. M., Aijo, T., Kim, E. Y., Marangoni, F., Pipkin, M. E., et al. (2015). The transcription factor NFAT promotes exhaustion of activated CD8+ T cells. *Immunity* 42, 265–278. doi: 10.1016/j.immuni.2015.01.006

Mazzeo, R. S., Rajkumar, C., Rolland, J., Blaher, B., Jennings, G., and Esler, M. (1998). Immune response to a single bout of exercise in young and elderly subjects. *Mech. Ageing Dev.* 100, 121–132. doi: 10.1016/S0047-6374(97)00130-9

Monteith, G. R., Mcandrew, D., Faddy, H. M., and Roberts-Thomson, S. J. (2007). Calcium and cancer: targeting Ca^{2+} transport. *Nat. Rev. Cancer* 7, 519–530. doi: 10.1038/nrc2171

Mooren, F. C., and Kinne, R. K. (1998). Cellular calcium in health and disease. *Biochim. Biophys. Acta* 1406, 127–151. doi: 10.1016/s0925-4439(98)00006-4

Mooren, F. C., Lechtermann, A., Fromme, A., Thorwesten, L., and Volker, K. (2001). Alterations in intracellular calcium signaling of lymphocytes after exhaustive exercise. *Med. Sci. Sports Exerc.* 33, 242–248. doi: 10.1097/00005768-200102000-00012

Ohta, A., Mohri, T., and Ohyashiki, T. (1989). Effect of lipid peroxidation on membrane-bound Ca^{2+}-ATPase activity of the intestinal brush-border membranes. *Biochim. Biophys. Acta* 984, 151–157. doi: 10.1016/0005-2736(89)90210-1

Pellegrini, M., Finetti, F., Petronilli, V., Ulivieri, C., Giusti, F., Lupetti, P., et al. (2007). p66SHC promotes T cell apoptosis by inducing mitochondrial dysfunction and impaired Ca^{2+} homeostasis. *Cell Death Differ.* 14, 338–347. doi: 10.1038/sj.cdd.4401997

Potteiger, J. A., Chan, M. A., Haff, G. G., Mathew, S., Schroeder, C. A., Haub, M. D., et al. (2001). Training status influences T-cell responses in women following acute resistance exercise. *J. Strength Cond. Res.* 15, 185–191.

Quah, B. J., and Parish, C. R. (2010). The use of carboxyfluorescein diacetate succinimidyl ester (CFSE) to monitor lymphocyte proliferation. *J. Vis. Exp.*:2259. doi: 10.3791/2259

Randall Simpson, J. A., Hoffman-Goetz, L., Thorne, R., and Arumugam, Y. (1989). Exercise stress alters the percentage of splenic lymphocyte subsets in response to mitogen but not in response to interleukin-1. *Brain Behav. Immun.* 3, 119–128. doi: 10.1016/0889-1591(89)90012-3

Sage, S. O., Merritt, J. E., Hallam, T. J., and Rink, T. J. (1989). Receptor-mediated calcium entry in fura-2-loaded human platelets stimulated with ADP and thrombin. Dual-wavelengths studies with Mn^{2+}. *Biochem. J.* 258, 923–926. doi: 10.1042/bj2580923

Shin, S. Y., Kim, M. W., Cho, K. H., and Nguyen, L. K. (2019). Coupled feedback regulation of nuclear factor of activated T-cells (NFAT) modulates activation-induced cell death of T cells. *Sci. Rep.* 9:10637. doi: 10.1038/s41598-019-46592-z

Silberman, D. M., Zorrilla-Zubilete, M., Cremaschi, G. A., and Genaro, A. M. (2005). Protein kinase C-dependent NF-kappaB activation is altered in T cells by chronic stress. *Cell. Mol. Life Sci.* 62, 1744–1754. doi: 10.1007/s00018-005-5058-7

Simpson, R. J., Campbell, J. P., Gleeson, M., Krüger, K., Nieman, D. C., Pyne, D. B., et al. (2020). Can exercise affect immune function to increase susceptibility to infection? *Exerc. Immunol. Rev.* 26, 8–22.

Squier, T. C., and Bigelow, D. J. (2000). Protein oxidation and age-dependent alterations in calcium homeostasis. *Front. Biosci.* 5, D504–D526. doi: 10.2741/squier

Subedi, K. P., Ong, H. L., and Ambudkar, I. S. (2017). Assembly of ER-PM junctions: A critical determinant in the regulation of SOCE and TRPC1. *Adv. Exp. Med. Biol.* 981, 253–276. doi: 10.1007/978-3-319-55858-5_11

Tanner, M. R., and Beeton, C. (2018). Differences in ion channel phenotype and function between humans and animal models. *Front. Biosci.* 23, 43–64. doi: 10.2741/4581

Zweifach, A., and Lewis, R. S. (1996). Calcium-dependent potentiation of store-operated calcium channels in T lymphocytes. *J. Gen. Physiol.* 107, 597–610. doi: 10.1085/jgp.107.5.597

Conflict of Interest: The authors declare that the research was conducted in the absence of any commercial or financial relationships that could be construed as a potential conflict of interest.

Publisher's Note: All claims expressed in this article are solely those of the authors and do not necessarily represent those of their affiliated organizations, or those of the publisher, the editors and the reviewers. Any product that may be evaluated in this article, or claim that may be made by its manufacturer, is not guaranteed or endorsed by the publisher.

frontiers in Pharmacology

BRIEF RESEARCH REPORT
published: 20 December 2021
doi: 10.3389/fphar.2021.734078

Genetic Ablation of the Mitochondrial Calcium Uniporter (MCU) Does not Impair T Cell-Mediated Immunity *In Vivo*

Hao Wu[1†], *Benjamin Brand*[1†], *Miriam Eckstein*[1], *Sophia M. Hochrein*[1], *Magdalena Shumanska*[2], *Jan Dudek*[3], *Alexander Nickel*[3], *Christoph Maack*[3], *Ivan Bogeski*[2] *and Martin Vaeth*[1*]

[1]*Würzburg Institute of Systems Immunology, Max Planck Research Group at the Julius-Maximilians-Universität Würzburg, Würzburg, Germany,* [2]*Molecular Physiology, Institute of Cardiovascular Physiology, University Medical Center, Georg-August-University, Göttingen, Germany,* [3]*Comprehensive Heart Failure Center (CHFC), University Hospital, Julius-Maximilians University of Würzburg, Würzburg, Germany*

OPEN ACCESS

Edited by:
Heike Wulff,
University of California, Davis, United States

Reviewed by:
Murali Prakriya,
Northwestern University, United States
Wolfgang F. Graier,
Medical University of Graz, Austria

***Correspondence:**
Martin Vaeth
Martin.vaeth1@uni-wuerzburg.de

[†]*These authors have contributed equally to this work*

Specialty section:
This article was submitted to Pharmacology of Ion Channels and Channelopathies, a section of the journal Frontiers in Pharmacology

Received: *30 June 2021*
Accepted: *22 November 2021*
Published: *20 December 2021*

Citation:
Wu H, Brand B, Eckstein M, Hochrein SM, Shumanska M, Dudek J, Nickel A, Maack C, Bogeski I and Vaeth M (2021) Genetic Ablation of the Mitochondrial Calcium Uniporter (MCU) Does not Impair T Cell-Mediated Immunity In Vivo. *Front. Pharmacol. 12:734078. doi: 10.3389/fphar.2021.734078*

T cell activation and differentiation is associated with metabolic reprogramming to cope with the increased bioenergetic demand and to provide metabolic intermediates for the biosynthesis of building blocks. Antigen receptor stimulation not only promotes the metabolic switch of lymphocytes but also triggers the uptake of calcium (Ca^{2+}) from the cytosol into the mitochondrial matrix. Whether mitochondrial Ca^{2+} influx through the mitochondrial Ca^{2+} uniporter (MCU) controls T cell metabolism and effector function remained, however, enigmatic. Using mice with T cell-specific deletion of MCU, we here show that genetic inactivation of mitochondrial Ca^{2+} uptake increased cytosolic Ca^{2+} levels following antigen receptor stimulation and store-operated Ca^{2+} entry (SOCE). However, ablation of MCU and the elevation of cytosolic Ca^{2+} did not affect mitochondrial respiration, differentiation and effector function of inflammatory and regulatory T cell subsets *in vitro* and in animal models of T cell-mediated autoimmunity and viral infection. These data suggest that MCU-mediated mitochondrial Ca^{2+} uptake is largely dispensable for murine T cell function. Our study has also important technical implications. Previous studies relied mostly on pharmacological inhibition or transient knockdown of mitochondrial Ca^{2+} uptake, but our results using mice with genetic deletion of MCU did not recapitulate these findings. The discrepancy of our study to previous reports hint at compensatory mechanisms in MCU-deficient mice and/or off-target effects of current MCU inhibitors.

Keywords: mitochondrial calcium uniporter (MCU), store-operated Ca^{2+} entry, mitochondria, oxidative phosphorylation, calcium (Ca^{2+}), immunometabolism, mitochondrial Ca^{2+} handling

INTRODUCTION

Mitochondria play a pivotal role in cellular metabolism by producing large amounts of ATP through oxidative phosphorylation (OXPHOS) and fatty acid oxidation (FAO). In addition, intermediates of mitochondrial metabolism, such as tricarboxylic acid (TCA) cycle, glutaminolysis and FAO, control the fate and function of immune cells by regulating signaling pathways, the cellular redox balance, apoptosis and epigenetic rewiring through DNA and histone modifications. Not surprisingly, mitochondrial metabolism has been (re-)

discovered as an important regulator of lymphocyte function and "immunometabolism" has become a major research focus.

The observation that mitochondria can rapidly take up calcium (Ca^{2+}) from the cytosol was made over half a century ago (Finkel et al., 2015). Studies in myocytes and other non-immune cells demonstrated that mitochondrial Ca^{2+} handling can regulate mitochondrial metabolism and function, including the activity of the TCA cycle and the electron transport chain (ETC), the production of reactive oxygen species (ROS) and apoptosis through opening of the mitochondrial permeability transition pore (mPTP) (Finkel et al., 2015; Wang P. et al., 2020). Although the outer mitochondrial membrane is permeable to most inorganic ions, transport of Ca^{2+} at the inner mitochondrial membrane (IMM) is tightly regulated and requires specific transporters. Following an intensive search over decades, two groups identified the predicted *mitochondrial Ca^{2+} uniporter* (MCU) using an *in silico* approach and demonstrated that the MCU protein forms a highly selective, inwardly rectifying Ca^{2+} channel. After the molecular identification of MCU, it became clear that mitochondrial Ca^{2+} uptake is mediated by a larger protein complex that not only contains MCU as the pore-forming subunit but is composed of additional regulatory and structural elements. *Essential MCU regulator* (EMRE) and its homologue MCUb were shown to be part of the channel pore, whereas the two EF hand domain-containing proteins *mitochondrial Ca^{2+} uptake 1* (MICU1), 2 and 3 function as "gatekeepers" of the MCU complex (Wang P. et al., 2020).

Ca^{2+} influx into the mitochondrial matrix is driven by a negatively charged membrane potential at the IMM that is established by the ETC. The opening of the MCU channel is initiated by conformational changes of MICU1/2 after binding of free cytosolic Ca^{2+} to their EF hand domains. Given the relatively low affinity of MICU1/2 for Ca^{2+} it was originally believed that the extramitochondrial Ca^{2+} levels required for MCU activation could not be achieved under physiological conditions. However, most Ca^{2+} signals are not uniformly distributed throughout the cytosol but are locally restricted to the site of Ca^{2+} influx. These Ca^{2+} "microdomains" can be generated by Ca^{2+} release from ER stores and/or extracellular calcium influx pathways, such as *store-operated Ca^{2+} entry* (SOCE) through *Ca^{2+} release-activated Ca^{2+}* (CRAC) channels, and reach the required local Ca^{2+} concentration to induce MCU channel opening. In activated T cells, mitochondria are in proximity to the ER and move actively towards the immunological synapse at which Ca^{2+} influx *via* SOCE is elicited (Quintana et al., 2007; Lioudyno et al., 2008; Quintana et al., 2011). We showed recently that CRAC channels and SOCE not only control mitochondrial size and function but also mitochondrial metabolism, including TCA cycle and OXPHOS (Vaeth et al., 2017a; Kahlfuss et al., 2020). These effects could be explained by a direct, MCU-mediated uptake of cytosolic Ca^{2+} into the mitochondrial matrix and the positive regulation of Ca^{2+}-sensitive TCA cycle enzymes. On the other hand, SOCE may also mediate these effects indirectly by regulating gene expression of nuclear-encoded mitochondrial proteins. To clarify how MCU-dependent mitochondrial Ca^{2+} uptake contributes to T cell metabolism and function *in vivo*, we investigated mice with genetic deletion of MCU in T cells using models of autoimmunity and viral infection.

MATERIALS AND METHODS

Mice

$Mcu^{fl/fl}$ (Kwong et al., 2015) (strain 029817), $Foxp3^{Cre}$ (strain 016959) and $Cd4^{Cre}$ mice (strain 022071) were purchased from the Jackson laboratories and housed at the University of Würzburg. All animals were on a pure C57BL/6J genetic background and maintained under SPF conditions.

T cell cultures and treatments

T cells were isolated using MojoSort Mouse T cell isolation kits (BioLegend) and cultured in complete RPMI 1640 medium (Gibco) containing 1 g/L glucose. 24-well plates were pre-coated with 12 μg/ml polyclonal anti-hamster IgG, washed with PBS and activated with either 0.25 μg/ml (for Th17) or 0.5 μg/ml (for Th1 and iTreg subsets) of anti-CD3 (clone 145-2C1) together with 1 μg/ml anti-CD28 (37.51). The following culture conditions were used: Th1 cells: 2.5 μg/ml anti-IL-4 (clone 11B11), 10 ng/ml rhIL-2 and 10 ng/ml rmIL-12. iTreg cells: 2.5 μg/ml anti-IL-4, 2.5 μg/ml anti-IFNγ, 10 ng/ml rhIL-2 and 5 ng/ml rhTGF-beta. Th17 cells: 2.5 μg/ml anti-IL-4, 2.5 μg/ml anti-IFNγ, 20 ng/ml rmIL-6 and 0.5 ng/ml rhTGFβ. Tc1 cells: 2.5 μg/ml anti-IL-4, 10 ng/ml rhIL-2 and 10 ng/ml rmIL-12. Tc17 cells: 2.5 μg/ml anti-IL-4, 2.5 μg/ml anti-IFNγ, 20 ng/ml rmIL-6 and 0.5 ng/ml rhTGFβ. All antibodies and cytokines were from Bio X Cell and Peprotech, respectively. To detect cytokine expression, cells were stimulated with 1 μM ionomycin plus 30 nM phorbol myristate acetate (Calbiochem) for 5 h in the presence of brefeldin A (BioLegend). In some experiments, T cell were treated for 72 h with 2–10 μM Ruthenium red (Sigma).

Experimental Autoimmune Encephalomyelitis

$MOG_{35–55}$ peptide (Synpeptide) was emulsified in CFA with 5 mg/ml *M tuberculosis* H37Ra (BD Difco). 200 mg $MOG_{35–55}$ was injected subcutaneously at the flanks of the mice, followed by intraperitoneal injection of 250 ng pertussis toxin (Enzo) on day 0 and 2. The EAE score was assigned as described before (Stromnes and Goverman, 2006). Mice were sacrificed and spinal cords were isolated, minced into small pieces and digested with 1 mg/ml collagenase D (Roche) and 20 μg/ml DNase I (Sigma) for 40 min at 37°C. CNS-infiltrating lymphocytes were enriched by percoll gradient centrifugation and analyzed by flow cytometry.

LCMV Infections

The LCMV clone 13 strain was kindly provided by R. Ahmed (Emory University). LCMV was grown in BHK-21 cells and viral titers (PFU) in the supernatant were determined as described (Vaeth et al., 2016; Ataide et al., 2020). For chronic viral

infections, mice were injected intravenously with 4×10^6 PFU of LCMV and analyzed 23 days post infection.

Flow Cytometry

Cells were blocked with anti-FcγRII/FcγRIII (Bio X Cell; clone 2.4G2) and debris was excluded using the viability dye eFluor780 (eBioscience). Staining of surface molecules with fluorochrome-conjugated antibodies was performed in PBS containing 0.1% BSA. Intracellular (IC) and transcription factor (TF) staining was carried out with the IC Staining and TF Staining Buffer Kit, respectively (eBioscience). Samples were acquired on a BD FACSCelesta flow cytometer and analyzed with FlowJo Software (Tree Star). The following antibodies were used: anti-mouse CD4 (clones 53–6.7 and GK1.5), anti-mouse IL-17A (C11-18H10.1), anti-mouse IFNγ (XMG1.2), anti-mouse GM-CSF (MP1-22E9), anti-mouse TNFα (MP6-XT22), anti-mouse IL-2 (JES6-5H4), anti-mouse Foxp3 (FJK-16s), anti-mouse T-bet (4B10), anti-mouse RORγt (Q31-378), anti-mouse CD25 (PC61), anti-mouse Ki-67 (B56), anti-CD44 (IM7), anti-CXCR5 (SPRCL5), anti-PD-1 (RMP1-30), anti-CD38 (90), anti-GL.7 (GL7), anti-CD8α (53–6.7), anti-Tim3 (RMT3-23). All antibodies were from BioLegend or eBiosciences. PE-labelled tetramers loaded with the LCMV peptides GP_{33-41} and GP_{66-77} were provided by the NIH Tetramer Core Facility.

T Cell Proliferation Analysis

T cells were labelled with CellTrace Violet (Thermo Scientific) according to the manufacturer's instructions. Cells were blocked with 50% FBS, washed twice with RPMI and stimulated with 1 μg/ml plate-bound anti-CD3 (clone 2C11) and anti-CD28 antibodies (37.51; both Bio X Cell) with 50 U/ml IL-2 (Peprotech). CTV dilution was monitored daily by flow cytometry.

Ca^{2+} Influx Measurements

T cells were labelled with 2 μM Fura-2-AM (Thermo Scientific) as described earlier (Vaeth et al., 2017b). Cells were attached to 96-well imaging plates coated with 0.01% poly-L-lysine (Sigma) and washed with Ca^{2+}-free Ringer solution. Changes in intracellular Ca^{2+} concentration were analyzed using a FlexStation3 plate reader (Molecular Devices) at 340 and 380 nm. Cells were stimulated with 1 μM thapsigargin (TG) (Sigma) in Ca^{2+}-free Ringer solution and SOCE was analyzed after re-addition of 2 mM Ca^{2+}. Alternatively, whole splenocytes were loaded with 2 μM Fluo4-AM (Thermo Scientific) and incubated with anti-CD4-APC and anti-CD8a-BV421 antibodies (BioLegend). Measurements of intracellular Ca^{2+} changes were recorded by flow cytometry. Baseline cytosolic Ca^{2+} levels acquired in 0 mM Ca^{2+} Ringer solution, before cells were stimulated with 1 μM thapsigargin and re-addition of 2 mM Ca^{2+}. Mitochondrial uptake of free Ca^{2+} was monitored in the presence of digitonin-permeabilized T cells (0.04%; preincubation time 10 min). 1×10^6 cells per well were re-suspended in PTP buffer (125 mM KCl, 2 mM K_2HPO_4, 1 mM $MgCl_2$, 10 mM HEPES, 20 μM EGTA, pH 7.4) containing 2 mM succinate, 2 μM thapsigargin and 1 μM CalciumGreen-5N (Thermo Scientific). Fluorescence (503/535 nm) was monitored using a Tecan M200 Pro reader in a 96-well plate with injection of 25 μM Ca^{2+} pulses.

Histochemistry

CNS specimens were fixed in 4% PFA, embedded in paraffin and stained with Luxol fast blue and Cresyl violet (both Carl Roth) to detect myelin and nuclei, respectively.

Quantitative RT-PCR

RNA was extracted using the RotiPrep RNA mini kit (Carl Roth), followed by cDNA synthesis with the iScript cDNA synthesis Kit (BioRad). qRT-PCR was performed using iTaq Universal SYBR Green SuperMix (Bio-Rad) and the CFX RT-PCR thermocycler (BioRad). For quantitation, C_T values were normalized to *18S* gene expression and analyzed using the $2^{-\Delta CT}$ method. *Mcu*-for: TTAGCAGAAAAGCAGAGAAGAG, *Mcu*-rev: TGATGAAGT AGGTGACGGG, *Letm1*-for: CGGGGTAGTCTGAGGGATCG, *Letm1*-rev: TGGAGTACAGCAACGAGACAG, *Slc8b1*-for: CTG GAAGTGTCAACCAGACTG, *Slc8b1*-rev: AGTCACAGCGAT CAGATGTGT, *18S*-for: CGGCGACGACCCATTCGAAC, *18S*-rev: GAATCGAACCCTGATTCCCCGT.

Western Blot

Cells were resuspended in RIPA lysis buffer with complete protease inhibitor cocktail (Thermo Scientific). 40 μg of total protein was fractionated by SDS-PAGE and transferred onto a nitrocellulose membrane. Membranes were incubated with antibodies against β-Actin (1:5,000, mouse, clone C4; SCBT), VDAC (1:1,000, mouse, N152B/23; BioLegend), GAPDH (1:200, mouse, 6C5; SCBT) and MCU (1:1,000, rabbit polyclonal; CST). For detection, peroxidase-coupled secondary anti-mouse or anti-rabbit antibodies (BioRad) and ECL Substrate (Thermo Scientific) were used.

Metabolic Flux Analyses

Glycolytic proton efflux rate (PER) and oxygen consumption rate (OCR) were measured using a XFe96 extracellular flux analyzer (Seahorse Bioscience) as described before (Vaeth et al., 2017a; Kahlfuss et al., 2020).

Statistical Analyses

All results are means with standard error of the means (SEM). The statistical significance of differences between experimental groups was determined by unpaired Student's *t*-test. Differences were considered significant for p values < 0.05.

RESULTS

Ablation of MCU Elevates Cytosolic Ca^{2+} Levels After Antigen Receptor Stimulation

To investigate the role of MCU (CCDC109A) and mitochondrial Ca^{2+} uptake in primary T cells, we generated mice with T cell-specific deletion of the *Mcu* gene by crossing $Mcu^{fl/fl}$ mice (Kwong et al., 2015) to $Cd4^{Cre}$ animals that express *Cre* recombinase under the control of the *Cd4* promoter. $Mcu^{fl/fl}Cd4^{Cre}$ mice were

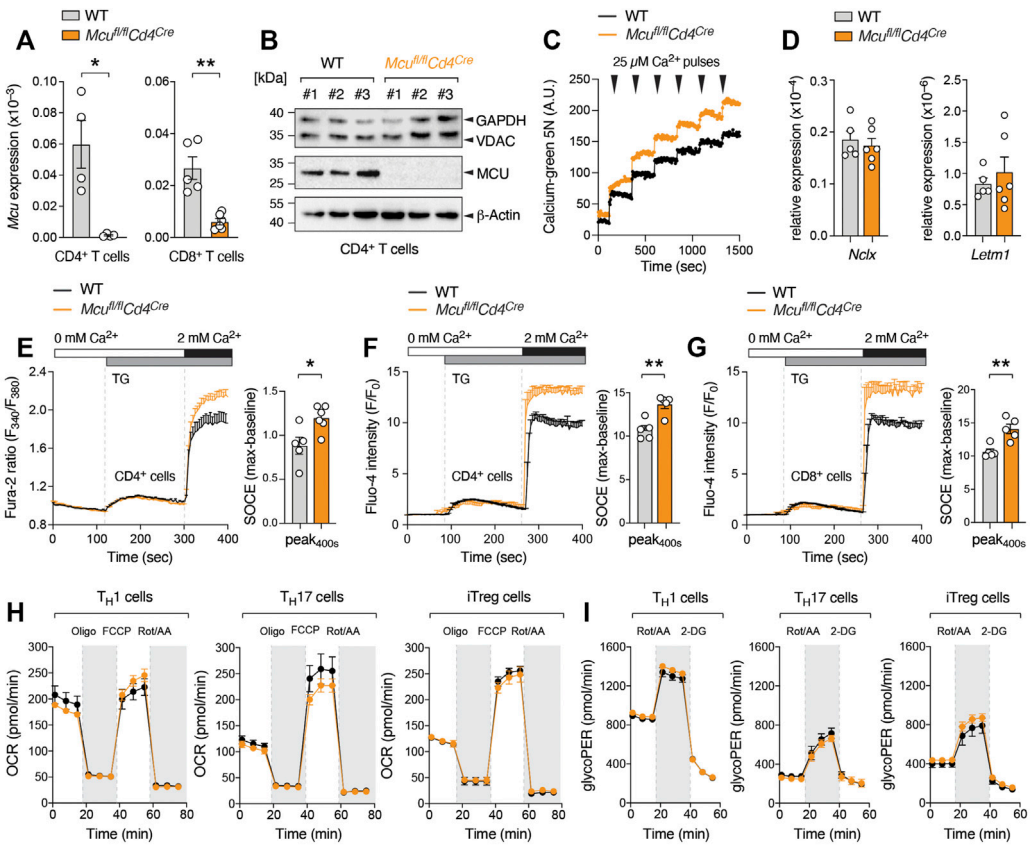

FIGURE 1 | Deletion of MCU attenuates mitochondrial Ca^{2+} uptake but increases cytosolic Ca^{2+} levels after store depletion. **(A)** *Mcu* gene expression in $CD4^+$ and $CD8^+$ T cells of WT and MCU-deficient mice (*Mcu*$^{fl/fl}$*Cd4*^{Cre}) analyzed by qRT-PCR; means ± SEM of 4-6 mice. **(B)** Immunoblot assay detecting MCU, VDAC and GAPDH protein expression in anti-CD3/CD28 stimulated $CD4^+$ T cells, three independent WT and MCU-deficient mice. **(C)** Ca^{2+} retention capacity of digitonin-permeabilized WT and MCU-deficient T cells after repetitive addition of 25 μM extracellular Ca^{2+} measured by CalciumGreen-5N. **(D)** Analysis of *Slc8b1* (NCLX) and *Letm1* gene expression in activated WT and MCU-deficient $CD8^+$ T cells by qRT-PCR; means ± SEM of 5-6 mice. **(E)** Measurement of Ca^{2+} store depletion and SOCE in $CD4^+$ T cells isolated from WT and *Mcu*$^{fl/fl}$*Cd4*^{Cre} mice using a FlexStation3 plate reader. Cells were loaded with Fura-2 and stimulated with thapsigargin (TG) in Ca^{2+} free Ringer solution followed by re-addition of 2 mM Ca^{2+} **(left panel)**. The traces were baseline normalized and the quantification of maximal SOCE (peak-baseline) was calculated as F340/380 emission ratios; means ± SEM of 4-6 mice **(right panel)**. **(F, G)** *Ex vivo* analysis of store depletion and SOCE in $CD4^+$ **(F)** and $CD8^+$ **(G)** T cells of WT and *Mcu*$^{fl/fl}$*Cd4*^{Cre} mice loaded with Fluo-4 and analyzed by flow cytometry. Addition of TG and 2 mM extracellular Ca^{2+} as indicated. Baseline normalized (F/F_0) means ± SEM of 4-5 mice. **(H, I)** Seahorse extracellular flux analyses to measure oxygen consumption rate (OCR) **(H)** and glycolytic proton efflux rate (glycoPER) **(I)** in WT and MCU-deficient Th1, Th17 and iTreg cells; means ± SEM of 3-5 mice.

indistinguishable from their littermates and showed a normal composition of thymic T cell populations (**Supplementary Figure S1A**). The frequencies and numbers of peripheral conventional and regulatory (Treg) T cells were also unaltered (**Supplementary Figures S1B–D**). Naïve and effector T cell composition was comparable between WT and *Mcu*$^{fl/fl}$*Cd4*^{Cre} mice and MCU-deficient mice showed no spontaneous immune dysregulation (**Supplementary Figure S1E**). We next confirmed that the expression of MCU was completely abolished in T cells at the mRNA (**Figure 1A**) and protein level (**Figure 1B**). We next measured mitochondrial Ca^{2+} uptake in digitonin-permeabilized WT and MCU-deficient T cells after extracellular Ca^{2+} addition (**Figure 1C**). Although we observed a reduced mitochondrial Ca^{2+} uptake in absence of MCU, primary mouse T cells showed only a moderate capacity to buffer extracellular Ca^{2+} elevations. Typically, the extracellular Ca^{2+} pulses are rapidly taken up by the mitochondria until mPTP opening becomes visible by a sudden elevation of free cytosolic Ca^{2+}. Our best explanation why we did not measure significant mitochondrial Ca^{2+} uptake in these experiments is that primary T cells have fewer and relatively small mitochondria compared to other immune cells, such as macrophages, which makes it difficult to monitor their Ca^{2+} buffering capacity. In addition, other mitochondrial Ca^{2+} transporters, such as the $Na^+/Ca^{2+}/Li^+$ exchanger NCLX and the H^+/Ca^{2+} exchanger Letm1, may compensate for the loss of MCU. Although expression of NCLX and Letm1 was unchanged (**Figure 1D**), this data does not exclude adaptational changes in mitochondrial Ca^{2+} handling and other compensatory mechanisms, when MCU is genetically ablated.

Previous reports presented conflicting results regarding MCU's effect on cytosolic Ca^{2+} elevations. In most studies, genetic or pharmacological inhibition of MCU attenuated ER store depletion and SOCE (Hoth et al., 1997; Gilabert et al., 2001; Samanta et al., 2014; Samanta et al., 2020), presumably due to a

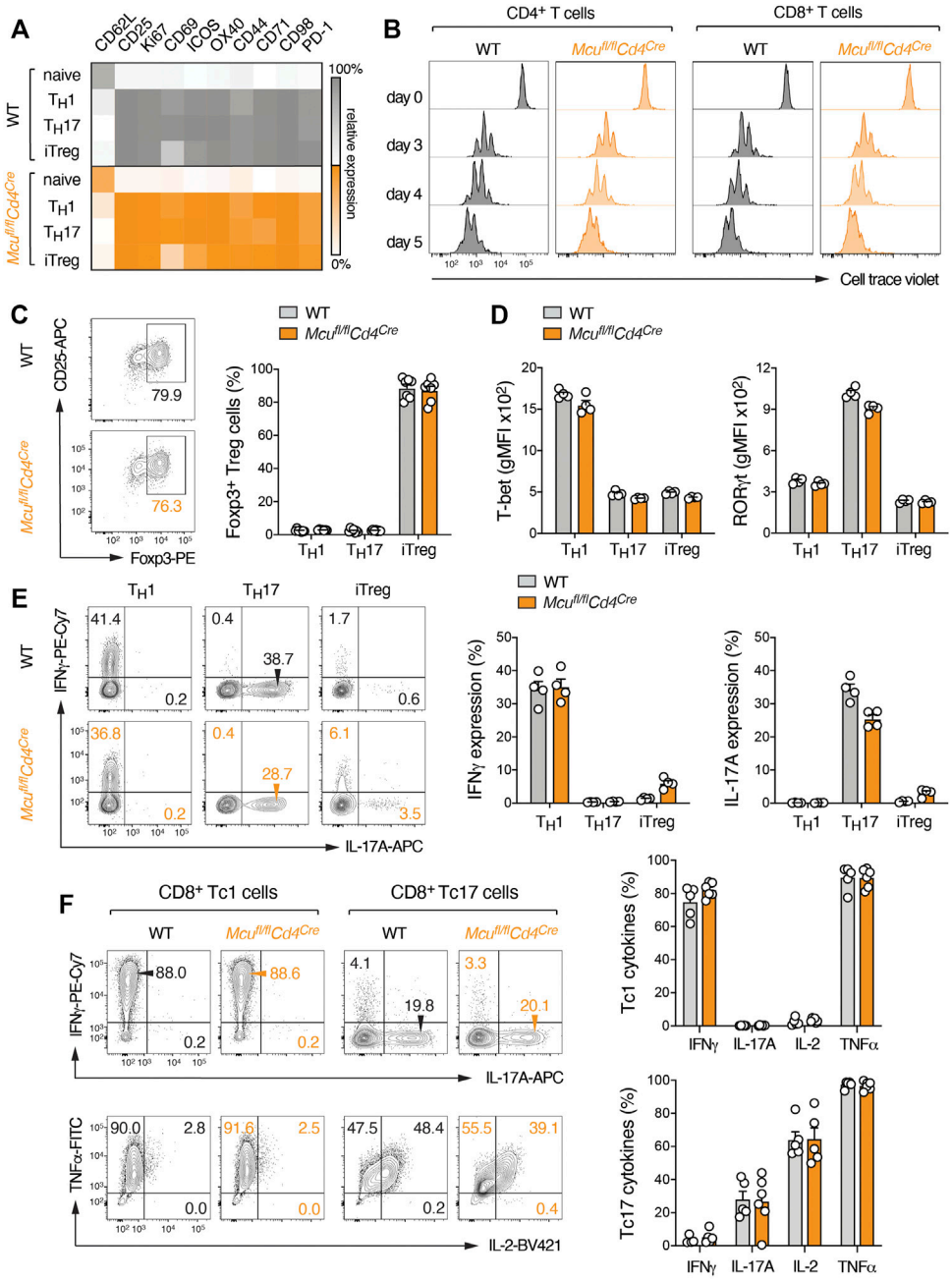

FIGURE 2 | Ablation of MCU does not impair activation, differentiation and effector function of murine T cells *in vitro*. **(A)** Flow cytometric analysis of CD62L and activation marker (CD25, Ki-67, CD69, ICOS, OX-40, CD44, CD71, CD98 and PD-1) expression on WT and MCU-deficient T cells after anti-CD3/CD28 stimulation. Naive CD4$^+$ T cells were cultured for 3 days under Th1, Th17 and iTreg culture conditions; heatmap showing row-normalized geometric MFIs as means of 3 individual mice. **(B)** Representative proliferation analysis of WT and MCU-deficient CD4$^+$ and CD8$^+$ T cells by CellTrace Violet dilution after anti-CD3/CD28 stimulation over the course of 5 days. **(C)** Analysis of Foxp3 expression in WT and MCU-deficient T cells cultured for 3 days under Th1, Th17 and iTreg-polarizing conditions; means ± SEM of 7 mice. **(D)** Flow cytometric analyses of T-bet and RORγt expression in WT and MCU-deficient T cells cultured under Th1, Th17 and iTreg-polarizing conditions; means ± SEM of 4 mice. **(E)** Quantification of IFNγ and IL-17A protein expression in WT and MCU-deficient CD4$^+$ T cells differentiated into Th1, Th17 and iTreg cells for 3 days and re-stimulated with PMA/ionomycin for 5 h; means ± SEM of 4 mice. **(F)** Quantification of IFNγ, IL-17A, IL-2 and TNFα production by WT and MCU-deficient CD8$^+$ T cells differentiated into Tc1 and Tc17 cells for 6 days and re-stimulated with PMA/ionomycin for 5 h; means ± SEM of 5-6 mice.

negative feedback regulation known as Ca^{2+}-dependent inactivation (CDI) of IP_3R and/or CRAC channels (Samanta et al., 2014; Deak et al., 2014; Tang et al., 2015). By contrast, other studies reported unchanged or elevated SOCE upon silencing of MCU (Paupe and Prudent, 2018; Wang P. et al., 2020; Seegren et al., 2020). In our experiments using primary

MCU-deficient T cells, we observed a small but reproducible increase in cytosolic Ca^{2+} levels after ER store depletion with the sarco/endoplasmic reticulum Ca^{2+} ATPase (SERCA) inhibitor thapsigargin (TG) (**Figures 1E–G**). Although unexpected, our results are in line with recent data that also found that deletion of MCU by CRISPR/Cas9-mediated genome editing elevates SOCE and NFAT nuclear translocation in different lymphocytic cell lines and in primary T and B cells (Yoast et al., 2021).

MCU is Dispensable for T Cell Proliferation, Differentiation and Effector Function *In Vitro*

To determine how impaired mitochondrial Ca^{2+} buffering and elevated SOCE affects the activation and effector function of T cells, we isolated naïve $CD4^+$ T cells from WT and $Mcu^{fl/fl}Cd4^{Cre}$ mice and differentiated these cells into different T helper (Th) subsets. The expression of MCU was similar in all Th cells tested (**Supplementary Figure S2A**). We focused on Th1, Th17 and iTreg cells for further analyses as these subsets are not only well-defined by their (inflammatory) cytokine profiles but also differ in their dependency on mitochondrial metabolism. However, we did not detect differences in oxygen consumption rate (OCR) or extracellular acidification (glycoPER) as measures of mitochondrial and glycolytic activity, respectively, when we compared MCU-deficient T cells to WT controls (**Figures 1H,I**). Stimulation of WT and MCU-deficient T cells under Th1, Th17 and iTreg-polarizing conditions revealed also no difference in the expression of activation markers (**Figure 2A**). Cell cycle entry (**Supplementary Figure S2B**) and proliferation of MCU-deficient $CD4^+$ and $CD8^+$ T cells was also comparable to WT controls (**Figure 2B**), indicating that MCU is dispensable for T cell metabolism and activation. To test whether MCU affects T cell differentiation, we analyzed the expression of T-bet, RORγt and Foxp3 as the "signature" transcription factors of Th1, Th17 and iTreg cells, respectively. We observed, however, no differences in the generation of iTreg (**Figure 2C**) or inflammatory Th1 and Th17 cells *in vitro* (**Figure 2D**, **Supplementary Figure S2C**), suggesting that mitochondrial Ca^{2+} is not required for T cell differentiation. Finally, we tested whether MCU plays a role in the effector function of T cells by re-stimulating Th1, Th17 and iTreg cells with PMA and ionomycin and analyzed the cytokine expression of WT and MCU-deficient cells by flow cytometry. However, we did not observe significant differences in IFNγ and IL-17A expression by Th1 and Th17 cells, respectively (**Figure 2E**). Likewise, GM-CSF and IL-2 expression was unaltered in MCU-deficient T cells (**Supplementary Figure S2D**). Similar as "helper" $CD4^+$ T cells, "cytotoxic" $CD8^+$ T cells can be also polarized into Tc1 and Tc17 cells that are not only characterized by an inflammatory (Tc1) and memory (Tc17) phenotype but also differ greatly by their mitochondrial activity (Flores-Santibáñez et al., 2018). As in $CD4^+$ T cells, ablation of MCU did not affect differentiation and cytokine expression of Tc1 and Tc17 cells (**Figure 2F**). Collectively, these data suggest that genetic deletion of MCU does not alter T cell metabolism, differentiation and effector function *in vitro*. By contrast, the widely used, but unspecific, MCU inhibitor Ruthenium Red attenuated T cell metabolism, proliferation and survival (**Supplementary Figures S3A–F**). Because pharmacological blockade of MCU does not recapitulate the findings of MCU-deficient T cells, this data hints at compensatory mechanisms in MCU knockout mice and/or off-target effects of pharmacological inhibitors.

Loss of MCU Does not Affect Adaptive Immune Responses in Autoimmunity and Infection

Although *in vitro* assays are useful to evaluate basic functions of T cells, the complexity of T cell interaction with lymphoid and non-lymphoid cell types and the varying metabolic conditions in different target tissues cannot be fully emulated *in vitro*. We therefore employed two complementary animal models of T cell-mediated inflammation; experimental autoimmune encephalomyelitis (EAE) (**Figure 3**), which resembles aspects of human multiple sclerosis, and persistent viral infection with the lymphocytic choriomeningitis virus (LCMV) strain clone 13 (**Figure 4**). We first induced EAE in $Mcu^{fl/fl}Cd4^{Cre}$ and littermate control mice by immunization with MOG_{35-55} peptide emulsified in CFA and monitored the disease progression over the course of 20 days. T cell-specific deletion of MCU did not alter EAE immunopathology, including the paralysis of their extremities (**Figure 3A**), inflammation-induced weight loss (**Figure 3B**) and the demyelination of the spinal cord (**Figure 3C**). The infiltration of lymphocytes into the CNS was also similar in $Mcu^{fl/fl}Cd4^{Cre}$ mice compared to control animals (**Figure 3D**). In line with our *in vitro* data, the production of IFNγ, IL-17A, GM-CSF, IL-2 and TNFα by encephalitogenic Th1 and Th17 cells following re-stimulation with PMA and ionomycin was not impaired in absence of MCU (**Figures 3E,F**). Because mitochondrial Ca^{2+} uptake is impaired in all T cells of $Mcu^{fl/fl}Cd4^{Cre}$ mice, defects in both inflammatory and regulatory T cells could potentially mask subset-specific functions of MCU. To explore a cell-intrinsic role of MCU in Treg cells, we generated $Mcu^{fl/fl}Foxp3^{Cre}$ mice that lack MCU expression specifically in $Foxp3^+$ Treg cells. As observed in mice with ablation of MCU in all T cells, $Mcu^{fl/fl}Foxp3^{Cre}$ mice were indistinguishable from their littermates and showed normal frequencies of thymocytes and peripheral T cells (**Supplementary Figure S4A–D**). Importantly, $Mcu^{fl/fl}Foxp3^{Cre}$ mice showed no signs of an overt immune activation (**Supplementary Figure S4E**) and the numbers of Treg cells in peripheral lymphoid organs were unaltered. The differentiation of thymus-derived Treg cells into $CD44^+CD62L^-$ effector Treg cells was also not perturbed in absence of MCU (**Supplementary Figures S4F,G**), suggesting that MCU is not required for Treg development and their suppressive function *in vivo*. In addition to autoimmunity and T cell responses to self-antigens, we tested the anti-viral activity of $CD4^+$ and $CD8^+$ T cells in WT and $Mcu^{fl/fl}Cd4^{Cre}$ mice after infection with the LCMV strain clone 13 (**Figure 4**). LCMV infection promotes the differentiation of $CD4^+$ T cells into T follicular helper (Tfh) cells to support affinity maturation of germinal center (GC) B cells and anti-viral humoral immunity. We did not detect differences in the activation of $CD4^+$

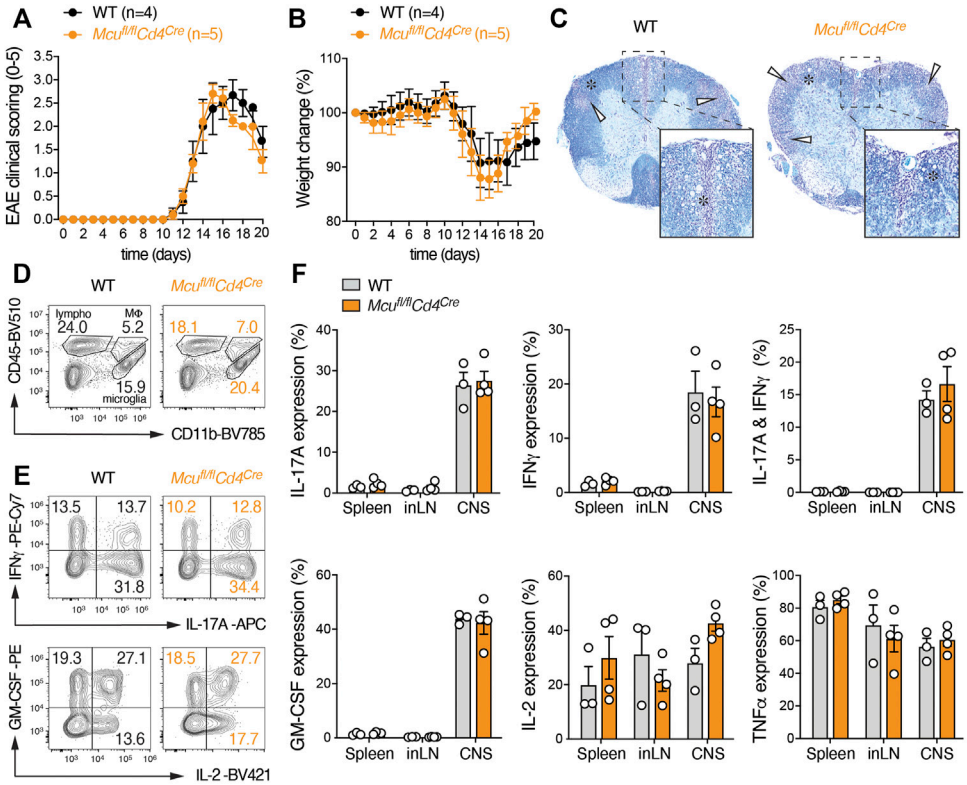

FIGURE 3 | Mice with T cell-specific deletion of MCU are susceptible to experimental autoimmune encephalomyelitis (EAE). **(A)** Clinical EAE scores of WT and MCU-deficient (*Mcu*$^{fl/fl}$*Cd4*^{Cre}) mice after immunization with MOG_{35-55} peptide; means ± SEM of 4-5 mice per cohort. **(B)** Relative weight change of WT and MCU-deficient mice after immunization with MOG_{35-55} peptide emulsified in CFA; means ± SEM of 4-5 mice per cohort. **(C)** Histopathological examination of spinal cord sections of WT and MCU-deficient mice 20 days after MOG_{35-55} immunization stained with Luxol fast blue (myelin) and Cresyl violet (nuclei). White arrows indicate leukocytic infiltrates and areas of demyelination (denoted with an asterisk). **(D)** Analyses of lymphocytic infiltrations in the CNS of WT and MCU-deficient mice 20 days after MOG_{35-55} immunization. **(E)** Flow cytometric analyses of IFNγ, IL-17A, IL-2 and GM-CSF production of $CD4^+$ T cells isolated from the CNS of WT and *Mcu*$^{fl/fl}$*Cd4*^{Cre} mice 20 days after MOG_{35-55} peptide immunization and stimulation with PMA/Iono for 5 h. **(F)** Frequencies of IL-17A, IFNγ, GM-CSF, IL-2 and TNFα-producing $CD4^+$ T cells in the spleen, inLN and CNS of MOG_{35-55}-imunized WT and *Mcu*$^{fl/fl}$*Cd4*^{Cre} mice after stimulation with PMA/ionomycin for 5 h; means ± SEM of 3-4 mice.

T cells and $Foxp3^+$ Treg cells in *Mcu*$^{fl/fl}$*Cd4*^{Cre} mice compared to WT controls (**Figure 4A**). The clonal expansion of LCMV-specific $CD4^+$ T cells, which were monitored with tetramers loaded with the LCMV-derived GP_{66-77} peptide, was also unaltered (**Figure 4A**). Furthermore, Tfh cell differentiation (**Figure 4B**) and GC B cell responses (**Figure 4C**) were intact in *Mcu*$^{fl/fl}$*Cd4*^{Cre} mice, demonstrating that MCU is dispensable for 'helper' T cell responses during viral infection. Although LCMV induces a strong $CD8^+$ T cell-mediated immune response, persistent antigenic stimulation during chronic LCMV infection also promotes T cell 'exhaustion' that is characterized by an upregulation of inhibitory receptors (such as PD-1 and Tim3), loss of effector function (e.g., cytokine expression) and apoptosis of $CD8^+$ T cells (McLane et al., 2019). Using GP_{33-41} tetramers to identify LCMV-specific $CD8^+$ T cells, we did not observe differences in the generation and/or expansion of cytotoxic immune responses in *Mcu*$^{fl/fl}$*Cd4*^{Cre} mice compared to control animals (**Figure 4D**). T cell exhaustion (**Figure 4E**) and cytokine expression (**Figure 4F**) of MCU-deficient T cells were also comparable to those in WT mice, suggesting that MCU is also expendable for 'cytotoxic' anti-viral immune responses.

Collectively, these data demonstrate that, despite attenuating mitochondrial Ca^{2+} uptake and elevating cytosolic Ca^{2+} levels after antigen receptor stimulation, MCU is largely dispensable for T cell-mediated immune responses *in vitro* and in models of autoimmunity and persistent viral infection.

DISCUSSION

Mitochondrial Ca^{2+} uptake is crucial for many cellular functions, including oxidative metabolism, ROS production, signal transduction and the regulation of cell death. In stressed or chronically activated cells, MCU triggers mitochondrial Ca^{2+} overload that causes the opening of the mPTP and the release of pro-apoptotic factors. Thus, tight control of mitochondrial Ca^{2+} uptake safeguards cellular survival and alterations in mitochondrial Ca^{2+} handling have been linked to a variety of diseases. Not surprisingly, MCU gained attention as a target for therapeutic interventions in different pathologies, including cancer, cardiovascular, and inflammatory disorders.

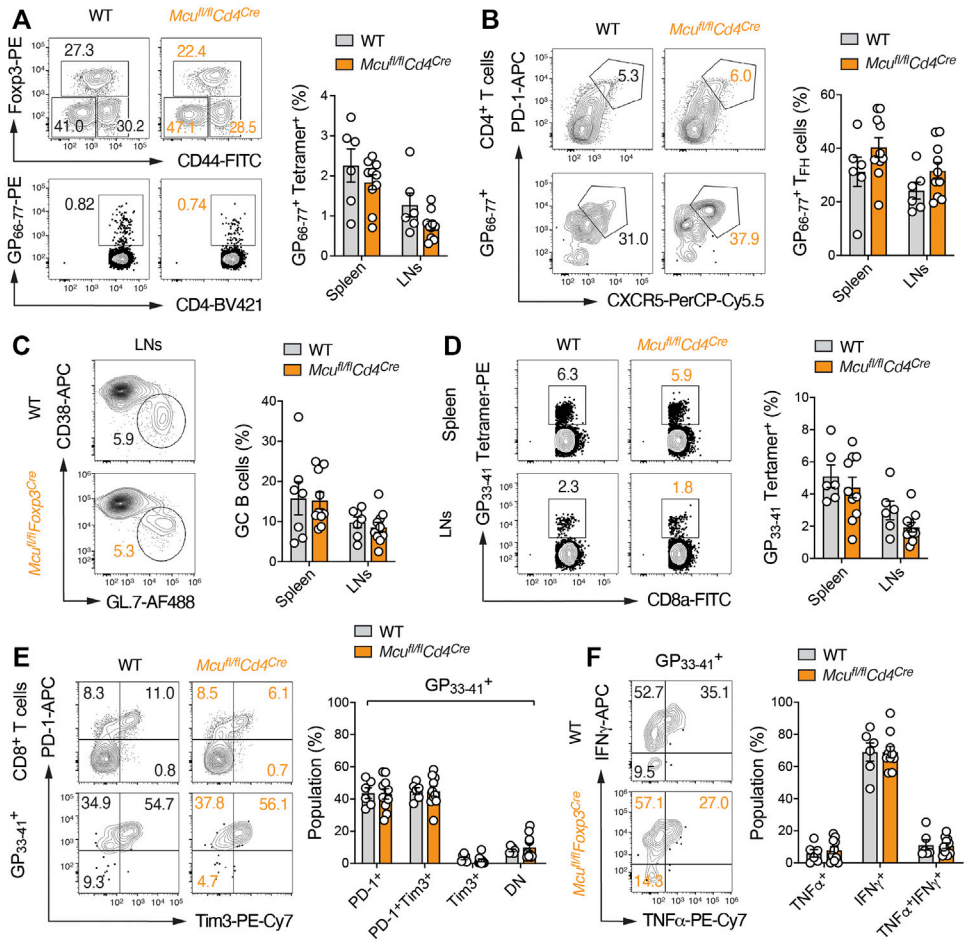

FIGURE 4 | T cell-specific ablation of MCU does not affect adaptive immune responses to persistent LCMV infection. **(A–C)** $CD4^+$ T cell immune responses in chronically infected WT and MCU-deficient (*Mcu*$^{fl/fl}$*Cd4*^{Cre}) mice. **(A)** Analysis of $Foxp3^+$ Treg and LCMV-specific (GP_{66-77} tetramer$^+$) effector $CD4^+$ T cell populations in WT and MCU-deficient mice 23 days after LCMV infection; means ± SEM of 6–10 mice. **(B)** Flow cytometric analysis of T follicular helper (T_{FH}) cells in total $CD4^+$ and LCMV-specific (GP_{66-77} tetramer$^+$) T cells 23 days after LCMV infection; means ± SEM of 6–10 mice. **(C)** Quantification of germinal center (GC) B cells in spleen and LNs of WT and *Mcu*$^{fl/fl}$*Cd4*^{Cre} mice; means ± SEM of 6–10 mice. **(D–F)** $CD8^+$ T cell immune responses in chronically infected WT and MCU-deficient mice. **(D)** Flow cytometric quantification of LCMV-specific (GP_{33-41} tetramer$^+$) effector $CD8^+$ T cell populations in the spleens and LNs of WT and MCU-deficient mice 23 days after infection; means ± SEM of 6-9 mice. **(E)** Analysis of PD-1 and Tim3 expression on total $CD8^+$ and LCMV-specific (GP_{66-77} tetramer$^+$) T cells 23 days after LCMV infection; means ± SEM of 6–10 mice. **(F)** Frequencies of IFNγ and TNFα-producing LCMV-specific (GP_{33-41} tetramer$^+$) T cells in WT and *Mcu*$^{fl/fl}$*Cd4*^{Cre} mice 10 d post infection and re-stimulation with PMA/ionomycin for 5 h; means ± SEM of 6-9 mice.

Ca^{2+} signals play fundamental roles in the immune system. They not only control the differentiation and effector function of lymphocytes at the transcriptional level but also promote their metabolic re-programming (Vaeth et al., 2020). We have recently shown that SOCE regulates multiple metabolic pathways in T cells, including glycolysis, mitochondrial metabolism and OXPHOS (Vaeth et al., 2017a; Wang Y. et al., 2020; Kahlfuss et al., 2020). SOCE-mediated NFAT signaling induces the expression of glucose transporters and glycolytic enzymes, resulting in an impaired glucose uptake and metabolism when extracellular Ca^{2+} influx or NFAT is inhibited (Vaeth et al., 2017a; Vaeth et al., 2020). The regulation of mitochondrial metabolism by SOCE is, however, less well understood (Wang Y. et al., 2020). Ca^{2+} influx through SOCE triggers MCU opening and the uptake of cytosolic Ca^{2+} into the mitochondrial matrix could directly stimulate OXPHOS and mitochondrial ATP synthesis. On the other hand, many SOCE-dependent mitochondrial proteins are encoded in the nucleus, arguing that cytosolic Ca^{2+} could also control mitochondrial metabolism independently of MCU.

We here show, contrary to our expectation, that ablation of MCU has no obvious effects on T cell metabolism, differentiation and effector function *in vitro* and in animal models of autoimmunity and viral infection. Although our results were unexpected, they are in line with the unaltered or mild phenotypes of mice with global or conditional deletion of MCU in various non-immune tissues (Wang P. et al., 2020). Of note, all published MCU-deficient mouse strains did not reveal an energy crisis, suggesting MCU-mediated Ca^{2+} uptake is largely dispensable for mitochondrial metabolism under basal conditions. Only after acute stimulation and/or stress of

tissues with a high mitochondrial workload, such as skeletal or cardiac muscle, genetic inhibition of mitochondrial Ca^{2+} uptake revealed moderate effects, albeit not consistently observed in all MCU-deficient strains (Wang P. et al., 2020). The findings presented in this study and previous reports using MCU-deficient mice are in stark contrast to the expected importance of mitochondrial Ca^{2+} uptake that was predicted from *in vitro* experiments. This discrepancy may be explained by the presence of additional, so far undefined, mitochondrial Ca^{2+} handling molecules or other (ionic) adaptions that compensate for the lack of MCU *in vivo* (Wang P. et al., 2020).

The consequences of mitochondrial Ca^{2+} uptake on cytosolic Ca^{2+} levels remain complex (Paupe and Prudent, 2018; Wang P. et al., 2020; Yoast et al., 2021). In most previous reports, MCU blockade by pharmacological inhibition or RNAi attenuated ER store depletion and SOCE (Hoth et al., 1997; Gilabert et al., 2001; Deak et al., 2014; Samanta et al., 2014; Tang et al., 2015; Samanta et al., 2020). Other studies found that MCU-deficient lymphocytes and macrophages showed enhanced store depletion and/or SOCE (Seegren et al., 2020; Yoast et al., 2021). Impaired cytosolic Ca^{2+} influx in absence of MCU was explained by an accelerated CDI of IP_3R and/or CRAC channels that causes their premature closing when incoming Ca^{2+} cannot be taken up by adjacent mitochondria (Quintana et al., 2007; Lioudyno et al., 2008; Quintana et al., 2011; Deak et al., 2014; Samanta et al., 2014; Tang et al., 2015). In this study, we found that genetic ablation of MCU did not impair store depletion and SOCE but, instead, caused a slightly enhanced extracellular Ca^{2+} influx in primary T cells. These observations are in line with recent reports of macrophages and lymphocytes from MCU-deficient mice that showed a similar increase of cytosolic Ca^{2+} (Seegren et al., 2020; Yoast et al., 2021). Furthermore, complete deletion of mitochondria in activated T cells enhanced SOCE (Lisci et al., 2021), indicating that mitochondria *per se* and, thus, mitochondrial Ca^{2+} buffering are not essential for SOCE in primary T cells. Our seemingly contradictory findings compared to other reports may have a simple explanation: defective Ca^{2+} uptake from the cytosol into the mitochondrial matrix in MCU-deficient lymphocytes causes an accumulation of cytoplasmic Ca^{2+}, resulting in a net increase of SOCE. Enhanced SOCE in MCU-deficient T cells could have been expected to amplify and augment T cell effector function and metabolism, which was, however, not the case. These observations are reminiscent of our previous findings using ORAI2-deficient mice that show a similar elevation of SOCE without increasing the effector functions of T cells in animal models of infection and autoimmunity (Vaeth et al., 2017b).

A possible explanation for our finding that MCU is largely dispensable for murine T cell function is that adaptational changes in the mitochondria may compensate for the "chronic" loss of MCU in $Mcu^{fl/fl}Cd4^{Cre}$ mice. It was shown before that deletion of MCU alone is not sufficient to completely abolish mitochondrial Ca^{2+} uptake in neurons (Hamilton et al., 2018). Furthermore, mitochondria store large amounts of Ca^{2+} as precipitates and acidification of the mitochondrial matrix during respiration dissolves these crystals and releases intra-mitochondrially free Ca^{2+} ions in an MCU-independent fashion (Hernansanz-Agustín et al., 2020). Although we did not find significant effects of MCU on T cell proliferation, differentiation and effector function, our results do not exclude a potential role of MCU in the adaptive immune system. It is noteworthy that we could not test all scenarios in which T cells play an important role and that MCU's importance could be different in human T cells. Our findings also have important technical implications as previous studies relied frequently on pharmacological MCU inhibitors but the genetic deletion of MCU does not recapitulate these findings. However, Ruthenium-based inhibitors are taken up inefficiently by intact cells, have a poor selectivity for MCU and affect, in addition, other Ca^{2+} channels, such as ryanodine receptors, TRP channels and SERCA pumps (Finkel et al., 2015; Woods and Wilson, 2020). Thus, future studies using genetic approaches are warranted to better define MCU's role in murine and human T cells and other (non-)immune cell types.

DATA AVAILABILITY STATEMENT

The raw data supporting the conclusions of this article will be made available by the authors, without undue reservation.

ETHICS STATEMENT

The animal studies were reviewed and approved by the Government of Lower Franconia.

AUTHOR CONTRIBUTIONS

Participated in research design: MV, JD, IB, AN, CM. Conducted experiments: HW, ME, SH, BB, MS, AN. Performed data analysis: MV, MS, AN, IB, BB, SH. Wrote the manuscript: MV.

FUNDING

This work was supported by the Deutsche Forschungsgemeinschaft (German Research Foundation) SFB-TRR 124/3 2021 210879364, SFB-TRR 338/1 2021 452881907, VA882/2-1 (to M.V.), SFB 1027, SFB 1190 and IRTG1816 (to I.B.), DU1839/2-1 (to D.U.), SFB 894, SFB-TRR 219, Ma 2528/7-1 (to C.M.) and the Federal Ministry of Education and Research (BMBF) 01EO1504 (to C.M.).

ACKNOWLEDGMENTS

We thank the Vaeth, Bogeski and Dudek labs for helpful discussions and Anja Sauer for excellent technical

assistance. The LCMV-specific tetramers used in this study were kindly provided by the NIH Tetramer Core Facility. We thank Drs. Wolfgang Kastenmüller and Mercedes Gomez de Agüero for critically reading the manuscript.

REFERENCES

Ataide, M. A., Komander, K., Knöpper, K., Peters, A. E., Wu, H., Eickhoff, S., et al. (2020). BATF3 Programs CD8 T Cell Memory. *Nat. Immunol.* 21 (11), 1397–1407. doi:10.1038/s41590-020-0786-2

Deak, A. T., Blass, S., Khan, M. J., Groschner, L. N., Waldeck-Weiermair, M., Hallström, S., et al. (2014). IP3-mediated STIM1 Oligomerization Requires Intact Mitochondrial Ca2+ Uptake. *J. Cel Sci* 127 (Pt 13), 2944–2955. doi:10.1242/jcs.149807

Finkel, T., Menazza, S., Holmström, K. M., Parks, R. J., Liu, J., Sun, J., et al. (2015). The Ins and Outs of Mitochondrial Calcium. *Circ. Res.* 116 (11), 1810–1819. doi:10.1161/CIRCRESAHA.116.305484

Flores-Santibáñez, F., Cuadra, B., Fernández, D., Rosemblatt, M. V., Núñez, S., Cruz, P., et al. (2018). In Vitro-Generated Tc17 Cells Present a Memory Phenotype and Serve as a Reservoir of Tc1 Cells *In Vivo*. *Front. Immunol.* 9, 209. doi:10.3389/fimmu.2018.00209

Gilabert, J. A., Bakowski, D., and Parekh, A. B. (2001). Energized Mitochondria Increase the Dynamic Range over Which Inositol 1,4,5-trisphosphate Activates Store-Operated Calcium Influx. *EMBO J.* 20 (11), 2672–2679. doi:10.1093/emboj/20.11.2672

Hamilton, J., Brustovetsky, T., Rysted, J. E., Lin, Z., Usachev, Y. M., and Brustovetsky, N. (2018). Deletion of Mitochondrial Calcium Uniporter Incompletely Inhibits Calcium Uptake and Induction of the Permeability Transition Pore in Brain Mitochondria. *J. Biol. Chem.* 293 (40), 15652–15663. doi:10.1074/jbc.RA118.002926

Hernansanz-Agustín, P., Choya-Foces, C., Carregal-Romero, S., Ramos, E., Oliva, T., Villa-Piña, T., et al. (2020). Na+ Controls Hypoxic Signalling by the Mitochondrial Respiratory Chain. *Nature* 586 (7828), 287–291. doi:10.1038/s41586-020-2551-y

Hoth, M., Fanger, C. M., and Lewis, R. S. (1997). Mitochondrial Regulation of Store-Operated Calcium Signaling in T Lymphocytes. *J. Cel Biol* 137 (3), 633–648. doi:10.1083/jcb.137.3.633

Kahlfuss, S., Kaufmann, U., Concepcion, A. R., Noyer, L., Raphael, D., Vaeth, M., et al. (2020). STIM1-mediated Calcium Influx Controls Antifungal Immunity and the Metabolic Function of Non-pathogenic Th17 Cells. *EMBO Mol. Med.* 12 (8), e11592. doi:10.15252/emmm.201911592

Kwong, J. Q., Lu, X., Correll, R. N., Schwanekamp, J. A., Vagnozzi, R. J., Sargent, M. A., et al. (2015). The Mitochondrial Calcium Uniporter Selectively Matches Metabolic Output to Acute Contractile Stress in the Heart. *Cell Rep* 12 (1), 15–22. doi:10.1016/j.celrep.2015.06.002

Lioudyno, M. I., Kozak, J. A., Penna, A., Safrina, O., Zhang, S. L., Sen, D., et al. (2008). Orai1 and STIM1 Move to the Immunological Synapse and Are Up-Regulated during T Cell Activation. *Proc. Natl. Acad. Sci. U S A.* 105 (6), 2011–2016. doi:10.1073/pnas.0706122105

Lisci, M., Barton, P. R., Randzavola, L. O., Ma, C. Y., Marchingo, J. M., Cantrell, D. A., et al. (2021). Mitochondrial Translation Is Required for Sustained Killing by Cytotoxic T Cells. *Science* 374 (6565), eabe9977. doi:10.1126/science.abe9977

McLane, L. M., Abdel-Hakeem, M. S., and Wherry, E. J. (2019). CD8 T Cell Exhaustion during Chronic Viral Infection and Cancer. *Annu. Rev. Immunol.* 37, 457–495. doi:10.1146/annurev-immunol-041015-055318

Paupe, V., and Prudent, J. (2018). New Insights into the Role of Mitochondrial Calcium Homeostasis in Cell Migration. *Biochem. Biophys. Res. Commun.* 500 (1), 75–86. doi:10.1016/j.bbrc.2017.05.039

Quintana, A., Pasche, M., Junker, C., Al-Ansary, D., Rieger, H., Kummerow, C., et al. (2011). Calcium Microdomains at the Immunological Synapse: How ORAI Channels, Mitochondria and Calcium Pumps Generate Local Calcium Signals for Efficient T-Cell Activation. *EMBO J.* 30 (19), 3895–3912. doi:10.1038/emboj.2011.289

Quintana, A., Schwindling, C., Wenning, A. S., Becherer, U., Rettig, J., Schwarz, E. C., et al. (2007). T Cell Activation Requires Mitochondrial Translocation to the Immunological Synapse. *Proc. Natl. Acad. Sci. U S A.* 104 (36), 14418–14423. doi:10.1073/pnas.0703126104

Samanta, K., Bakowski, D., Amin, N., and Parekh, A. B. (2020). The Whole-Cell Ca2+ Release-Activated Ca2+ Current, ICRAC , Is Regulated by the Mitochondrial Ca2+ Uniporter Channel and Is Independent of Extracellular and Cytosolic Na. *J. Physiol.* 598 (9), 1753–1773. doi:10.1113/JP276551

Samanta, K., Douglas, S., and Parekh, A. B. (2014). Mitochondrial Calcium Uniporter MCU Supports Cytoplasmic Ca2+ Oscillations, Store-Operated Ca2+ Entry and Ca2+-dependent Gene Expression in Response to Receptor Stimulation. *PLoS One* 9 (7), e101188. doi:10.1371/journal.pone.0101188

Seegren, P. V., Downs, T. K., Stremska, M. E., Harper, L. R., Cao, R., Olson, R. J., et al. (2020). Mitochondrial Ca2+ Signaling Is an Electrometabolic Switch to Fuel Phagosome Killing. *Cel Rep* 33 (8), 108411. doi:10.1016/j.celrep.2020.108411

Stromnes, I. M., and Goverman, J. M. (2006). Active Induction of Experimental Allergic Encephalomyelitis. *Nat. Protoc.* 1 (4), 1810–1819. doi:10.1038/nprot.2006.285

Tang, S., Wang, X., Shen, Q., Yang, X., Yu, C., Cai, C., et al. (2015). Mitochondrial Ca^{2+} Uniporter Is Critical for Store-Operated Ca^{2+} Entry-dependent Breast Cancer Cell Migration. *Biochem. Biophys. Res. Commun.* 458 (1), 186–193. doi:10.1016/j.bbrc.2015.01.092

Vaeth, M., Eckstein, M., Shaw, P. J., Kozhaya, L., Yang, J., Berberich-Siebelt, F., et al. (2016). Store-Operated Ca(2+) Entry in Follicular T Cells Controls Humoral Immune Responses and Autoimmunity. *Immunity* 44 (6), 1350–1364. doi:10.1016/j.immuni.2016.04.013

Vaeth, M., Kahlfuss, S., and Feske, S. (2020). CRAC Channels and Calcium Signaling in T Cell-Mediated Immunity. *Trends Immunol.* 41 (10), 878–901. doi:10.1016/j.it.2020.06.012

Vaeth, M., Maus, M., Klein-Hessling, S., Freinkman, E., Yang, J., Eckstein, M., et al. (2017a). Store-Operated Ca2+ Entry Controls Clonal Expansion of T Cells through Metabolic Reprogramming. *Immunity.* 47 (4), 664–679.e6. doi:10.1016/j.immuni.2017.09.003

Vaeth, M., Yang, J., Yamashita, M., Zee, I., Eckstein, M., Knosp, C., et al. (2017b). ORAI2 Modulates Store-Operated Calcium Entry and T Cell-Mediated Immunity. *Nat. Commun.* 8, 14714. doi:10.1038/ncomms14714

Wang, P., Fernandez-Sanz, C., Wang, W., and Sheu, S. S. (2020). Why Don't Mice Lacking the Mitochondrial Ca2+ Uniporter Experience an Energy Crisis? *J. Physiol.* 598 (7), 1307–1326. doi:10.1113/JP276636

Wang, Y., Tao, A., Vaeth, M., and Feske, S. (2020). Calcium Regulation of T Cell Metabolism. *Curr. Opin. Physiol.* 17, 207–223. doi:10.1016/j.cophys.2020.07.016

Woods, J. J., and Wilson, J. J. (2020). Inhibitors of the Mitochondrial Calcium Uniporter for the Treatment of Disease. *Curr. Opin. Chem. Biol.* 55, 9–18. doi:10.1016/j.cbpa.2019.11.006

Yoast, R. E., Emrich, S. M., Zhang, X., Xin, P., Arige, V., Pathak, T., et al. (2021). The Mitochondrial Ca2+ Uniporter Is a central Regulator of Interorganellar Ca2+ Transfer and NFAT Activation. *J. Biol. Chem.* 297 (4), 101174. doi:10.1016/j.jbc.2021.101174

SUPPLEMENTARY MATERIAL

The Supplementary Material for this article can be found online at: https://www.frontiersin.org/articles/10.3389/fphar.2021.734078/full#supplementary-material

Conflict of Interest: The authors declare that the research was conducted in the absence of any commercial or financial relationships that could be construed as a potential conflict of interest.

Publisher's Note: All claims expressed in this article are solely those of the authors and do not necessarily represent those of their affiliated organizations, or those of the publisher, the editors and the reviewers. Any product that may be evaluated in this article, orclaim that may be made by its manufacturer, is not guaranteed or endorsed by the publisher.

frontiers | Frontiers in Pharmacology

ORIGINAL RESEARCH
published: 24 May 2022
doi: 10.3389/fphar.2022.795176

Distinct Gene Expression Patterns of Calcium Channels and Related Signaling Pathways Discovered in Lymphomas

Shawna R. Stanwood[1,2,3,4], *Lauren C. Chong*[5], *Christian Steidl*[6,7] and *Wilfred A. Jefferies*[1,2,3,4,8,9,10,11]*

[1]Michael Smith Laboratories, University of British Columbia, Vancouver, BC, Canada, [2]Vancouver Prostate Centre, Vancouver General Hospital, Vancouver, BC, Canada, [3]Centre for Blood Research, University of British Columbia, Vancouver, BC, Canada, [4]Department of Microbiology and Immunology, University of British Columbia, Vancouver, BC, Canada, [5]Centre for Lymphoid Cancer, British Columbia Cancer Research Institute, Vancouver, BC, Canada, [6]Lymphoid Cancer Research, British Columbia Cancer Research Institute, Vancouver, BC, Canada, [7]Department of Pathology and Laboratory Medicine, University of British Columbia, Vancouver, BC, Canada, [8]Djavad Mowafaghian Centre for Brain Health, University of British Columbia, Vancouver, BC, Canada, [9]Department of Medical Genetics, University of British Columbia, Vancouver, BC, Canada, [10]Department of Urological Sciences, University of British Columbia, Vancouver, BC, Canada, [11]Department of Zoology, University of British Columbia, Vancouver, BC, Canada

OPEN ACCESS

Edited by:
Heike Wulff,
University of California, Davis,
United States

Reviewed by:
Isaac Jardin,
University of Extremadura, Spain
Indu Ambudkar,
National Institute of Dental and Craniofacial Research (NIH),
United States

***Correspondence:**
Wilfred A. Jefferies
wilf@msl.ubc.ca

Specialty section:
This article was submitted to Pharmacology of Ion Channels and Channelopathies, a section of the journal Frontiers in Pharmacology

Received: 14 October 2021
Accepted: 24 March 2022
Published: 24 May 2022

Citation:
Stanwood SR, Chong LC, Steidl C and Jefferies WA (2022) Distinct Gene Expression Patterns of Calcium Channels and Related Signaling Pathways Discovered in Lymphomas. Front. Pharmacol. 13:795176. doi: 10.3389/fphar.2022.795176

Cell surface calcium (Ca^{2+}) channels permit Ca^{2+} ion influx, with Ca^{2+} taking part in cellular functions such as proliferation, survival, and activation. The expression of voltage-dependent Ca^{2+} (Ca_V) channels may modulate the growth of hematologic cancers. Profile analysis of Ca^{2+} channels, with a focus on the Ca^{2+} release-activated Ca^{2+} (CRAC) and L-type Ca_V channels, was performed on RNA sequencing data from lymphoma cell lines and samples derived from patients with diffuse large B cell lymphoma (DLBCL). $Ca_V1.2$ expression was found to be elevated in classical Hodgkin lymphoma (CHL) cell lines when compared to other B cell lymphoma cell lines. In contrast, CHL exhibited reduced expression of ORAI2 and STIM2. In our differential expression analysis comparing activated B cell-like DLBCL (ABC-DLBCL) and germinal centre B cell-like DLBCL (GCB-DLBCL) patient samples, ABC-DLBCL revealed stronger expression of $Ca_V1.3$, whereas $Ca_V1.1$, $Ca_V1.2$, and $Ca_V1.4$ showed greater expression levels in GCB-DLBCL. Interestingly, no differences in ORAI/STIM expression were noted in the patient samples. As Ca^{2+} is known to bind to calmodulin, leading to calcineurin activation and the passage of nuclear factor of activated T cells (NFAT) to the cell nucleus, pathways for calcineurin, calmodulin, NFAT, and Ca^{2+} signaling were also analyzed by gene set enrichment analysis. The NFAT and Ca^{2+} signaling pathways were found to be upregulated in the CHL cell lines relative to other B cell lymphoma cell lines. Furthermore, the calmodulin and Ca^{2+} signaling pathways were shown to be downregulated in the ABC-DLBCL patient samples. The findings of this study suggest that L-type Ca_V channels and Ca^{2+}-related pathways could serve as differentiating components for biologic therapies in targeted lymphoma treatments.

Keywords: calcium channel, lymphoma, leukaemia, signaling pathway, sequencing

INTRODUCTION

Hodgkin lymphoma, non-Hodgkin lymphoma (NHL), and leukemia collectively constitute 5.7% of all new cases of cancer (Sung et al., 2021). The ability to conduct expression profiling of genes has greatly contributed to knowledge pertaining to leukemia and lymphoma in terms of categorization of subtypes (Hoefnagel et al., 2005; Bobée et al., 2020), disease aggressiveness (Glas et al., 2005), and relapse (Yeoh et al., 2002). Differences in the expression of subunits of ion channels, including potassium (K^+) channels, sodium (Na^+) channels, and calcium (Ca^{2+}) channels, have been noted in relapsed follicular lymphoma compared to counterparts who have not relapsed (Magi et al., 2019). The Ca^{2+} release-activated Ca^{2+} (CRAC) channel, a well-characterized example of a Ca^{2+} channel, consists of stromal interacting molecule (STIM) and ORAI proteins (Putney, 2018). Orai3 expression has been shown to be elevated in leukemia/multiple myeloma cell lines sensitive to tipifarnib when compared to a resistant myeloma cell line (Yanamandra et al., 2011). Furthermore, upregulation and downregulation of voltage-dependent Ca^{2+} (Ca_V) channel expression have been established for leukemia and lymphoma, along with many additional kinds of cancer (by publicly accessible data from microarrays), suggesting that the channels are engaged in the development of cancer (Wang et al., 2015; Phan et al., 2017).

Ca^{2+} channels are known to be positioned at the plasma membrane of the cell (Omilusik et al., 2013). Once Ca^{2+} is in the cell, it can guide proliferation, homeostasis, differentiation, survival, and activation by taking part in intracellular pathways (Omilusik

TABLE 1 | Sequencing conditions used for RNA sequencing of lymphoma cell lines. Cell lines of various pathologies were included for analysis.

Cell Line	Read Length	Sequencer	Pathology	Source
HDLM-2	75bp	HiSeq	Classical Hodgkin Lymphoma	BC Cancer
HDMYZ	151bp	MiSeq	Classical Hodgkin Lymphoma	BC Cancer
KM-H2	50bp	GA	Classical Hodgkin Lymphoma	BC Cancer
L-1236	75bp	HiSeq	Classical Hodgkin Lymphoma	BC Cancer
L-428	50bp	GA	Classical Hodgkin Lymphoma	BC Cancer
L-540	75bp	HiSeq	Classical Hodgkin Lymphoma	BC Cancer
L-591	75bp	HiSeq	Classical Hodgkin Lymphoma	BC Cancer
SUP-HD1	75bp	HiSeq	Classical Hodgkin Lymphoma	BC Cancer
U-H01	75bp	HiSeq	Classical Hodgkin Lymphoma	BC Cancer
Farage	151bp	MiSeq	Primary Mediastinal B-cell Lymphoma	BC Cancer
GRANTA519	75bp	HiSeq	Mantle Cell Lymphoma	BC Cancer
Jeko-1	75bp	HiSeq	Mantle Cell Lymphoma	BC Cancer
JVM2	75bp	HiSeq	Mantle Cell Lymphoma	BC Cancer
Mino	75bp	HiSeq	Mantle Cell Lymphoma	BC Cancer
REC-1	75bp	HiSeq	Mantle Cell Lymphoma	BC Cancer
SP-49	75bp	HiSeq	Mantle Cell Lymphoma	BC Cancer
SP-53	75bp	HiSeq	Mantle Cell Lymphoma	BC Cancer
Z138	75bp	HiSeq	Mantle Cell Lymphoma	BC Cancer
Karpas-1106P	50bp	GA	Primary Mediastinal B-cell Lymphoma	BC Cancer
MedB-1	75bp	HiSeq	Primary Mediastinal B-cell Lymphoma	BC Cancer
U-2940	75bp	HiSeq	Primary Mediastinal B-cell Lymphoma	BC Cancer
Raji	75bp	HiSeq	Burkitt's Lymphoma	BC Cancer
Ramos	75bp	HiSeq	Burkitt's Lymphoma	BC Cancer
DEV	50bp	GA	Nodular lymphocyte-predominant Hodgkin lymphoma	BC Cancer
DB	36bp	GA	Diffuse Large B-cell Lymphoma (Germinal Centre B-cell-like)	BC Cancer
DOHH-2	50bp	GA	Diffuse Large B-cell Lymphoma (Germinal Centre B-cell-like)	BC Cancer
HBL-1	75bp	HiSeq	Diffuse Large B-cell Lymphoma (Activated B-cell-like)	BC Cancer
HT	75bp	HiSeq	Diffuse Large B-cell Lymphoma (Germinal Centre B-cell-like)	BC Cancer
Karpas422	50bp	GA	Diffuse Large B-cell Lymphoma (Germinal Centre B-cell-like)	BC Cancer
MD903	75bp	HiSeq	Diffuse Large B-cell Lymphoma (Activated B-cell-like)	BC Cancer
NU-DHL-1	50bp	GA	Diffuse Large B-cell Lymphoma (Germinal Centre B-cell-like)	BC Cancer
NU-DUL-1	50bp	GA	Diffuse Large B-cell Lymphoma (Activated B-cell-like)	BC Cancer
OCI-Ly1	50bp	GA	Diffuse Large B-cell Lymphoma (Germinal Centre B-cell-like)	BC Cancer
OCI-Ly10	75bp	HiSeq	Diffuse Large B-cell Lymphoma (Activated B-cell-like)	BC Cancer
OCI-Ly3	75bp	HiSeq	Diffuse Large B-cell Lymphoma (Activated B-cell-like)	BC Cancer
OCI-Ly7	50bp	GA	Diffuse Large B-cell Lymphoma (Germinal Centre B-cell-like)	BC Cancer
Pfeiffer	75bp	HiSeq	Diffuse Large B-cell Lymphoma (Germinal Centre B-cell-like)	BC Cancer
SU-DHL-10	75bp	HiSeq	Diffuse Large B-cell Lymphoma (Germinal Centre B-cell-like)	BC Cancer
SU-DHL-4	75bp	HiSeq	Diffuse Large B-cell Lymphoma (Germinal Centre B-cell-like)	BC Cancer
SU-DHL-5	75bp	HiSeq	Diffuse Large B-cell Lymphoma (Germinal Centre B-cell-like)	BC Cancer
SU-DHL-6	50bp	GA	Diffuse Large B-cell Lymphoma (Germinal Centre B-cell-like)	BC Cancer
SU-DHL-8	75bp	HiSeq	Diffuse Large B-cell Lymphoma (Activated B-cell-like)	BC Cancer
Toledo	75bp	HiSeq	Diffuse Large B-cell Lymphoma (Germinal Centre B-cell-like)	BC Cancer
WSU-DLCL2	50bp	GA	Diffuse Large B-cell Lymphoma (Germinal Centre B-cell-like)	BC Cancer

TABLE 2 | BioCarta and KEGG pathways. Components of the calcineurin, calmodulin, NFAT, and Ca^{2+} signaling pathways are listed.

Pathway	Components
Calcineurin (BioCarta)	CALM1, CALM2, CALM3, CDKN1A, CYCSP35, GNAQ, LOC124827, LOC147908, MARCKS, NFATC1, NFATC2, NFATC3, NFATC4, PLCG1, PPP3CA, PPP3CB, PPP3CC, PRKCA, PRKCB, SP1, and SP3
Calmodulin (BioCarta)	CALM1, CALM2, CALM3, CAMK1, CAMK1G, CAMK2A, CAMK2B, CAMK2D, CAMK2G, CAMK4, CAMKK1, CAMKK2, CREB1, CYCSP35, LOC124827, and LOC147908
Nuclear factor of activated T cells (NFAT) (BioCarta)	ACTA1, AGT, AKT1, CALM1, CALM2, CALM3, CALR, CAMK1, CAMK1G, CAMK4, CREBBP, CSNK1A1, CTF1, CYCSP35, EDN1, ELSPBP1, F2, FGF2, FKBP1A, GATA4, GSK3B, HAND1, HAND2, HBEGF, HRAS, IGF1, LIF, LOC124827, LOC147908, MAP2K1, MAPK1, MAPK14, MAPK3, MAPK8, MEF2C, MYH2, NFATC1, NFATC2, NFATC3, NFATC4, NKX2-5, NPPA, PIK3CA, PIK3CG, PIK3R1, PPP3CA, PPP3CB, PPP3CC, PRKACB, PRKACG, PRKAR1A, PRKAR1B, PRKAR2A, PRKAR2B, RAF1, and RPS6KB1
Ca^{2+} signaling (KEGG)	ADCY1, ADCY2, ADCY3, ADCY4, ADCY7, ADCY8, ADCY9, ADORA2A, ADORA2B, ADRA1A, ADRA1B, ADRA1D, ADRB1, ADRB2, ADRB3, AGTR1, ATP2A1, ATP2A2, ATP2A3, ATP2B1, ATP2B2, ATP2B3, ATP2B4, AVPR1A, AVPR1B, BDKRB1, BDKRB2, BST1, CACNA1A, CACNA1B, CACNA1C, CACNA1D, CACNA1E, CACNA1F, CACNA1G, CACNA1H, CACNA1I, CACNA1S, CALM1, CALM2, CALM3, CALML3, CALML5, CALML6, CAMK2A, CAMK2B, CAMK2D, CAMK2G, CAMK4, CCKAR, CCKBR, CD38, CHP, CHP2, CHRM1, CHRM2, CHRM3, CHRM5, CHRNA7, CYSLTR1, CYSLTR2, DRD1, DRD5, EDNRA, EDNRB, EGFR, ERBB2, ERBB3, ERBB4, F2R, GNA11, GNA14, GNA15, GNAL, GNAQ, GNAS, GRIN1, GRIN2A, GRIN2C, GRIN2D, GRM1, GRM5, GRPR, HRH1, HRH2, HTR2A, HTR2B, HTR2C, HTR4, HTR5A, HTR6, HTR7, ITPKA, ITPKB, ITPR1, ITPR2, ITPR3, LHCGR, LOC729317, LTB4R2, MYLK, MYLK2, MYLK3, NOS1, NOS2, NOS3, NTSR1, OXTR, P2RX1, P2RX2, P2RX3, P2RX4, P2RX5, P2RX6, P2RX7, PDE1A, PDE1B, PDE1C, PDGFRA, PDGFRB, PHKA1, PHKA2, PHKB, PHKG1, PHKG2, PLCB1, PLCB2, PLCB3, PLCB4, PLCD1, PLCD3, PLCD4, PLCE1, PLCG1, PLCG2, PLCZ1, PLN, PPID, PPP3CA, PPP3CB, PPP3CC, PPP3R1, PPP3R2, PRKACA, PRKACB, PRKACG, PRKCA, PRKCB, PRKCG, PRKX, PTAFR, PTGER1, PTGER3, PTGFR, PTK2B, RYR1, RYR2, RYR3, SLC25A31, SLC25A4, SLC25A5, SLC25A6, SLC8A1, SLC8A2, SLC8A3, SPHK1, SPHK2, TACR1, TACR2, TACR3, TBXA2R, TNNC1, TNNC2, TRHR, TRPC1, VDAC1, VDAC2, and VDAC3

et al., 2013). In T lymphocytes, for example, Ca^{2+} can bind to calmodulin, enabling the latter to activate the enzyme calcineurin once bound (Omilusik et al., 2013). Nuclear factor of activated T cells (NFAT) is dephosphorylated by calcineurin, leading to NFAT moving into the cell nucleus (Omilusik et al., 2013). NFAT has long been known to bind to the interleukin-2 (IL-2) promoter with activating protein-1 (AP-1) (Rao et al., 1997). Several other "transcriptional partners" of NFAT include T-bet at the 5' enhancer for interferon (IFN)-γ and IFN-regulatory factor 4 (IRF4) at the promoter for interleukin-4 (IL-4) (Macian, 2005).

Considering the involvement of Ca^{2+} in lymphocyte processes, it would be useful to study Ca^{2+} channel expression more thoroughly in lymphoma. In order to accomplish this objective, patient samples and cell lines were assessed in the current study. This investigation focuses on diagnostic tissue from patients with diffuse large B cell lymphoma (DLBCL) and cell lines representing diverse types of lymphoma. Expanding on the calmodulin/calcineurin/NFAT signaling pathway, several pathways from BioCarta and the Kyoto Encyclopedia of Genes and Genomes (KEGG) were also examined. Here, we present expression profiles relating to Ca^{2+} channels - the CRAC and Ca_V channels in particular - and these pathways. This characterization of expression may aid in cultivating a comprehensive understanding of the molecular basis of lymphoma.

MATERIALS AND METHODS

RNA Sequencing Data

RNA sequencing data were generated at the British Columbia Cancer Research Centre (BC Cancer) from 44 lymphoma cell lines representing multiple pathologies. These datasets were generated at multiple time points and were consolidated for analysis in this study (**Table 1**).

RNA sequencing reads from each cell line were aligned to the hg19 reference using the STAR aligner (v2.5.2a), which also generated per-gene counts with HTSeq.

RNA sequencing data from a previously published cohort of DLBCL patients were also analyzed (Ennishi et al., 2019). Patients whose tumours were successfully assigned to a subtype by the Lymph2Cx assay (Scott et al., 2014) were retained for analysis (N = 301). This included tumours classified as germinal centre B cell-like (GCB-DLBCL; N = 171), activated B cell-like (ABC-DLBCL; N = 96), or unclassified (N = 34). Sequencing data were re-aligned to the hg19 reference to generate counts using the same method as the cell lines.

Comparison of Ca^{2+} Channel Gene Expression

To compare the expression of the Ca^{2+} channel genes between different pathological groups, RNA sequencing counts from all samples were analyzed in R (v3.6.1) using the DESeq2 package (v1.26.0).

For cell lines, counts from all samples were read into a merged *DESeqDataSet* object, and lowly expressed genes (1 or fewer counts across all samples) were removed. The count data were then normalized using a variance-stabilizing transformation (*vst* function). Pairwise t-tests were used to compare normalized counts of numerous genes, such as Ca^{2+} channel genes of interest, between each combination of pathologies. For specific comparisons of interest, differential expression was also performed between pathological pairs (*DESeq* function), and the results for the Ca^{2+} channel genes (p value, adjusted p value (q value), and log2 fold change) were assessed. The same process was performed merging count data from all DLBCL patients and comparing groups by DLBCL subtype.

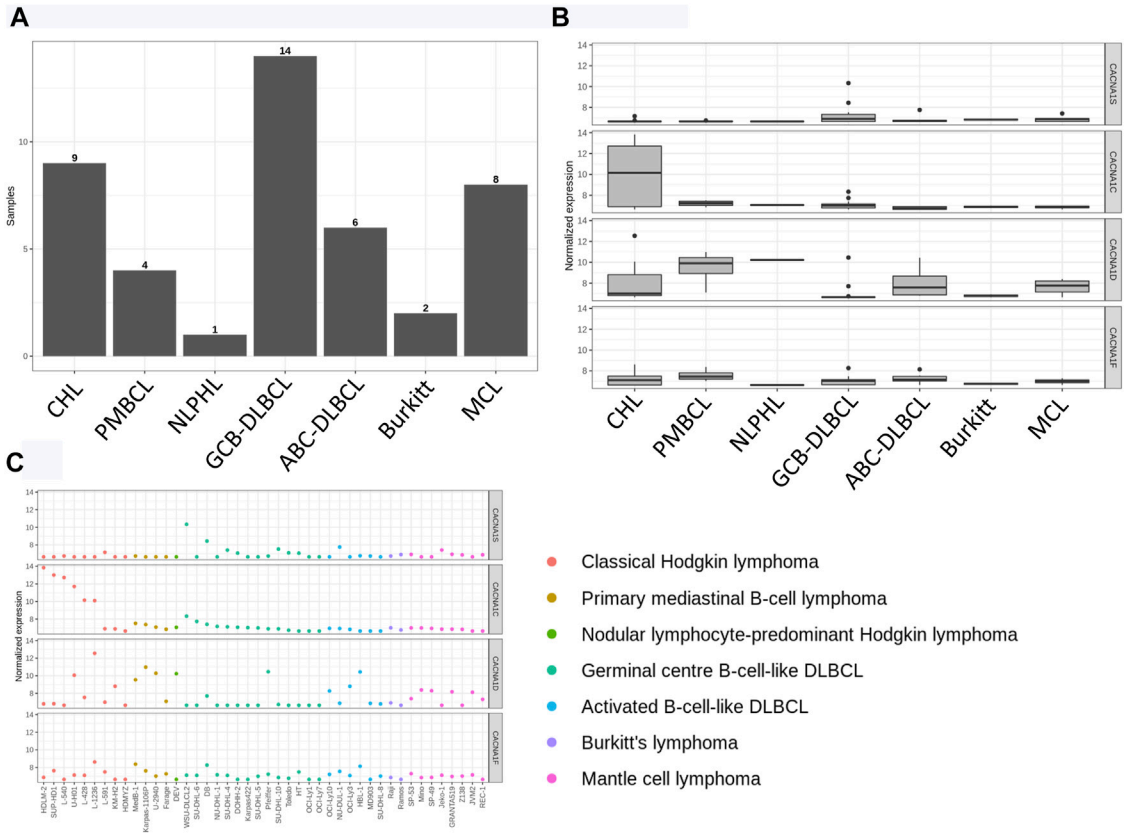

FIGURE 1 | Ca_V1 channel expression in lymphoma cell lines. **(A)** Cell lines were classified according to pathology. **(B)** Expression (normalized and log-transformed counts) of the Ca_V1 channels (CACNA1S, $Ca_V1.1$; CACNA1C, $Ca_V1.2$; CACNA1D, $Ca_V1.3$; CACNA1F, $Ca_V1.4$). The boxes signify the interquartile range. The vertical lines correspond to the largest value that is no further than 1.5 times the interquartile range. The dots designate outliers. **(C)** Ca_V1 channel expression is shown for each cell line.

Gene Set Enrichment Analysis

In order to identify Ca^{2+} channel pathways that were potentially enriched in certain pathological comparisons, the differential expression results were used to perform gene set enrichment using the GSEA tool (v4.1.0). The GSEAPreranked module was used, ranking genes by their differential expression log2 fold change and investigating specific pathways of interest (**Table 2**).

RESULTS

ORAI Expression Varies Among Lymphoma Cell Lines

The included cell line categories consisted of classical Hodgkin lymphoma (CHL), primary mediastinal B cell lymphoma (PMBCL), nodular lymphocyte-predominant Hodgkin lymphoma (NLPHL), GCB-DLBCL, ABC-DLBCL, Burkitt's lymphoma, and mantle cell lymphoma (MCL) (**Figure 1A**). Engagement at the T cell receptor leads to Ca^{2+} release from stores, such as the endoplasmic reticulum (ER), and Ca^{2+} entry at the plasma membrane in a process known as store-operated Ca^{2+} entry (SOCE) (Omilusik et al., 2013). STIM1 and STIM2 act as ER Ca^{2+} sensors, whereas ORAI1 (as well as ORAI2 and ORAI3) is a pore-forming molecule at the cell surface (Omilusik et al., 2013). RNA sequencing data were used to perform pairwise expression comparisons between the different cell line pathologies for multiple genes of interest, including those belonging to the ORAI/STIM family. In the current study, MCL cell lines exhibited greater ORAI1 expression when compared to those representing GCB-DLBCL (adjusted p value = 0.028) (**Supplementary Table S1**). As increased expression of cyclin D1 is a feature of MCL (Vogt et al., 2017), and cyclin D1 has been linked to Ca^{2+} signaling (Kahl and Means, 2004), the high ORAI1 expression in MCL was expected. Moreover, ORAI2 showed increased expression in ABC-DLBCL cell lines relative to CHL cell lines (adjusted p value = 0.046) (**Supplementary Table S1**). Interestingly, the pairwise cell line analysis did not indicate any significant differences in expression level for STIM1/2 (**Supplementary Table S1**), suggesting that ER Ca^{2+} sensing might not vary to a great extent across different types of lymphoma, although this would require further investigation.

TABLE 3 | Comparisons of L-type Ca^{2+} channel expression in cell lines. Statistical analysis is presented in the form of *p* values and *q* values.

Ca_V	Comparison with the Lowest *p* Value and q Value	Category with Higher Expression	*p* value	*q* value
1.1	GCB-DLBCL versus PMBCL	GCB-DLBCL	0.0521351928659242	0.254503787844234
1.2	ABC-DLBCL versus CHL	CHL	0.00651509770928301	0.091494633047757
1.3	Burkitt versus MCL	MCL	0.021600429461562	0.1687969044214
1.4	Burkitt versus PMBCL	PMBCL	0.0645300423866672	0.273783609609632

Although ORAI and STIM play important roles, other Ca^{2+} channels have been shown to be involved in lymphocyte function as well. We have previously provided evidence of voltage-dependent Ca^{2+} channel expression in the Jurkat cell line and peripheral blood T cells (Kotturi et al., 2003). Furthermore, we have previously characterized the role of $Ca_V1.4$ in lymphocytes, particularly T cells, highlighting its importance in SOCE and lymphocyte immune responses (Omilusik et al., 2011). In terms of B cells, increased $Ca_V1.2$ expression has been recorded for B cell childhood acute lymphoblastic leukemia and marginal zone B cell lymphoma (Wang et al., 2015). Given this, we investigated the Ca_V1 family in the current study to assess differences in expression among various lymphoma cell lines, with the normalized expression of the four Ca_V1 channels shown in **Figures 1B,C**. No statistically significant differences in Ca_V1 channel expression were observed for the comparisons listed in **Table 3**. As these comparisons already had the lowest *q* values (**Table 3**), differences in expression for other comparisons were also deemed not significant.

CHL Exhibits Reduced $Ca_V1.1$ and Higher $Ca_V1.2$ Expression Levels Relative to Other Kinds of B Cell Lymphoma

The cell lines of the CHL category were of interest for further study due to the relatively high expression of $Ca_V1.2$ (**Figure 1B**). Differential expression was performed between the CHL cell lines and the other B cell lymphoma cell lines to assess the expression of the L-type Ca^{2+} channels (**Figure 2A**). Expression of $Ca_V1.1$ was significantly lower in CHL (adjusted *p* value = 0.004), and the expression of the $Ca_V1.2$ channel was significantly greater in CHL (adjusted *p* value = 1.8×10^{-16}). Differential expression also showed that the expression levels of ORAI2 (adjusted *p* value = 0.00034) and STIM2 (adjusted *p* value = 0.0016) were lower in the CHL cell lines. In order to determine whether pathways related to Ca^{2+} were affected in CHL, three pathways from BioCarta and one from the KEGG were evaluated. Although no significant enrichment was detected between CHL and other B cell lymphomas for the calcineurin and calmodulin pathways, the NFAT (nominal *p* value <0.001; FDR *q* value <0.001; FWER *p* value <0.001) and KEGG Ca^{2+} signaling (nominal *p* value <0.001; FDR q value <0.001; FWER *p* value <0.001) pathways were found to be significantly upregulated in CHL (**Figures 2B–E**).

Another category of cell lines that underwent more assessment was PMBCL due to the $Ca_V1.3$ channel showing relatively elevated expression (**Figure 1B**). However, differential expression analysis of the Ca_V1 channels found no significant differences when comparing PMBCL to other B cell lymphoma cell lines (data not shown). Similarly, differential expression did not show any differences in ORAI/STIM expression (data not shown). In PMBCL, none of the four pathways showed significant upregulation or downregulation according to GSEA (data not shown).

TABLE 4 | Comparisons of ORAI/STIM expression in DLBCL patient samples. The *p* value and *q* value for each comparison are shown.

Gene	COO A	COO B	Mean A	Mean B	*p* value	q value
ORAI1	GCB	ABC	7.71096066894052	7.83107649954498	0.208403954574778	0.41883124851436
	GCB	Unclassified	7.71096066894052	7.82500105710116	0.32273153927664	0.538753456695682
	ABC	Unclassified	7.83107649954498	7.82500105710116	0.962399139380119	0.986380548158669
ORAI2	ABC	Unclassified	11.4239520360561	11.0771101686768	0.0756808552933548	0.246707670011409
	GCB	ABC	11.2701801394973	11.4239520360561	0.219636549829334	0.428912885044076
	GCB	Unclassified	11.2701801394973	11.0771101686768	0.299007694731689	0.520122628650921
ORAI3	GCB	ABC	9.38887758513438	9.29082762801457	0.143491212884708	0.343481033490216
	ABC	Unclassified	9.29082762801457	9.43745538376645	0.180810083575845	0.396852604528146
	GCB	Unclassified	9.38887758513438	9.43745538376645	0.638326098387733	0.808155977775295
STIM1	GCB	ABC	10.2794800129143	10.1798834785399	0.314227244848016	0.53315606297983
	ABC	Unclassified	10.1798834785399	10.3018108011769	0.422786360206746	0.651958096371479
	GCB	Unclassified	10.2794800129143	10.3018108011769	0.87562962451273	0.959022922085371
STIM2	ABC	Unclassified	10.6677890074025	10.5761563926166	0.52196480309146	0.738890716785782
	GCB	Unclassified	10.6595800398733	10.5761563926166	0.56420482060024	0.766037193868797
	GCB	ABC	10.6595800398733	10.6677890074025	0.921572084819698	0.973292967131008

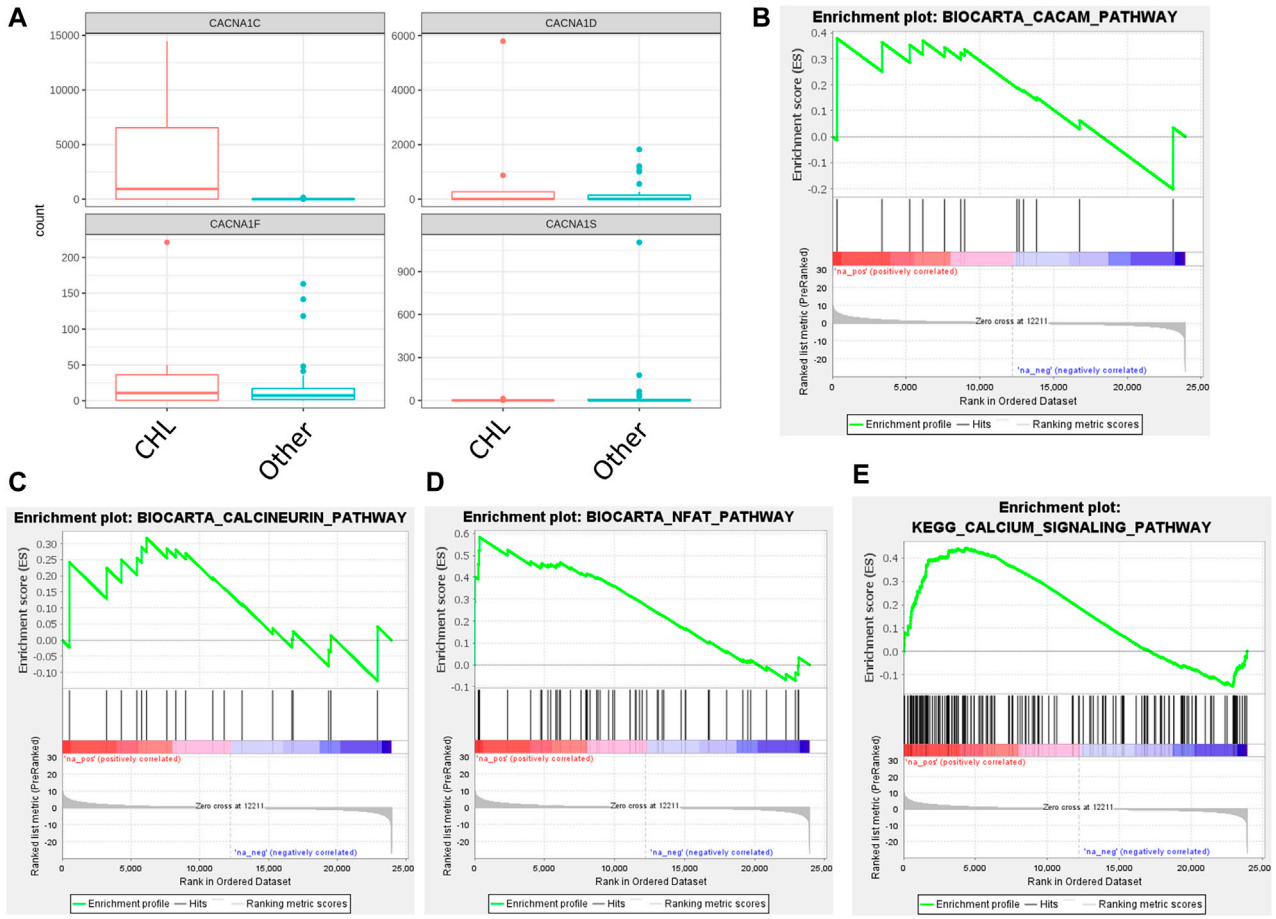

FIGURE 2 | Ca_V1 channel expression and BioCarta/KEGG pathways in CHL cell lines. **(A)** Ca_V1 channel expression (CACNA1S, $Ca_V1.1$; CACNA1C, $Ca_V1.2$; CACNA1D, $Ca_V1.3$; CACNA1F, $Ca_V1.4$) in CHL and other B cell lymphomas. **(B–E)** Pathways for **(B)** calmodulin (BioCarta), **(C)** calcineurin (BioCarta), **(D)** NFAT (BioCarta), and **(E)** Ca^{2+} signaling (KEGG) were assessed for enrichment in the CHL cell lines relative to other varieties of B cell lymphoma.

Expression Profile of $Ca_V1.3$ is Distinct From the Profiles of the Other Ca_V1 Channels in DLBCL Patient Samples

Aside from cell lines, the study of samples from patients with DLBCL was also conducted. Cell of origin was defined for patient samples, assigning each to ABC-DLBCL, GCB-DLBCL, or unclassified DLBCL (**Figure 3**). Numerous genes were evaluated for their expression levels with the use of RNA sequencing data, including the ORAI/STIM family. No differences in ORAI/STIM expression were observed from the pairwise comparisons (**Table 4**). To further assess the differences associated with DLBCL cell of origin, differential expression analysis was performed between ABC-DLBCL and GCB-DLBCL patient samples and used to assess the four Ca_V1 channels (**Figure 4A**). GCB-DLBCL demonstrated higher expression of $Ca_V1.1$ (adjusted p value = 2.2×10^{-10}), $Ca_V1.2$ (adjusted p value = 2.5×10^{-6}), and $Ca_V1.4$ (adjusted p value = 0.0013). In contrast, ABC-DLBCL displayed greater expression of $Ca_V1.3$ (adjusted p value = 0.0016). Differential expression analysis of the patient samples did not indicate any significant differences in ORAI/STIM expression between ABC-DLBCL and GCB-DLBCL (data not shown). For pathways associated with Ca^{2+}, the calcineurin and NFAT pathways were unchanged between GCB-DLBCL and ABC-DLBCL (**Figures 4C,D**). However, the calmodulin (nominal p value = 0.037; FDR q value = 0.037; FWER p value = 0.032) and KEGG (nominal p value = 0.04; FDR q value = 0.04; FWER p value = 0.04) pathways were both downregulated in ABC-DLBCL (**Figures 4B,E**).

DISCUSSION

As a range of lymphocyte functions are affiliated with Ca^{2+}, such as proliferation and activation (Omilusik et al., 2013), a study of Ca^{2+} channel expression and signaling pathway expression was conducted in an attempt to disentangle some of the complexities of lymphoma. The results presented here refer to cell lines and DLBCL patient samples, with a discussion regarding each of these groups

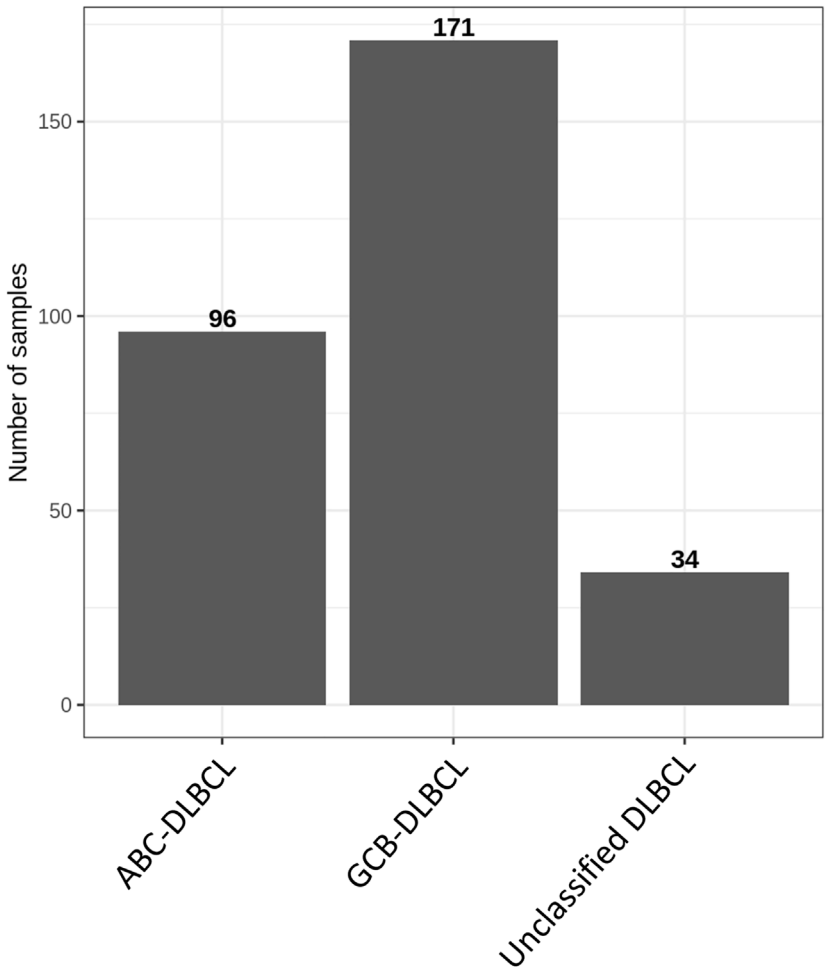

FIGURE 3 | DLBCL patient cohort by cell of origin subtype. DLBCL patient samples (N = 301) were categorized as ABC-DLBCL (N = 96), GCB-DLBCL (N = 171), or unclassified DLBCL (N = 34) according to the Lymph2Cx assay.

being provided below. Methods have been used previously (Aoki et al., 2020) to reaffirm the expression pattern of certain genes; however, a notable limitation of the current study is that no such validation has been completed.

The CHL cell lines included in this study consisted of the HDLM-2, HDMYZ, KM-H2, L-1236, L-428, L-540, L-591, SUP-HD1, and U-H01 cell lines (**Table 1**). Differential expression analysis revealed that $Ca_V1.2$ was more highly expressed in CHL cell lines relative to cell lines belonging to other types of B cell lymphoma. $Ca_V1.2$ has been linked to interleukin-13 (IL-13) in the context of T helper 2 (T_H2) cells in that IL-13 levels drop in response to $Ca_V1.2$ knockdown (Robert et al., 2014). IL-13 has been shown to be expressed by cell lines of Hodgkin lymphoma (Kapp et al., 1999). Furthermore, in a study published soon afterward (Skinnider et al., 2001), it was shown that most CHL patients exhibited expression of IL-13, whereas this trait was either observed in none or fewer than 50% of patients with other forms of lymphoma, such as DLBCL. Signal transducer and activator of transcription 6 (STAT6), which is activated by IL-13, was found to be phosphorylated in cell lines of Hodgkin lymphoma (Skinnider et al., 2002). Therefore, $Ca_V1.2$ could possibly be playing a role in the regulation of IL-13 and STAT6 in CHL. Since the NFAT and KEGG Ca^{2+} signaling pathways (**Table 2**) were shown to be upregulated in the CHL cell lines, it is also possible that $Ca_V1.2$ influences the components of these pathways. In contrast to $Ca_V1.2$, reduced expression of ORAI2 and STIM2 was noted in the CHL cell lines via differential expression analysis. Given that STIM1 is known to activate ORAI channels and hinder $Ca_V1.2$ (Wang et al., 2010), it was surprising that the differential expression analysis in the current study did not show a significant reduction in STIM1 expression in the CHL cell lines. As STIM1 and STIM2 differ in their expression profiles (at least in T cells) and the ER Ca^{2+} concentration to which they respond (Shaw and Feske, 2012), this could potentially explain why only one of them, STIM2, showed a change in expression between CHL and other B cell lymphomas.

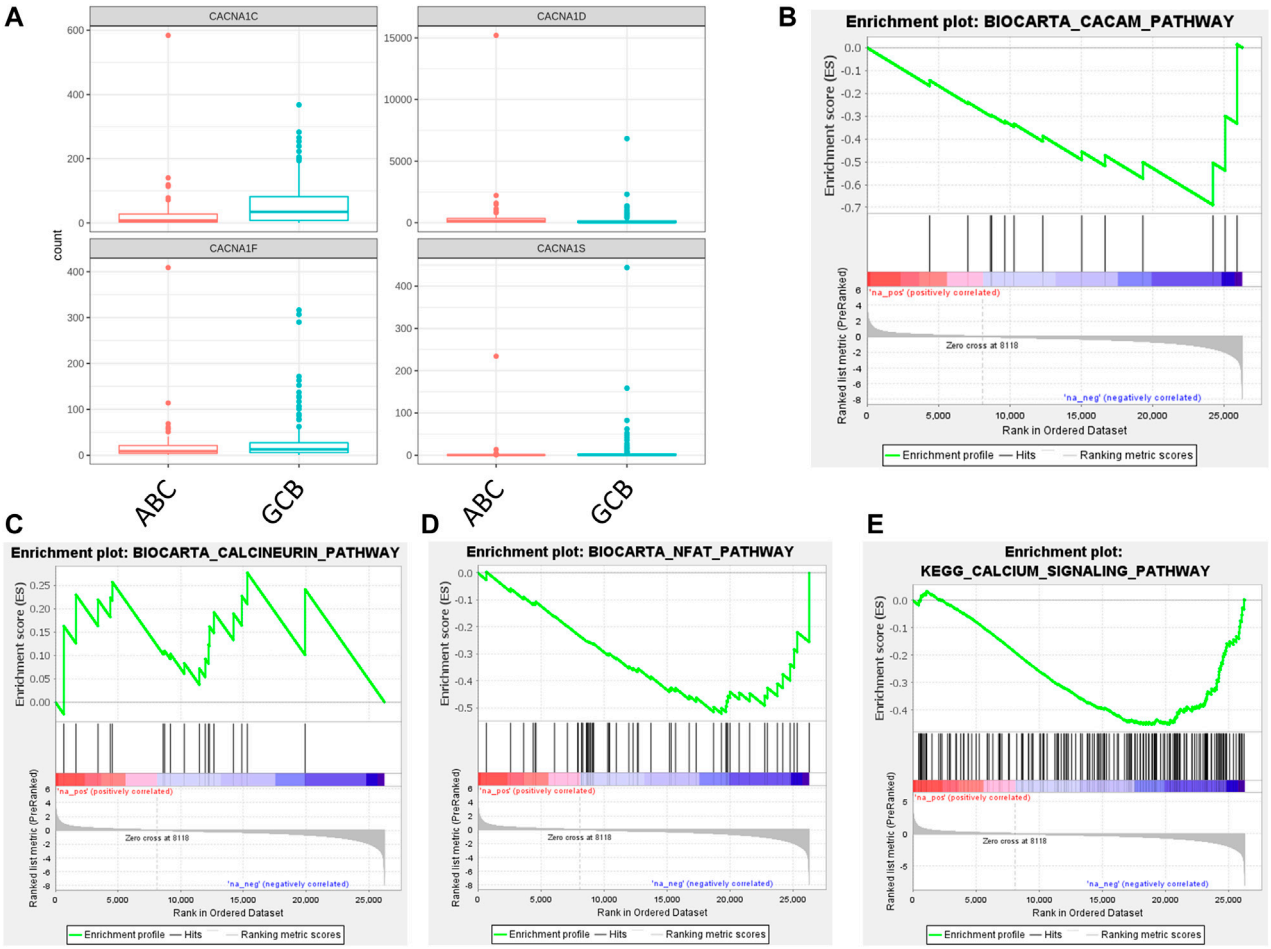

FIGURE 4 | Ca_V1 channel expression and BioCarta/KEGG pathways in ABC-DLBCL and GCB-DLBCL patient samples. **(A)** Ca_V1 channel expression (CACNA1S, $Ca_V1.1$; CACNA1C, $Ca_V1.2$; CACNA1D, $Ca_V1.3$; CACNA1F, $Ca_V1.4$) in ABC-DLBCL and GCB-DLBCL. **(B–E)** Differential expression results were assessed for pathway enrichment of **(B)** calmodulin (BioCarta), **(C)** calcineurin (BioCarta), **(D)** NFAT (BioCarta), and **(E)** Ca^{2+} signaling (KEGG).

Among the GCB-DLBCL and ABC-DLBCL patients, the expression of the $Ca_V1.3$ channel was found to be higher in ABC-DLBCL by differential expression. It is known that L-type Ca_V channel constraint leads to reduced function of the transcription factor nuclear factor kappa B (NF-κB) (Lilienbaum and Israël, 2003). Within the promoter for the *bcl-2* gene, which encodes the B cell leukemia/lymphoma-2 (Bcl-2) "anti-apoptosis" protein, there exists at least one binding site for NF-κB (Catz and Johnson, 2001). BCL2, as part of a network of genes, was deemed to be upregulated in ABC-DLBCL (Blenk et al., 2007). Another component of this network that was ascertained as being upregulated in the ABC kind of DLBCL was IRF4 (Blenk et al., 2007), and the promoter for this gene is known to have NF-κB binding sites as well (Sharma et al., 2002). Future studies could potentially further characterize these components in terms of how they might functionally relate to the $Ca_V1.3$ Ca^{2+} channel in the specific context of DLBCL, particularly since no differences in ORAI/STIM expression were detected in the patient samples in our study. This latter finding suggests that ORAI channels might not be contributing to differences in DLBCL phenotype in patients and that other Ca^{2+} channels, such as $Ca_V1.3$, could be playing this role instead. Furthermore, the calmodulin and KEGG Ca^{2+} signaling pathways (**Table 2**) were downregulated in ABC-DLBCL relative to GCB-DLBCL, suggesting that these pathways could also be linked to differences in DLBCL phenotype. The DLBCL patient sample RNA sequencing did not cover control B cells due to a lack of normal matches at the time. Investigation of Ca_V channels from this perspective would potentially be valuable as well. In order to validate these suggested mechanisms linked to Ca^{2+}, follow-up experiments would need to be conducted.

To conclude, the L-type Ca_V channels represent a potential target class in the field of anti-lymphoma therapeutics. By targeting specific Ca_V1 channels and, by extension, the mechanisms associated with each channel, this could lead to updated strategies to treat lymphoma.

DATA AVAILABILITY STATEMENT

RNA sequencing data for the lymphoma cell lines generated at BC Cancer are available via controlled access through GEO (accession number GSE189927). Data for the DLBCL patients were previously reported, and information on the accession is available in the original article (Ennishi et al., 2019).

ETHICS STATEMENT

Human studies were reviewed and approved by the University of British Columbia - BC Cancer Research Ethics Board (H14-02304: Biomarkers in Lymphoid Cancer), in accordance with the Declaration of Helsinki. We obtained written informed consent from the patients or informed consent was waived for the samples used in this retrospective study.

AUTHOR CONTRIBUTIONS

WJ conceived of the project; WJ, SS, and LC wrote the manuscript; WJ, SS, CS, and LC edited the manuscript; SS and LC prepared tables; LC conducted analyses (including statistical analysis) and produced images for figures; SS and LC discussed analyses and points of interest to investigate; CS provided access to datasets; WJ and CS supervised the research.

FUNDING

SS was supported by the John Richard Turner Fellowship in Microbiology. This work was supported by a Canadian Institutes of Health Research (CIHR) Operating grant to WJ (MOP-102698) and by donations to the Sullivan Urology Foundation at Vancouver General Hospital.

ACKNOWLEDGMENTS

The authors would like to thank the patients whose samples were invaluable to this study.

SUPPLEMENTARY MATERIAL

The Supplementary Material for this article can be found online at: https://www.frontiersin.org/articles/10.3389/fphar.2022.795176/full#supplementary-material

REFERENCES

Aoki, T., Chong, L. C., Takata, K., Milne, K., Hav, M., Colombo, A., et al. (2020). Single-Cell Transcriptome Analysis Reveals Disease-Defining T-Cell Subsets in the Tumor Microenvironment of Classic Hodgkin Lymphoma. *Cancer Discov.* 10, 406–421. doi:10.1158/2159-8290.CD-19-0680

Blenk, S., Engelmann, J., Weniger, M., Schultz, J., Dittrich, M., Rosenwald, A., et al. (2007). Germinal center B Cell-like (GCB) and Activated B Cell-like (ABC) Type of Diffuse Large B Cell Lymphoma (DLBCL): Analysis of Molecular Predictors, Signatures, Cell Cycle State and Patient Survival. *Cancer Inform.* 3, 399–420. doi:10.1177/117693510700300004

Bobée, V., Drieux, F., Marchand, V., Sater, V., Veresezan, L., Picquenot, J. M., et al. (2020). Combining Gene Expression Profiling and Machine Learning to Diagnose B-Cell Non-hodgkin Lymphoma. *Blood Cancer J.* 10, 59. doi:10.1038/s41408-020-0322-5

Catz, S. D., and Johnson, J. L. (2001). Transcriptional Regulation of Bcl-2 by Nuclear Factor Kappa B and its Significance in Prostate Cancer. *Oncogene* 20, 7342–7351. doi:10.1038/sj.onc.1204926

Ennishi, D., Jiang, A., Boyle, M., Collinge, B., Grande, B. M., Ben-Neriah, S., et al. (2019). Double-hit Gene Expression Signature Defines a Distinct Subgroup of Germinal center B-cell-like Diffuse Large B-Cell Lymphoma. *J. Clin. Oncol.* 37, 190–201. doi:10.1200/JCO.18.01583

Glas, A. M., Kersten, M. J., Delahaye, L. J., Witteveen, A. T., Kibbelaar, R. E., Velds, A., et al. (2005). Gene Expression Profiling in Follicular Lymphoma to Assess Clinical Aggressiveness and to Guide the Choice of Treatment. *Blood* 105, 301–307. doi:10.1182/blood-2004-06-2298

Hoefnagel, J. J., Dijkman, R., Basso, K., Jansen, P. M., Hallermann, C., Willemze, R., et al. (2005). Distinct Types of Primary Cutaneous Large B-Cell Lymphoma Identified by Gene Expression Profiling. *Blood* 105, 3671–3678. doi:10.1182/blood-2004-04-1594

Kahl, C. R., and Means, A. R. (2004). Regulation of Cyclin D1/Cdk4 Complexes by Calcium/calmodulin-dependent Protein Kinase I. *J. Biol. Chem.* 279, 15411–15419. doi:10.1074/jbc.M312543200

Kapp, U., Yeh, W. C., Patterson, B., Elia, A. J., Kägi, D., Ho, A., et al. (1999). Interleukin 13 Is Secreted by and Stimulates the Growth of Hodgkin and Reed-Sternberg Cells. *J. Exp. Med.* 189, 1939–1946. doi:10.1084/jem.189.12.1939

Kotturi, M. F., Carlow, D. A., Lee, J. C., Ziltener, H. J., and Jefferies, W. A. (2003). Identification and Functional Characterization of Voltage-dependent Calcium Channels in T Lymphocytes. *J. Biol. Chem.* 278, 46949–46960. doi:10.1074/jbc.M309268200

Lilienbaum, A., and Israël, A. (2003). From Calcium to NF-Kappa B Signaling Pathways in Neurons. *Mol. Cel Biol.* 23, 2680–2698. doi:10.1128/MCB.23.8.2680-2698.2003

Macian, F. (2005). NFAT Proteins: Key Regulators of T-Cell Development and Function. *Nat. Rev. Immunol.* 5, 472–484. doi:10.1038/nri1632

Magi, A., Masselli, M., Sala, C., Guerriero, A., Laise, P., Puccini, B., et al. (2019). The Ion Channels and Transporters Gene Expression Profile Indicates a Shift in Excitability and Metabolisms during Malignant Progression of Follicular Lymphoma. *Sci. Rep.* 9, 8586. doi:10.1038/s41598-019-44661-x

Omilusik, K., Priatel, J. J., Chen, X., Wang, Y. T., Xu, H., Choi, K. B., et al. (2011). The Ca(v)1.4 Calcium Channel Is a Critical Regulator of T Cell Receptor Signaling and Naive T Cell Homeostasis. *Immunity* 35, 349–360. doi:10.1016/j.immuni.2011.07.011

Omilusik, K. D., Nohara, L. L., Stanwood, S., and Jefferies, W. A. (2013). Weft, Warp, and Weave: the Intricate Tapestry of Calcium Channels Regulating T Lymphocyte Function. *Front. Immunol.* 4, 164. doi:10.3389/fimmu.2013.00164

Phan, N. N., Wang, C. Y., Chen, C. F., Sun, Z., Lai, M. D., and Lin, Y. C. (2017). Voltage-gated Calcium Channels: Novel Targets for Cancer Therapy. *Oncol. Lett.* 14, 2059–2074. doi:10.3892/ol.2017.6457

Putney, J. W. (2018). Forms and Functions of Store-Operated Calcium Entry Mediators, STIM and Orai. *Adv. Biol. Regul.* 68, 88–96. doi:10.1016/j.jbior.2017.11.006

Rao, A., Luo, C., and Hogan, P. G. (1997). Transcription Factors of the NFAT Family: Regulation and Function. *Annu. Rev. Immunol.* 15, 707–747. doi:10.1146/annurev.immunol.15.1.707

Robert, V., Triffaux, E., Paulet, P. E., Guéry, J. C., Pelletier, L., and Savignac, M. (2014). Protein Kinase C-dependent Activation of CaV1.2 Channels Selectively Controls Human TH2-Lymphocyte Functions. *J. Allergy Clin. Immunol.* 133, 1175–1183. doi:10.1016/j.jaci.2013.10.038

Scott, D. W., Wright, G. W., Williams, P. M., Lih, C. J., Walsh, W., Jaffe, E. S., et al. (2014). Determining Cell-Of-Origin Subtypes of Diffuse Large B-Cell

Lymphoma Using Gene Expression in Formalin-Fixed Paraffin-Embedded Tissue. *Blood* 123, 1214–1217. doi:10.1182/blood-2013-11-536433

Sharma, S., Grandvaux, N., Mamane, Y., Genin, P., Azimi, N., Waldmann, T., et al. (2002). Regulation of IFN Regulatory Factor 4 Expression in Human T Cell Leukemia Virus-I-Transformed T Cells. *J. Immunol.* 169, 3120–3130. doi:10.4049/jimmunol.169.6.3120

Shaw, P. J., and Feske, S. (2012). Regulation of Lymphocyte Function by ORAI and STIM Proteins in Infection and Autoimmunity. *J. Physiol.* 590, 4157–4167. doi:10.1113/jphysiol.2012.233221

Skinnider, B. F., Elia, A. J., Gascoyne, R. D., Patterson, B., Trumper, L., Kapp, U., et al. (2002). Signal Transducer and Activator of Transcription 6 Is Frequently Activated in Hodgkin and Reed-Sternberg Cells of Hodgkin Lymphoma. *Blood* 99, 618–626. doi:10.1182/blood.v99.2.618

Skinnider, B. F., Elia, A. J., Gascoyne, R. D., Trümper, L. H., von Bonin, F., Kapp, U., et al. (2001). Interleukin 13 and Interleukin 13 Receptor Are Frequently Expressed by Hodgkin and Reed-Sternberg Cells of Hodgkin Lymphoma. *Blood* 97, 250–255. doi:10.1182/blood.v97.1.250

Sung, H., Ferlay, J., Siegel, R. L., Laversanne, M., Soerjomataram, I., Jemal, A., et al. (2021). Global Cancer Statistics 2020: GLOBOCAN Estimates of Incidence and Mortality Worldwide for 36 Cancers in 185 Countries. *CA Cancer J. Clin.* 71, 209–249. doi:10.3322/caac.21660

Vogt, N., Dai, B., Erdmann, T., Berdel, W. E., and Lenz, G. (2017). The Molecular Pathogenesis of Mantle Cell Lymphoma. *Leuk. Lymphoma* 58, 1530–1537. doi:10.1080/10428194.2016.1248965

Wang, C. Y., Lai, M. D., Phan, N. N., Sun, Z., and Lin, Y. C. (2015). Meta-Analysis of Public Microarray Datasets Reveals Voltage-Gated Calcium Gene Signatures in Clinical Cancer Patients. *PLoS One* 10, e0125766. doi:10.1371/journal.pone.0125766

Wang, Y., Deng, X., Mancarella, S., Hendron, E., Eguchi, S., Soboloff, J., et al. (2010). The Calcium Store Sensor, STIM1, Reciprocally Controls Orai and CaV1.2 Channels. *Science* 330, 105–109. doi:10.1126/science.1191086

Yanamandra, N., Buzzeo, R. W., Gabriel, M., Hazlehurst, L. A., Mari, Y., Beaupre, D. M., et al. (2011). Tipifarnib-induced Apoptosis in Acute Myeloid Leukemia and Multiple Myeloma Cells Depends on Ca2+ Influx through Plasma Membrane Ca2+ Channels. *J. Pharmacol. Exp. Ther.* 337, 636–643. doi:10.1124/jpet.110.172809

Yeoh, E. J., Ross, M. E., Shurtleff, S. A., Williams, W. K., Patel, D., Mahfouz, R., et al. (2002). Classification, Subtype Discovery, and Prediction of Outcome in Pediatric Acute Lymphoblastic Leukemia by Gene Expression Profiling. *Cancer Cell* 1, 133–143. doi:10.1016/s1535-6108(02)00032-6

Conflict of Interest: The authors declare that the research was conducted in the absence of any commercial or financial relationships that could be construed as a potential conflict of interest.

Publisher's Note: All claims expressed in this article are solely those of the authors and do not necessarily represent those of their affiliated organizations, or those of the publisher, the editors and the reviewers. Any product that may be evaluated in this article, or claim that may be made by its manufacturer, is not guaranteed or endorsed by the publisher.

Advantages of publishing in Frontiers

OPEN ACCESS
Articles are free to read for greatest visibility and readership

FAST PUBLICATION
Around 90 days from submission to decision

HIGH QUALITY PEER-REVIEW
Rigorous, collaborative, and constructive peer-review

TRANSPARENT PEER-REVIEW
Editors and reviewers acknowledged by name on published articles

Frontiers
Avenue du Tribunal-Fédéral 34
1005 Lausanne | Switzerland

Visit us: www.frontiersin.org
Contact us: frontiersin.org/about/contact

REPRODUCIBILITY OF RESEARCH
Support open data and methods to enhance research reproducibility

DIGITAL PUBLISHING
Articles designed for optimal readership across devices

FOLLOW US
@frontiersin

IMPACT METRICS
Advanced article metrics track visibility across digital media

EXTENSIVE PROMOTION
Marketing and promotion of impactful research

LOOP RESEARCH NETWORK
Our network increases your article's readership